

Numerische Simulation des Mikroklimas im Innenhof

Von der Fakultät für Bauingenieurwesen und Geodäsie
der Gottfried Wilhelm Leibniz Universität Hannover zur Erlangung des
Grades

Doktorin der Ingenieurwissenschaften

Dr.-Ing.

genehmigte Dissertation von

M.Sc. Aysan Forouzandeh

2020

Prüfungskommission

Referent/in	Univ.-Prof. Dr.-Ing. Nabil A. Fouad
Ko-Referent/in:	Univ.-Prof. Dr.-Ing. Udo Nackenhorst
Externe Referent/in:	Univ.-Prof. Dr. Michael Bruse
Tag der Promotion:	08.01.2020

Numerical Simulation of Microclimate in Courtyard

From the Department of Civil Engineering and Geodetic Science
Leibniz University of Hanover to obtain the academic degree

Doctor in engineering

Dr.-Ing.

Submitted by

M.Sc. Aysan Forouzandeh

Published- 2020

Danksagungen

Diese Dissertation ist im Rahmen meiner Tätigkeit als wissenschaftliche Mitarbeiterin und Doktorandin am Institut für Bauphysik der Leibniz Universität Hannover entstanden. Hierbei wurde ich von vielen Personen unterstützt, denen ich an dieser Stelle herzlich danken möchte. Zuerst möchte ich mich bei meinem Doktorvater Herr Prof. Dr. Nabil Fouad bedanken. Bei Herrn Dr. Torsten Richter bedanke ich mich für seine Unterstützung zur Ermöglichung der Messungen im Gebäude der VHV-Gruppe. Neben den oben genannten Personen möchte ich mich ebenfalls bei allen anderen Institutskollegen bedanken. Sie hätte ich während meiner Dissertationszeit nicht missen wollen.

Ein persönlicher Dank geht an Herrn Prof. Michael Bruse. Er hat mich während meiner Dissertation durch die Bereitstellung der Softwarelizenz und des Programm (ENVI-met) unterstützt, welches für Simulationen in meiner Forschung dringend benötigt werde. Schließlich gilt mein größter Dank meiner Familie und meinem Mann Shahin, die mich während dieser Zeit in jeglicher Hinsicht unterstützt haben. Daher widme ich ihnen diese Dissertation mit meinem ganzen Herzen.

Hannover, Juni 2019

Aysan Forouzandeh

Abstract

It is widely accepted that the courtyard concept can modify the climate and with moderating the extreme hot or cold climate condition is considered as one of the old passive design strategies. However, despite the effect of the courtyard on climatic variables, the heat loss calculation methods mostly consider the weather file of the courtyard the same as the ambient weather file. Regarding the low thermal resistance of the courtyard surrounding glass envelopes against heat conduction, these façades are more sensitive in front of the environmental parameters and this simplification in the calculation can overestimate the heat load for the surrounding rooms of the courtyard.

This study seeks to understand the effect of the courtyard and its various configurations on the environmental parameters and to suggest appropriate adjustment factors to consider the courtyard's special microclimate in the calculation of the heat loss through the building's envelope. In this way, the parametric analysis was implemented using the three-dimensional computational microclimate model "ENVI-met".

Hence as a first step of the research processes, the numerical simulations were validated by experimental in-situ investigations and the accuracy of the computational model in predicting air temperature, wind speed, relative humidity and mean radiant temperature inside the courtyard was evaluated.

The next steps following the linking the climatic variables inside the courtyard in the thermal balance of surrounding building envelopes and the heat loss calculation. Since the biggest advantage of the courtyard semi-closed space related to the wind protection offered by the courtyard and its heat island during the winter, this study was focused on the effect of the courtyard and its configuration on two building physics parameters including the convective heat transfer coefficient (CHTC) and temperature adjustment factor ($F_{x, \text{heat load}}$).

The outcomes of the research, which were calculated for the experimental case in the Hanover climate region, showed that the CHTC through the façade inside the courtyard is less than exposed building envelopes. This decrease is particularly noticeable at higher ambient wind speeds. In addition, the aspect ratio of the courtyard has a great effect on wind speed inside it. So that, inside the deep courtyards ($H/W \geq 2.67$) the wind speed is almost zero at low levels of the courtyard and CHTC can be considered with the minimum value and is about $4 \text{ (W m}^{-2}\text{K}^{-1}\text{)}$ according to DIN EN ISO 6946.

Investigating the air temperature difference between the courtyard and outside standard temperature for Hanover also proposes an $F_{x, \text{heat load}}$ between 0.9 and 2.2 for courtyard semi-closed space, which varies depending on the courtyard aspect ratio and glazing percentage of the surrounding envelopes.

Keywords: Courtyard microclimate, Heat loss through building's envelope, Ambient temperature correction factor, External convective heat transfer coefficient

Zusammenfassung

Es ist allgemein akzeptiert, dass das Innenhofkonzept das Klima verändern kann und mit der Milderung des extrem heißen oder kalten Klimas als eine der alten passiven Designstrategien betrachtet wird. Trotz der Einflüsse des Innenhofs auf die Klimavariablen, werden die Innenhofwetterdaten bei den Wärmeverlustberechnungen oft mit den Umgebungswetterdaten gleichgesetzt. Aufgrund des geringen Wärmewiderstands der Glasfassaden werden die Berechnungsergebnisse dieser Fassaden durch die Umgebungsparameter stark beeinflusst. Der zuvor genannte Annahmefehler bei den Berechnungen führt zu einer Überschätzung der Wärmebelastungen für die umliegenden Räume des Innenhofes.

Im Rahmen dieser Arbeit wurden die Auswirkungen des Innenhofs auf die Wetterdaten untersucht und geeignete Anpassungsfaktoren wurden in Abhängigkeit der Eigenschaften des Innenhofs vorgeschlagen. Auf dieser Art wurde die Parameteranalyse mittels eines dreidimensionalen Computergeschützten Mikroklimamodells „ENVI-met“ implementiert.

Im ersten Schritt der Forschungsprozesse wurden die numerischen Simulationen mittels der experimentellen In-Situ-Untersuchungen validiert und die Genauigkeit des Berechnungsmodells bei der Vorhersage von Lufttemperatur, Windgeschwindigkeit, relative Luftfeuchtigkeit und mittlere Strahlungstemperatur im Innenhof bewertet.

Die nächsten Schritte folgen der Verknüpfung der klimatischen Variablen im Innenhof in der Wärmebilanz der umgebenden Gebäudehüllen und der Berechnung der Wärmeverluste. Da der größte Vorteil des halbgeschlossenen Innenhofes der Windschutz des Innenhofes und die Ausbildung einer Wärmeinsel im Winter ist, konzentrierte sich diese Studie auf die Auswirkungen des Innenhofes und seiner Konfiguration auf zwei bauphysikalische Parameter, einschließlich des konvektiven Wärmeübertragungskoeffizienten (CHTC) und des Temperaturanpassungsfaktors (F_x , Wärmebelastung).

Die experimentellen Forschungsergebnisse, die für die Klimaregion Hannover ermittelt wurden, zeigen, dass das CHTC der Fassade im Innenhof geringer ist als bei freiliegenden Gebäudehüllen. Dieser Unterschied ist insbesondere bei höheren Umgebungswindgeschwindigkeiten bemerkbar. Darüber hinaus hat das Seitenverhältnis der Innenhöfe einen großen Einfluss auf die Windgeschwindigkeit. In den tiefen Innenhöfen ($H / W \geq 2,67$) ist die Windgeschwindigkeit bei niedrigen Fassadenhöhen des

Innenhofs kann zu einen minimal wert angenommen werden (ca. $4 \text{ (W m}^{-2} \text{K}^{-1})$ gemäß DIN EN ISO 6946).

Die Untersuchung der Lufttemperaturdifferenz zwischen Innenhof- und Außentemperatur für Hannover schlägt für halb geschlossene Innenhofräume eine F_x -Wärmebelastung zwischen 0,9 und 2,2 vor, der je nach Seitenverhältnis des Innenhofs und Verglasungsgrade variiert.

Schlüsselwörter: Innenhof-Mikroklima, Wärmeverlust durch die Gebäudehülle, Umgebungstemperatur-Korrekturfaktor, Konvektive Wärmedurchgangskoeffizient

Papers

Numerical modeling validation for the microclimate thermal condition of semi-closed courtyard spaces between buildings

Paper A

Forouzandeh, A. Numerical modeling validation for the microclimate thermal condition of semi-closed courtyard spaces between buildings, Sustain. Cities Soc. 36 (2018).

doi:10.1016/j.scs.2017.07.025

Parametric analysis of influence of courtyard microclimate on diminution of convective heat transfer through building's envelope

Paper B

Forouzandeh, A. Parametric analysis of influence of courtyard microclimate on diminution of convective heat transfer through building's envelope, Build. Simul. (2019).

doi:10.1007/s12273-019-0528-2

Accurate prediction of heating energy demand of courtyard's surrounding envelopes using temperature correction factor

Paper C

Forouzandeh, A. , Richter, A. Forouzandeh, T. Richter, Accurate prediction of heating energy demand of courtyard's surrounding envelopes using temperature correction factor, Energy Build. 193 (2019).

doi:10.1016/j.enbuild.2019.03.030

Structure of the Dissertation

The dissertation consists of two parts: The research summary (Part A) and the papers of the dissertation (Part B).

Part A introduces the topic (Section 1) by giving an overall motivation, stating the problem and deriving the research questions (1.1).

Introduction includes the theoretical background (1.2) which focuses on the effective environmental parameters on the heat loss through the building's envelopes (1.2.1) and the courtyard special microclimate and its effect on the climatic variables (1.2.2) this part is concluded with the effect of courtyard microclimate on the heat loss through the building's envelope (1.2.3). Finally, the introduction section ends with presenting the main research objectives (1.3).

Part A is followed by the explanation of the overall research approach (Section 2) on the evaluating methods of the courtyard microclimate (2.1), case study selection (2.1.1), modeling software selection and validation (2.1.2). By giving an overview and a synopsis on each paper of the dissertation the results are presented in section 3. This part concludes with a summary and discussion, which provide a positioning of the dissertation as well as future research (Section 4).

Part B comprises the papers of the dissertation and introduces each paper with a summary table presenting its bibliographical information.

Table of Contents

Abstract.....	II
Zusammenfassung	IV
Papers.....	VI
Structure of the Dissertation	VII
Table of Contents.....	VIII
List of Figures.....	XIII
List of Tables	XVII
Part A - Research Summary	1
1 Introduction	2
1.1. Concept of motivation	2
1.2. Theoretical Background	7
1.2.1. Effective environmental parameters on heat loss through building's envelope	7
1.2.2. Effect of courtyard on climatic variables	9
1.2.3. Conclusion	11
1.3. Research Objectives	12
2 Research process	13
2.1 Research design.....	13
2.1.1 Selection of research reference case.....	15
2.1.2 Computational software selection	16
3 Discussion of results.....	23
4 Conclusions and future developments.....	26
5 References	27
Part B - Papers of the Dissertation	34
Paper A - Numerical modeling validation for the microclimate thermal condition of semi-closed courtyard spaces between buildings.....	35
Abstract	36
1. Introduction	37

2. The microclimate model ENVI-met	40
3. Methods	41
3.1. Field experiment	42
3.1.1. Study area.....	42
3.1.2. Site-measurements.....	43
3.1.3. ENVI-met model.....	44
3.1.4. Weather data.....	48
3.1.5. Model area.....	50
3.1.6. Building, plants, soil physical properties	55
3.1.7. Boundary condition.....	60
3.1.7.1. Temperature and humidity	60
3.1.7.2. Wind and turbulence	60
3.1.8. Simulation time	61
3.1.9. Model timing.....	61
4. Results and discussion.....	62
4.1. ENVI-met model verification.....	62
4.2. validation results and discussion	67
5. Discussion.....	77
5. References	78
Paper B - Parametric analysis of influence of courtyard microclimate on diminution of convective heat transfer through building's envelope.....	86
Abstract	87
1. Introduction ..	89
2. Methodology	98
2.1. Study site and simulation days.....	99
2.2. Characteristics of computational model and studied cases.. ..	100
2.3. Reliability of software	111
3. Results and analysis	112
3.1. Flow pattern inside the courtyards ..	112

3.2. Diurnal variation of WS	117
3.3. Effect of courtyard on WS and CHTC	120
3.3.1. Effect of courtyard aspect ratio (H/W).....	120
3.3.2. Effect of step-up and step-down notch.....	121
3.3.3. Effect of courtyard enclosure's depth	123
3.3.4. Effect of courtyard orientation, facing into prevailing wind direction.....	125
3.3.5. Effect of surrounding roof pitches	126
3.3.6. Effect of ambient wind speed	127
4. Discussion.....	129
5. Conclusion	134
References.....	134
Paper C - Accurate prediction of heating energy demand of courtyard's surrounding envelopes using temperature correction factor.....	143
Author contribution statements.....	144
Abstract	145
1. Introduction ..	147
2. Methodology	155
2.1. Description of experimental studies ..	156
2.1.1. Selected courtyards and field measurement	156
2.1.2. Experimental results.....	161
2.2. Computational studies: method and validation	164
2.2.1. Computational method and adjustments	164
2.2.2. Validation using experimental results.....	173
2.2.3. Results and discussions	175
2.2.3.1. Phase 1: normal winter day	175
2.2.3.2. Phase 2: standard-external temperature and $F_{x, \text{Heat load}}$	181
3. Conclusions and future developments	189
References.....	190

Appendix

Appendix 1: Existing correlations for convective heat transfer coefficient at exterior building surface	197
1. Flat plate.....	197
2. Full- scale experiments	199
3. Wind- tunnel experiments.....	199
4. Computational fluid dynamics experiments	200
References.....	203
Appendix 2: Effect of courtyard on surface temperature of its surrounding envelopes and accuracy of ENVI-met in predicting building's surface temperature....	206
Appendix 3: Software: Microclimate model ENVI-met, features and codes	209
1. General model properties.....	210
1.1. 1D boundary model.....	210
1.2. The 3D core model	210
1.2.1. The atmosphere model	211
1.2.1.1. Wind flow	211
1.2.1.2. Temperature and humidity	212
1.2.1.3. Atmospheric Turbulence.....	213
1.2.1.4. Gas and particle dispersion model	213
1.2.1.5. Radiation	214
1.2.2. Surface model: Ground and building surfaces	217
1.2.2.1. Ground surfaces	217
1.2.2.2. Building surfaces.....	218
1.2.3. Soil model	225
1.2.4. Vegetation model	225
1.2.5. Biometeorological model	227
1.2.5.1. Calculation of the mean radiant temperature in ENVI-met	227
2. Numerical solution techniques in ENVI-met.....	228
3. Shortcoming of ENVI-met	229
4. Example data for ENVI-met model (.SIM files)	231

References.....	237
Appendix 4: Original Published Papers- first page	240
1. Paper A.	240
2. Paper B.....	241
3. Paper C.....	242
Curriculum Vitae	243

List of Figures

Part A

Fig. A. 1.	Typical courtyard buildings in different climates.....	3
Fig. A. 2.	Different resistance between building's envelope inside and outside courtyard.....	6
Fig. A. 3.	Heat transfer through external wall	8
Fig. A. 4.	Radiation exchange inside courtyard.....	10
Fig. A. 5.	Research process	14
Fig. A. 6.	Experimental area.....	16
Fig. A. 7.	Courtyard's vertical section; including (a) Stratification; (b) Convection; (c) Wind flow	18

Part B

Paper A. Fig. 1.	The process of achieving a valid ENVI-met model of the outdoor environment.....	44
Paper A. Fig. 2.	An experimental area and the layout of measurement points.....	45
Paper A. Fig. 3.	Views of the instruments during the experiment.....	46
Paper A. Fig. 4.	An experimental area and the layout of measurement points.....	46
Paper A. Fig. 5.	Representation of the model input (including buildings and vegetation) for each area	57
Paper A. Fig. 6.	Respectively from left to right: The structure of Courtyard's surrounding walls, defined structure for the courtyard's surrounding walls in ENVI-met- Database.....	58
Paper A. Fig. 7.	Model area, including the buildings, Plants and soil color-chart	58
Paper A. Fig. 8.	Compares the difference between the calculated and site measurement meteorological values for three experimental models.....	65
Paper A. Fig. 9.	Comparison of the difference between the calculated and site measurement meteorological values with three different model boundary condition for turbulence	66
Paper A. Fig. 10.	Comparison of the difference between the calculated and site measurement meteorological values with four different time intervals for flow.....	67
Paper A. Fig. 11.	Comparison of the observed and modeled Air temperature at 1.5 m above ground.	68

Paper A. Fig. 12.	Comparison of the observed and modeled Air temperature at 1.5 m above ground, for the different part of the courtyard on August 17, 2016.....	69
Paper A. Fig. 13.	Comparison of the observed and modeled Air temperature at 1.5 m above ground, outside the courtyard on August 16, 2016.....	69
Paper A. Fig. 14.	Comparison of the observed and modeled Relative humidity at 1.5 m above ground.....	71
Paper A. Fig. 15.	Comparison of the observed and modeled Relative Humidity at 1.5 m above ground, for different part of the courtyard on August 17, 2016.....	72
Paper A. Fig. 16.	Comparison of the observed and modeled Relative Humidity at 1.5 m above ground, outside the courtyard on August 16, 2016.....	72
Paper A. Fig. 17.	Comparison of the observed and modeled wind velocity (m s^{-1}) at 1.5 m above ground.....	73
Paper A. Fig. 18.	Comparison of the observed and modeled wind speed at 1.5 m above ground, for the different part of the courtyard on August 17, 2016.....	74
Paper A. Fig. 19.	Comparison of the observed and modeled wind speed at 1.5 m above ground, outside the courtyard on August 16, 2016.....	74
Paper A. Fig. 20.	Comparison of the observed and modeled Mean Radiant Temperature at 1.5 m above ground.....	76
Paper A. Fig. 21.	Comparison of the observed and modeled Mean Radiant Temperature at 1.5 m above ground, outside the courtyard on August 16, 2016.....	77
Paper B. Fig. 1.	Study cases.....	103
Paper B. Fig. 2.	A model description, computational domain in x - z plane including the boundaries.....	108
Paper B. Fig. 3.	Heat balances on outside and inside of the exterior walls, respectively on the Airtec glass façade and on the heat protection glass.....	110
Paper B. Fig. 4.	Layout of the measured points.....	111
Paper B. Fig. 5.	Comparison of observed and modeled WS at 1.5 m above ground, for measured points on 16-17 August 2016.....	112
Paper B. Fig. 6.	Sketches of flow pattern in courtyard of different cases. The sketches are not to scale and separate have been exaggerated.....	114
Paper B. Fig. 7.	Position of investigated planes relative to courtyard convention related to wind direction, respectively on side and top view.....	118
Paper B. Fig. 8.	Diurnal wind speed on courtyard windward surfaces based on mean hourly values for 27 January 2017.....	119
Paper B. Fig. 9.	Diurnal wind speed on courtyard leeward surfaces based on mean hourly values for 27 January 2017.....	119

Paper B. Fig. 10.	$v(\text{m} \cdot \text{s}^{-1})$ and $h_c (\text{W} \cdot \text{m}^{-2} \cdot \text{K}^{-1}) = 4 + 4v(\text{m} \cdot \text{s}^{-1})$ for the simulation period with various aspect ratios; right y- axis: maximum on LW (Points 1-4) (black), WW (Points 5-8) (red); left y-axis: minimum on outside in middle of WW wall (green)	122
Paper B. Fig. 11.	$v(\text{m} \cdot \text{s}^{-1})$ and $h_c (\text{W} \cdot \text{m}^{-2} \cdot \text{K}^{-1}) = 4 + 4v(\text{m} \cdot \text{s}^{-1})$ for the simulation period with step-down /step-up; right y- axis: maximum on LW (Points 1-4) (black), WW (Points 5-8) (red); left y-axis: minimum on outside in middle of WW wall (green)	123
Paper B. Fig. 12.	$v(\text{m} \cdot \text{s}^{-1})$ and $h_c (\text{W} \cdot \text{m}^{-2} \cdot \text{K}^{-1}) = 4 + 4v(\text{m} \cdot \text{s}^{-1})$ for the simulation period with various depth-to-width ratios; right y- axis: maximum on LW (Points 1-4) (black), WW (Points 5-8) (red); left y-axis: minimum on outside in middle of WW wall (green)	124
Paper B. Fig. 13.	$v(\text{m} \cdot \text{s}^{-1})$ and $h_c (\text{W} \cdot \text{m}^{-2} \cdot \text{K}^{-1}) = 4 + 4v(\text{m} \cdot \text{s}^{-1})$ for the simulation period with various dominant wind directions; maximum on LW (Points 1-4) (black), WW (Points 5-8) (red)	126
Paper B. Fig. 14.	$v(\text{m} \cdot \text{s}^{-1})$ and $h_c (\text{W} \cdot \text{m}^{-2} \cdot \text{K}^{-1}) = 4 + 4v(\text{m} \cdot \text{s}^{-1})$ for the simulation period with various roof slopes; right y- axis: maximum on LW (Points 1-4) (black), WW (Points 5-8) (red); left y-axis: minimum on outside in middle of WW wall (green).....	127
Paper B. Fig. 15.	$v(\text{m} \cdot \text{s}^{-1})$ for base model ($H/W= 1.17$) with various U_{10} ; right y-axis: LW (Points 1-4) (black), WW (Points 5-8) (red); left y-axis: outside in middle of WW wall (green)	128
Paper B. Fig. 16.	$v(\text{m} \cdot \text{s}^{-1})$ for case study 4 ($H/W= 2.17$) with various U_{10} ; right y-axis: LW (Points 1-4) (black), WW (Points 5-8) (red); left y-axis: outside in middle of WW wall (green)	128
Paper C. Fig. 1.	An overview of methodology	155
Paper C. Fig. 2.	Microbiological institute with the studied courtyard and measurment setup in courtyard	157
Paper C. Fig. 3.	VHV- group office building with the studied courtyard spaces- photo, plan and elevation drawing of measurment setup	158
Paper C. Fig. 4.	Comparison of observed air temperature at 1.5 m above ground inside IfMB- Hanover with measured average hourly air temperature at IMUK meteorological weather station.....	161
Paper C. Fig. 5.	Comparison of observed air temperature inside 3 courtyards of VHV with measured average hourly air temperature at roof level, 5-12 February	162
Paper C. Fig. 6.	Schematic diagram of heat exchange between courtyard and its surrounding.....	165
Paper C. Fig. 7.	Experimental models with different aspect ratios.....	169
Paper C. Fig. 8.	Domain of Computational model showing boundary conditions	171
Paper C. Fig. 9.	Thermo-physical properties of building envelope	172

Paper C. Fig. 10.	Location and height levels of measurement points	173
Paper C. Fig. 11.	Comparison of SVF at different height levels of the courtyard for each study case	175
Paper C. Fig. 12.	Diurnal courses of θ_u °C for rectangular courtyards with different aspect ratios - (typical winter day 27.01. 2017)	177
Paper C. Fig. 13.	Hourly distribution of temperature at different height levels of courtyard and it's outside for various aspect ratios on 27 th February - (Min (1-6): the minimum recorded value inside the courtyard at point 1-6, out: minimum recorded value near the outside façade)	179
Paper C. Fig. 14.	Comparison of minimum air temperature at the different height of the courtyards with corresponding outside condition for various aspect ratio and glass cover percentage; the forced input air temperature is set - 14°C for all hours of the day	184
Paper C. Fig. 15.	The diurnal variation of temperature inside courtyard as affected by type of the surrounding glass façade, including clear glass (CG-black), reflecting glass (RG- red) and heat- absorbing glass (AG- green)	186

Appendix

Appendix 2. Fig. 1.	Views of the instruments and sensors position inside and outside of courtyard	207
Appendix 2. Fig. 2.	Comparison of building surface temperature inside and outside of courtyard on west façade of IfMB, Hanover (3 - 5 th June 2017).....	207
Appendix 2. Fig. 3.	Comparison of building surface temperature inside and outside of courtyard on west façade of IfMB, Hanover (22 - 24 th December 2017)	208
Appendix 2. Fig. 4.	Comparison of difference between calculated and site measurement surface temperature inside IfMB courtyard (west façade), 5 - 6 th June 2017	208
Appendix 3. Fig. 1.	Schematic of sub models of ENVI-met (left) and basic model layout (right).....	210
Appendix 3. Fig. 2.	Schematic of the new 3-node model.....	220

List of Tables

Part A

Table. A. 1.	Comparison of features of simulation software tools	19
--------------	---	----

Part B

Paper A. Table 1.	Measurement variables, technical data of instruments and observation arrangements	45
Paper A. Table 2.	Schedule of the measurements conducted inside courtyard	47
Paper A. Table 3.	Major input variables for ENVI-met simulation.....	48
Paper A. Table 4.	Description of the model meteorological boundary conditions	52
Paper A. Table 5.	The size of the model area in previous studies	54
Paper A. Table 6.	Description of the model dimensions of each area	55
Paper A. Table 7.	Physical properties of the materials used in the simulation.....	59
Paper A. Table 8.	Mean difference comparison of the validation criteria between the on-site measured and the simulated data, at different model calibration stages on July 7, 2016, Point A	64
Paper A. Table 9.	The root mean squared error for selected variables at measured points in the model	78
Paper B. Table 1.	Wind speed inside courtyard investigated through previous studies	92
Paper B. Table 2.	Major input variables for ENVI-met simulation.....	109
Paper B. Table 3.	Comparison between minimum CHTC on outside windward facade and maximum CHTC inside courtyard on windward façade for all experimental models.....	130
Paper C. Table 1.	Air temperature inside the courtyard investigated through previous studies.....	150
Paper C. Table 2.	Geometrical dimensions of experimental courtyards and location of sensors	160
Paper C. Table 3.	Comparison between minimum air temperature inside experimental courtyards and outside in exposed area with suggested $F_{x, \text{Heat load}}$ in each case (Inside temperature: 22°C)	163
Paper C. Table 4.	Overview of computational model.....	170
Paper C. Table 5.	RMSE of comparing air temperature for different spans of time during winter (27 th January and 2 th February) at IfMB	174

Paper C. Table 6.	Predicted F_x factor at different height levels inside the courtyards with various aspect ratios, simulation with minimum standard outside air temperature = -14°C and Inside temperature = 20°C	188
-------------------	--	-----

Appendix

Appendix 1. Table 1.	CHTC correlations derived from full-scale measurements on building surface	201
Appendix 1. Table 2.	CHTC correlations derived from CFD simulations	203

Part A- Research Summary

List of Abbreviations and Nomenclature	
α_s	Solar absorptance of the surface, dimensionless
CFD	Computational fluid dynamics
CHTC	Convective heat transfer coefficient, ($\text{W m}^{-2} \text{K}^{-1}$)
C_p	Pressure coefficients, dimensionless number
$F_{x, \text{Heat load}}$	Temperature correction factor for heat load calculation, dimensionless
G	Total solar irradiance incident upon the surface, (W m^{-2})
h_c	Convective heat transfer coefficient, ($\text{W m}^{-2} \text{K}^{-1}$)
h_e	External surface heat transfer coefficient, ($\text{W m}^{-2} \text{K}^{-1}$)
h_r	Radiation heat transfer coefficient, ($\text{W m}^{-2} \text{K}^{-1}$)
L	Total (incoming or outgoing) long wave irradiance incident upon the surface, (W m^{-2})
LES	Large Eddy Simulation
q	Net heat flow from or into the surface, (W m^{-2})
RANS	Reynolds-averaged Navier–Stokes
RH	Relative Humidity, %
Ri_b	Bulk Richardson Number, dimensionless
SVF	Sky view factor, dimensionless
T_o	External air temperature, K
T_i	Internal air temperature, K
T_s	External surface temperature, K
U	Mean thermal transmittance coefficient of building element, ($\text{W m}^{-2} \text{K}^{-1}$)
v	Wind speed in front of wall/ roof element, (m s^{-1})
Greek letter	
σ	Stefan - Boltzmann constant $5.6697 \times 10^{-8} (\text{Wm}^{-2}\text{K}^{-4})$
ε	Long-wave emittance of the surface (assumed equal to the long-wave absorptance), dimensionless

1. Introduction

1.1. Concept of motivation

The courtyard typology knows a long tradition of uses around the world. The first records of the courtyard settlements date back from 5000 years old to the Chaldean City of Ur before 2000 B.C (Oliver, 1987). Excavations in Greece also suggest that the houses of the wealthy in Ancient Greece were also characteristically inward-looking, with rooms arranged around a central open space called the atrium. Jumping a few centuries to the Ming dynasty (1368 – 1644) and Qing dynasty (1644 – 1911) in China, we can see that the courtyard typology plays a central role in Beijing urban planning and the creation of communities (Edwards, Sibley, Land, & Hakmi, 2006).

The courtyard house arrived in Spain with the first wave of Arab Muslim conquest from North Africa in about 750AD and by the end of the thirteenth century, the courtyard house had reached a high level of refinement and ingenuity in its environmental and cultural adaptation (Polyzoides, Sherwood, & Tice, 1992).

Courtyards remain popular and used around the world today, spreading with the various configurations for different building functions. Figure A. 1. shows typical courtyard buildings in various climatic conditions in four categories based on the Taleghani et al. (Mohammad Taleghani, Tenpierik, & van den Dobbelen, 2012) evolution.

Generally, the courtyard is a private and isolated space through which all living rooms grouped around it receive sunlight, natural ventilation and visual as well as physical communications (Hussein Alwan. Al-Azzawi, 2019). In other words, the courtyard design idea provides useful and sheltered open space between the building's external envelopes. It can see in Fig. A. 1. that the special microclimate of the courtyard under extreme climatic conditions – where the buildings were designed with few or no windows at all and constructed of thick masonry walls – can create an in-built shelter space for a light façade with large openings (Fig. A. 2.).

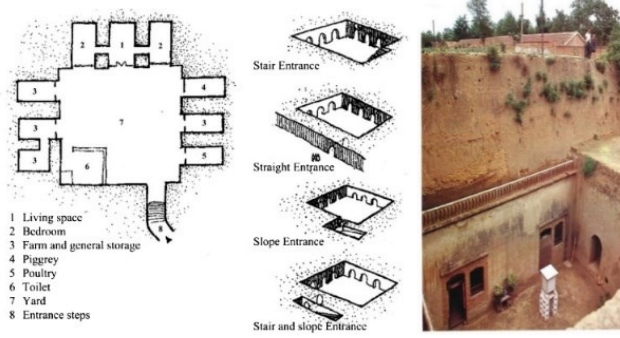
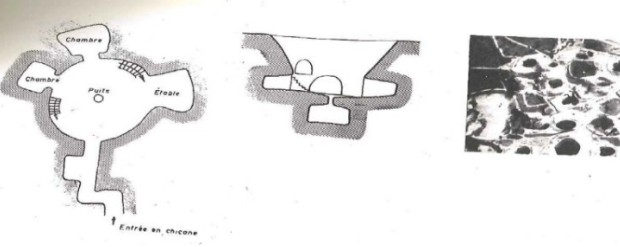
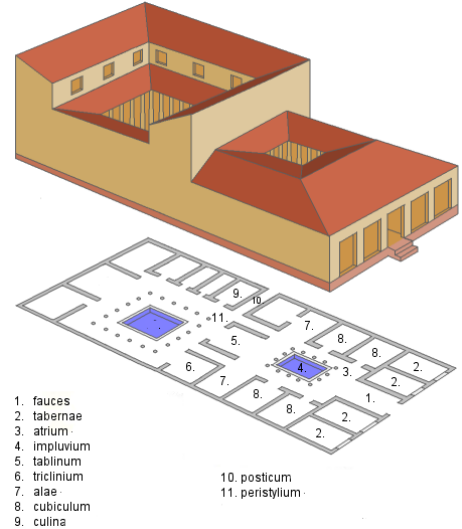
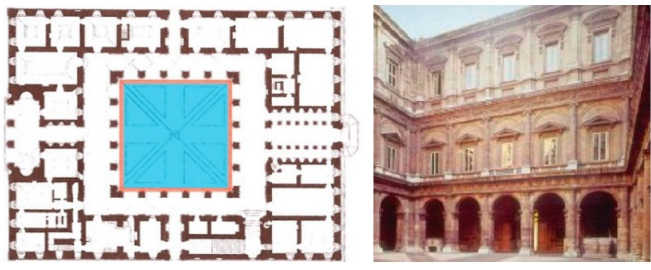
Name/ Location	Climate	Plans
(a) Ancient civilization from north Africa to China		
<p>Lian Jiazhuang, Shanxi Province, North-western China (Sun, 1982) (Anselm, 2008)</p>	<p>Humid Subtropical Climate "Cfa"</p>	
<p>Matmata, Tunisia (Adeeb, 1966)</p>	<p>Mediterranean Climate "Csa"</p>	
(b) Classical civilization in Greece and Rome		
<p>Ancient Roman dwelling, a domus (Kokko, 2006)</p>	<p>Mediterranean Climate "Csa"</p>	
<p>Palazzo Farnese- Rome (Rojas, Galán-Marín, & Fernández-Nieto, 2012)</p>	<p>Mediterranean Climate "Csa"</p>	

Fig. A. 1. Typical courtyard buildings in different climates

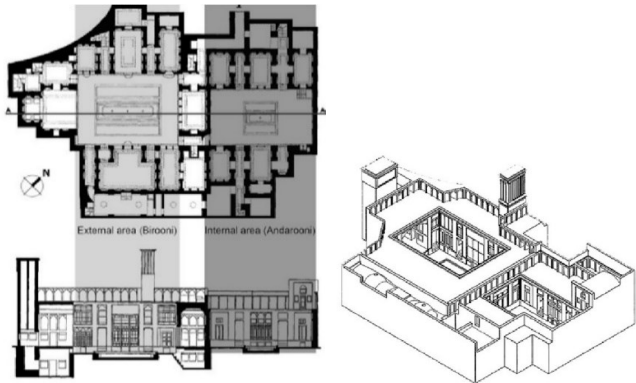
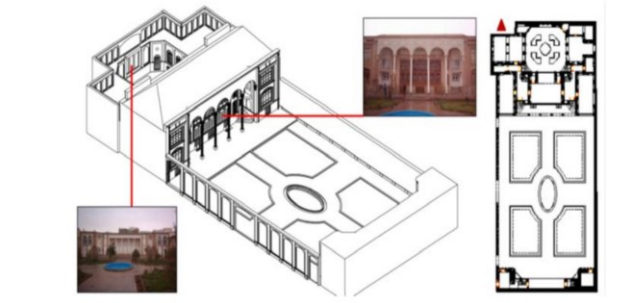
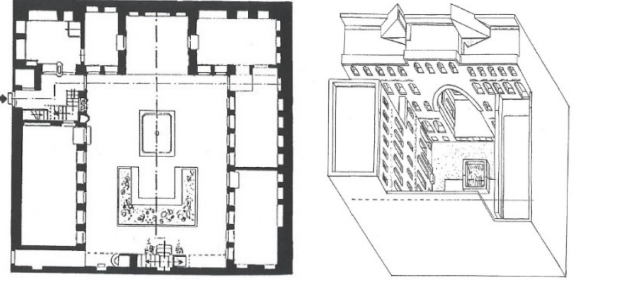
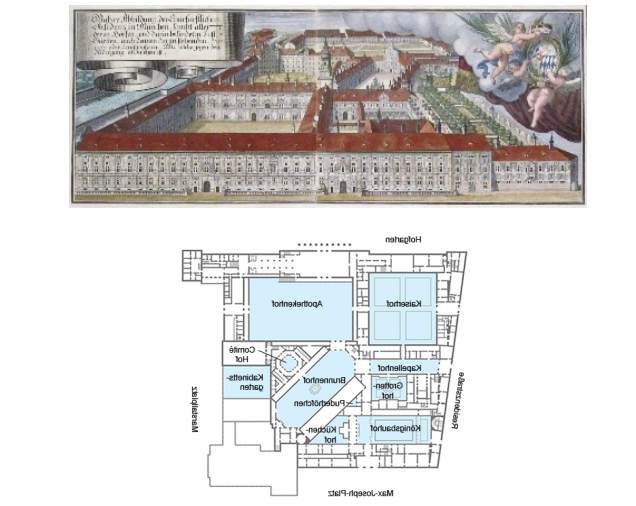
Name/ Location	Climate	Plans
(c) The middle ages		
<p>Gerami House, Yazd, Iran (Raviz, Nik Eteghad, Uson Guardiola, & Armesto Aira, 2015)</p>	<p>Tropical and Subtropical Desert Climate "Bwk"</p>	
<p>Behnam house, Tabriz, Iran (Kalantari, Kheradmand, & Jourshari, 2014)</p>	<p>Tropical and Subtropical Steppe Climate "BSk"</p>	
<p>Baleet house, Aleppo.Syria (Edwards et al., 2006)</p>	<p>Mediterran Climate "Csa"</p>	
(d) Modern area		
<p>Residenz, Munich Germany (Bayerische Schlösserverwaltung, n.d.)</p>	<p>Oceanic "Cfb"</p>	

Fig. A. 1. Typical courtyard buildings in different climates (Continued)


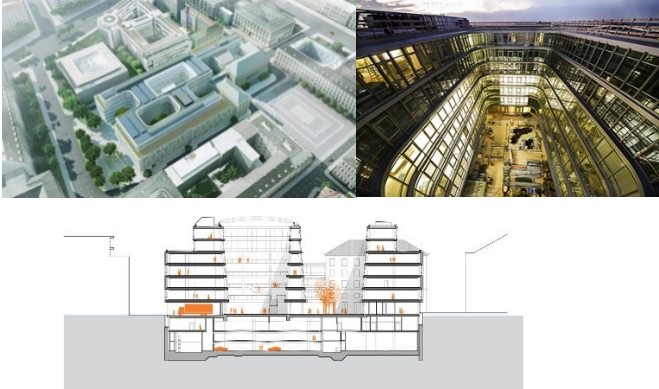
Name/ Location	Climate	Plans
(a) UNESCO building, Paris; (b) Bordie house (Golany, 1983)	Marine West Coast Climate "Cfb"	
Tuwaig Palace in Riyadh, Saudi Arabia (Aga Khan Foundation, 2018)	Tropical and Subtropical Desert Climate "Bwh"	
Siemens new company headquarters, Munich, Germany (AchDaily, 2016)	Oceanic "Cfb"	

Fig. A. 1. Typical courtyard buildings in different climates (Continued)

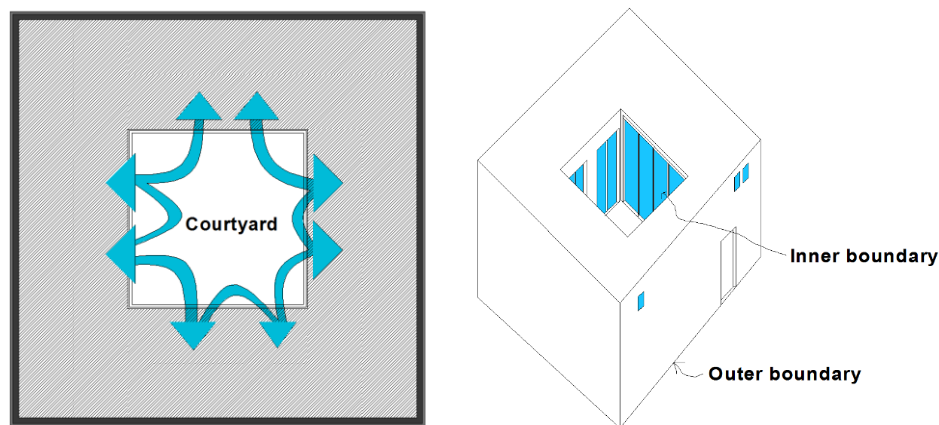


Fig. A. 2. Different resistance between building's envelope inside and outside courtyard

Many research studies have approved that the courtyard semi-closed space acts as a climatic modifier (Rojas et al., 2012) and helps to improve the thermal environment and reduce the cooling and heating energy consumption of buildings (Aldawoud, 2008; Mohammad Taleghani, Tenpierik, van, & Dobbelsteen, 2013; Zamani, Heidari, & Hanachi, 2018). These studies have mainly utilized building simulation software tools that integrate the building with its outside environment and the detailed field simulation, while the annual energy consumption is considered in a combined manner. However, in fact the largest group of current building simulation tools and heat loss calculation standards require all environmental information to input as default data at the beginning of the calculation. Therefore, there is a limitation to applying the courtyard's special microclimate in a calculation and in many of the existing technical standards (European Standard, ASHRAE und etc.) the heat loss through the building fabric facing the courtyard is calculated with the same boundary condition as other exterior envelopes. Considering the physical properties and heat loss through courtyard envelopes the same as other exterior façade over-estimates the building's heating and cooling load and increases the costs through applying unnecessary insulation materials as well as heating and air-conditioning systems.

This research is motivated by the questions: Can all courtyard configurations modify their microclimate? If so, which design concepts are more effective and which environmental factors modify within the courtyard's semi-closed spaces? Finally, how we can consider the special boundary conditions created by a courtyard in calculating the building's thermal load?

This thesis comprises three self-contained research articles with relevant literature reviews. The entire exercise has been carried out using a validated building simulation program (Paper 1). In the following, the effect of the courtyard's microclimate on the physical-environmental variables of wind speed and the air temperature inside the courtyard are investigated. In this regard, in Paper 2 the difference between the CHTC inside and outside

the courtyard is considered. By considering the heat island effect of the courtyard microclimate, Paper 3 aims to suggest an appropriate temperature correction factor ($F_{x, \text{Heat load}}$) for various courtyard configurations.

Finally, this study helps to understand the effect of the courtyard building configurations and their potential for climate modifying in the temperate climate of Hanover, as well as suggesting appropriate adjustment factors to consider the heat loss through the building's envelope surrounding the courtyard compared with the other exposed façade.

1.2. Theoretical background

1.2.1. Effective environmental parameters on heat loss through building's envelope

The building envelope provides a thermal barrier between the indoor and outdoor environments, and it is clear that the more heat that escapes via an external envelope, the more heat that has to be produced for the users' comfort (Goggins, Moran, Armstrong, & Hajdukiewicz, 2016).

According to the net sensible energy balance at the external surface of the building, Eq. (1), the heat loss through the external surface of the building beside the physical properties of its materials is affected by its surrounding environment (Turner & Doty, 2013).

$$q + \alpha_s G + \varepsilon L = \varepsilon \sigma T_s^4 + h_c (T_s - T_o) \quad (1)$$

The interaction between the outdoor environment and the building is described using the external surface heat transfer coefficient ($h_e = h_r + h_c$), which includes radiative (h_r) and convective (h_c) components (Fig. A. 3.).

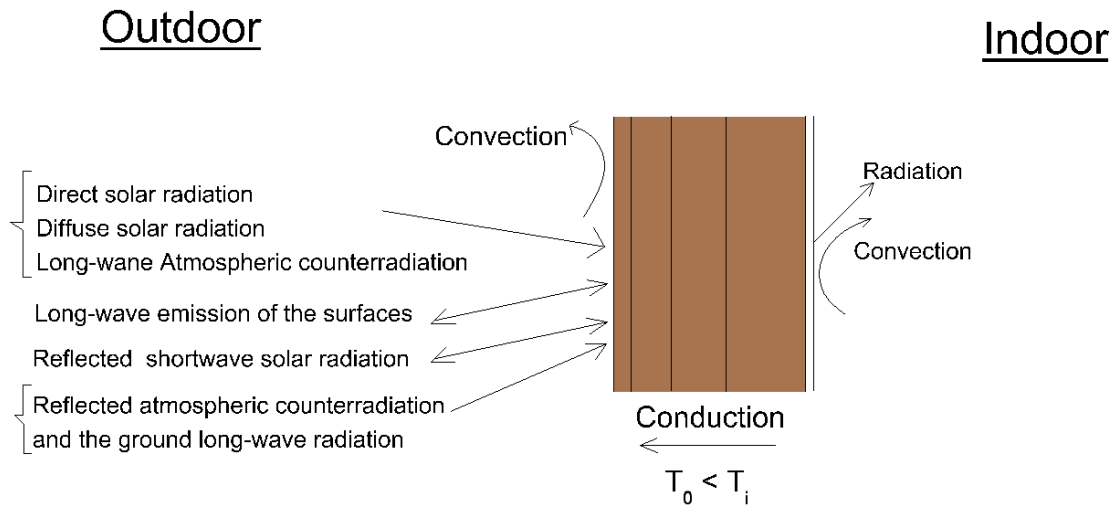


Fig. A. 3. Heat transfer through external wall

Thermal radiation comprises the energy emitted and absorbed between an external building surface and its surroundings. The radiative coefficient (h_r) can be derived from Eq. (2):

$$h_r = \varepsilon \sigma (T_s + T_o)(T_s^2 + T_o^2) \quad (2)$$

Convection is the interaction between the building and moving air and it is dependent on the temperature difference between the surface and air (free convection), as well as the air movement induced in a natural environment by wind (forced convection).

According to well-established heat transfer theory (Hens, 2012), several features should be taken into account when determining the value of the convective heat transfer coefficient (h_c), including the flow conditions (laminar or turbulent), the shape of the surface and the physical properties of the air.

Different approaches to calculating the external CHTC have been developed. The literature review by Defraeye et al. (Defraeye, Blocken, & Carmeliet, 2011) and Palyvos (Palyvos, 2008) shows the various correlations in this field (Appendix 1). However, many of these correlations incorporate dimensionless numbers such as the Nusselt number and Sherwood number, which in turn are functions of the Prandtl number and Reynolds number. Setting a value for these numbers requires an appropriate representative length, which is difficult to define in complex and varied urban environments (Erell, Pearlmutter, & Williamson, 2012).

There have also been several simple linear attempts to express h_c ($\text{W m}^{-2} \text{K}^{-1}$) as a function of air speed near outdoor surfaces, in the distance between 13cm to as much as 10m.

In this research, the linear method according to German DIN EN ISO 6946 (DIN, 2015) was used to consider the CHTC for the outside wall from Eq. (3).

$$h_c = 4 + 4v \quad (3)$$

This is calculated for the wind speed (v (m s^{-1})) at about 1m distance in front of the wall/roof element to avoid the effect of inhomogeneity in the building surfaces (Xiaoshan Yang, Zhao, Bruse, & Meng, 2012).

These coefficients can be evaluated in calculating of heat loss through envelopes using the outdoor infrared thermography technique (O'Grady, Lechowska, & Harte, 2017), where U-value is considered based on the simplified following equation (Eq. (4)):

$$U = \frac{5.67\varepsilon \left[\left(\frac{T_s}{100} \right)^4 - \left(\frac{T_o}{100} \right)^4 \right] + (4 + 4v)(T_s - T_o)}{T_i - T_o} \quad (4)$$

According to the above heat transfer theory, several climatic variables should be taken into account when determining the sensible heat transfer through a building's envelope. Such variables include wind velocity (v), external air temperature (T_o) and the effect of environmental radiation balance (long-wave and short-wave) on the building's surface temperature (T_s).

1.2.2. Effect of courtyard on climatic variables

Many research works have considered the climatic performance of the courtyard in different climate regions and considered the thermal, shading, daylight and airflow characteristics inside the various courtyard configurations (among others (Al-Hemiddi & Megren Al-Saud, 2001; Aldawoud, 2008; Meir, I.A., Pearlmutter, & Etzion, 1995; Muhaisen, 2006; Muhaisen & Gadi, 2006; Sharples & Bensalem, 2001)). They have found that the courtyard semi-closed space can change the following climatic parameters:

a. Radiation balance: A Compact courtyard form reduces the total exposed surface area and minimizes the solar radiation gain for its surrounding envelopes compared with the exposed surfaces. During the day, the absorbed solar radiation on the surface of the ground and the walls of the courtyard raises the surface temperature of the ground and walls. One part of the absorbed heat is used to warm the air in the courtyard, while the other is kept until sunset and released back into the courtyard. Meanwhile, compared with the exposed building envelopes, inside the courtyard a lesser part of surface long-wave radiation is emitted directly to the sky and the major part is reflected repetitiously and absorbed among

the surrounding surfaces of the courtyard (Fig. A. 4.). Accordingly, the courtyard creates a microclimate whereby the air temperature of the courtyard is higher than that on the outside in the winter and (F. Wang & Liu, 2002) and lower than outside during the summer (Soflaei, Shokouhian, & Soflaei, 2017).

In this way, various studies have indicated that the shading and isolation condition can be varied inside the courtyard semi-closed space depending on the courtyard form and orientation (Almhafdy, Ibrahim, Ahmad, & Yahya, 2013; Muhaisen, 2006; Muhaisen & Gadi, 2005; Yaşa & Ok, 2014).

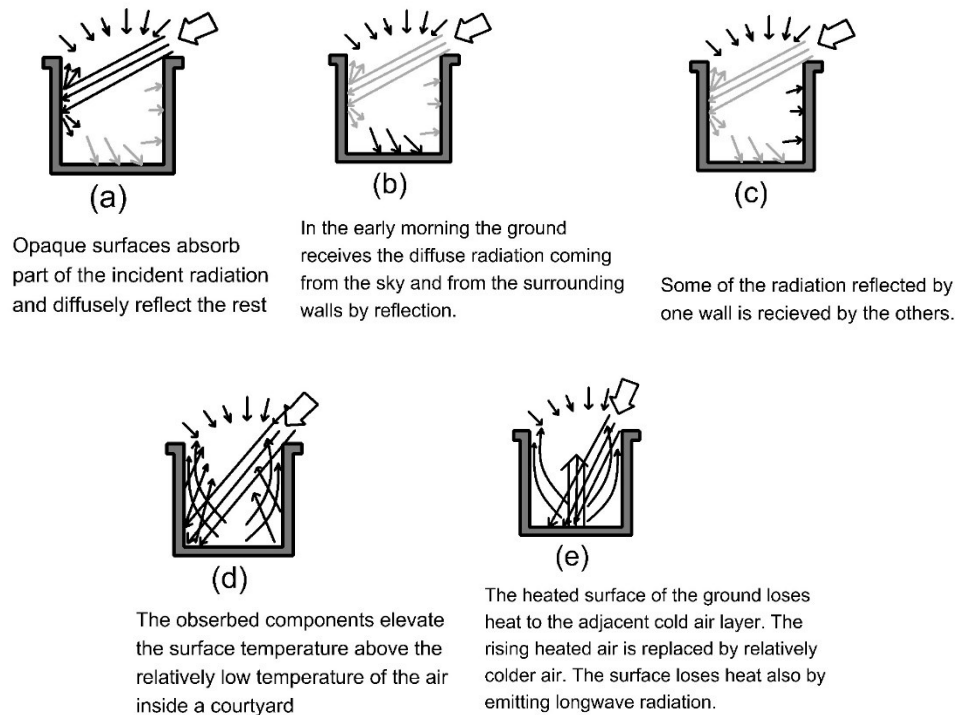


Fig. A. 4. Radiation exchange inside courtyard (Mohsen, 1979)

b. Wind: Local sheltering effects in a courtyard can change the flow pattern inside it (ALVAREZ, SANCHEZ, & MOLINA, 1998). In general, the pattern of wind velocity inside the courtyard is characterized by (a) eddies at the top level of the courtyard; and (b) calm at the bottom of the enclosed courtyards (Chandler, 1976). However, as shown through many previous studies (among others (Almhafdy, Ibrahim, Ahmad, & Yahya, 2015; ALVAREZ et al., 1998; Hall, Walker, & Spanton, 1999; Micallef, Buhagiar, & Borg, 2016; Rojas et al., 2012; TABLADA, BLOCKEN, CARMELIET, TROYER, & VERSCHURE, 2005)), the courtyards' geometry and orientation can strongly affect flow patterns and wind speed distortion inside it (Berkovic, Yezioro, & Bitan, 2012; F. Wang & Liu, 2002).

c. Humidity: Existing microclimate modifiers such as vegetation and water pools inside the courtyard increase the relative humidity. Meanwhile, due to the low air change rate

between low levels of the courtyard and its outside, the courtyard depth should be considered in the design to prevent the accommodation of additional humidity within it (Edwards et al., 2006).

1.2.3. Conclusion

A courtyard pattern is one of the traditional methods for optimizing of the building with its extremely hot and cold external climate and it can change the boundary condition – including flow pattern and velocity, air temperature, radiation balance and humidity accommodation (Hao, Yu, Xu, & Song, 2019) – in front of the envelope walls.

By considering the thermal balance on the building's external surface, the effect of the courtyard on the outside thermal condition during the winter and heat loss through the building's envelope can be studied under the following subjects:

1. Effect of courtyard on external temperature: Since the courtyard exerts effects on the extreme cold or hot weather conditions, it can be expected that the localized heating within buildings can be reduced by diminishing the thermal interaction due to the difference in temperature of the courtyard and the building surrounding it (Littlefair, 2000).
2. Effect of courtyard on the CHTC through envelopes: Courtyard with its buffer effects shelters the wind and reduces its impact on the façade. Therefore, CHTC at exterior building surfaces facing the courtyard can be considered less than the exposed surfaces.
3. Effect of courtyard on the surface temperature and radiation heat transfer coefficient: the courtyard limits the solar radiation on the façade and reduces the heat gain and the surface temperature of the surrounding walls (Tsoka, 2017). On the other hand, it limits the long-wave radiation to the atmosphere by limiting the sky view factor (SVF) of the courtyard's surrounding envelopes. Therefore, it is expected that during cloudy winter days and during the night, the average exterior surface temperature of the courtyard surrounding façade – with high insulation – differs less compared with the outside exposed façade (The measurements during the June and December 2017 are also approved this (Appendix 2)). However, for glass façades with low thermal resistance, the effect of the courtyard on the radiation heat transfer coefficient should be investigated in detail.
4. In addition, the wind pressure on the façades (C_p) – which affects the infiltration rate through the cracks and windows – is quite low inside the courtyard's semi-closed space. This effect was previously approved by Tablada et al. (TABLADA et al., 2005), who found that the C_p at low levels inside the narrow courtyards with ($W/H = 0.33 - 0.66$) is almost less (≈ 0.005).

1.3. Research Objectives

According to the aforementioned variables, three main objectives have been defined in this study related to the comparative parametric analysis depending on the geometrical characteristics of small courtyards in Hanover, Germany.

1. Numerical modeling of the microclimate of the courtyard's semi-closed spaces and validation of the model accuracy in predicting the climatic variables inside the small courtyard spaces (Paper 1).
2. Performing a comparative analysis of the flow pattern inside the courtyard, focusing on the relationship between aspect ratio, orientation, surrounding depth and roof forms on wind speed near the façade and CHTC (Paper 2).
3. Suggesting an appropriate $F_{x, \text{Heat load}}$ for courtyard semi-closed space based on the effect of the courtyard's aspect ratio and the physical properties of the surrounding envelopes (Paper 3).

2. Research process

Figure A.5 describes the overall research process applied in this study. In a first step, a library study was conducted on the concept of a courtyard semi-closed space, its typology and form in various climatic regions and its effect on the climatic variables. Parallel studies have explored on the effect of environmental parameters on the heat loss through the building's envelope.

The combination of these two fields – the field of the courtyard and the field of heat loss through the building's envelope – provides the underlying principles of the research concepts for this thesis.

2.1. Research design

The design of research methods is related to research questions and their problems (Silverman & Marvasti, 2008). The function of the courtyard depends on its basic design characteristics, including its form and aspect ratio, boundary conditions and degree of exposure, orientation and physical properties of the surrounding envelopes (Reynolds, 2002). Therefore, a comparative parametric analysis is suggested in this study.

According to the literature review on the climatic aspects of the courtyards have done by Zamani et al. (Zamani et al., 2018), the microclimate of the courtyard can be investigated through the three dominant research methods in urban physics, namely field experiments, wind tunnel experiments and numerical simulations based on the Computational Fluid Dynamics (CFD) (Peter Moonen, Defraeye, Dorer, Blocken, & Carmeliet, 2012).

Field experiments show the real complexity of the problem under examination, namely that wind tunnel measurements and computational simulations cannot fully reproduce this real complexity. In addition, in many cases field experiments are necessary to validate the wind tunnel measurements and computational simulations (Peter Moonen et al., 2012). However, this method is only suitable for existing buildings and cannot be applied in parametric analysis.

Wind tunnel tests are mostly executed on a scale model of the real geometry. In order to apply the results of the wind tunnel test in real cases, some general similarity criteria – including geometric similarity, kinematic similarity, dynamic similarity and thermal similarity – have to be satisfied. Therefore, one of the most important steps in wind tunnel modeling is an appropriate selection of the dimensionless parameters, such as the Reynolds-number to obtain similitude of the flow field, the Richardson or Froude number to properly scale thermal effects and the Schmidt-number to control dispersion processes

and determine the test conditions (VDI-Standard, 2000). Furthermore, the wind tunnel is involved with limitations for complex building configurations and model design.

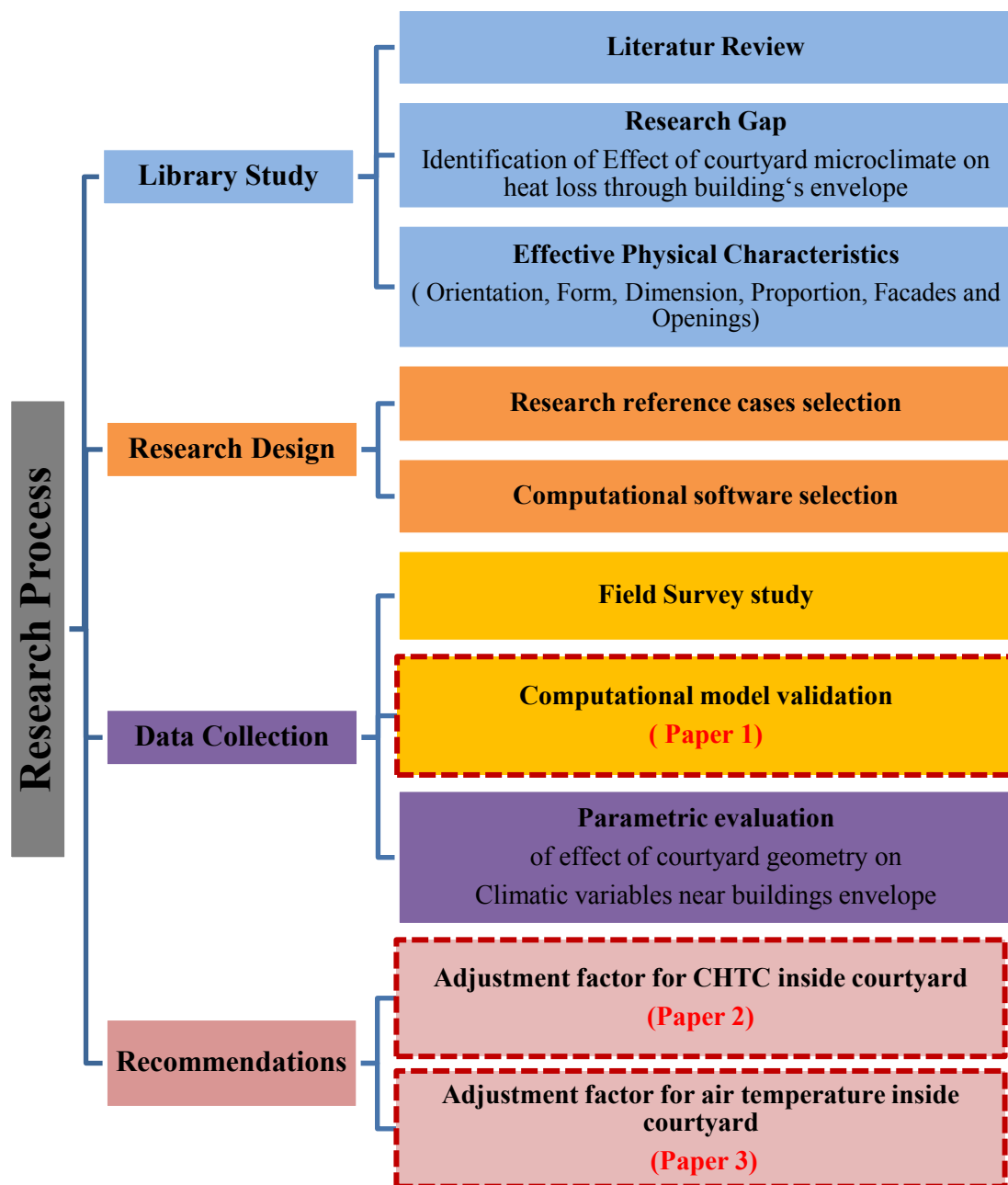


Fig. A. 5. Research process

Meanwhile, computational simulation has specific advantages compared with the two mentioned methods and there are essentially no restrictions regarding the geometry of the model (van Hooff, Blocken, Timmermans, & Hensen, 2016). In addition, a strong degree of flexibility exists for the imposed boundary conditions, which are exactly known or can be taken exactly the same as in the corresponding analysis.

However, this method also has some important aspects – including the degree of the turbulence modeling, boundary-layer modeling, grid resolution and the computational domain – that have to be selected appropriately to ensure sufficient accuracy of the simulation with a logical computational cost and time (Defraeye, Blocken, & Carmeliet, 2012; Saneinejad, Moonen, Defraeye, Derome, & Carmeliet, 2012; Zhai & Chen, 2004). Accordingly, a CFD urban microclimate study in the sub-category of “real urban areas” with validation based on the site measurements is selected as the research method in this study.

2.1.1. Selection of research reference case

As the case study, a field survey was conducted on a university building in the temperate oceanic climate (Cfb) of Hanover. The selection process of cases was conducted based on the following steps:

a. Climate and city selection: This study aims to consider the effect of the courtyard on the heat loss through the building’s envelope and the heating load. Since performing the simulations with validation for various climatic regions and countries would have been time-consuming and cost-intensive (compared to accessible resources), it was decided to select one reference city for comparative analysis. Hanover has mostly cold days and – like in other German cities – the heating energy demand is more than cooling (Mathiesen, 2017). Therefore, it can be a good and affordable choice for this study.

b. Courtyard selection: The reference model is a new university building with two small courtyards. The main characteristics of the building that make it ideal for parametric analysis include the following:

1. The meteorological weather conditions in this part of the urban context can be obtained from the IMUK meteorological station, located at a small distance from the building (80m). It is a major advantage of the study case since the suitability and availability of climate data for scientific use and especially for validation of the model are necessary (Measuring such data is not easily possible for each area due to the complexity and inherent variability of the meteorological conditions and it requires careful measurement of a large number of parameters (Schatzmann & Leitzl, 2011; Toparlar, Blocken, Maiheu, & van Heijst, 2017)).
2. The building and courtyards are designed with regular simple geometric and covered with the same material in all sides (Fig. A. 6.). This makes the selected area ideal for the parametric analysis and reduces the effect of unpredicted variables on the results. That is important, because the variety of the size, shape and composition of the element within the courtyard means that it is very difficult to select an appropriate scale for each of the parameters that describes the space.

3. The geometry of the building is simple and has the potential to test various design scenarios, including various aspect ratios, depths and roof shapes.
4. The size of the courtyard is not too large and measuring the climatic variables at different points inside it is possible.
5. The ventilated two-skin high insulated façade limits the influence of heat gain by conduction through the building's envelope and makes it possible to consider the surface temperature of the courtyard's surrounding envelopes (Paper 4 – not published) based on the external radiation and convection interaction with the courtyard's microclimate.



Fig. A. 6. Experimental area

2.1.2. Computational software selection

In the second step, in order to develop the research idea and comparative analysis, the appropriate software for simulating the microclimate of the courtyard's semi-closed space was selected and validated.

A courtyard – as a semi-enclosed space exposed to ambient weather – has its own special characteristics and its microclimate depends on both the interior thermal conditions of the buildings surrounding the courtyard space and the exterior weather conditions (Bagneid, 1992). The limitation of most building energy simulation software tools is their focus on indoor and physical properties of the building envelopes, whereas they cannot generate an outdoor microclimate environment (M Taleghani, 2015). Consequently, this software can only simulate the courtyard as an indoor environment. Therefore, there is a need for specialized analysis and simulation software dealing with the building's physical phenomena and heat transfer through envelopes, as well as tools focusing on analyzing environmental variables such as solar radiation and wind flow.

Reviewing the previous studies in this area shows two main simulation methods for predicting the thermal conditions inside the courtyard semi-closed spaces, namely:

a. A multi-zone model: In this method, the courtyard is divided into a series of semi-enclosed 'zones' resembling roofless buildings. The air within each zone exchanges mass

and energy with the other zone's surrounding the courtyard. In order to facilitate the process, it is assumed that the airflow is induced by pressure, density and temperature differences (Huang, Jones, Peng, A Li, & A Hou, 2017). This method has been used to consider thermal condition inside the courtyard or its surrounding rooms with simulation tools, such as Energy Plus (Bagheri, 2016), TRNSYS (Hassan, 2012) and Design-Builder (Al-Hafith, B K, Bradbury, & de Wilde, 2017).

This method can be appropriate for calculating the energy consumption or thermal comfort of surrounding envelopes for deep courtyards where wind-driven flow is often stagnant, at which time buoyancy flow dominates (ALVAREZ et al., 1998). However, it is unsuitable for a wide range of courtyard aspect ratios.

Another limitation of this method relates to its limitation in predicting the effect of the courtyard's microclimate on wind speed and forced convection heat loss through the façade.

b. Microclimate model: In this method, the courtyard's thermal condition is simulated with microclimate modeling software, which is created to simulate the interaction between ground and building surfaces, plants and air in an urban environment.

There are various numerical models in this area, each of which has its own characteristics, outputs, strength and weaknesses (Table 1). Considering the existing software tools for analyzing the climatic variables inside a microclimate space shows limitations in a holistic approach. Some of the modeling tools in this area predict climate variables such as wind speed and air temperature near the building envelope with low sensitivity and are not appropriate for small courtyard spaces, while others can only simulate one specific parameter such as turbulence flow with high accuracy.

The first criterion for selecting appropriate software is its capacity to simulate the three main flows inside the courtyard (Fig. A. 7.), namely flow induced by wind, thermal buoyancy and free convection with the courtyard surrounding the envelopes (Rojas et al., 2012).

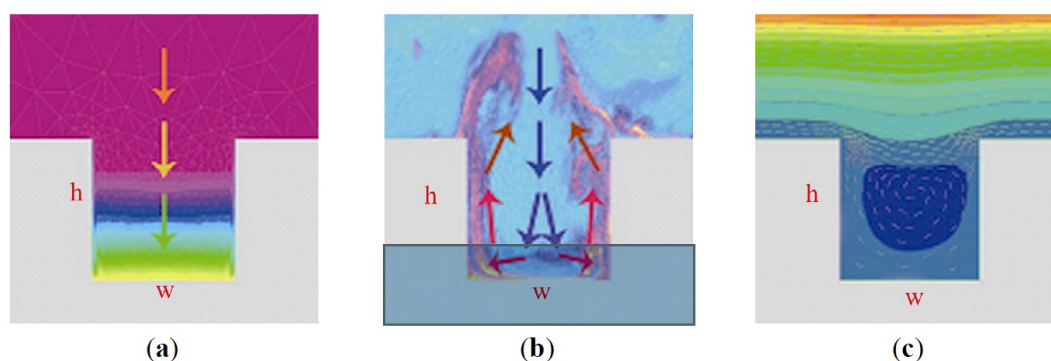


Fig. A. 7. Courtyard's vertical section; including (a) Stratification; (b) Convection; (c) wind flow (image after (Rojas et al., 2012))

In addition, regarding the research objectives the selected model should include the following parameters:

- Thermal networking between the building's inside and outside
- A short-wave and long-wave radiation network between courtyard envelope surfaces and sky
- Evaporation of water on surfaces, or water bodies
- A coupled CFD model with the courtyard microclimate model to obtain better predictions related to airflow

In this way, the holistic microclimate model ENVI-met (RANS) (Michael Bruse & Flear, 1998a) was selected for numerical simulations. The selection was made considering the capability of the program to deal with the required application, provide the basic necessary outputs (Air temperature and Wind speed at various points inside the courtyard), predict the variables with acceptable accuracy and regarding the cost and accessibility of the software, as well as its simplicity to learn and use.

Furthermore, In a survey of nearly 100 microclimate modeling papers over the past eight years (Singh & Laefer, 2015), several have noted a growing trend for ENVI-met software. In addition, Vidmar and Roset (Vidmar & Roset, 2013) have indicated that the ENVI-met, as a user-friendly software, can simulate the physical interactions in urban environments with acceptable accuracy. Appendix 3 describes the general model properties of the microclimate model ENVI-met.

Table A.1. Comparison of features of simulation software tools

Features	Simulation tool				
	ENVI-met	PALM-4U	TEB + Trnsys	Ecotect + Winair	IES-VE
Developed	University of Mainz, Mainz, Germany Prof. M. Bruse (M Bruse, 2016)	Leibniz university Hanover, Germany Prof. Raasch (Maronga et al., 2015)(Raasch & Schröter, 2001)	The concept of Town Energy Balance (TEB) (Masson, Grimmond, & Oke, 2002) is presented in 2015 to add in building energy model TRNSYS, named Type 201 (Ali-Toudert & Böttcher, 2018)	Marsh University of Cardiff, Wales, Dr Andrew (Anand, Deb, & Alur, 2017) (Shouzhi, Jiang, & Zhao, 2018)	IES was founded in 1994 by Dr Don McLean. In June 2012, the company announced the acquisition of North American consulting firm BVM Engineering (BVME) (McLean, 2011)
Incoming shortwave solar radiation	Yes	Yes	Yes	Yes	Yes
Long wave Sky radiation	Yes	No clouds in urban area	Yes	No. just consider sky view factor	Cloud cover is not exist
Irradiation (Long-wave emission and reflection between surfaces)	High resolution modelling of multiple reflections using the IVS algorithm	No reliable emission model (Resler et al., 2017a).	Yes	Yes	No
Conduction heat transfer	Yes. 3 Layer for envelopes	Yes. Includes 3 layer wall material model (Resler et al., 2017b)	Yes. Includes Multi-layer facets	Yes	Yes

Table A.1. Comparison of features of simulation software tools (Continued)

Features	ENVI-met	PALM-4U	TEB + Trnsys	Ecotect + Winair	IES-VE
Surface Convection heat transfer based on wind speed	Yes	Yes	Yes	No. R _{se} = 0.04 (Wm ⁻² k ⁻¹) as per EN ISO 6946	Yes
Materials assignment	3 layers wall and roof model 3 layer Soil model	Yes	Yes	Yes	Yes
Air exchange (CFD)	Turbulence and Flow around and between buildings	Turbulence and Flow around and between buildings	The air flows within the canyon is not simulated as in a CFD software (that have 3D or 2D atmospheric grids of 1m of resolution). Turbulence simulated based on Monin-Obukhov Theory	Yes	Yes. MicroFlo. Interface
CFD method	RANS (E-Epsilon model)	1. RANS mode (TKE-epsilon closure) 2. LES	-	-	RANS 1. k-ε (Default) 2. Constant effective viscosity
Turbulence flow	Yes	Yes	Simple	Not accurate	Yes
Thermal buoyancy	Yes	Yes	Yes	No	No
Air movement due to Surface free convection	Yes	Yes	Yes	No	No
Water bodies	Yes	No	Yes	No	Yes
Humidity & evaporation	Yes	-	Yes	No	Just for internal spaces

Table A.1. Comparison of features of simulation software tools (Continued)

Features	ENVI-met	PALM-4U	TEB + Trnsys	Ecotect + Winair	IES-VE
Vegetation (trees & green areas)	Yes	No	No	Yes	The effect of vegetation considered on shading and not on wind and flow
3D modeling	Detailed 3D simulation	Yes	The 3D shape of the city is not kept completely and TEB is idealized for 2D canyons	Yes	Yes
loading climate data	Yes	Yes	Yes	Yes	Yes
Bioclimatology and PMV	Yes	Yes	-	Yes	Yes
Particle	Dispersion of air pollutants including NO-NO2 ozone chemistry	Chemistry module for the transport and conversion of reactive species	No	No	Just for internal spaces
Data validation and accuracy	Validated through site measurement (because the results are based on sun, vegetation , humidity, pollutant)	Released from October 2018 and not extensively validated	TEB itself validated (Lemonsu, Masson, Shashua-Bar, Erell, & Pearlmutter, 2012) but TEB Type 201 in combination with Trnsys is new and not validated.	Simplified the flow around building	Not for urban areas

Table A.1. Comparison of features of simulation software tools (Continued)

Features	ENVI-met	PALM-4U	TEB + Trnsys	Ecotect + Winair	IES-VE
Application interoperability (coupling possibility)	No	-	Yes	Yes	No export options to use the data in other applications.
Calculation speed	Good	LES Need supercomputer	Fast in computation	Fast in computation	Medium
Ease of use & learning curve	User family and for Architects and urban designer	Low	Medium	High	High
Community & technical support	Yes	Yes	Yes	Yes	Yes
license, cost	Full Student and Science license 300 Euro	Open	TRNSYS 18, Research 1 user license: 2400,00 €	Education version-free of cost	30 days trail \$4,400 per seat
Operating system	Windows	Linux	Windows	Windows	Windows

3. Discussions of results

Improving the microclimate conditions in front of the building's exterior surfaces is one of the sustainable design methods from the past. In this regard, due to its climatic buffering and filtering characteristics, the courtyard design idea is one of the oldest methods to control extreme external conditions and it has been applied in many regions of the world.

It has been experimentally proven that the heating and cooling energy consumption of envelope spaces surrounding the courtyard are mostly less than other exposed ones. However, in most calculation standards, the courtyard special microclimate is not considered in calculations and the heat loss or gain through the courtyard envelope walls is evaluated the same as other envelopes. Accordingly, this study aims to answer the research question concerning how a courtyard – as a microclimate modifier – affects heat loss through its surrounding envelopes.

In order to answer this question, in a first step it is necessary to understand courtyard microclimate and effective parameters on the thermal conditions and in a second step to evaluate the effect of each climate variables in the thermal balance of the surrounding building envelopes.

Reviewing the previous studies in the field of courtyard shows that significant elements in the courtyard microclimate are related to the effects of sun, wind, trees, water and the thermal condition of the courtyard's surrounding spaces. In addition, numerous studies indicate that the courtyard geometry has a strong effect on the flow pattern inside it, as well as the radiative exchange between the courtyard and its outside. Therefore, a parametric analysis is suggested here to consider the effect of courtyard geometric properties on the thermal balance of its surrounding building envelopes.

Regarding, a computational model is mostly suggested to study a particular environment variable such as air temperature or wind speed inside various design scenarios, which is more flexible in testing the effect of various parameters on climatic conditions in comparison with wind tunnel or site measurements. Considering the potential of ENVI-met in simulating the various climatic parameters – including the distribution of heat, momentum and humidity inside the courtyard's semi-closed spaces – it is decided to simulate the courtyard microclimate with a holistic ENVI-met model.

The main difficulty with CFD microclimate modeling of a built environment is an appropriate definition of input parameters and computational model size and resolution. In this regard, site-specific climate data is essential to develop and evaluate the accuracy of the computational model. Accordingly, in the first paper the numerical ENVI-met has been

calibrated and tested using experimental data obtained in the extended measuring program in Hanover, Germany, during the summer and winter.

Field measurements were conducted by measuring the air temperature, relative humidity, wind speed, mean radiant temperature and external surface temperature of building envelopes recorded inside the courtyard space and multiple simulations were conducted with ENVI-met (version 4.0) to adjust a reliable model that accurately represents the real courtyard microclimate. According to the results of this paper, appropriate computational domain size, grid resolution, the lateral boundary condition for turbulence and time step were defined for the case study.

The results of this section show that the calibrated ENVI-met model predicts the air temperature, relative humidity and wind speed inside the courtyard with good accuracy to represent the real environment. However, the main weakness of the model lies in predicting the mean radiant temperature for solar irradiance on the sun-exposed areas and simulating the turbulence in front of the façade, which is directly exposed to forces of wind. In these cases, the model mostly overestimates solar irradiance and wind speed.

In the next step, as one project (Paper 2), the wind speed near the façade and CHTC difference between the courtyard's semi-closed space and outside exposed façade was calculated through a simple linear correlation ($h_c = 4 + 4v$). The study started with a literature review and considering the wind speed reduction inside the courtyard's semi-closed space regarding its geometry. According to the precious studies' results, comparative parametric simulations are planned and the effect of different courtyard geometry on wind speed near the façade and CHTC at different height levels has been investigated in the five phases through considering various common strategies, including different proportions of height to width, step-up and step-down design concepts, the various thickness for surrounding buildings, three main different wind directions and various roof pitches.

The results of simulations show $\approx 15 - 30\%$ difference between CHTC inside the courtyard correspond to the outside exposed façade for ambient wind speed $2.3 \text{ (m s}^{-1}\text{)}$. CHTC is increasingly reduced when increasing the height of the courtyard enclosures. The findings also show that the difference between CHTC inside and outside the courtyard continually increased with increasing the ambient wind speed.

In the next project (Paper 3), the idea of the courtyard heat island is linked to the issue of heat loss through the building's envelope. This study aims to present a new idea in the calculation of heat loss through the courtyard envelope walls with the temperature adjustment factor.

Site measurements and previous studies show that the courtyard design idea is more efficient in extreme weather conditions. Therefore, in this study the effect of the courtyard on heat losses through the building's envelope is considered according to the standard DIN

EN 12831-1 (DIN, 2017b), which considers the extreme cold condition outside the buildings in heat loss and heat load calculation in comparison with DIN 4108-6 (DIN, 2003b).

According to the results of the field measurements and the simulations, the thermal condition of the courtyard is mostly affected by its geometry and physical properties of its surrounding walls. As much as the limited convection heat exchange between the courtyard and its outside, sheltered surface exposure to solar radiation during the day and low long-wave radiation loss during the night has a major effect on the thermal condition inside the courtyard, the amount of the heat courtyard gains through its surrounding rooms can also change the thermal condition inside the courtyard during cold winter times. According to the results of the experimental studies in Hanover, the air temperature near the building external envelope for deep courtyards with more than ~70% low insulated glass façades is higher than the open space outside the courtyard. However, the recorded values show relatively lower temperatures inside the courtyards with high insulated envelopes.

The findings of this research recommend considering the temperature of courtyards depending on their aspect ratio and glazing percentage (or thermal resistance of surrounding envelope) with a temperature correction factor ($F_{x, \text{Heat load}}$) between 0.9 and 2.2. According to the results, the heat island inside the courtyard is more intense under high aspect-ratio, lower wind speed and more glazing ratio.

4. Conclusions and future developments

The growing trend of using a glass façade and the low thermal resistance of this material increase the effect of the local microclimate near the façade on the heat transfer through the envelopes. Meanwhile, the semi-closed space of the courtyard creates a special microclimate, which can be effective in improving the heating and cooling energy demand of the buildings. In this regard, looking at courtyard buildings shows that the mechanical systems are relatively rare in the courtyard's surrounding rooms – contrary to electric lighting systems for lights.

The understanding of how courtyard controls heat, light and sound is one of the research fields in building physics. A review of studies in the field of microclimate shows that the air temperature and wind speed near the courtyard surrounding walls as well as the amount of incoming short-wave radiation and outgoing long-wave radiation through the façade can be different compared with exposed envelopes.

Through a parametric analysis in Hanover, this study aims to answer some of the questions in the field of courtyard microclimate by calculating a number of effective environmental variables and their effect on heat loss through the building's envelope surrounding the courtyard. Two building physic parameters including CHTC and $F_{x, \text{heat load}}$ are investigated here for the courtyard space. As a new project, it is also planned to analyze the effect of the courtyard on radiation balance and external surface temperature.

Since the findings of this research are limited to experimental cases in a maritime temperate climate of Hanover, as the future developments and in order to obtain general results it is recommended for further research to explore a special microclimate of courtyard's semi-closed space and its changes under the effect of various parameters including geometry, vegetation, water bodies and weather conditions.

In addition, this study has focused on the effect of the courtyard on the calculation of the heat loss during the winter for courtyard envelope walls. Accordingly, it is also necessary to consider the effect of various scenarios on the microclimate condition of the courtyard during the summer and suggest the adjustment factors in calculating the heat gain through building envelopes.

References

- AchDaily. (2016). Siemens Headquarters / Henning Larsen Architects. Retrieved May 8, 2019, from <https://www.archdaily.com/791741/siemens-headquarters-henning-larsen-architects>
- Adeeb, H. E. (1966). *Building Technology in Hot Dry Climates*. Kolb Organization. Retrieved from <https://books.google.de/books?id=3rl8vQEACAAJ>
- Aga Khan Foundation. (2018). Tuwaiq Palace. Retrieved May 8, 2019, from <https://www.akdn.org/architecture/project/tuwaiq-palace>
- Al-Hafith, O., B K, S., Bradbury, S., & de Wilde, P. (2017). The Impact of Courtyard parameters on its shading level An experimental study in Baghdad, Iraq. *Energy Procedia*, 134, 99–109. <https://doi.org/https://doi.org/10.1016/j.egypro.2017.09.539>
- Al-Hemiddi, N. A., & Megren Al-Saud, K. A. (2001). The effect of a ventilated interior courtyard on the thermal performance of a house in a hot–arid region. *Renewable Energy*, 24(3), 581–595. [https://doi.org/http://dx.doi.org/10.1016/S0960-1481\(01\)00045-3](https://doi.org/http://dx.doi.org/10.1016/S0960-1481(01)00045-3)
- Aldawoud, A. (2008). Thermal performance of courtyard buildings. *Energy and Buildings*, 40(5), 906–910. <https://doi.org/http://dx.doi.org/10.1016/j.enbuild.2007.07.007>
- Ali-Toudert, F., & Böttcher, S. (2018). Urban microclimate prediction prior to dynamic building energy modelling using the TEB model as embedded component in TRNSYS. *Theoretical and Applied Climatology*, 134(3), 1413–1428. <https://doi.org/10.1007/s00704-018-2621-3>
- Almhafdy, A., Ibrahim, N., Ahmad, S. S., & Yahya, J. (2013). Courtyard Design Variants and Microclimate Performance. *Procedia - Social and Behavioral Sciences*, 101, 170–180. <https://doi.org/https://doi.org/10.1016/j.sbspro.2013.07.190>
- Almhafdy, A., Ibrahim, N., Ahmad, S. S., & Yahya, J. (2015). Thermal Performance Analysis of Courtyards in a Hot Humid Climate Using Computational Fluid Dynamics CFD Method. *Procedia - Social and Behavioral Sciences*, 170, 474–483. <https://doi.org/http://dx.doi.org/10.1016/j.sbspro.2015.01.012>
- ALVAREZ, S., SANCHEZ, F., & MOLINA, J. L. (1998). Air flow pattern at courtyards. *Environmentally Freindly Cities*, 503–506. Retrieved from http://www.aivc.org/sites/default/files/airbase_11854.pdf
- Anand, P., Deb, C., & Alur, R. (2017). A simplified tool for building layout design based on thermal comfort simulations. *Frontiers of Architectural Research*, 6(2), 218–230. <https://doi.org/https://doi.org/10.1016/j.foar.2017.03.001>
- Anselm, A. J. (2008). Passive annual heat storage principles in earth sheltered housing, a supplementary energy saving system in residential housing. *Energy and Buildings*, 40(7), 1214–1219. <https://doi.org/https://doi.org/10.1016/j.enbuild.2007.11.002>
- Bagheri, H. (2016). *EnergyPlus Validation of a Courtyard House in Yazd-Iran*. *Engineering and Applied Sciences* (Vol. 11).

- Bagneid, A. A. (1992). The microclimate of courtyards: Experiments on three evaporative cooling floor treatments. *Ekistics*, 59(354/355), 217–229. Retrieved from <http://www.jstor.org/stable/43622251>
- Bayerische Schlösserverwaltung. (n.d.). Munich Residenz. Retrieved April 26, 2019, from <http://www.residenz-muenchen.de/englisch/residenc/bau.htm>
- Berkovic, S., Yezioro, A., & Bitan, A. (2012). Study of thermal comfort in courtyards in a hot arid climate. *Solar Energy*, 86(5), 1173–1186. <https://doi.org/10.1016/j.solener.2012.01.010>
- Bruse, M. (2016). ENVI-met 4.0, (Science). ESSEN.
- Bruse, Michael, & Fleer, H. (1998). Simulating surface–plant–air interactions inside urban environments with a three dimensional numerical model. *Environmental Modelling & Software*, 13(3), 373–384. [https://doi.org/https://doi.org/10.1016/S1364-8152\(98\)00042-5](https://doi.org/https://doi.org/10.1016/S1364-8152(98)00042-5)
- Chandler, T. J. (1976). *Urban Climatology and Its Relevance to Urban Design*. Secretariat of the World Meteorological Organization. Retrieved from <https://books.google.de/books?id=eSgkAQAIAAJ>
- Defraeye, T., Blocken, B., & Carmeliet, J. (2011). Convective heat transfer coefficients for exterior building surfaces: Existing correlations and CFD modelling. *Energy Conversion and Management*, 52(1), 512–522. <https://doi.org/http://doi.org/10.1016/j.enconman.2010.07.026>
- Defraeye, T., Blocken, B., & Carmeliet, J. (2012). Analysis of convective heat and mass transfer coefficients for convective drying of a porous flat plate by conjugate modelling. *International Journal of Heat and Mass Transfer*, 55(1), 112–124. <https://doi.org/https://doi.org/10.1016/j.ijheatmasstransfer.2011.08.047>
- DIN. (2003). *DIN 4108-6*. Berlin: Deutsches Institut für Normung e. V. <https://doi.org/https://dx.doi.org/10.31030/9493310>
- DIN. (2015). *DIN EN ISO 6946*. Berlin.
- DIN. (2017). *DIN EN 12831-1*. Berlin: Deutsches Institute für Normung e.V.
- Edwards, B., Sibley, M., Land, P., & Hakmi, M. (2006). *Courtyard Housing: Past, Present and Future*. Taylor & Francis.
- Erell, E., Pearlmuter, D., & Williamson, T. (2012). *Urban Microclimate: Designing the Spaces Between Buildings*. Taylor & Francis. Retrieved from <https://books.google.de/books?id=LHwnWaYfPNkC>
- Goggins, J., Moran, P., Armstrong, A., & Hajdukiewicz, M. (2016). Lifecycle environmental and economic performance of nearly zero energy buildings (NZEB) in Ireland. *Energy and Buildings*, 116, 622–637. <https://doi.org/https://doi.org/10.1016/j.enbuild.2016.01.016>
- Golany, G. (1983). *Earth-sheltered habitat: history, architecture, and urban design*. Van Nostrand Reinhold. Retrieved from <https://books.google.de/books?id=BWDM0QOfb0UC>
- Hall, D. J., Walker, S., & Spanton, A. M. (1999). Dispersion from courtyards and other enclosed spaces. *Atmospheric Environment*, 33(8), 1187–1203. [https://doi.org/10.1016/S1352-2310\(98\)00284-2](https://doi.org/10.1016/S1352-2310(98)00284-2)

- Hao, S., Yu, C., Xu, Y., & Song, Y. (2019). The Effects of Courtyards on the Thermal Performance of a Vernacular House in a Hot-Summer and Cold-Winter Climate. *Energies*, 12(6). <https://doi.org/10.3390/en12061042>
- Hassan, M. H. (2012). Ventilated courtyard as a passive cooling strategy in the hot desert climate. In *33rd AIVC Conference " Optimising Ventilative Cooling and Airtightness for [Nearly] Zero-Energy Buildings, IAQ and Comfort*. Copenhagen, Denmark: AIVC. Retrieved from <https://www.aivc.org/resource/ventilated-courtyard-passive-cooling-strategy-hot-desert-climate>
- Hens, H. S. L. (2012). *Building Physics -- Heat, Air and Moisture: Fundamentals and Engineering Methods with Examples and Exercises*. Wiley. Retrieved from <https://books.google.de/books?id=rYsRnsYTl4gC>
- Huang, J., Jones, P., Peng, R., A Li, X., & A Hou, S. (2017). An Integrated Model for Urban Microclimate and Building Energy in High-Density Cities for Early Stage Design. In *Building Simulation 2017: 15th Conference of International Building Performance Simulation Association*. San Francisco, USA. <https://doi.org/10.26868/25222708.2017.313>
- Hussein Alwan. Al-Azzawi, S. (2019). *A descriptive, analytical and comparative study of traditional courtyard houses and modern non-courtyard houses in Baghdad : (in the context of urban design in the hot-dry climates of the sub-tropics)*.
- Kalantari, N. N. P., Kheradmand, A. S., & Jourshari, S. R. (2014). Adaptive comparison of thermal and ventilation behavior aboriginal buildings of Iran. *Trends in Life Sciences*, 3(3), 578–592. Retrieved from http://sciencejournal.in/data/documents/Life-Sci.-Special-Issue-Vol-3-3-69_2.pdf
- Kokko, O. (2006). File:Domus suomi.png. Retrieved April 26, 2019, from https://commons.wikimedia.org/wiki/File:Domus_suomi.png
- Lemonsu, A., Masson, V., Shashua-Bar, L., Erell, E., & Pearlmutter, D. (2012). *Inclusion of vegetation in the Town Energy Balance model for modelling urban green areas. Geoscientific Model Development* (Vol. 5). <https://doi.org/10.5194/gmd-5-1377-2012>
- Littlefair, P. J. (2000). *Environmental site layout planning: solar access, microclimate and passive cooling in urban areas*. Building Research Establishment. Retrieved from <https://books.google.de/books?id=pYQeAQAAIAAJ>
- Maronga, B., Gryschka, M., Heinze, R., Hoffmann, F., Kanani-Sühring, F., Keck, M., ... Raasch, S. (2015). The Parallelized Large-Eddy Simulation Model (PALM) version 4.0 for atmospheric and oceanic flows: model formulation, recent developments, and future perspectives. *Geoscientific Model Development*, 8(8), 2515–2551. <https://doi.org/10.5194/gmd-8-2515-2015>
- Masson, V., Grimmond, C. S. B., & Oke, T. R. (2002). Evaluation of the Town Energy Balance (TEB) Scheme with Direct Measurements from Dry Districts in Two Cities. *Journal of Applied Meteorology*, 41(10), 1011–1026. [https://doi.org/10.1175/1520-0450\(2002\)041<1011:EOTTEB>2.0.CO;2](https://doi.org/10.1175/1520-0450(2002)041<1011:EOTTEB>2.0.CO;2)

- Mathiesen, B. V. (2017). *2015 Final Heating & Cooling Demand in Germany*. Retrieved from http://www.heatroadmap.eu/resources/HRE4-Country_presentation-Germany.pdf
- McLean, D. (2011). IES. Retrieved May 5, 2019, from [https://www.iesve.com/discoveries/author/6192/Don McLean](https://www.iesve.com/discoveries/author/6192/Don%20McLean)
- Meir, I.A., Pearlmutter, D., & Etzion, Y. (1995). On the microclimatic behavior of two semi-enclosed attached courtyards in a hot dry region. *Building and Environment*, *30*(4), 563–572.
- Micallef, D., Buhagiar, V., & Borg, S. P. (2016). Cross-ventilation of a room in a courtyard building. *Energy and Buildings*, *133*, 658–669. <https://doi.org/http://dx.doi.org/10.1016/j.enbuild.2016.09.053>
- Mohsen, M. A. (1979). Solar radiation and courtyard house forms—I. A mathematical model. *Building and Environment*, *14*(2), 89–106. [https://doi.org/https://doi.org/10.1016/0360-1323\(79\)90014-3](https://doi.org/https://doi.org/10.1016/0360-1323(79)90014-3)
- Moonen, P., Defraeye, T., Dorer, V., Blocken, B., & Carmeliet, J. (2012). Urban Physics: Effect of the micro-climate on comfort, health and energy demand. *Frontiers of Architectural Research*, *1*(3), 197–228. <https://doi.org/https://doi.org/10.1016/j.foar.2012.05.002>
- Muhaisen, A. S. (2006). Shading simulation of the courtyard form in different climatic regions. *Building and Environment*, *41*(12), 1731–1741. <https://doi.org/https://doi.org/10.1016/j.buildenv.2005.07.016>
- Muhaisen, A. S., & Gadi, M. B. (2005). Mathematical model for calculating the shaded and sunlit areas in a circular courtyard geometry. *Building and Environment*, *40*(12), 1619–1625. <https://doi.org/http://dx.doi.org/10.1016/j.buildenv.2004.12.018>
- Muhaisen, A. S., & Gadi, M. B. (2006). Effect of courtyard proportions on solar heat gain and energy requirement in the temperate climate of Rome. *Building and Environment*, *41*(3), 245–253. <https://doi.org/http://dx.doi.org/10.1016/j.buildenv.2005.01.031>
- O’Grady, M., Lechowska, A. A., & Harte, A. M. (2017). Quantification of heat losses through building envelope thermal bridges influenced by wind velocity using the outdoor infrared thermography technique. *Applied Energy*, *208*, 1038–1052. <https://doi.org/https://doi.org/10.1016/j.apenergy.2017.09.047>
- Oliver, P. (1987). *Dwellings: the house across the world*. University of Texas Press. Retrieved from <https://books.google.de/books?id=uz9UAAAAMAAJ>
- Palyvos, J. A. (2008). A survey of wind convection coefficient correlations for building envelope energy systems’ modeling. *Applied Thermal Engineering*, *28*(8–9), 801–808. <https://doi.org/10.1016/j.applthermaleng.2007.12.005>
- Polyzoides, S., Sherwood, R., & Tice, J. (1992). *Courtyard Housing in Los Angeles*. Princeton Architectural Press.
- Raasch, S., & Schröter, M. (2001). PALM - A large-eddy simulation model performing on massively parallel computers. *Meteorologische Zeitschrift*, *10*(5), 363–372. <https://doi.org/10.1127/0941-2948/2001/0010-0363>

- Raviz, S., Nik Eteghad, A., Uson Guardiola, E., & Armesto Aira, A. (2015). *Iranian courtyard housing: The role of social and cultural patterns to reach the spatial formation in the light of an accentuated privacy* (Vol. 10). <https://doi.org/10.5821/ace.11.29.2653>
- Resler, J., Krč, P., Belda, M., Juruš, P., Benešová, N., Lopata, J., ... Kanani-Sühring, F. (2017a). PALM-USM v1.0: A new urban surface model integrated into the PALM large-eddy simulation model. *Geoscientific Model Development*, *10*(10), 3635–3659. <https://doi.org/10.5194/gmd-10-3635-2017>
- Resler, J., Krč, P., Belda, M., Juruš, P., Benešová, N., Lopata, J., ... Kanani-Sühring, F. (2017b). PALM-USM v1.0: A new urban surface model integrated into the PALM large-eddy simulation model. *Geoscientific Model Development*, *10*(10), 3635–3659. <https://doi.org/10.5194/gmd-10-3635-2017>
- Reynolds, J. (2002). *Courtyards: Aesthetic, Social, and Thermal Delight*. Wiley. Retrieved from <https://books.google.de/books?id=BTWnUjH3j2AC>
- Rojas, J. M., Galán-Marín, C., & Fernández-Nieto, E. D. (2012). Parametric study of thermodynamics in the mediterranean courtyard as a tool for the design of eco-efficient buildings. *Energies*, *5*(7), 2381–2403. <https://doi.org/10.3390/en5072381>
- Saneinejad, S., Moonen, P., Defraeye, T., Derome, D., & Carmeliet, J. (2012). Coupled CFD, radiation and porous media transport model for evaluating evaporative cooling in an urban environment. *Journal of Wind Engineering and Industrial Aerodynamics*, *104–106*, 455–463. <https://doi.org/https://doi.org/10.1016/j.jweia.2012.02.006>
- Schatzmann, M., & Leidl, B. (2011). Issues with validation of urban flow and dispersion CFD models. *Journal of Wind Engineering and Industrial Aerodynamics*, *99*(4), 169–186. <https://doi.org/https://doi.org/10.1016/j.jweia.2011.01.005>
- Sharples, S., & Bensalem, R. (2001). Airflow in courtyard and atrium buildings in the urban environment: a wind tunnel study. *Solar Energy*, *70*(3), 237–244. [https://doi.org/https://doi.org/10.1016/S0038-092X\(00\)00092-X](https://doi.org/https://doi.org/10.1016/S0038-092X(00)00092-X)
- Shouzhi, C., Jiang, Q., & Zhao, Y. (2018). *Integrating CFD and GIS into the Development of Urban Ventilation Corridors: A Case Study in Changchun City, China*. *Sustainability* (Vol. 10). <https://doi.org/10.3390/su10061814>
- Silverman, D., & Marvasti, A. (2008). *Doing Qualitative Research: A Comprehensive Guide*. SAGE Publications. Retrieved from <https://books.google.de/books?id=C7AbqNdwbiAC>
- Singh, M., & Laefer, D. F. (2015). Recent Trends and Remaining Limitations in Urban Microclimate Models. *Demography Journal*, *1*, 1–12. <https://doi.org/10.2174/2352631901401010001>
- Soflaei, F., Shokouhian, M., & Soflaei, A. (2017). Traditional courtyard houses as a model for sustainable design: A case study on BWHS mesoclimate of Iran. *Frontiers of Architectural Research*, *6*(3), 329–345. <https://doi.org/https://doi.org/10.1016/j.foar.2017.04.004>
- Sun, P. (1982). Underground Houses. In H.-U. Khan (Ed.), *Mimar 3: Architecture in Development*. Singapore: Concept Media Ltd.

- Tablada, A., Blocken, B., Carmeliet, J., Troyer, F. DE, & Verschure, H. (2005). Geometry of Building's courtyards to favour natural ventilation: comparison between wind tunnel experiment and numerical simulation. In *World Sustainable Building Conference*. Tokyo. Retrieved from <http://www.irbnet.de/daten/iconda/CIB3858.pdf>
- Taleghani, M. (2015). *Dwelling on Courtyards*. TU Delft. Retrieved from <https://books.google.de/books?id=GblcCwAAQBAJ>
- Taleghani, Mohammad, Tenpierik, M., van, A., & Dobbelsteen, A. (2013). *Optimisation of Heating Energy Demand and Thermal Comfort of a Courtyard-Atrium Dwelling*. <https://doi.org/10.13140/2.1.1096.8968>
- Taleghani, Mohammad, Tenpierik, M., & van den Dobbelsteen, A. (2012). Environmental impact of courtyards- A review and comparison of residential courtyard buildings in different climates. *Journal of Green Building*, 7(2), 113–136. <https://doi.org/10.3992/jgb.7.2.113>
- Toparlar, Y., Blocken, B., Maiheu, B., & van Heijst, G. J. F. (2017). A review on the CFD analysis of urban microclimate. *Renewable and Sustainable Energy Reviews*, 80, 1613–1640. <https://doi.org/https://doi.org/10.1016/j.rser.2017.05.248>
- Tsoka, S. (2017). Investigating the Relationship Between Urban Spaces Morphology and Local Microclimate: A Study for Thessaloniki. *Procedia Environmental Sciences*, 38, 674–681. <https://doi.org/https://doi.org/10.1016/j.proenv.2017.03.148>
- Turner, W. C., & Doty, S. (2013). *Energy Management Handbook: 8th Edition*. Lulu.com. Retrieved from <https://books.google.de/books?id=T6IUCAAAQBAJ>
- van Hooff, T., Blocken, B., Timmermans, H. J. P., & Hensen, J. L. M. (2016). Analysis of the predicted effect of passive climate adaptation measures on energy demand for cooling and heating in a residential building. *Energy*, 94, 811–820. <https://doi.org/https://doi.org/10.1016/j.energy.2015.11.036>
- VDI-Standard. (2000). Environmental meteorology - Physical modelling of flow and dispersion processes in the atmospheric boundary layer - Application of wind tunnels. Berlin. Retrieved from http://www.vdi.eu/nc/guidelines/vdi_3783_blat_12-umweltmeteorologie_physikalische_modellierung_von_stroemungs_und_ausbreitungsvorgaengen_in_der_/
- Vidmar, J., & Roset, J. (2013). Evaluation of simulation tools for assessment of urban form based on physical performance.
- Wang, F., & Liu, Y. (2002). Thermal environment of the courtyard style cave dwelling in winter. *Energy and Buildings*, 34(10), 985–1001. [https://doi.org/10.1016/S0378-7788\(01\)00145-1](https://doi.org/10.1016/S0378-7788(01)00145-1)
- Yang, X., Zhao, L., Bruse, M., & Meng, Q. (2012). An integrated simulation method for building energy performance assessment in urban environments. *Energy and Buildings*, 54(Supplement C), 243–251. <https://doi.org/https://doi.org/10.1016/j.enbuild.2012.07.042>
- Yaşa, E., & Ok, V. (2014). Evaluation of the effects of courtyard building shapes on solar heat gains and energy efficiency according to different climatic regions. *Energy and Buildings*, 73, 192–199. <https://doi.org/http://dx.doi.org/10.1016/j.enbuild.2013.12.042>

- Zamani, Z., Heidari, S., & Hanachi, P. (2018). Reviewing the thermal and microclimatic function of courtyards. *Renewable and Sustainable Energy Reviews*, 93, 580–595. <https://doi.org/https://doi.org/10.1016/j.rser.2018.05.055>
- Zhai, Z., & Chen, Q. (Yan). (2004). Numerical determination and treatment of convective heat transfer coefficient in the coupled building energy and CFD simulation. *Building and Environment*, 39(8), 1001–1009. <https://doi.org/https://doi.org/10.1016/j.buildenv.2004.01.023>

Part B - Papers of the Dissertation

Paper A **Numerical modeling validation for the microclimate thermal condition of semi-closed courtyard spaces between buildings**

Paper B **Parametric analysis of influence of courtyard microclimate on diminution of convective heat transfer through building's envelope**

Paper C **Accurate prediction of heating energy demand of courtyard's surrounding envelopes using temperature correction factor**

Paper A

Note. Reprinted from “Numerical modeling validation for the microclimate thermal condition of semi-closed courtyard spaces between buildings” by A. Forouzandeh, 2018, Journal of Sustainable Cities and Society, Volume 36 (Supplement C), page 327-345. Copyright (2017) by Elsevier Ltd. (Appendix 4)

Title	Numerical modeling validation for the microclimate thermal condition of semi-closed courtyard spaces between buildings
Author(s)	Aysan Forouzandeh
Publication outlet	Journal of Sustainable Cities and Society
Publication type	Journal paper
Publication year	2018
Publication status	Published
Volume	36
Issue	Supplement C
Pages	327-345
DOI	https://doi.org/10.1016/j.scs.2017.07.025
Journal Impact Factor	4.5
Highlights	<ul style="list-style-type: none"> • A proper choice of input parameters for numerical simulations of semi-closed spaces with the software ENVI-met. • Experimental measures of microclimatic variables inside medium-narrow courtyard spaces. • Comparison between the ENVI-met outputs and the values measured experimentally under various seasonal conditions. • The model showed very similar results between measured and simulated data, with acceptable range of RMSE.

Numerical modeling validation for the microclimate thermal condition of semi-closed courtyard spaces between buildings

Abstract

In this study, the microclimate model ENVI-met version 4 was evaluated with field data inside courtyard spaces. The measurements were planned in different climate conditions in summer and winter at different points inside the courtyard located in Hannover, Germany. Climate variables — including air temperature (T_a), relative humidity (RH), wind speed (WS) and mean radiant temperature (T_{mrt}) — were investigated. The comparison between observation and prediction was performed while considering the accuracy of the model with the different domain and cell sizes, the different lateral boundary conditions for turbulence (LBC for TKE) and the time step size for flow. Consequently, the $2 \times 2 \times 1 \text{ m}^3$ cell-sized model with cyclic LBC for TKE and $t_{\text{flow}} = 0 \text{ s}$ lead to quicker simulation and reliable results.

This study provides further confidence that the ENVI-met model is capable of predicting the microclimate variables inside medium-narrow courtyards with an acceptable accuracy. The root mean square error (RMSE) value at the center of the shaded courtyard was calculated as approximately $0.73 \text{ }^\circ\text{C}$ for T_a , 3.34% for RH, $0.01 \text{ (m s}^{-1}\text{)}$ for WS and $8.44 \text{ }^\circ\text{C}$ for T_{mrt} . However, due to the model resolution, inaccuracies in the values are displayed for T_{mrt} in the sun-exposed areas.

Keywords: Courtyard microclimate variables, ENVI-met model, Field experiment, Model evaluation

Nomenclature			
dx	Horizontal dimension of the cell, m	WS	Wind Speed, (m s ⁻¹)
dy	Vertical dimension of the cell, m	y ⁺	Non-dimensional distance- able to characterize the influences in the wall-adjacent cells
H	Height above ground, m	y _p	The distance (normal) of the center point P of the ground-adjacent cell to the ground, m
H _c	Height of the courtyard's surrounding walls, m	u,v,w	Wind speed vector component, (m s ⁻¹)
LAD	Leaf area density of the Plant, (m ² m ⁻³)	<i>Greek letter</i>	
RH	Relative Humidity, %	ΔT	Air temperature difference between modeled and measured values, °C
RMSE	Root Mean Square Error	ΔT _{mrt}	Mean radiant temperature difference between modeled and measured values, °C
T _a	Air temperature, °C	ΔWS	Wind speed difference between modeled and measured values, (m s ⁻¹)
T _B	Temperature near ground, °C	Δz _s	Height of the cells in Lowest box
t _{flow}	Time step for flow, s	Δz	Height of the equidistant cell
T _D	Dew point temperature, °C	τ _w	The shear stress at the surface, (kg m ⁻¹ s ⁻²)
T _g	Black globe temperature, °C	ρ	The air density, (kg m ⁻³)
T _H	Air temperature T (in °C) at height H (in meter)	ν	The kinematic viscosity of air, (m ² s ⁻¹)
T _{mrt}	Mean radiant temperature, °C		
V _a	Air velocity, (m s ⁻¹)		
W	The courtyard's width, m		

1. Introduction

The courtyard as a private and isolated space through which all living rooms are grouped around, offered an endemic sense of well-being, permitting residents to live either indoors or outdoors in natural surroundings more protected from the external climatic agents such as sun, wind and strong temperature fluctuations (among others (Berkovic et al., 2012; Edwards et al., 2006; Polyzoides et al., 1992; Randhawa, 1999; Rojas et al., 2012)). This space with special microclimate conditions can also reduce heat loss or gain through building envelopes, consequently reducing the heating and cooling energy demand of buildings.

The courtyard microclimate thermal condition can be significantly influenced by the geometry and orientation of buildings (among others (Edwards et al., 2006; Fabbri, Di Nunzio, Gaspari,

Antonini, & Boeri, 2017; Hall et al., 1999; Martinelli & Matzarakis, 2017; Muhaisen, 2006; Muhaisen & B Gadi, 2006; Rojas et al., 2012; Yaşa & Ok, 2014)) and other elements (e.g. Vegetation)(Berkovic et al., 2012; Mohammad Taleghani, Tenpierik, van den Dobbelsteen, & Sailor, 2014b), the materials used in construction (Nazarian & Kleissl, 2015; F. Wang & Liu, 2002) and land use characteristics (Collier, 2006). Therefore, the best approach to assess the impact of geometrical parameters on courtyard microclimate and building envelope heat loss is to simulate the project with the help of microclimate modeling software that meets the following requirements (Huttner, 2012)(Noro & Lazzarin, 2015):

- The model should have an adequate grid size – i.e. $\leq 10\text{m}$ –, according to building resolution
- The model has to implement the energy balance of surfaces of all types
- The model has to simulate the physical and physiological properties of plants
- The model should calculate the atmospheric processes, prognostic and transient

Accordingly, in this project, as a first step the appropriate modeling software should be selected based on the required accuracy and project resources.

Common turbulence models can be classified based on computational expense into two main approaches, The Reynolds-averaged Navier–Stokes (RANS) and Large Eddy Simulation (LES). Despite the increasing popularity of LES methods over the past three years, this method has the drawback that most LES microscale models only focus on a single aspect of microclimate – like wind field –and thus do not fulfill all of the aforementioned requirements.

One of the few microscale models that meets all of the above-cited criteria is the three-dimensional microclimate model ENVI-met (M . Bruse, 2016). In a survey of nearly 100 microclimate modeling papers over the past eight years (Singh & Laefer, 2015), even with the continuing dominance of RANS-based methods and the software Fluent, several trends were noted, including a growing trend towards ENVI-met software to consider the thermal environment inside different urban spaces in various climates all over the world (among others(Ali-Toudert & Mayer, 2007; Barakat, Ayad, & El-Sayed, 2017; Defraeye et al., 2011; Fabbri et al., 2017; Fahmy & Sharples, 2009; Jamei & Rajagopalan, 2017; Lee, Mayer, & Chen, 2016; Lu et al., 2017)). Due to the aforementioned reasons, whereas the PALM LES model was still included as a candidate in the description of the work, it was decided to continue with ENVI-met only, as the latter contains more detail of the flow field.

It is widely known that model performance evaluation is an essential prerequisite for confident numerical modeling (Bennett et al., 2013). Some studies have undertaken to validate the performance of ENVI-met by comparing the simulation results with field experimental data. Yang et al. (Xiaoshan Yang, Zhao, Bruse, & Meng, 2013) compared the ENVI-met outputs to the observed soil temperature at different depths and air temperature and humidity at different heights in a hot-humid city in south China. They showed that ENVI-met is capable of simulating the thermal performance of different ground surfaces and their effects on the local air temperature and humidity. Taleghani et.al (Mohammad Taleghani, Tenpierik, van den Dobbelsteen, & Sailor, 2014a) reported that the air temperatures predicted by ENVI-met were consistent with the field data in a courtyard building (aspect ratio $H_c/W \leq 1$) on the campus of Delf University in the Netherlands. Middel et al. (Middel, Hüb, Brazel, Martin, & Guhathakurta, 2014), Kong et al. (Kong et al., 2016) and Gusson et al. (Gusson & Duarte, 2016) concluded that ENVI-met tends to underestimate afternoon 2m – air temperature and overestimate during the night but shows clear agreement in the morning. Besides, Middel et al. validated the modeled surface temperature in semi-arid Phoenix, Arizona and showed that the surface temperatures are overestimated by ENVI-met Version 3.1 in the morning with a better fit in the afternoon and at night. Acero et al. (Acero & Herranz-Pascual, 2015) compared the ENVI-met results to the Climate variables and measured in four different areas with different regional climate conditions in Bilbao in the north of the Iberian Peninsula. This research showed that modeled wind speed and mean radiant temperature values present relevant differences with respect to measurements. Salata et.al (Salata, Golasi, de Lieto Vollaro, & de Lieto Vollaro, 2016) evaluated the accuracy of ENVI-met to simulate the different microclimate variables and predicted mean vote (PMV) inside the cloister of the faculty of engineering in Rome. In addition, they considered the effect of different cell sizes and lateral boundary conditions on results. They indicated that ENVI-met can simulate the air temperature and relative humidity reasonably; however, the weakness of the model to predict the global radiation was revealed.

These studies showed that the ENVI-met model is suited for modeling outdoor thermal environment for different climates. However, there was no investigation to analyze the capacity of ENVI-met for thermal modeling of the semi-closed spaces such as medium- narrow courtyards with aspect ratio $H_c/W \geq 1$. Furthermore, the older versions of ENVI-met were mostly used in the earlier studies. This paper describes the validation of the ENVI-met (v.4.1.0) model for the microclimate of semi-enclosed courtyards based on field measurements, conducted in Hanover, Germany from 7 July to 4 September 2016 and from 27 January to 3 February 2017. In the first step of model validation, three different domain sizes with various

vertical and horizontal resolutions were analyzed to obtain the proper computational domain. This step was followed by a comparison of different climatic variables predicted by ENVI-met and those measured experimentally. Afterward, the model physical boundary conditions and the time step variations for flow were investigated and the influence of the lateral boundary condition for turbulence on the results was analyzed. Based on validation results and usage of previous experimental data, the reliable model that accurately represents the courtyard real environment is formed. Finally, the reliability of a model was proved for 10 different days during the summer and winter. The Root Mean Square Error index of agreement for the air temperature, relative humidity, wind speed and mean radiant temperature were evaluated. With respect to the continuing popularity of the courtyard as an architectural style and the special microclimate of this space, the study emphasizes the following issues on simulation with ENVI-met: (i) proper setting of the geometric domain size and resolution, (ii) advisable physical lateral boundary condition, (iii) an appropriate simulation time step for flow.

The report starts with a brief introduction to ENVI-met in section 2. Section 3 describes the methodology including the field experiment and the numerical simulation. The results and outcomes are presented in sections 4 and 5, respectively. Based on the results, identification of modeling limitations for further steps is established.

2. The microclimate model ENVI-met

This research investigated a three-dimensional microclimate model ENVI-met (v 4.1.0) (M Bruse, 2016), which was designed to simulate the microclimate thermal condition with a fine spatial resolution (0.5 – 10m) and a time step between 1 and 5s.

ENVI-met is a prognostic model based on the fundamental laws of fluid dynamics and thermodynamics, including simulation of several phenomena: heat and steam transition around and between buildings envelope and at soil level, turbulence, thermo-hygrometric exchange in vegetation, bioclimatology and fluid dynamics of polluting species and small particles (M. Bruse, 1999, 2004, 2016). This is the reason in many studies it was used to simulate the influence of urban greening and vegetation (Barakat et al., 2017; Hofman & Samson, 2014; Kong et al., 2016; Lee et al., 2016; Skelhorn, Lindley, & Levermore, 2014; Tsoka, 2017), urban forms and density (Chatzidimitriou & Yannas, 2017; Paramita & Fukuda, 2013; Wei Yang, Wong, & Lin, 2015) and physical properties of used materials for ground, walls and roofs (Alchapar & Correa, 2016; Ketterer & Matzarakis, 2014; Salata et al., 2016; Salata, Golasi, Vollaro, & Vollaro, 2015) on the outdoor thermal condition and pollutant dispersion.

The ENVI-met model essentially comprises of a one-dimensional boundary model that includes vertical profiles of different meteorological parameters up to a height of 2500 meters (approx. the height of the planetary boundary layer) – which provides stable laminar condition – and a three-dimensional core model that includes all atmosphere, soil, building and vegetation processes (M. Bruse, 1999).

Notwithstanding that ENVI-met (v. 4.1.0) is a perfect simulation of reality to simulate the meteorological components of the urban environment – which has been approved through various studies (Conry et al., 2015; De Ridder & Acero, J.; Lauwaet, D.; Lefebvre, W.; Maiheu, B.; Mendizabal, 2014; Duarte, Shinzato, Gusson, & Alves, 2015; Elnabawi, Hamza, & Dudek, 2015; Hedquist & Brazel, 2014; Jänicke, Meier, Hoelscher, & Scherer, 2015; Lee et al., 2016; Middel et al., 2014; Qaid & Ossen, 2015; Salata et al., 2016; Song & Park, 2015; Srivanit & Hokao, 2013; Mohammad Taleghani, Sailor, & Ban-Weiss, 2016) –, it has some (major) limitations that should be considered in the evaluation process. For instance, the wind speed and direction as well as cloudiness rate remain constant throughout the diurnal simulation and only air temperature and relative humidity boundary conditions are updated. Additionally, the standard E-ε closure used by ENVI-met has a known tendency to overestimate the turbulent production in areas with a high acceleration or deceleration and thus wind speed estimation.

ENVI-met is able to simulate the effects of plants onto the microclimate quite accurately, but is not capable of assessing the effects of microclimate on plants (Simon, 2016) and the attenuation of the diffuse radiation by vegetation is not yet taken into account. Finally, the calculation of radiation fluxes is not accurate; for example, the short-wave downward radiation in ENVI-met is overestimated and the scattering of the upward and downward diffuse radiation is considered isotropic (Huttner, 2012).

3. Methods

The validation processes that were used in this study include the following: 1) an on-site measurement and 2) computer-based simulation.

The on-site measurement program was designed to measure the current microclimate conditions, including air temperature, relative humidity, wind velocity and black globe temperature at the 1.5m level of field experiment which was located in Hanover, Germany. The accuracy of the model was verified based on these results.

Figure 1 describes the validation processes applied in this research. According to the validation graph, in the first step several grid sizes were analyzed to consider how the accuracy of the model was affected by the different mesh sizes. This step was followed by a comparison between the values of wind speed predicted by different turbulence lateral boundary condition adjustments in ENVI-met and those measured experimentally. Finally, the effect of different time-steps for the flow was investigated.

3.1. Field experiment

3.1.1. Study area

The study has been performed in the city of Hanover, Germany (52° 22' 13.87" N 9° 43' 59.59" E, elevation 57m a.s.l). This city is associated with the Cfb category of Köppen's climate classification (Kottek, Grieser, Beck, Rudolf, & Rubel, 2006). Hanover has a warm, humid temperate climate with warm summers and no dry season. The warm season lasts from June to September with an average daily high temperature above 20 °C. The cold season lasts from November to February with an average daily high temperature below 7 °C (Deutscher Wetterdienst, n.d.; "Weather Spark," 2016).

The examined location is a courtyard located in the moderately vegetated urban center with average surrounded building elevation of 8 m, whereby most buildings in this part of the city are not more than two stories. According to the Oke classification of the local climate zone scheme (Stewart & Oke, 2012), the study site can be characterized as LCZ 8B (large low rise with scattered trees). As part of the Institute of Microbiology's building, the courtyard is 6 × 14m and completely enclosed by a building 7m tall (aspect ratio on the windward side (H_C/W) ≥ 1). Figure 2 shows the layout of the project and the surrounding environments. According to the site plan, the north side of the case study is open and flat. The main mass of the buildings are located on the south and east side of the building.

Regular geometric forms, the same facade materials, low urban density and displacement height and low distance from the meteorological station (The Herrenhausen station, for Institute of Meteorology and Climatology, Leibniz University of Hanover, has been installed about 80m away from the experimental site on its south- east side) make this case appropriate for parametric studies.

3.1.2. Site-measurements

Air temperature, relative humidity, mean radiant temperature and wind velocity were monitored using TESTO 480 data loggers placed in solar radiation shields (home-made Stevenson box), at a height of 1.5m in the courtyard (Fig. 3.). Table 1 summarizes the measured variables, the measuring devices and the observation arrangements.

It is generally accepted that the flow pattern and direction inside the courtyard differ between summer and winter, as well as between day and night (in winter and during the nighttime, the stratification flows are stronger than in summer) (Berkovic et al., 2012; Edwards et al., 2006; Farahat, 1980; Hall et al., 1999; Rojas et al., 2012; F. Wang & Liu, 2002). Therefore, the measurements were carried out during the period from 7 July — 30 August 2016 as summer weather data and 27 January – 15 February 2017 as winter weather data.

Figure 4 and Table 2 respectively show the location and time of the observation points. The measurements at points A and B – defined at the center of the courtyard – correspond to the general courtyard thermal condition. For these points, all mentioned parameters are measured. Points C – I are defined to consider the wind velocity and temperature near the windward and leeward facade and corner of courtyards that are strongly affected by the main wind direction and intensity. The measured values at points H and G correspond to the thermal situation that plants can create.

The whole system recorded one-minute average values for all points and all parameters, which were stored in the device's own storage space.

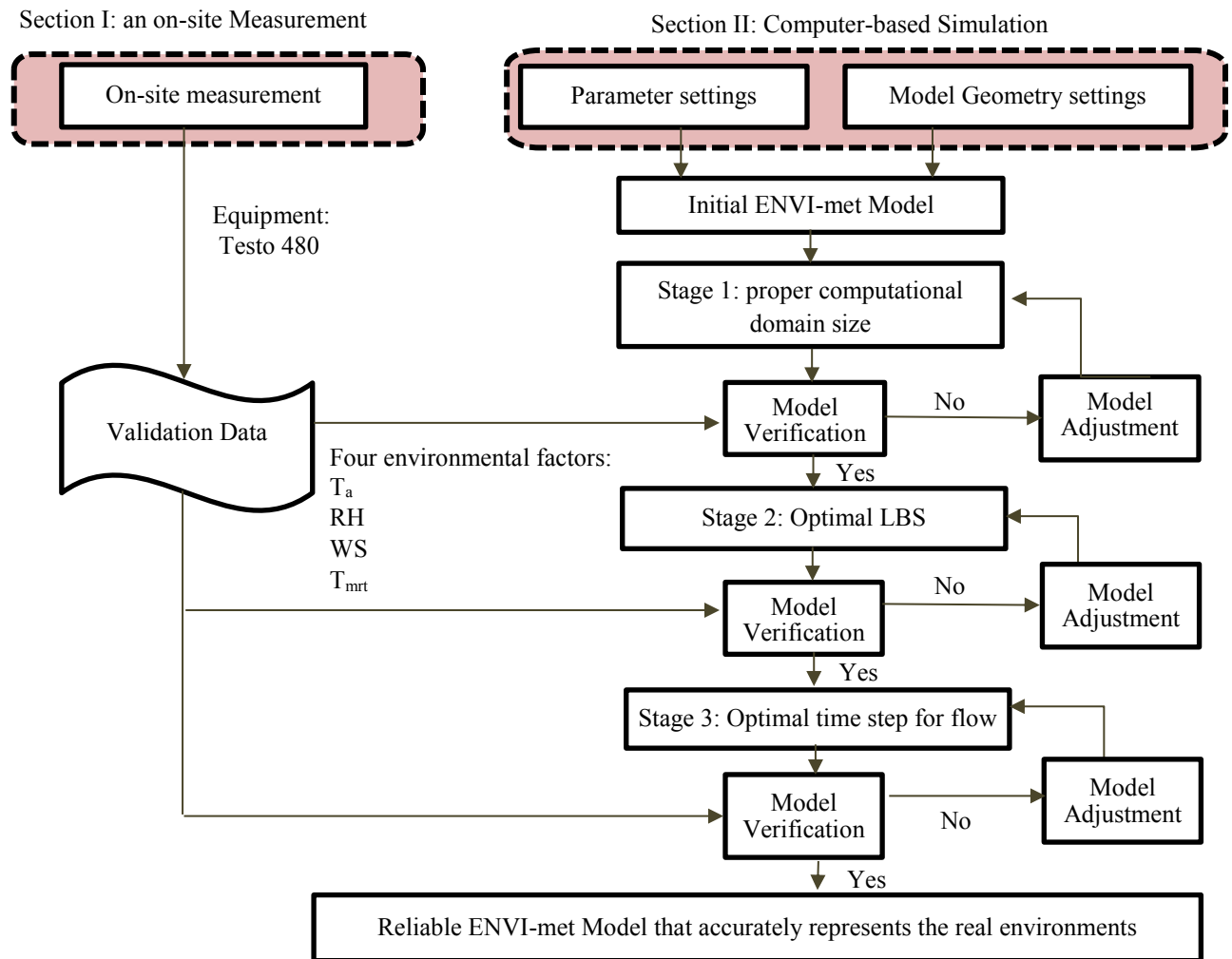


Fig. 1. The process of achieving a valid ENVI-met model of the outdoor environment

3.1.3. ENVI-met model

The ENVI-met software uses input values for building, vegetation, surface characteristics, soil, climatic conditions and pollutant emissions. Table 3 describes the major input variables for the ENVI-met simulation.

Table 1. Measurement variables, technical data of instruments and observation arrangements

Variable	Sensor type	Accuracy	Range	Output resolution	sample
T_a	Testo 480, IAG-probe 0632 1543	$\pm 0.5 \text{ }^{\circ}\text{C}$	0 to +50 $^{\circ}\text{C}$	0.1 $^{\circ}\text{C}$	1 min
RH	Testo 480, IAG-probe 0632 1543	$\pm (1.8\% \text{ RH} + 0.7\% \text{ of reading})$	0 to +100% RH	0.1% RH	1 min
Wind velocity	Testo 480, The comfort probe 0628 0143	$\pm (0.03 \text{ (m s}^{-1}) + 4 \% \text{ of meas. Val.)}$	0 to +5 (m s ⁻¹)	0.01 (m s ⁻¹)	1 min
Black globe temperature	Testo 480, Globe probe 0602 0743 (D = 150mm)	Accuracy class 1 at 22 $^{\circ}\text{C}$, ± 1 digit	0 to +120 $^{\circ}\text{C}$		1 min

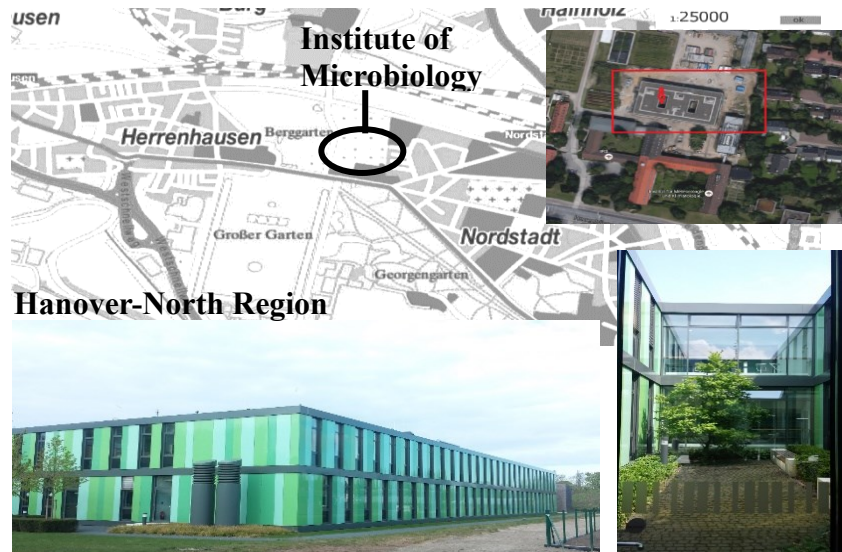


Fig. 2. An experimental area and the layout of measurement points (“ENVI-met EagleEye”, 2016)

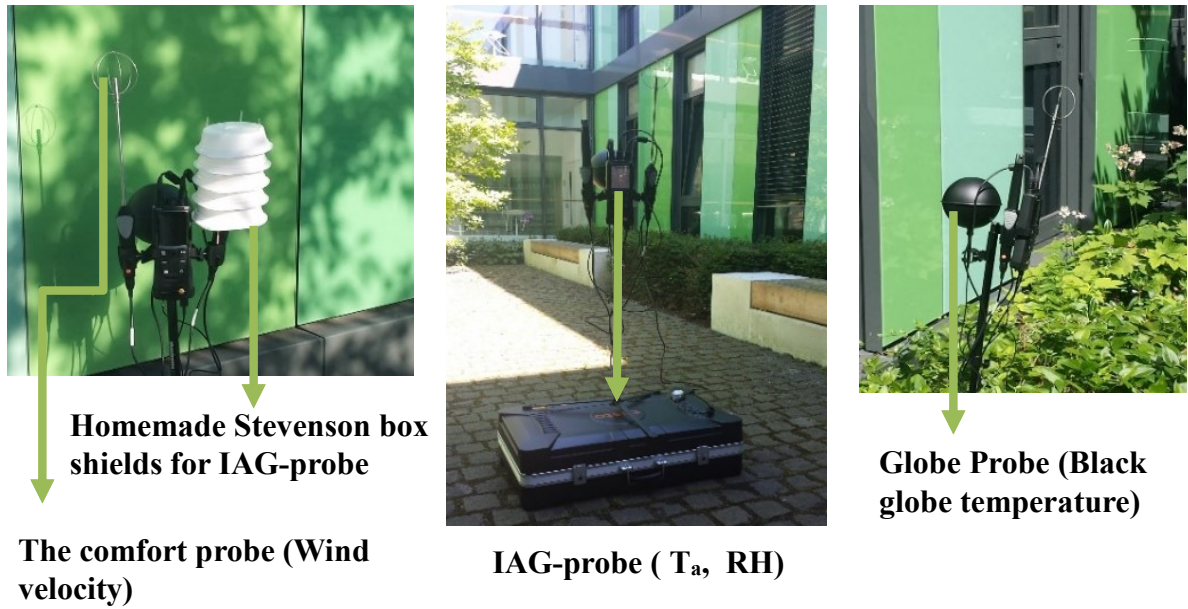


Fig. 3. Views of the instruments during the experiment

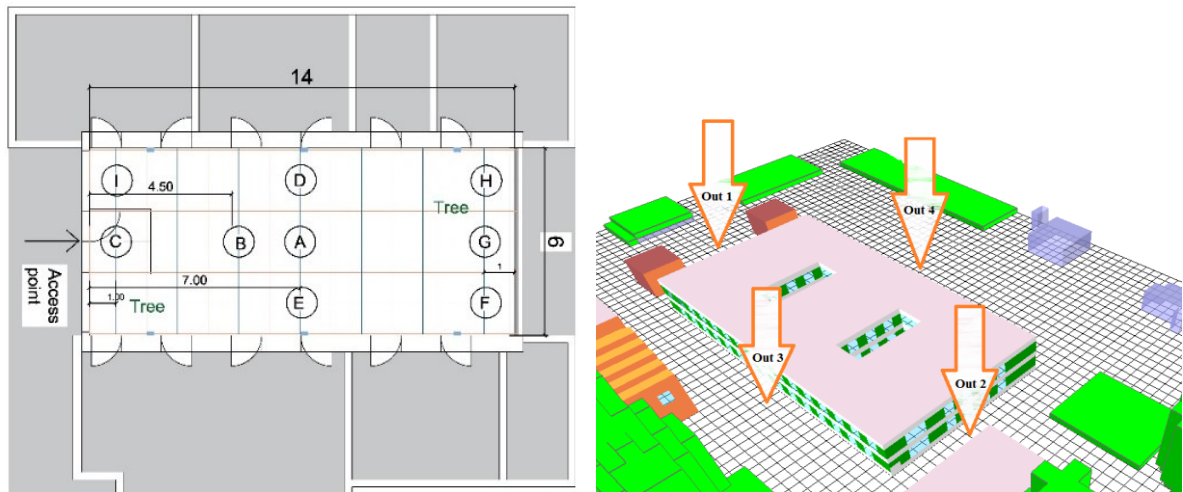


Fig. 4. An experimental area and the layout of measurement points

Table 2. Schedule of the measurements conducted inside courtyard

Nr.	Day	Point/ Station	07.07. 2016	08.07. 2016	19.07. 2016	20.07. 2016	04.08. 2016	16.08. 2016	17.08. 2016	04.10. 2016	27.01. 2017	02.02. 2017
1	Start	A	05:00	00:01					12:01			
	End		00:00	04:00					12:30			
2	Start	D			09:45				12:31			
	End				14:00				13:00			
3	Start	B				10:00					12:00	07:00
	End					18:00					18:00	12:00
4	Start	E					09:52		11:31			
	End						16:10		12:00			
5	Start	Out 1						07:00				
	End							09:00				
6	Start	Out 2						09:01		13:00		
	End							11:00		14:00		
7	Start	Out 3						11:01				
	End							13:00				
8	Start	Out 4						13:01		14:00		
	End							15:00		15:00		
9	Start	C						15:01	13:31			
	End							16:00	14:00			
10	Start	F							10:00			
	End								10:30			
11	Start	G							10:31			
	End								11:00			
12	Start	H							11:01			
	End								11:30			
13	Start	I							13:01			
	End								13:30			

Table 3. Major input variables for ENVI-met simulation

Meteorological inputs	Air temperature and relative humidity	Hourly data from Herrenhausen meteorological station
	Wind speed and direction	Table 4. Hourly data from meteorological station
	Solar radiation: SW diffuse and Global	Table 4. Hourly data from meteorological station
	Specific humidity in 2500 m	Table 4
	Roughness length at reference point	0.1 m
Plants	3D tree	Crown/width 5m, height 10 m , LAD = 2 (m ² m ⁻³)
	1D grass	Height 0.63/ Albedo 0.2/ LAD=0.3 (m ² m ⁻³)
	1D grass	Height 0.2/ Albedo 0.2/ LAD=0.3 (m ² m ⁻³)
Building	Detailed individual surface material for walls and roofs	Table 7
	Indoor Temperature	293 K
	Unsealed soil	Initial condition for soil (default)
Soil (Fig. 7.)	Concrete pavement Gray	Upper layer (0 – 20cm): 293 K/ 50%
	Asphalt road	Middle Layer (20 – 50cm): 293 K/ 60% Deep Layer (50 – 200cm) : 293 K/ 60%

3.1.4. Weather data

The weather data used for simulation are obtained from Measuring Field in the area of the Institute of Meteorology and Climatology at Herrenhaeuserstr., Hanover, Germany. There is an ultrasonic anemometer at the top of the 50m – high measuring mast, which measures wind velocity and its direction. Nearby the mast temperature, humidity and pressure at 2m, wind velocity at 10m and precipitation are measured (IMUK, 2016) .

In this case, the low distance between the case study and meteorological station reduce the errors in air temperature and wind velocity caused by the urban heat island (UHI) phenomena (Oke, 1982) and high displacement height in city areas.

The hourly meteorological data from the IMUK meteorological station is used to generate the forcing air temperature and relative humidity file for the simulation. The cloud cover and solar adjust factor during simulation periods are also derived from the direct observation of the hourly variation of global and diffuse radiation in the IMUK meteorological station (IMUK, 2016). The amount of specific humidity at 2500m can be determined through the radiosoundings (Indian Space Research Organisation. Dept., 1994). In this study, it was calculated using the psychrometric chart (ASHRAE, 1992). Under the simple standard atmospheric condition, the average temperature decrease is 0.65 °C for every 100 meters. Therefore, the Air temperature at 2500m was calculated from the following formula (Mennerich, 2016):

$$T_H = T_B - \frac{H}{100} \times 0.65C^\circ \quad (1)$$

With T_B as the temperature near ground – here 2m above ground – and H as the height above ground (2500m).

An amount of relative humidity (%) at 2500m is derived from the dew point temperature at 2500 m (T_D) (Dew point temperature gradient: 0.18 °C /100m (Mennerich, 2016)) from the following equation (Wanielista, Kersten, & Eaglin, 1997):

$$RH = 100 \left(\frac{112 - 0.1T_a T_D}{112 + 0.9 T_a} \right) (\%) \quad (2)$$

In this research, the expert version of ENVI-met is not accessible (wind simulation with forced boundary condition is only possible for internal use). To solve this problem, the simulations for one day are repeated with different wind velocity, direction and cloud cover factor, which are recorded on simulated days, while the results are exported separately for periods with the same mentioned values. Furthermore, it should be mentioned that in the simulations the wind direction is calculated based on 12 (deg) model rotation. Table 4 summarizes the weather parameters on simulations used.

3.1.5. Model area

The model area in this study is digitized by using aerial photos and pictures taken at ground level and bird's eye view pictures through the site. The height of the main building is measured on the site through a Leica Disto D2 laser distance meter. For other buildings, trees and shrubs, it was mainly estimated from the pictures and the number of levels of the buildings.

In the first step of model domain size and resolution definition, it is necessary to consider the results of previous studies to find an optimal model. Table 5 summarizes the defined model area, including the number of grids, their resolution and applied nesting grids in previous studies.

The size of the entire computational domain in the horizontal dimensions was modeled generally 2 H radios from the target building (Yoshihide Tominaga et al., 2008; Yoshie et al., 2007). The lateral size of the computational domain was selected to be at least five times the high of the highest building (Yoshihide Tominaga et al., 2008), however, for urban areas, it can be placed closer than this distance (Franke, J., Hellsten, A. , Schlünzen, H., Carissimo, 2007). The 'Nesting area' including 5 – 20 nesting grids is also created around the core zone of the model, offering the possibility to distance the boundaries of the model from the area under examination and minimize the undesired effects provoked by the boundary.

According to the ENVI-met simulation instrument, the total height of the model adjusted at least twice the height of the tallest structure and bigger than 30m in total (ENVI-met, 2013a). In addition, the blockage ratio of buildings, in the computational domain, limited to the range between 3% (Franke, J., Hellsten, A. , Schlünzen, H., Carissimo, 2007) and 10% (VDI-Standard, 2000).

In the case of suitable grid resolution, a brief look at previous studies (Table 5) shows that in most cases the simulation results from the model with a resolution equal to 2m are close to the real condition. Normally, the resolution of the grid should be fine enough to capture the important physical phenomena like shear layers and vortices with sufficient resolutions. It is recommended to set the minimum grid resolution to about 1/10 of the building scale and set the minimum of 10 grids on one side of the building. Moreover, the vertical grid resolution in all cases is arranged that the evaluation height is located at least 3rd or higher grid from the ground surface (Franke, J., Hellsten, A. , Schlünzen, H., Carissimo, 2007; Y Tominaga, Mochida, Murakami, & Sawaki, 2008; Yoshie et al., 2007).

Based on the mentioned assumptions and with regard to the limitations in the number of vertical grids and size of the horizontal grid cells in ENVI-met (Max. 40 vertical grids and 250 horizontal grid cells with resolution $\geq 0.5\text{m}$), four identical models were generated in order to examine the sensitivity of the simulation results with respect to the grid and domain size. The geometric characteristics of the experimental models are stated in Table 6 and Figure. 5.

According to Table 6, in the vertical direction, varying grid sizes were tested. Moreover, given that we focused on the near-ground microclimate in this study, for the courtyard space equidistant grids were used with a fine resolution (0.5 – 1m) and for the space above the courtyard, telescoping grids were used with a telescoping factor of 15% to 20%. Furthermore, the structure of the lowest grid cell above ground is normally split into 5 sub-cells, with size $\Delta z_s = 0.2 \Delta z$, to increase the accuracy in calculating surface processes. Consequently, the dimensionless wall distance (y^+) values for all four experimental models lie between the range of $30 < y^+ < 500$ (Table 6). Where y^+ is defined as:

$$y^+ = \frac{\sqrt{\frac{\tau_w}{\rho}} y_p}{\nu} \quad (3)$$

With y_p as the distance (normal) of the center point P of the ground-adjacent cell to the ground (m), τ_w is the shear stress at the surface ($\text{kg m}^{-1} \text{s}^{-2}$), ρ is the air density (kg m^{-3}) and ν is the kinematic viscosity of air ($\text{m}^2 \text{s}^{-1}$). This range is known as the log-low layer where a turbulent effect dominates (Salata et al., 2016; Tu, Yeoh, & Liu, 2012).

In this case, the study area has a different orientation (12 deg. Rotated) and it is not possible to model the buildings' form with existing grids. Therefore, the model area is rotated 12 degrees counter-clockwise above the original map.

The four mentioned experimental models are validated for the weather conditions on July 7. The validation results are explained in section 4.1.

Table 4. Description of the model meteorological boundary conditions

Datum (dd.mm.yyyy)	Hour (hh:nn)	Average wind speed at 10 m above ground (m s^{-1})	Average wind direction at 50 m above ground (deg) with 12 (deg) model rotation	Cloud cover			Adjustment Factor	Specific Humidity (2500m) (g Kg^{-1})
				low	Med.	High		
07.07.2016	06:00 – 13:00	2.73	244.62 - 12 = 232.62	0	0	0	1	3
	14:00 – 16:00	2.23	228.8 - 12 = 216.8	1	5	2	1	3
	17:00 – 18:00	1.4	219.85 – 12 = 207.85	1	7	0	0.5	3
	19:00 – 23:00	0.64	197.16 – 12 = 185.16	0	8	0	0.5	3
08.07.2016	00:00 – 02:00	0.64	197.16 - 12= 185.16	0	8	0	0.5	4
	03:00 – 05:00	1.03	164.73 - 12= 152.73	0	6	0	1	4
19.07.2016	10:00 – 13:00	1.73	241.33 - 12= 229.33	0	1	0	0.9	5
20.07.2016	10:00 – 17:00	2.28	112.58 - 12= 100.58	0	0	0	0.9	6
04.08.2016	10:00 – 14:00	3.96	235.78 - 12= 223.78	0	6	1	0.85	4
	15:00 – 17:00	2.17	230.43 - 12 = 218.43	8	0	0	0.7	4

Table 4. Description of the model meteorological boundary conditions (Continued)

Datum (dd.mm.yyyy)	Hour (hh:nn)	Average wind speed at 10 m above ground (m s^{-1})	Average wind direction at 50 m above ground (deg) with 12 (deg) model rotation	Cloud cover			Adjustment Factor	Specific Humidity (2500 m) (g Kg^{-1})
				low	Med.	High		
16.08.2016	07:00	1.73	213.8 - 12 = 201.8	0	0	0	1.1	3.5
	08:00 – 10:00	1.73	295.3 - 12 = 283.3	0	0	0	1.1	3.5
	11:00 – 14:00	2.02	223.4 - 12 = 211.4	0	3	0	0.75	3.5
	15:00 – 16:00	1.75	154.65 - 12 = 142.65	0	4	0	0.55	3.5
17.08.2016	10:00 – 14:00	1.86	86.8 - 12 = 74.8	0	1	0	0.9	2.8
04.08.2016	13:00 – 14:00	2.54	55 - 12 = 43	0	0	0	0.8	1.5
27.01.2017	12:00 – 18:00	2.3	143.5 - 12 = 131.5	0	2	0	0.7	1
02.02.2017	07:00 – 12:00	2.5	155.23 - 12 = 143.23	0	2	0	1	3

Table 5. The size of the model area in previous studies

Research	Grid	Resolution	Δz	Nesting grid
(Xiaoshan Yang et al., 2013)	85, 85, 30	3	0.2 until 2m, 20% telescoping	5
Ramses Project (De Ridder & Acero, J. ; Lauwaet, D.; Lefebvre, W.; Maiheu, B.; Mendizabal, 2014), RiberaDeusto	167, 104, 30	2	Increasing with height	6
Ramses Project, Miribilla	167, 146, 30	2	Increasing with height	6
Ramses Project, CasscoViejo	109, 101, 26	2	2	9
Ramses Project, RiberaDeusto	167, 167, 30	2	Increasing with height	6
Erbprinzenstrasse, (Huttner, 2012)	186, 118, 25	2	2	Not known
Vauban, (Huttner, 2012)	256, 197, 25	2	2	Not known
(Salata et al., 2016)	XX, XX, 29	2	0.5 until 3m, 20% telescoping	Not known
(Lee et al., 2016)	150, 150, 25	1	1	20 m
(Simon, 2016)	140, 116, 40	2	2	
(Ambrosini, Galli, Mancini, Nardi, & Sfarra, 2014)	80, 80, 30	dx = 4.5; dy = 3.5	1.2	Not known
(Srivanit & Hokao, 2013)	200, 246, 20	3	3	65!
(Elnabawi et al., 2015)	30, 140, 30	1	3	Not known

Table 6. Description of the model dimensions of each area

Parameter	Model 1	Model 2	Model 3	Model 4
Number of grid cells (x,y,z)	83, 83, 39	89, 89, 39	131, 131, 34	181, 125, 24
	2, 2, 1	2, 2, 1	1, 1, 0.6	0.5, 0.5, 0.5
Size of grid cells (meter) (x,y,z)	Telescoping Factor : 15%	Telescoping Factor : 15%	Telescoping Factor : 15%	Telescoping Factor : 20%
	Start telescoping after height : 12m	Start telescoping after height : 12m	Start telescoping after height : 8m	Start telescoping after height : 4m
Nesting grids	8	5	9	20
Blockage ratio	3%	5.9%	8%	3%
Y⁺ ≈	200	215	130	104
Model rotation out of grid north	12	12	12	12

3.1.6. Building, Plants, Soil physical properties

Since version 4.0, the simulation of the outdoor and indoor interactions on building's facade has been carried out using a multiple-node transient state model based on the works of Terjung and O'Rourke (Terjung & O'Rourke, 1980). This model allows the construction of up to three different layers which can vary in width and materials used. Every material can have its own physical properties (absorption, transmission, reflection, emissivity, specific heat capacity, thermal conductivity and density). This method allows the calculation of the temperature at seven points, including outside and inside surface of the wall, under a dynamically condition, and at the center of the wall for each layer in a transient-state. (Simon, 2016).

The material section in the Database allows to create new materials or edit their parameters. In this project the thermal properties of the building envelope were defined default characteristics by the ENVI-met-Database. The thermal properties of new materials were derived from local building codes – including DIN 4108-4 and DIN EN ISO 10456 (DIN, 2017a)(DIN, 2010b) – and material brochures. Table 7 describes the physical properties of the materials used in the simulation.

The courtyard's surrounding walls (Microbiological institute) are defined in three main layers, including a Quadroclad Glass panel (colored glass), the air layer and brick walls with a total thickness of 0.55m (Fig. 6.). For other neighboring buildings, the default brick and glass wall details adjusted with the same thickness and material for all three layers. All flat roofs were defined as concrete slabs with 30cm thickness and the 30cm terracotta roofing structure was selected for the pitched roofs.

The type of the soil and the sort and height of the plants through the model defined based on the field survey (Fig. 7.). As can be seen in Figure 7, the ground of the courtyard's center is covered with dark stone. The surrounding ground is partly covered by lightly colored concrete blocks and partly by loamy soil as well as grass.

The ENVI-met default values are set for the initial soil conditions, including its wetness and temperature in upper, middle and deep layers. Moreover, the default leaf area density (LAD) values in ENVI-met were used for plants (Table 3).

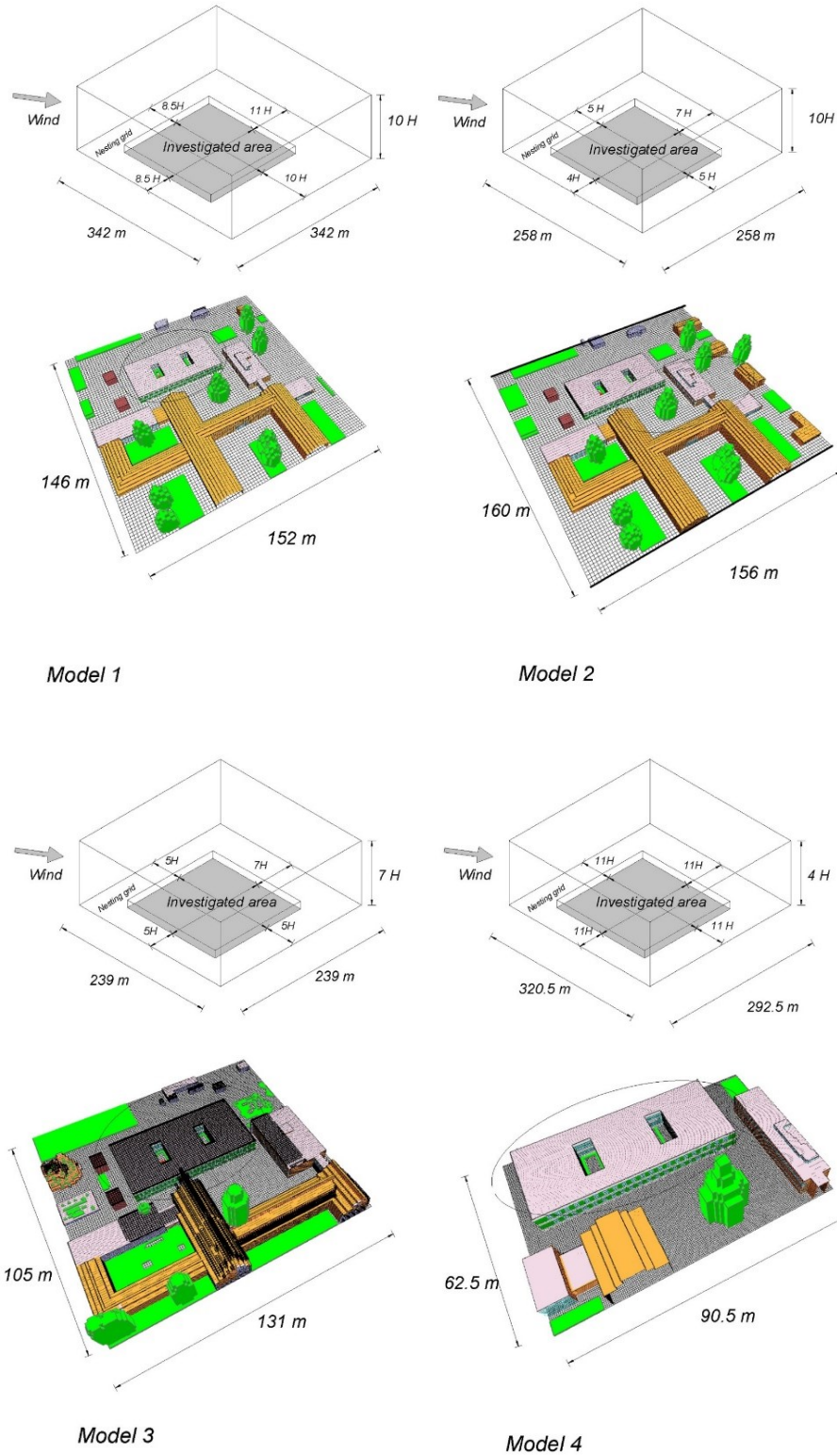


Fig. 5. Representation of the model input (including buildings and vegetation) for each area (“ENVI-met SPACES,” 2016)

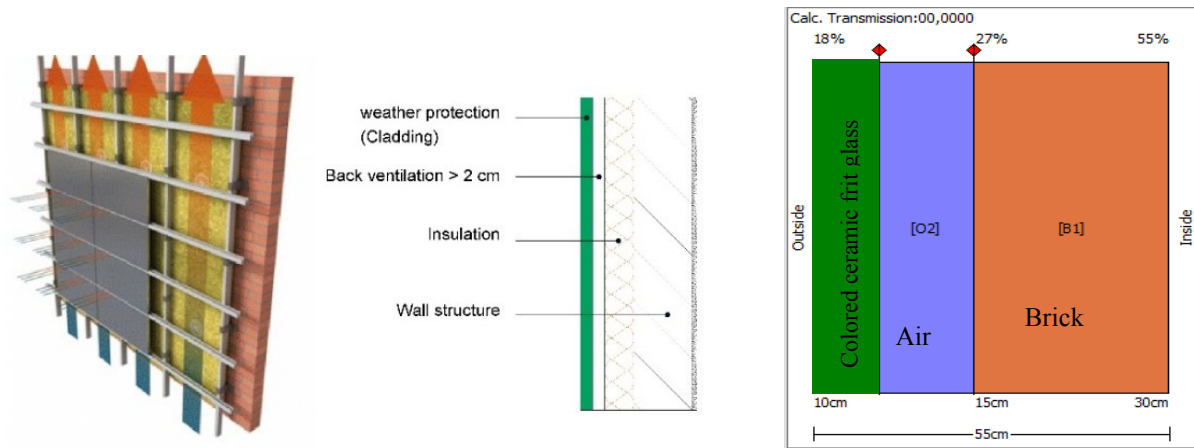


Fig. 6. Respectively from left to right: The structure of Courtyard’s surrounding walls (DIN, 2010a; Green Building Factory, 2014), defined structure for the courtyard’s surrounding walls in ENVI-met- Database

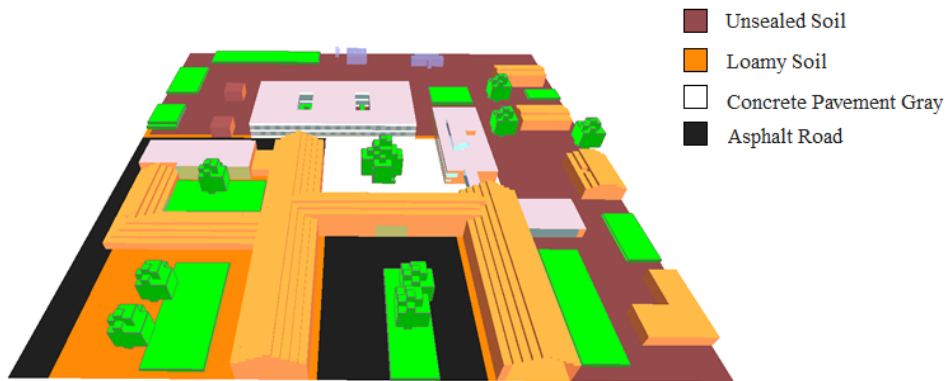


Fig. 7. Model area, including the buildings, Plants and soil color-chart

Table 7. Physical properties of the materials used in the simulation

Physical properties	Material							
	Concrete slab (hollow block)	Glass (clear float glass)	colored ceramic frit glass	wood facade panels	Brick	Roofing: Terracotta	Aluminum profiles	Air
Thickness (m)	0.3	0.02	0.02	0.1	0.3	0.05	0.03	0.15
Absorption	0.7	0.05	0.3	0.6	0.6	0.5	0.1	0.0
Transmission	0.00	0.9	0.1	0.00	0.00	0.00	0.00	1.0
Reflection	0.3	0.05	0.6	0.4	0.4	0.5	0.9	0.0
Emissivity	0.9	0.9	0.8	0.9	0.9	0.9	0.18	0.96
Specific Heat capacity (j kg⁻¹ K⁻¹)	840	750	1500	1700	650	840	880	1006
Thermal conductivity (W m⁻¹ K⁻¹)	0.86	1.05	0.19	0.26	0.44	0.81	203	0.025
Density (kg m⁻³)	930	2500	1200	1350	1500	1700	2700	1.2041

3.1.7. Boundary condition

3.1.7.1. Temperature and humidity

The ground, roof and wall surface temperatures are used as real physical boundaries. In order to compare the results of a numerical simulation with measured data or simulate a specific meteorological development, it is necessary to ‘force’ the simulation by adjusting the variables at the inflow boundaries of the model. The implementation of ‘forcing’ in ENVI-met uses this boundary condition and lets the user define the temporal and spatial development of the 1D model with the observed data from a meteorological station at 2m above ground level. By assuming the neutral stratification of the atmosphere for air temperature profile (constant potential temperature for all levels) and linearly interpolating the observed data at the ground level and the input specific humidity at 2500m above ground for the humidity profile, the 1D meteorological profiles for temperature and humidity are shaped and used to define the lateral and top inflow boundaries of the main model (3D).

3.1.7.2. Wind and Turbulence

The wind speed is always assumed to be 0 (m s^{-1}) at ground level (0m) and on walls (no-slip condition, $u = v = w = 0$). For the top of the model, it is extrapolated logarithmically to 2500m from the next lower height level for which a value is given (Huttner, 2012). All vertical motions, at the top boundary, are assumed to be zero (closed) and a zero-gradient condition is used at the outflow and lateral boundaries.

The turbulence closure scheme for 1D and 3D is set as the “Prognostic 1.5 Order E- Epsilon Closure Model”, which is able to estimate both temperature and humidity in the “main loop” of the model in a continuative way. However, the information concerning the boundaries cannot be obtained through the equations of the aforementioned model. For these reasons, it must be obtained in simpler ways. ENVI-met manages the boundaries of the model for turbulent in three ways (Michael Bruse, 2015):

- “Open Boundary Conditions”: the values of the inner points are copied back to the lateral inflow boundary for each time step;
- “Closed (or Forced) Boundary Conditions”: the values of the one dimensional model are copied to the border;

- “Cyclic Boundary Conditions”: the values of the downstream model border are copied to the upstream model border.

The default Lateral boundary condition for turbulence (LBC for TKE) in the first phase of the simulation is set to open, which least influences the inner parts of the model (Huttner, 2012). This assumption represents a situation where the neighborhood of the simulation area has a similar structure to the simulation area. With open LBC, the profile at the inflow boundary is more similar to the distribution inside the model area, which reduces the squeezing effect at the inflow boundary (ENVI-met, 2017).

At the second stage of validation, according to validation processes (Fig. 1.), the effect of various lateral boundary conditions for turbulence is analyzed.

3.1.8. Simulation Time

Based on the ENVI-met basic setting guideline (ENVI-met, 2013b), all simulations are started at sunrise or during the night, whereby the calculation can follow the atmospheric processes. Moreover, the total simulation time in all cases is set to a minimum of 12 hours. To reduce the numerical instability, the output values are considered after three hours' simulation.

3.1.9. Model timing

In this research, model time intervals that are too wide are avoided and the default values provided by ENVI-met were used. For this reason, the temperature and humidity of the surfaces receive an update every 30 s, the position of the sun, irradiative fluxes connected to it and shadows every 600 s and finally the data concerning the plants (leaves temperature, resistance determined by the stoma) every 600 s. In the first and second stage of model validation, the data concerning the wind and turbulence are updated every 900 s. However, since the size of the time intervals is another important parameter for the accuracy of the results, to assess the influence of the wind and turbulence updated intervals on the results, a systematic reduction of the time step was considered on 7 July. The results of this part are described in section 4.

For output, climate values of the model were available every 30 minutes and the whole grid outputs were recorded every hour.

4. Results and discussion

4.1. ENVI-met model Verification

Before comparing the experimental data with the values provided by the software, to adjust a reliable ENVI-met model that accurately represents the real environment, it is necessary to select the optimum model size and lateral boundary condition.

For this reason, four simulations were carried out with different meshes and model size (Table 6, Fig. 5) for July 7, 2016, during the period between 06:00 until 13:00. In this section, the comparison results for the air temperature, wind speed and the relative humidity at point “A”, are explained.

While examining the data reported in Figure 8, it is possible to note that there is not a major difference between the air temperature and relative humidity, measured and simulated for four experimental models. The large difference occurs for wind velocity in experimental model 3 with high resolution and small lateral domain extension, which shows approximately 0.14 (m s^{-1}) the mean difference between the modeled values and site measurement ones. Due to the E- ϵ closure method used in ENVI-met, it seems that by increasing the grid's resolution, due to the limitation in a number of the vertical grid, the computational domain height is reduced and the turbulent tendency inside the model is overestimated.

On the other hand, comparing the results for all micrometeorological variables between models 1 and 2 – with a different lateral extension of the domain – confirms that model 1, with big lateral domain, gives better results.

Based on earlier research (Table 5) and this project's results (Figure 8), for quicker simulation and to have a sufficient large model area for further research, model area 1 – with a horizontal resolution of 2m and a vertical resolution of 1m – was selected for further simulations.

Beside geometrical and model parameters, the boundary conditions set by the simulation play a key role in the acquisition of reliable data. This is why a further analysis here considers the influence of the lateral boundary conditions for turbulence on the results provided by the software. Figure 9 shows the effect of three different Turbulence lateral boundary conditions setting alternatives: open, forced and cyclic (Section 3.1.7.2) on air temperature, relative humidity and wind velocity inside the model.

It should be specified that it is not possible to predict which type of LBC is best for a specific case. As can be seen in figure 9, the turbulence lateral boundary condition has a negligible effect on air temperature and relative humidity. The simulations with different LBC show the differences in wind speed. The results show that between a different LBC for TKE, the cyclic LBC type leads to a smaller difference between the predicted and measured wind speed inside the courtyard ($\approx 0.02 \text{ (m s}^{-1}\text{)}$).

The appropriate time step for flow is also considered in this research (Fig. 10.). Due to the various air flow patterns inside the semi-closed courtyard spaces – buoyancy and wind flow pattern (ALVAREZ et al., 1998; Rojas et al., 2012) – smaller time steps improve the results of wind speed prediction.

Based on these results, the decision was made to continue the validation processes for other time periods with geometrical model area 1 with cyclic LBC for TKE and flow time step size $t_{\text{flow}} = 0 \text{ s}$.

Table 8. Mean difference comparison of the validation criteria between the on-site measured and the simulated data, at different model calibration stages on July 7, 2016, Point A

Validation criteria	Precision of required equipment	06:00 - 13:00				06:00 - 11:00		
		Calibrated model 1	Calibrated model 2	Calibrated model 3	Calibrated model 4	Calibrated model 1 (Open LBC for TKE)	Calibrated model 1 (Cyclic LBC for TKE)	Calibrated model 1 (Forced LBC for TKE)
Air temperature	± 0.5 °C	0.07	0.40	-0.06	-0.089	0.07	0.07	0.08
Relative humidity	$\pm 3\%$	2.96	1.95	2.99	4.16	3.10	2.96	3.11
Air velocity	± 0.05 (m s ⁻¹)	0.03	0.06	0.14	0.086	-0.055	-0.02	-0.055

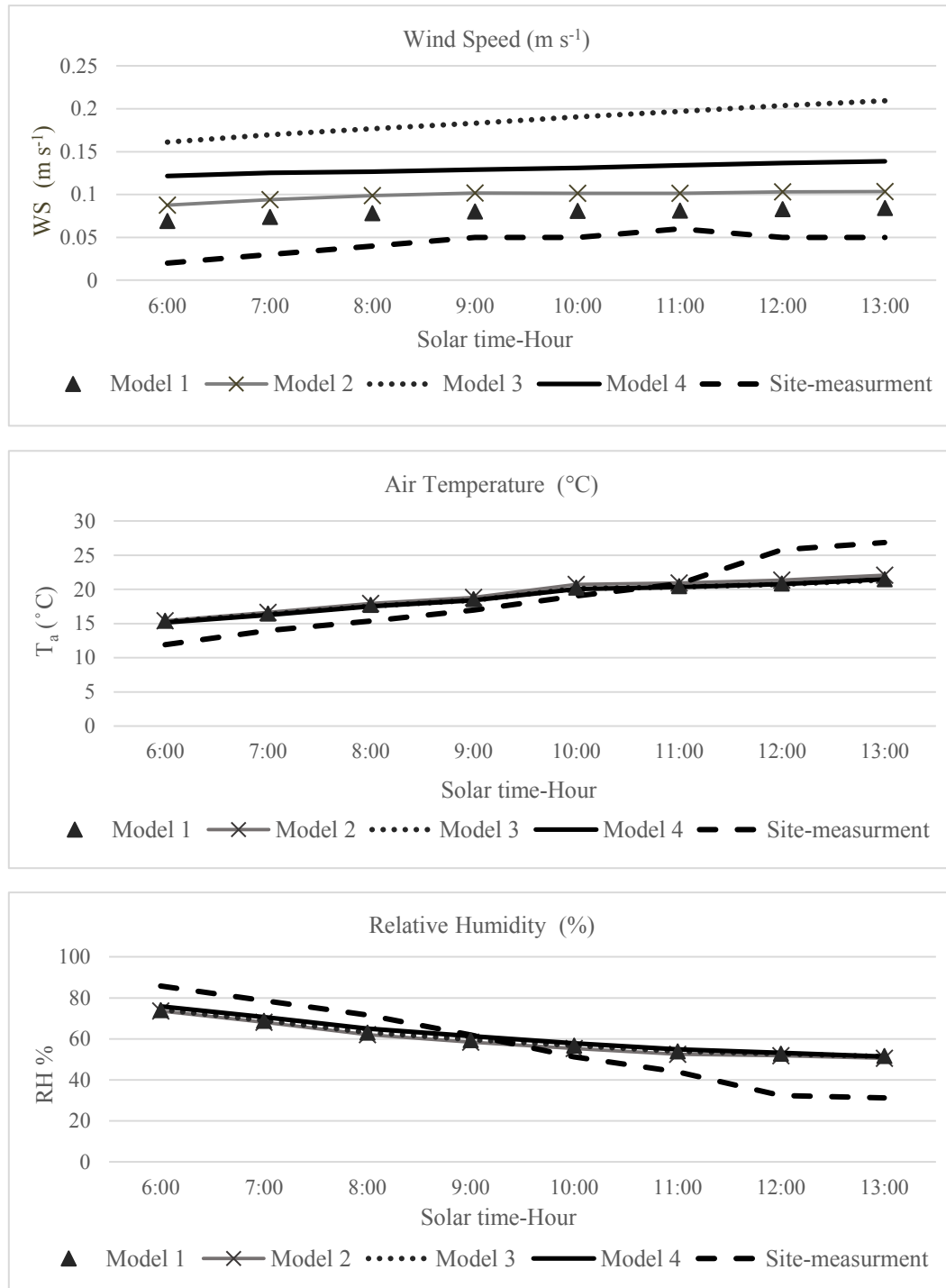


Fig. 8. Compares the difference between the calculated and site measurement meteorological values for four experimental models

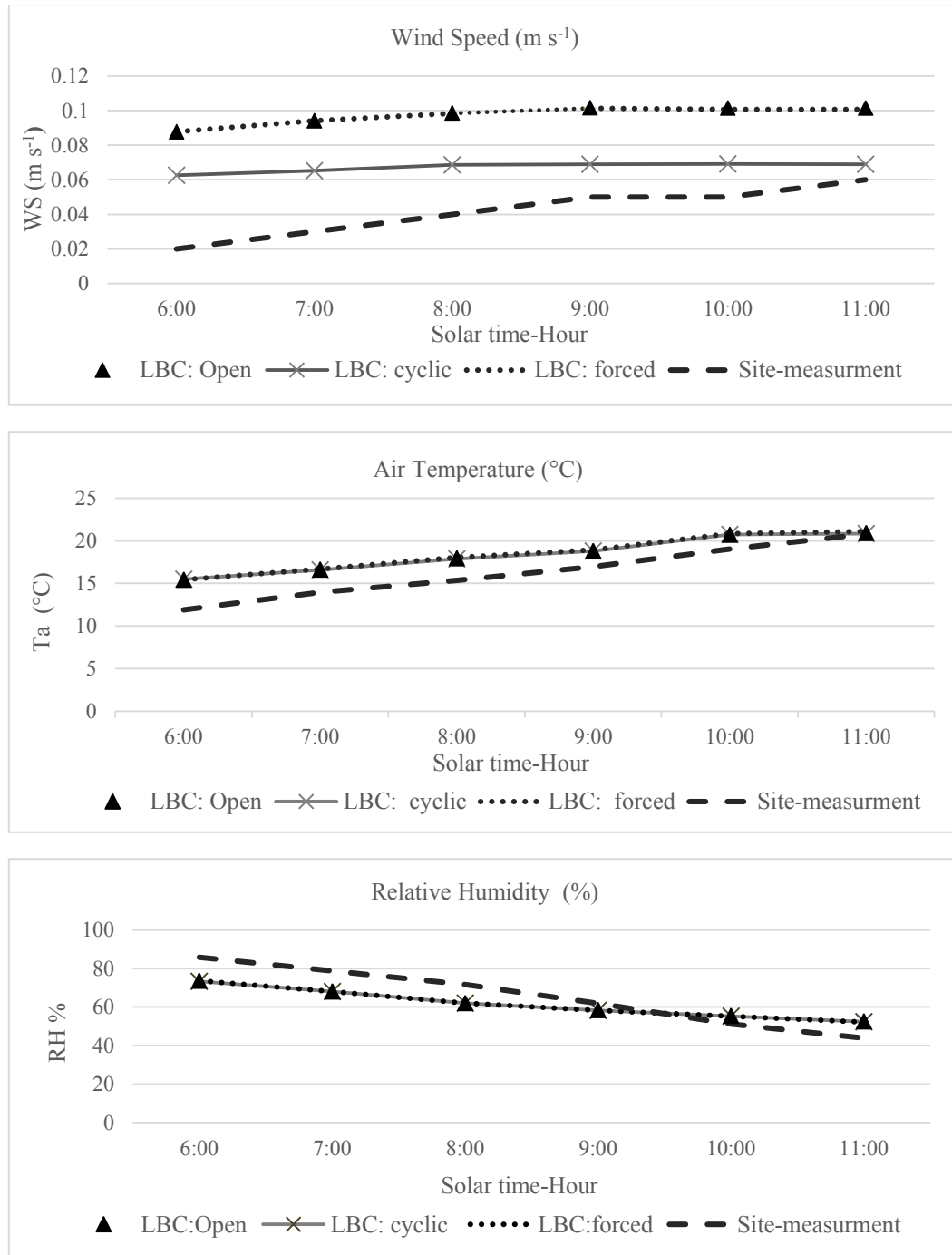


Fig. 9. Comparison of the difference between the calculated and site measurement meteorological values with three different model boundary condition for turbulence

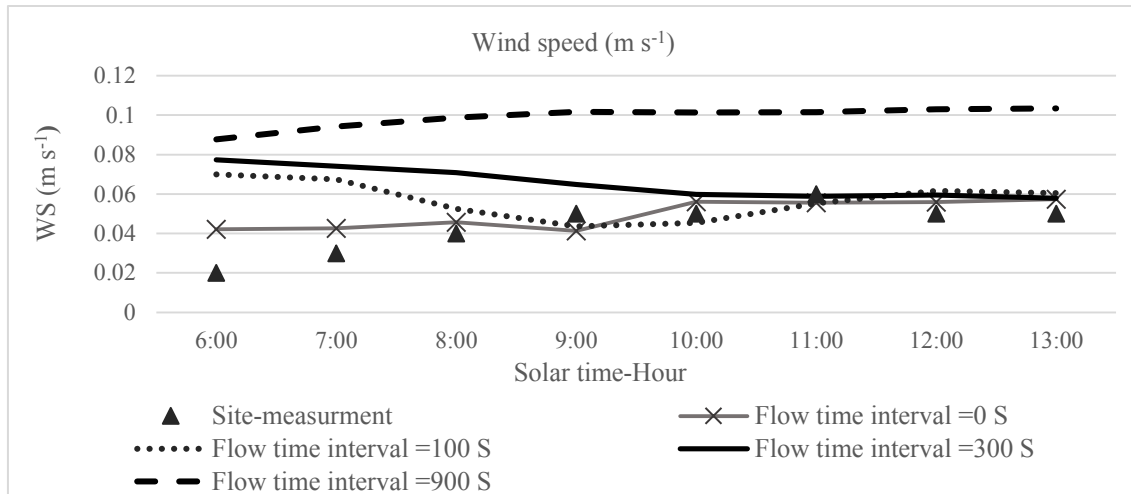


Fig. 10. Comparison of the difference between the calculated and site measurement meteorological values with four different time intervals for flow

4.2. Validation results and discussion

The evaluation of the model, for other simulation periods was achieved by comparing the measured data with the simulated temporal variations of T_a , RH, WS and T_{mrt} . The average hourly air temperature, relative humidity, wind velocity and mean radiant air temperature collected at the measuring points “A – F” and “Out. 1 – 4” at 1.5m height were compared with the corresponding ENVI-met model outputs.

Considering the results for air temperature at 1.5m above ground (Fig. 11 – 13.) shows good agreement between the simulated and measured data for shaded areas (Point B), as well as during the night. Furthermore, the measured values during cold periods of the year are in accordance with the simulations.

The mean air temperature difference between model and measured values (ΔT) for unshaded areas is higher ($T_{measured} > T_{modeled}$) during day time with clear sky, except during the first hours after sunrise (until 9:00 a.m.). The largest differences occur at the point ‘Out 3’, south side, during midday (~ 7 °C). This systematic aberration can be explained by the assumption made for the boundary conditions – i.e. a neutrally stratified atmosphere – which is not valid for a summer day with strong radiation input (Huttner, 2012), as well as also the effect of direct solar radiation and wind velocity on measurement devices (the home-made Stevenson box cannot completely cover the probe).

During the first period of the day, the urban surface has not been heated up by the sun's radiation and thus it is colder than the data forcing the model. The ΔT differences ($T_{\text{modeled}} > T_{\text{measured}}$) at point "Out 1" and point "A" during the first hours the day reflect this fact.

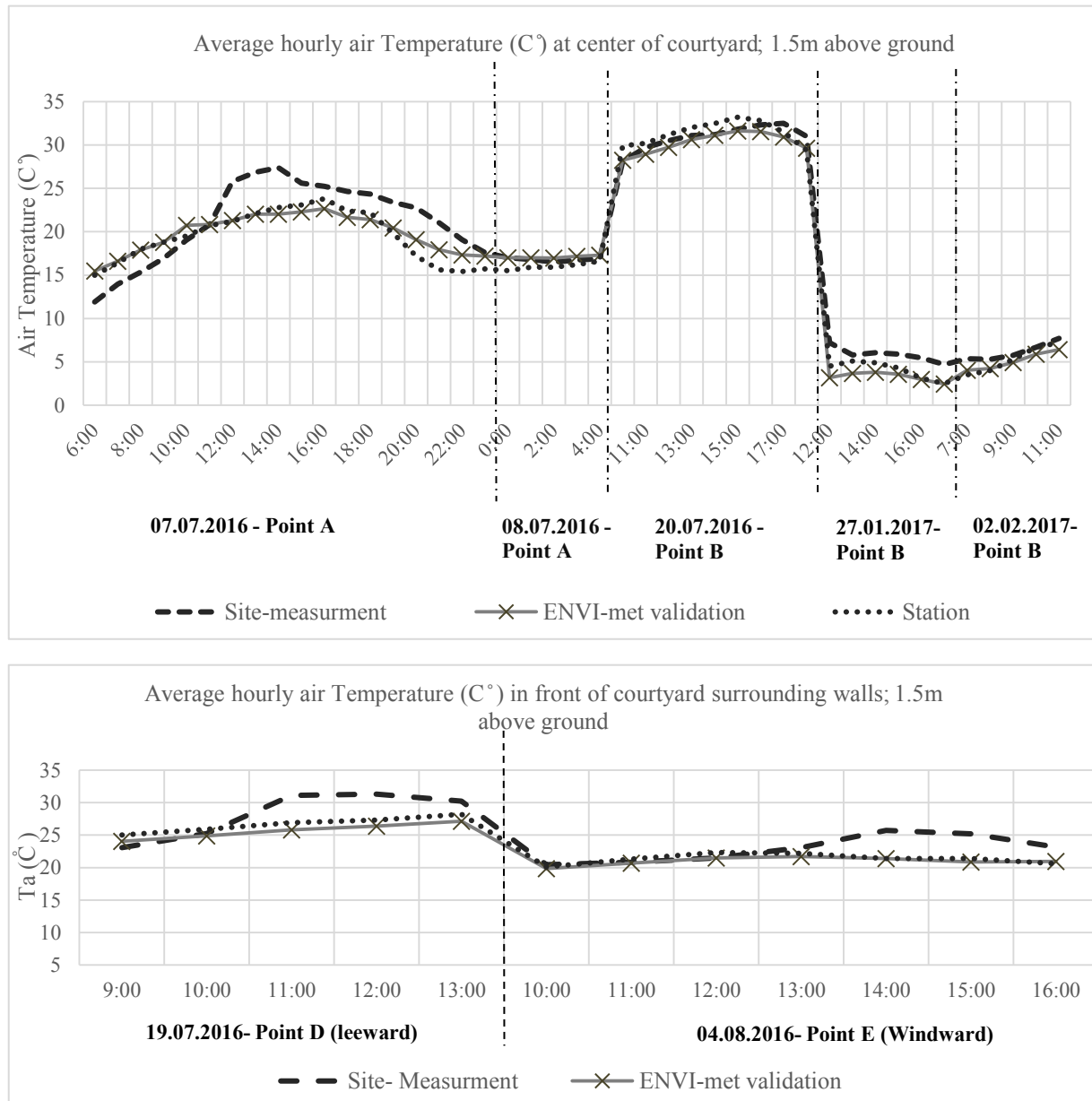


Fig. 11. Comparison of the observed and modeled Air temperature at 1.5m above ground. The dotted line shows the measured average hourly air temperature at the IMUK meteorological weather station.

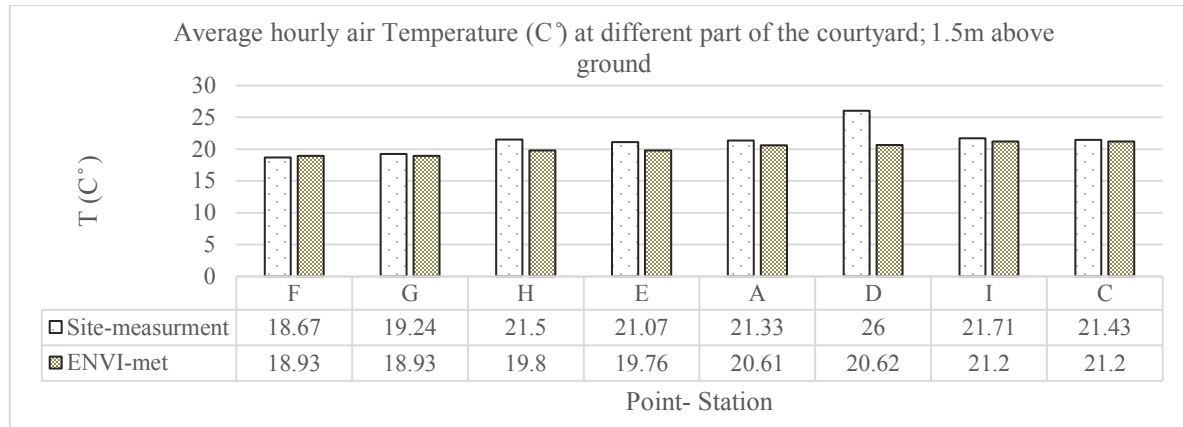


Fig. 12. Comparison of the observed and modeled Air temperature at 1.5m above ground, for the different part of the courtyard on August 17, 2016.

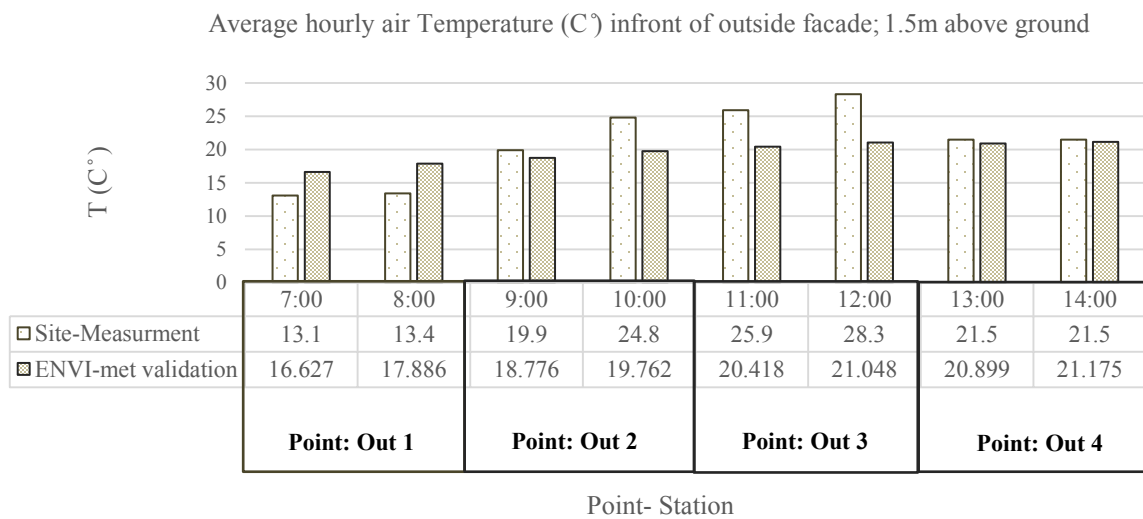


Fig. 13. Comparison of the observed and modeled Air temperature at 1.5m above ground, outside the courtyard on August 16, 2016.

In the case of RH, the best relationship occurs on cloudy days, during the night and in a shaded area (Point B) for winter and summer weather data. The lack of intense solar heating reduces heat accumulation in the urban area and thus reduces its influence on driving measured and modeled Ta and respectively RH values.

During the afternoon on the clear-sky day, the measured air temperature is higher than the simulated one, whereby consequently the measured relative humidity at nearly sunny times is lower than the modeled one.

Similarly, mean relative humidity deviations are higher during the clear-sky day around midday ($\sim 15\%$). However, given that the accuracy of the relative humidity probe is $\pm 1.8\%$ RH + 0.7% of reading, it can be said that the modeled relative humidity fits the observed values very well. Figures 14 – 16 show the comparison between the observed and modeled relative humidity at 1.5m above ground for each of the measured points.

The measured wind speed considering the accuracy of the air velocity probe, $\pm(0.03 \text{ (m s}^{-1}) + 4\%$ of means. Val.), fits the observed values in all points inside the courtyard semi-closed space, except for leeward corner (Point “F” with $\Delta WS \approx 0.07 \text{ (m s}^{-1})$).

By contrast, outside and surrounding the considered building – especially in front of windward facades – the simulated wind speed shows much more turbulence than the measured one. The Reynold Averaged Navier-Stokes (RANS) equation with a 1.5 order turbulence closure model causes this large difference. In the k - ϵ method – used for ENVI-met – the turbulent production (k) in areas with a high acceleration or deceleration such as the flow around a building is overestimated (Huttner, 2012). In addition, k - ϵ model shows poor performance in flow separations (BALDWIN & LOMAX, 1978), reattachment (Kato, M., Launder, 1993) and in flow between complex geometrical configurations (Tu et al., 2012).

The results of earlier studies also show the limitations of ENVI-met in terms of providing an accurate estimation of wind speed around buildings located in open areas, especially for wind speed greater than $2 \text{ (m s}^{-1})$. However, for semi-closed spaces such as courtyards that are not exposed to direct wind, the mean wind speed difference ($\sim 0.02 \text{ (m s}^{-1})$) is negligible. Figures 17 – 19 describe the comparison between the observed and modeled Wind speed at 1.5 meter above ground for the all measured points.

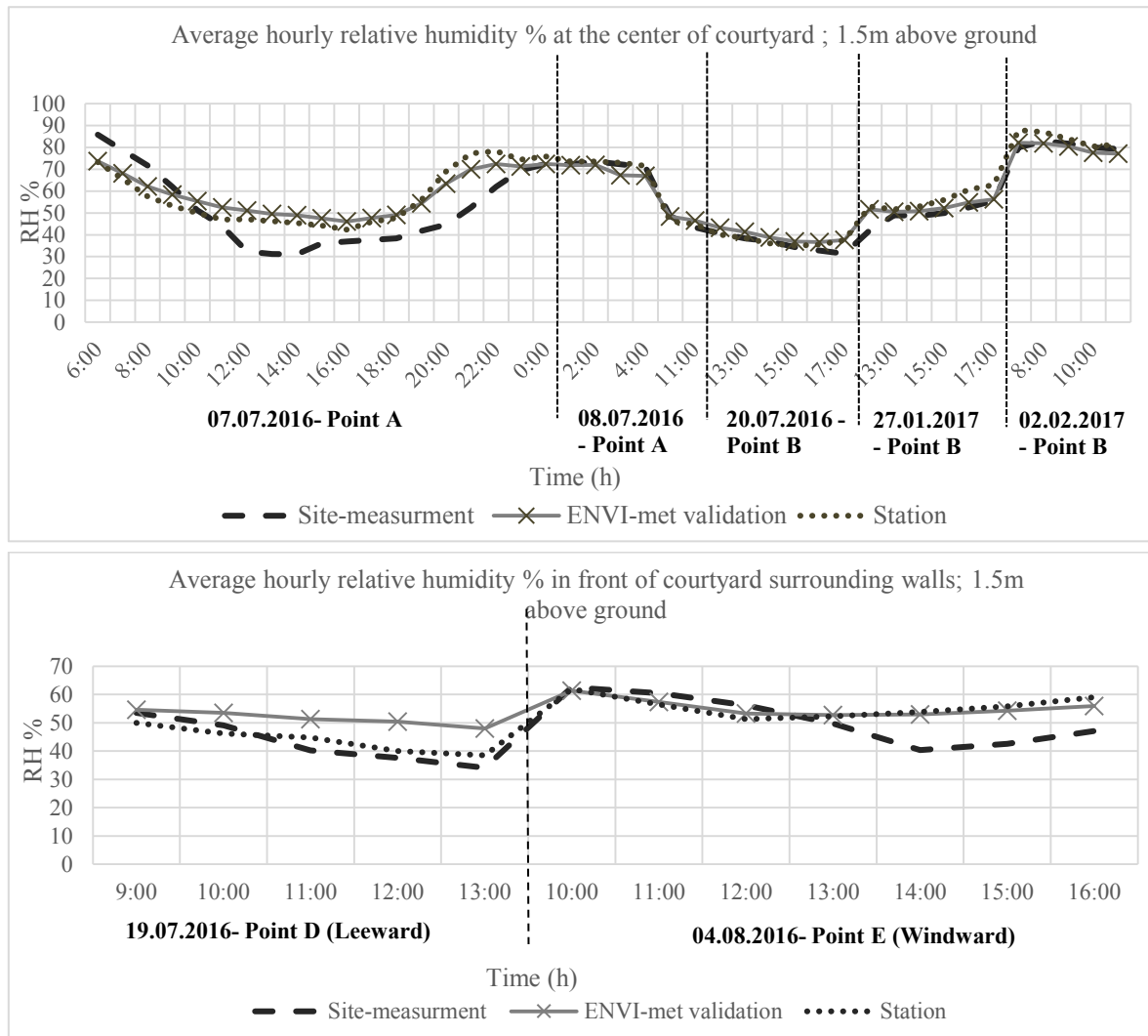


Fig. 14. Comparison of the observed and modeled relative humidity at 1.5m above ground. The dotted line shows the measured average hourly air temperature at the IMUK meteorological weather station.

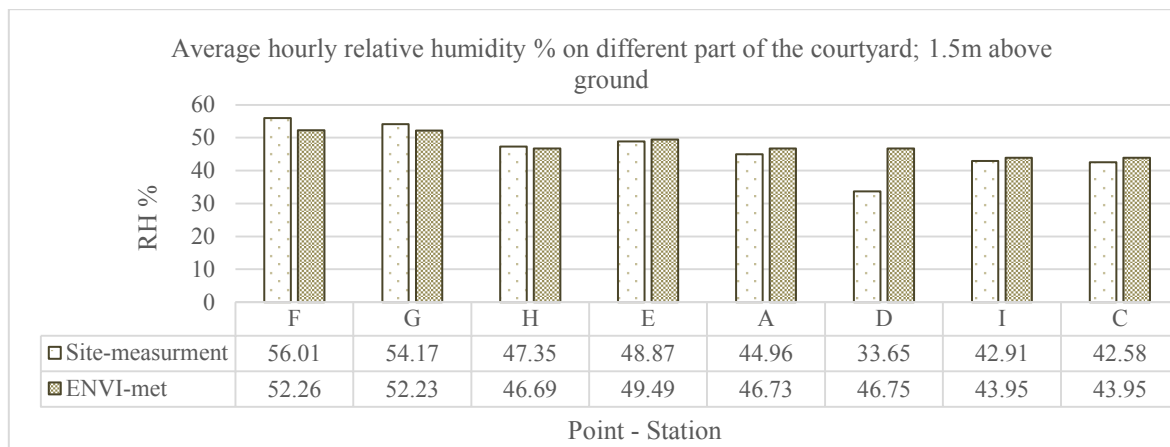


Fig. 15. Comparison of the observed and modeled Relative Humidity at 1.5m above ground, for different part of the courtyard on August 17, 2016

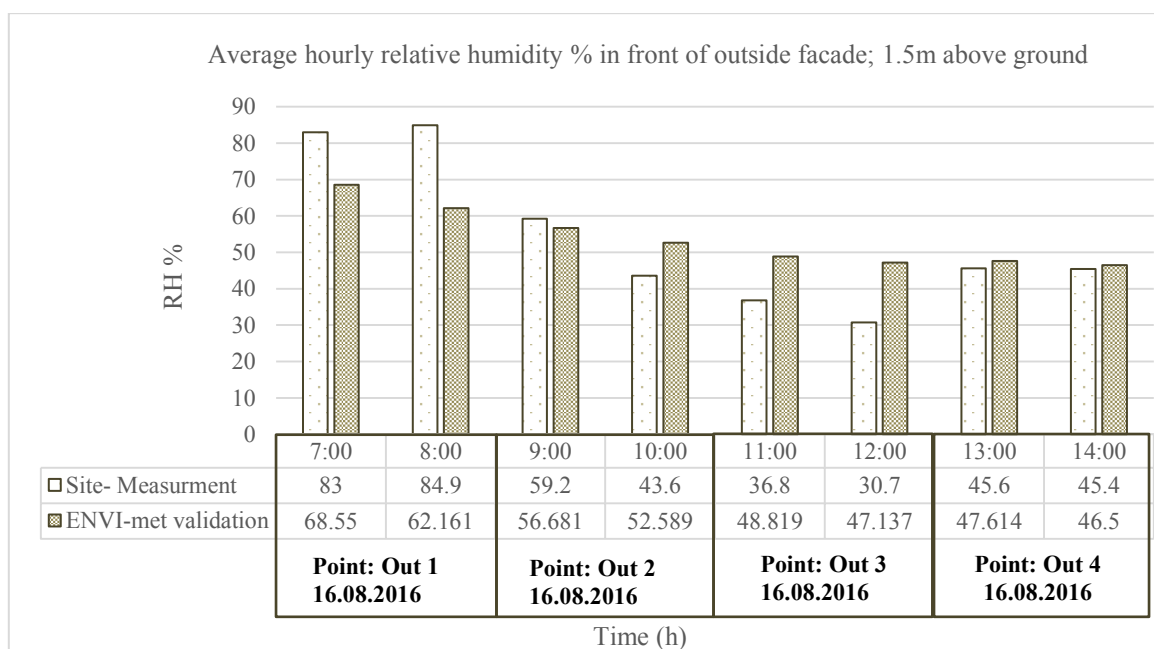


Fig. 16. Comparison of the observed and modeled Relative Humidity at 1.5m above ground, outside the courtyard on August 16, 2016

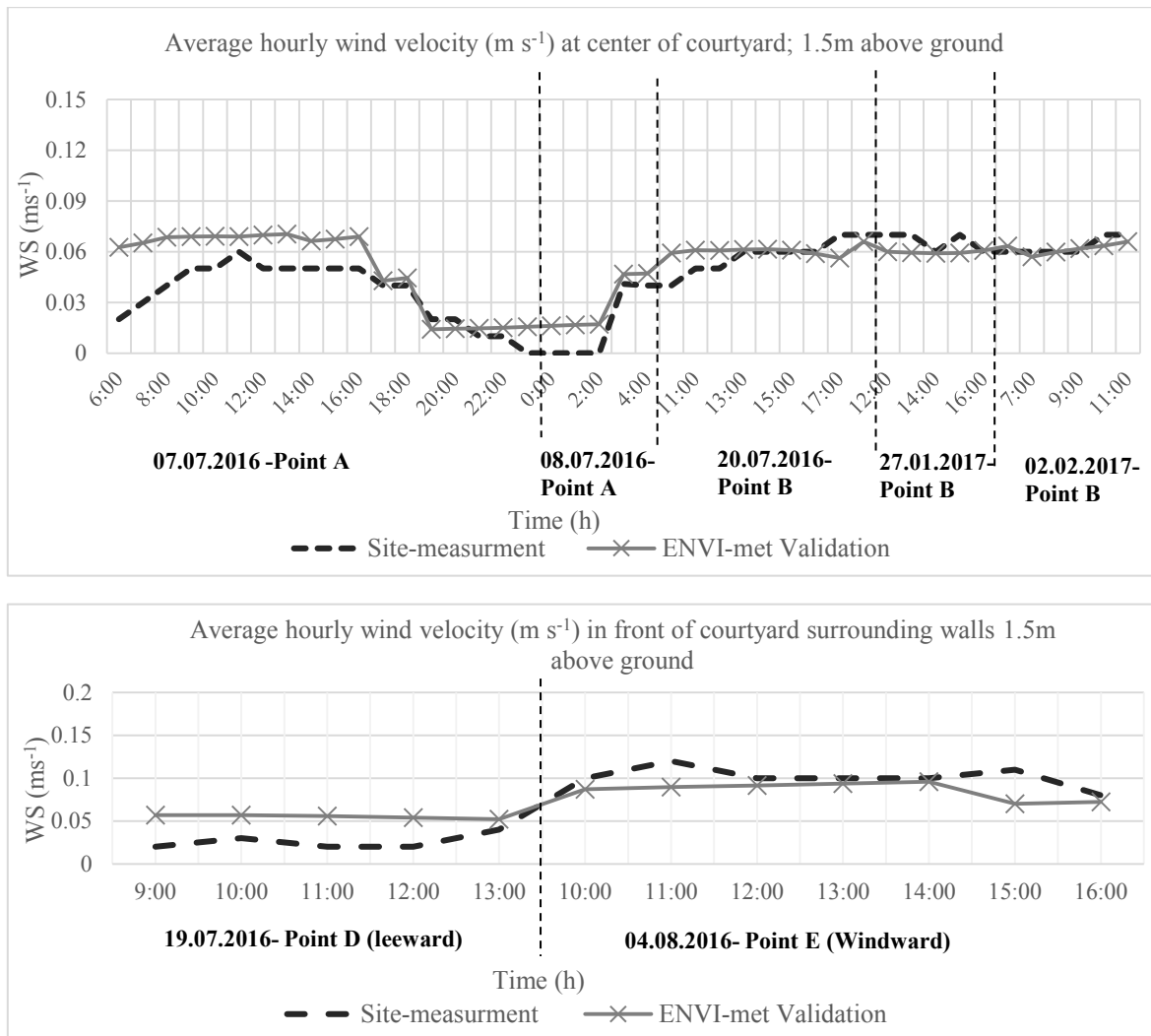


Fig. 17. Comparison of the observed and modeled Wind Velocity ($m s^{-1}$) at 1.5m above ground. The dotted line shows the measured average hourly air temperature at the IMUK meteorological weather station.

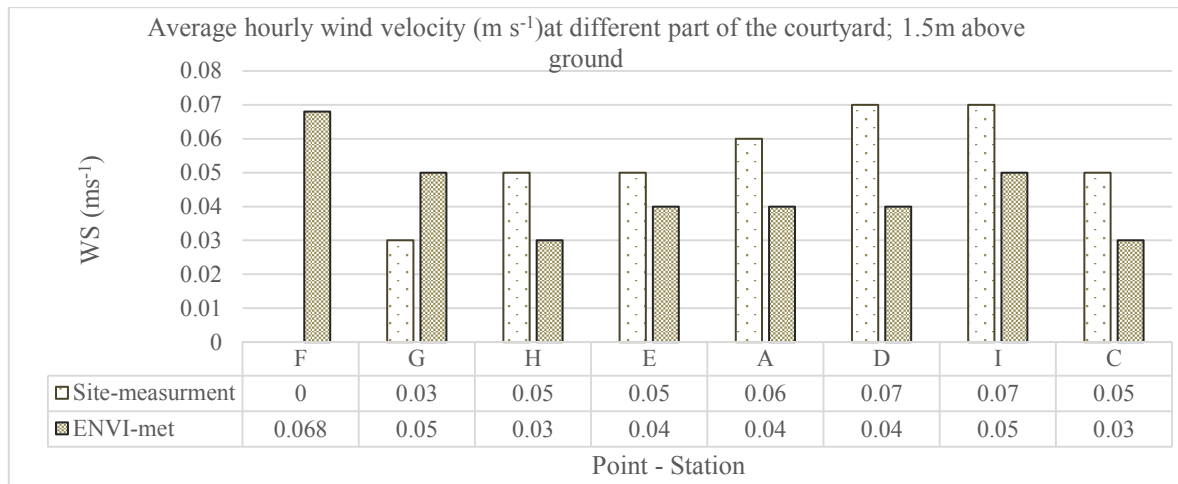


Fig. 18. Comparison of the observed and modeled Wind Speed at 1.5m above ground, for the different part of the courtyard on August 17, 2016

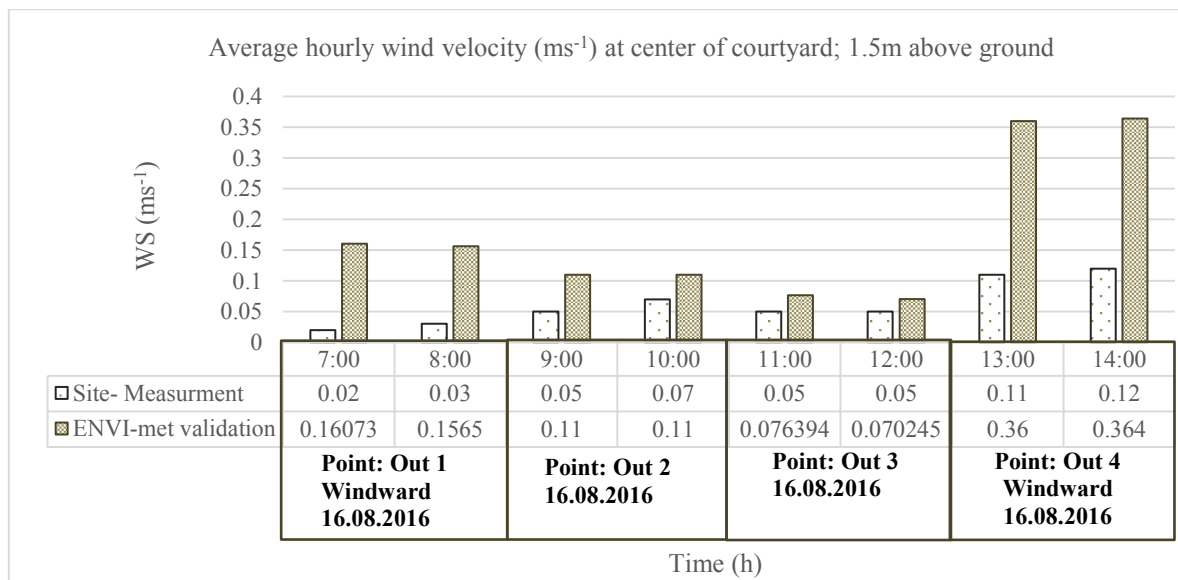


Fig. 19. Comparison of the observed and modeled Wind Speed at 1.5m above ground, outside the courtyard on August 16, 2016

In order to evaluate the software and its capacity to predict the courtyard thermal condition, the mean radiant temperature (MRT) at a height of 1.5m above ground for all measured points is also calculated based on the recorded values for black globe temperature. Testo 480, with 150mm globe thermometer and the emissivity of the globe $\epsilon = 0.95$, measures the radiation temperature according to following formula (DIN, 2002; “Testo 480 · Climate measuring instrument-Instruction manual,” 2016) :

$$T_{\text{mrt}} = [(T_g + 273)^4 + 2.5 \times 10^8 \times V a^{0.6} \times (T_g - T_a)]^{1/4} - 273 \quad (3)$$

Where T_g is recorded black globe temperature ($^{\circ}\text{C}$), V_a is Air velocity (m s^{-1}) and T_a is Air temperature ($^{\circ}\text{C}$).

While considering the results (Fig. 20 – 21), it can be noted that the mean radiant temperature (T_{mrt}) does not show a very good relationship between the measured and modeled values, mainly due to the following reasons:

- 1) Short-wave radiation (SW) is overestimated by the model, whereby simulated T_{mrt} shows higher values than the measured ones (where simulated direct SW radiation is null, the shadow is overestimated).
- 2) The model resolution and cubic grid structure does not correctly account for sun radiation exposure caused by certain urban elements, resulting in inaccuracies of the shading.
- 3) Incoming solar radiation is absorbed in the atmosphere by clouds, water vapor, dust, and ozone (Geiger, Aron, & Todhunter, 2003), but due to this information is usually not available, ENVI-met simplifies the calculation by only taking the effects of water vapor into account (M. Bruse, 1999; Simon, 2016).
- 4) The measurement device is not appropriate for outside spaces: in this research, the MRT is estimated by using 150mm copper globe thermometers, which were originally developed for measuring MRT indoors. A number of studies (Erell et al., 2012) have refined the use of this tool for outdoor application, replacing the standard 150 mm blackened hollow copper sphere with smaller ($\sim 38\text{mm}$), lighter variations to reduce its response time when exposed to rapidly-changing outdoor conditions.

The significant overestimation of the MRT ($\sim 25^{\circ}\text{C}$) is during the morning periods with a clear-sky day. At midday, the mean radiant temperature deviation for points with direct solar access is $\Delta T_{\text{mrt}} \sim + 10^{\circ}\text{C}$ and for shaded areas is $\Delta T_{\text{mrt}} \sim + 8^{\circ}\text{C}$.

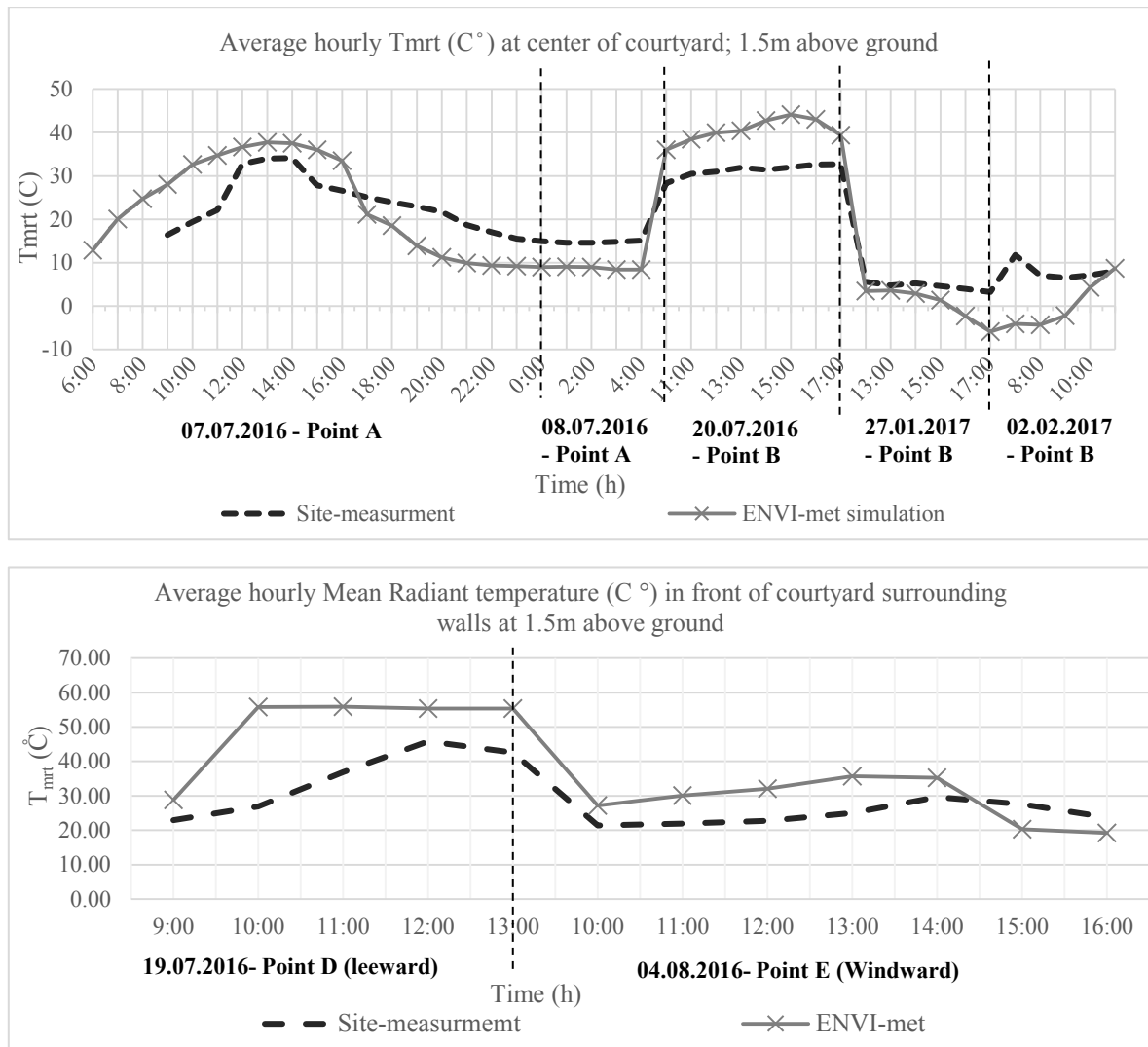


Fig. 20. Comparison of the observed and modeled Mean Radiant Temperature (T_{mrt}) at 1.5m above ground, the dotted line shows the measured average hourly air temperature at the IMUK meteorological weather station.

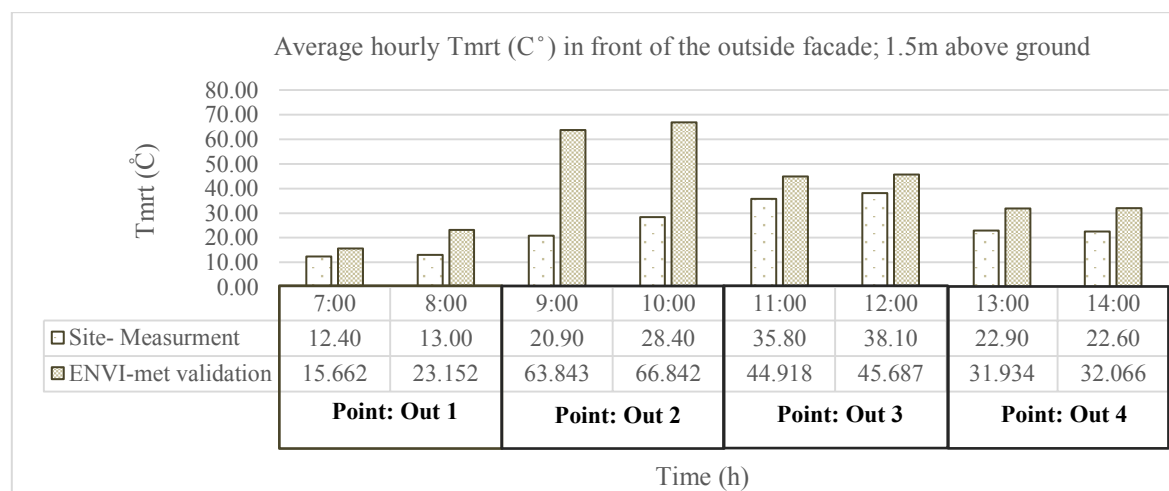


Fig. 21. Comparison of the observed and modeled Mean Radiant Temperature at 1.5m above ground, outside the courtyard on August 16, 2016.

5. Discussion

Analysis and spread of the concept of the isolated-courtyard spaces need accurate simulation models, which can reliably predict this space special microclimate. This paper focuses on the numerical modeling of courtyard semi-closed spaces with ENVI-met software and model validation.

The comparison between measurement values and the simulations performed with ENVI-met (4.0) shows that the model output fully depends on the quality of the data used for creating the boundary conditions of the model (Force LBC). In this research, the 1D input profiles for air temperature, specific humidity and wind speed and direction are derived from the recorded data at Herrenhausen weather station. The low distance (~ 80m) between the station and case study significantly reduced the errors. Furthermore, through an accurate choice of model input parameters together with a proper selection of the computational domain sizes and lateral boundary conditions and the analysis of the time step sensitivity, it can be considered satisfying with output data for narrow-courtyard spaces that are close to the values experimentally measured.

The systematical calibration process for the ENVI-met model based on the root mean square error (RMSE) in this project (Table 9) shows that the calibrated ENVI-met model predictions inside the courtyard agreed with all validation criteria and accurately represent the real environment, except for solar irradiance on the sun- exposed areas, which was higher than on-site measured values. The conclusions of the analysis are summarized as follows:

- Considering the results for air temperature and relative humidity shows a good agreement between simulated and measured data for shaded areas, nights and during cloudy hours in summer and winter.
- The measured wind speed inside the courtyard – which is not affected by direct wind flow – fits the observed values. However, for outside the courtyard, the model results show large discrepancies between measurements and simulations for turbulent in front of the facade, which are directly exposed to forces of wind.
- On sun exposed areas inaccuracies of the shading due to model resolution lead to the major difference in mean radiant temperature between the modeled and measurement values.

Even so, this study provides increased confidence that the microclimate model ENVI-met for a semi-closed courtyard space ($H_c/W \geq 1$) can be utilized as the reliable model for further research steps.

Table 9. The root mean squared error for selected variables at measured points in the model

Validation criteria	Precision of required equipment	Center of the courtyard (point B)	Inside courtyard leeward (Point D)	Inside courtyard Windward (Point E)	Out 1	Out 2	Out 3	Out 4
Air temperature	± 0.5 °C	0.73	3.55	2.52	4.04	3.65	6.43	0.48
Relative humidity	$\pm 3\%$	3.34	10.00	7.54	19.05	5.45	14.40	1.62
Air velocity	± 0.05 (m s ⁻¹)	0.010	0.03	0.02	0.13	0.05	0.02	0.24
Mean irradiative temperature	± 1 °C 21.142	8.44	2.65	2.19	7.54	40.75	8.39	9.25

References

- Acero, J. A., & Herranz-Pascual, K. (2015). A comparison of thermal comfort conditions in four urban spaces by means of measurements and modelling techniques. *Building and Environment*, 93, 245–257. <https://doi.org/10.1016/j.buildenv.2015.06.028>
- Alchapar, N. L., & Correa, E. N. (2016). The use of reflective materials as a strategy for urban

- cooling in an arid “OASIS” city. *Sustainable Cities and Society*, 27, 1–14. <https://doi.org/http://dx.doi.org/10.1016/j.scs.2016.08.015>
- Ali-Toudert, F., & Mayer, H. (2007). Effects of asymmetry, galleries, overhanging façades and vegetation on thermal comfort in urban street canyons. *Solar Energy*, 81(6), 742–754. <https://doi.org/https://doi.org/10.1016/j.solener.2006.10.007>
- ALVAREZ, S., SANCHEZ, F., & MOLINA, J. L. (1998). Air flow pattern at courtyards. *Environmentally Freindly Cities*, 503–506. Retrieved from http://www.aivc.org/sites/default/files/airbase_11854.pdf
- Ambrosini, D., Galli, G., Mancini, B., Nardi, I., & Sfarra, S. (2014). Evaluating mitigation effects of urban heat islands in a historical small center with the ENVI-Met?? climate model. *Sustainability (Switzerland)*, 6(10), 7013–7029. <https://doi.org/10.3390/su6107013>
- ASHRAE. (1992). *Psychrometric Chart 7 Normal Temperature - High Altitude (2250 m - 0 to 50 degrees C db) 11 x 17 (SI). 50-sheet pad.*
- BALDWIN, B., & LOMAX, H. (1978). Thin-layer approximation and algebraic model for separated turbulentflows. In *16th Aerospace Sciences Meeting*. American Institute of Aeronautics and Astronautics. <https://doi.org/doi:10.2514/6.1978-257>
- Barakat, A., Ayad, H., & El-Sayed, Z. (2017). Urban design in favor of human thermal comfort for hot arid climate using advanced simulation methods. *Alexandria Engineering Journal*. <https://doi.org/https://doi.org/10.1016/j.aej.2017.04.008>
- Bennett, N. D., Croke, B. F. W., Guariso, G., Guillaume, J. H. A., Hamilton, S. H., Jakeman, A. J., ... Andreassian, V. (2013). Characterising performance of environmental models. *Environmental Modelling & Software*, 40, 1–20. <https://doi.org/http://dx.doi.org/10.1016/j.envsoft.2012.09.011>
- Berkovic, S., Yezioro, A., & Bitan, A. (2012). Study of thermal comfort in courtyards in a hot arid climate. *Solar Energy*, 86(5), 1173–1186. <https://doi.org/10.1016/j.solener.2012.01.010>
- Bruse, M. (1999). *Die Auswirkungen kleinskaliger Umweltgestaltung auf das Mikroklima Michael Bruse aus Essen Bochum*, 1999.
- Bruse, M. (2004). ENVI-met documentation.
- Bruse, M. (2015). ENVI_met. A holistic microclimate model. Retrieved July 5, 2016, from <http://www.model.envi-met.com/hg2e/doku.php?id=kb:start>
- Bruse, M. (2016). ENVI_met. A holistic microclimate model. Retrieved September 1, 2016, from <http://www.model.envi-met.com/hg2e/doku.php?id=intro:modelconept>
- Bruse, M. (2016). ENVI-met 4.0, (Science). ESSEN.
- Bruse, M. . (2016). ENVI_met. A holistic microclimate model . Retrieved September 1, 2016, from <http://www.model.envi-met.com/hg2e/doku.php?id=apps:envimet>
- Chatzidimitriou, A., & Yannas, S. (2017). Street canyon design and improvement potential for

- urban open spaces; the influence of canyon aspect ratio and orientation on microclimate and outdoor comfort. *Sustainable Cities and Society*.
<https://doi.org/https://doi.org/10.1016/j.scs.2017.05.019>
- Collier, C. G. (2006). The impact of urban areas on weather. *Quarterly Journal of the Royal Meteorological Society*, *132*(614), 1–25. <https://doi.org/10.1256/qj.05.199>
- Conry, P., Sharma, A., Potosnak, M. J., Leo, L. S., Bensman, E., Hellmann, J. J., & Fernando, H. J. S. (2015). Chicago's heat island and climate change: Bridging the scales via dynamical downscaling. *Journal of Applied Meteorology and Climatology*, *54*(7), 1430–1448. <https://doi.org/10.1175/JAMC-D-14-0241.1>
- De Ridder, K. ; A., & Acero, J. ; Lauwaet, D.; Lefebvre, W.; Maiheu, B.; Mendizabal, M. (2014). *WP 4: Climate change scenarios for urban agglomerations D4 . 1: Validation of agglomeration-scale climate projections*. RAMSES - Science for cities in transition.
- Defraeye, T., Blocken, B., & Carmeliet, J. (2011). Convective heat transfer coefficients for exterior building surfaces: Existing correlations and CFD modelling. *Energy Conversion and Management*, *52*(1), 512–522. <https://doi.org/http://doi.org/10.1016/j.enconman.2010.07.026>
- Deutscher Wetterdienst. (n.d.). Langjährige Stationsmittelwerte für die Klimareferenzperiode 1981-2010, für aktuellen Standort und Bezugsstandort. Retrieved June 12, 2017, from <ftp://ftp-cdc.dwd.de/pub/CDC/>
- DIN. (2002). *DIN EN ISO 7726* (Deutsches). Berlin.
- DIN. (2010a). *DIN 18516-1*. Berlin.
- DIN. (2010b). *DIN EN ISO 10456*. Berlin.
- DIN. (2017). *DIN 4108-4*. Berlin.
- Duarte, D. H. S., Shinzato, P., Gusson, C. dos S., & Alves, C. A. (2015). The impact of vegetation on urban microclimate to counterbalance built density in a subtropical changing climate. *Urban Climate*. <https://doi.org/10.1016/j.uclim.2015.09.006>
- Edwards, B., Sibley, M., Land, P., & Hakmi, M. (2006). *Courtyard Housing: Past, Present and Future*. Taylor & Francis.
- Elnabawi, M. H., Hamza, N., & Dudek, S. (2015). Numerical modelling evaluation for the microclimate of an outdoor urban form in Cairo, Egypt. *HBRC Journal*, *11*(2), 246–251. <https://doi.org/10.1016/j.hbrj.2014.03.004>
- ENVI-met. (2013a). ENVI_met. A holistic microclimate model. Retrieved August 1, 2016, from <http://www.model.envi-met.com/hg2e/doku.php?id=kb:modelheight>
- ENVI-met. (2013b). ENVI_met. A holistic microclimate model. Retrieved June 15, 2017, from <http://www.envi-met.info/hg2e/doku.php?id=kb:lbc>
- ENVI-met. (2013c). ENVI_met. A holistic microclimate model. Retrieved June 5, 2016, from <http://www.model.envi->

- met.com/hg2e/doku.php?id=basic_settings&s[]=simulation&s[]=time
- ENVI-met EagleEye. (2016). ESSEN.
- ENVI-met SPACES. (2016). ESSEN.
- Erell, E., Pearlmutter, D., & Williamson, T. (2012). *Urban Microclimate: Designing the Spaces Between Buildings*. Taylor & Francis. Retrieved from <https://books.google.de/books?id=LHwnWaYfPNkC>
- Fabbri, K., Di Nunzio, A., Gaspari, J., Antonini, E., & Boeri, A. (2017). Outdoor Comfort: The ENVI-BUG tool to Evaluate PMV Values Output Comfort Point by Point. *Energy Procedia*, *111*, 510–519. <https://doi.org/https://doi.org/10.1016/j.egypro.2017.03.213>
- Fahmy, M., & Sharples, S. (2009). On the development of an urban passive thermal comfort system in Cairo, Egypt. *Building and Environment*, *44*(9), 1907–1916. <https://doi.org/https://doi.org/10.1016/j.buildenv.2009.01.010>
- Farahat, A. M. (1980). *Energy, Environment and New Communities in Hot-arid Areas of the Middle East*. Virginia Polytechnic Institute and State University. Retrieved from <https://books.google.de/books?id=N8lgnQEACAAJ>
- Franke, J., Hellsten, A., Schlünzen, H., Carissimo, B. (2007). *Best Practice Guideline for the CFD Simulation of Flows in the Urban Environment*. Brussel, Belgium. <https://doi.org/ISBN:3-00-018312-4>
- Geiger, R., Aron, R. H., & Todhunter, P. (2003). *The Climate Near the Ground*. Rowman & Littlefield. Retrieved from <https://books.google.de/books?id=KaJHBv9FbYIC>
- Green Building Factory. (2014). Innovation in technology. Retrieved March 14, 2017, from <http://www.greenbuildingfactory.com/en/innovations/ceramic-ventilated-fa-ade>
- Gusson, C. S., & Duarte, D. H. S. (2016). Effects of Built Density and Urban Morphology on Urban Microclimate - Calibration of the Model ENVI-met V4 for the Subtropical Sao Paulo, Brazil. *Procedia Engineering*, *169*, 2–10. <https://doi.org/http://dx.doi.org/10.1016/j.proeng.2016.10.001>
- Hall, D. J., Walker, S., & Spanton, A. M. (1999). Dispersion from courtyards and other enclosed spaces. *Atmospheric Environment*, *33*(8), 1187–1203. [https://doi.org/10.1016/S1352-2310\(98\)00284-2](https://doi.org/10.1016/S1352-2310(98)00284-2)
- Hedquist, B. C., & Brazel, A. J. (2014). Seasonal variability of temperatures and outdoor human comfort in Phoenix, Arizona, U.S.A. *Building and Environment*, *72*, 377–388. <https://doi.org/10.1016/j.buildenv.2013.11.018>
- Hofman, J., & Samson, R. (2014). Biomagnetic monitoring as a validation tool for local air quality models: A case study for an urban street canyon. *Environment International*, *70*, 50–61. <https://doi.org/http://dx.doi.org/10.1016/j.envint.2014.05.007>
- Huttner, S. (2012). Further development and application of the 3D microclimate simulation ENVI-

- met. Mainz: Johannes Gutenberg-Universität in Mainz, 147. Retrieved from <http://ubm.opus.hbz-nrw.de/volltexte/2012/3112/>
- IMUK. (2016). Weather & Climate > Measurement Data. Retrieved January 1, 2017, from <https://www.muk.uni-hannover.de/258.html?&L=1>
- Indian Space Research Organisation. Dept. (1994). *Scientific Results from ISRO Geosphere Biosphere Programme 1994*. Indian Space Research Organisation, Department of Space. Retrieved from <https://books.google.de/books?id=xF4RAQAIAAJ>
- Jamei, E., & Rajagopalan, P. (2017). Urban development and pedestrian thermal comfort in Melbourne. *Solar Energy*, *144*, 681–698. <https://doi.org/https://doi.org/10.1016/j.solener.2017.01.023>
- Jänicke, B., Meier, F., Hoelscher, M.-T., & Scherer, D. (2015). Evaluating the Effects of Façade Greening on Human Bioclimate in a Complex Urban Environment. *Advances in Meteorology*, *2015*, 1–15. <https://doi.org/http://dx.doi.org/10.1155/2015/747259>
- Kato, M., Launder, B. (1993). Three-dimensional modelling and heat-loss effects on turbulent flow in a nominally two-dimensional cavity. *Heat and Fluid Flow*, *16*, 171–177.
- Ketterer, C., & Matzarakis, A. (2014). Human-biometeorological assessment of heat stress reduction by replanning measures in Stuttgart, Germany. *Landscape and Urban Planning*, *122*, 78–88. <https://doi.org/http://dx.doi.org/10.1016/j.landurbplan.2013.11.003>
- Kong, F., Sun, C., Liu, F., Yin, H., Jiang, F., Pu, Y., ... Dronova, I. (2016). Energy saving potential of fragmented green spaces due to their temperature regulating ecosystem services in the summer. *Applied Energy*, *183*, 1428–1440. <https://doi.org/https://doi.org/10.1016/j.apenergy.2016.09.070>
- Kottke, M., Grieser, J., Beck, C., Rudolf, B., & Rubel, F. (2006). World map of the Köppen-Geiger climate classification updated. *Meteorologische Zeitschrift*, *15*(3), 259–263. <https://doi.org/10.1127/0941-2948/2006/0130>
- Lee, H., Mayer, H., & Chen, L. (2016). Contribution of trees and grasslands to the mitigation of human heat stress in a residential district of Freiburg, Southwest Germany. *Landscape and Urban Planning*, *148*, 37–50. <https://doi.org/10.1016/j.landurbplan.2015.12.004>
- Lu, J., Li, Q., Zeng, L., Chen, J., Liu, G., Li, Y., ... Huang, K. (2017). A micro-climatic study on cooling effect of an urban park in a hot and humid climate. *Sustainable Cities and Society*, *32*, 513–522. <https://doi.org/https://doi.org/10.1016/j.scs.2017.04.017>
- Martinelli, L., & Matzarakis, A. (2017). Influence of height/width proportions on the thermal comfort of courtyard typology for Italian climate zones. *Sustainable Cities and Society*, *29*, 97–106. <https://doi.org/https://doi.org/10.1016/j.scs.2016.12.004>
- Mennerich, I. (2016). *No TitleWettervorhersage in der Schule (1) Wasserdampf und Wolken in der Atmosphäre. Landeshauptstadt Hannover Fachbereich Bibliothek und Schule Schulbiologiezentrum*. Hannover. Retrieved from <http://www.schulbiologiezentrum.info/AH>

- 19.87 Wettervorhersage in der Schule (1).pdf
- Middel, A., Häb, K., Brazel, A. J., Martin, C. A., & Guhathakurta, S. (2014). Impact of urban form and design on mid-afternoon microclimate in Phoenix Local Climate Zones. *Landscape and Urban Planning*, *122*, 16–28. <https://doi.org/10.1016/j.landurbplan.2013.11.004>
- Muhaisen, A. S. (2006). Shading simulation of the courtyard form in different climatic regions. *Building and Environment*, *41*(12), 1731–1741. <https://doi.org/https://doi.org/10.1016/j.buildenv.2005.07.016>
- Muhaisen, A. S., & B Gadi, M. (2006). Shading performance of polygonal courtyard forms. *Building and Environment*, *41*(8), 1050–1059. <https://doi.org/https://doi.org/10.1016/j.buildenv.2005.04.027>
- Nazarian, N., & Kleissl, J. (2015). CFD simulation of an idealized urban environment: Thermal effects of geometrical characteristics and surface materials. *Urban Climate*, *12*, 141–159. <https://doi.org/https://doi.org/10.1016/j.uclim.2015.03.002>
- Noro, M., & Lazzarin, R. (2015). Urban heat island in Padua, Italy: Simulation analysis and mitigation strategies. *Urban Climate*, *14*, Part 2, 187–196. <https://doi.org/http://doi.org/10.1016/j.uclim.2015.04.004>
- Oke, T. R. (1982). The energetic basis of the urban heat island. *Quarterly Journal of the Royal Meteorological Society*, *108*(455), 1–24. <https://doi.org/10.1002/qj.49710845502>
- Paramita, B., & Fukuda, H. (2013). Study on the Affect of Aspect Building Form and Layout Case Study: Honjo Nishi Danchi, Yahatanishi, Kitakyushu-Fukuoka. *Procedia Environmental Sciences*, *17*, 767–774. <https://doi.org/http://dx.doi.org/10.1016/j.proenv.2013.02.094>
- Polyzoides, S., Sherwood, R., & Tice, J. (1992). *Courtyard Housing in Los Angeles*. Princeton Architectural Press.
- Qaid, A., & Ossen, D. R. (2015). Effect of asymmetrical street aspect ratios on microclimates in hot, humid regions. *International Journal of Biometeorology*, *59*(6), 657–677. <https://doi.org/10.1007/s00484-014-0878-5>
- Randhawa, T. S. (1999). *The Indian Courtyard House*. Prakash Books.
- Rojas, J. M., Galán-Marín, C., & Fernández-Nieto, E. D. (2012). Parametric study of thermodynamics in the mediterranean courtyard as a tool for the design of eco-efficient buildings. *Energies*, *5*(7), 2381–2403. <https://doi.org/10.3390/en5072381>
- Salata, F., Golasi, I., de Lieto Vollaro, R., & de Lieto Vollaro, A. (2016). Urban microclimate and outdoor thermal comfort. A proper procedure to fit ENVI-met simulation outputs to experimental data. *Sustainable Cities and Society*, *26*(August), 318–343. <https://doi.org/10.1016/j.scs.2016.07.005>
- Salata, F., Golasi, I., Vollaro, A. de L., & Vollaro, R. de L. (2015). How high albedo and traditional buildings' materials and vegetation affect the quality of urban microclimate. A case study. *Energy and Buildings*, *99*, 32–49.

- <https://doi.org/http://dx.doi.org/10.1016/j.enbuild.2015.04.010>
- Simon, H. (2016). New and Improved Calculation Methods for the, (MICROSCALE MODELS), 233.
- Singh, M., & Laefer, D. F. (2015). Recent Trends and Remaining Limitations in Urban Microclimate Models. *Demography Journal*, 1, 1–12. <https://doi.org/10.2174/2352631901401010001>
- Skelhorn, C., Lindley, S., & Levermore, G. (2014). The impact of vegetation types on air and surface temperatures in a temperate city: A fine scale assessment in Manchester, UK. *Landscape and Urban Planning*, 121, 129–140. <https://doi.org/http://dx.doi.org/10.1016/j.landurbplan.2013.09.012>
- Song, B., & Park, K. (2015). Contribution of greening and high-albedo coatings to improvements in the thermal environment in complex urban areas. *Advances in Meteorology*, 2015, 12–21. <https://doi.org/10.1155/2015/792172>
- Srivanit, M., & Hokao, K. (2013). Evaluating the cooling effects of greening for improving the outdoor thermal environment at an institutional campus in the summer. *Building and Environment*, 66, 158–172. <https://doi.org/10.1016/j.buildenv.2013.04.012>
- Stewart, I. D., & Oke, T. R. (2012). Local climate zones for urban temperature studies. *Bulletin of the American Meteorological Society*, 93(12), 1879–1900. <https://doi.org/10.1175/BAMS-D-11-00019.1>
- Taleghani, M., Sailor, D., & Ban-Weiss, G. A. (2016). Micrometeorological simulations to predict the impacts of heat mitigation strategies on pedestrian thermal comfort in a Los Angeles neighborhood. *Environ. Res. Lett.*, 11(2), 24003. <https://doi.org/10.1088/1748-9326/11/2/024003>
- Taleghani, M., Tenpierik, M., van den Dobbelsteen, A., & Sailor, D. J. (2014a). Heat in courtyards: A validated and calibrated parametric study of heat mitigation strategies for urban courtyards in the Netherlands. *Solar Energy*, 103, 108–124. <https://doi.org/https://doi.org/10.1016/j.solener.2014.01.033>
- Taleghani, M., Tenpierik, M., van den Dobbelsteen, A., & Sailor, D. J. (2014b). Heat mitigation strategies in winter and summer: Field measurements in temperate climates. *Building and Environment*, 81, 309–319. <https://doi.org/https://doi.org/10.1016/j.buildenv.2014.07.010>
- Terjung, W. H., & O'Rourke, P. A. (1980). Simulating the causal elements of urban heat islands. *Boundary-Layer Meteorology*, 19(1), 93–118. <https://doi.org/10.1007/BF00120313>
- Testo 480 · Climate measuring instrument–Instruction manual. (2016). Germany.
- Tominaga, Y., Mochida, A., Murakami, S., & Sawaki, S. (2008). Comparison of various revised k- ϵ models and LES applied to flow around a high-rise building model with 1:1:2 shape placed within the surface boundary layer. *Journal of Wind Engineering and Industrial Aerodynamics*, 96(4), 389–411. <https://doi.org/10.1016/j.jweia.2008.01.004>

- Tominaga, Y., Mochida, A., Yoshie, R., Kataoka, H., Nozu, T., Yoshikawa, M., & Shirasawa, T. (2008). AIJ guidelines for practical applications of CFD to pedestrian wind environment around buildings. *Journal of Wind Engineering and Industrial Aerodynamics*, 96(10), 1749–1761. <https://doi.org/http://dx.doi.org/10.1016/j.jweia.2008.02.058>
- Tsoka, S. (2017). Investigating the Relationship Between Urban Spaces Morphology and Local Microclimate: A Study for Thessaloniki. *Procedia Environmental Sciences*, 38, 674–681. <https://doi.org/https://doi.org/10.1016/j.proenv.2017.03.148>
- Tu, J., Yeoh, G. H., & Liu, C. (2012). *Computational Fluid Dynamics: A Practical Approach*. Butterworth-Heinemann. Retrieved from <https://books.google.de/books?id=IQAc3z-2QYIC>
- VDI-Standard. (2000). *Environmental meteorology - Physical modelling of flow and dispersion processes in the atmospheric boundary layer - Application of wind tunnels*. Berlin. Retrieved from http://www.vdi.eu/nc/guidelines/vdi_3783_blat_12-umweltmeteorologie_physikalische_modellierung_von_stroemungs_und_ausbreitungsvorgaengen_in_der/
- Wang, F., & Liu, Y. (2002). Thermal environment of the courtyard style cave dwelling in winter. *Energy and Buildings*, 34(10), 985–1001. [https://doi.org/10.1016/S0378-7788\(01\)00145-1](https://doi.org/10.1016/S0378-7788(01)00145-1)
- Wanielista, M. P., Kersten, R., & Eaglin, R. (1997). *Hydrology: Water Quantity and Quality Control*. Wiley. Retrieved from <https://books.google.de/books?id=mxsfAQAAIAAJ>
- Weather Spark. (2016). Retrieved August 1, 2016, from <https://weatherspark.com/averages/28636/Hanover-Niedersachsen-Germany>
- Yang, W., Wong, N. H., & Lin, Y. (2015). Thermal Comfort in High-rise Urban Environments in Singapore. *Procedia Engineering*, 121, 2125–2131. <https://doi.org/http://dx.doi.org/10.1016/j.proeng.2015.09.083>
- Yang, X., Zhao, L., Bruse, M., & Meng, Q. (2013). Evaluation of a microclimate model for predicting the thermal behavior of different ground surfaces. *Building and Environment*, 60, 93–104. <https://doi.org/10.1016/j.buildenv.2012.11.008>
- Yaşa, E., & Ok, V. (2014). Evaluation of the effects of courtyard building shapes on solar heat gains and energy efficiency according to different climatic regions. *Energy and Buildings*, 73, 192–199. <https://doi.org/http://dx.doi.org/10.1016/j.enbuild.2013.12.042>
- Yoshie, R., Mochida, A., Tominaga, Y., Kataoka, H., Harimoto, K., Nozu, T., & Shirasawa, T. (2007). Cooperative project for CFD prediction of pedestrian wind environment in the Architectural Institute of Japan. *Journal of Wind Engineering and Industrial Aerodynamics*, 95(9), 1551–1578. <https://doi.org/http://dx.doi.org/10.1016/j.jweia.2007.02.023>

Paper B

Note. Reprinted from “Parametric analysis of influence of courtyard microclimate on diminution of convective heat transfer through building's envelope” by A. Forouzandeh, 2019, Journal of Building Simulation, Volume 12 (Issue 5), page 759–779. Copyright (2020) by Springer Nature. (Appendix 4)

Title	Parametric analysis of influence of courtyard microclimate on diminution of convective heat transfer through building's envelope
Author(s)	Aysan Forouzandeh
Publication outlet	Journal of Building Simulation (Springer)
Publication type	Journal paper
Publication year	2019
Publication status	Published
Volume	12
Issue	5
Pages	759–779
DOI	https://doi.org/10.1007/s12273-019-0528-2
Journal Impact Factor	2.23
Highlights	<ul style="list-style-type: none"> • The courtyard design idea can reduce the convective heat transfer coefficient (CHTC) through the envelopes 15 to 35%. • Increasing the wind speed at 10 m above the ground has a negligible effect on wind speed and CHTC at low levels inside the courtyard. • Among various design parameters, the aspect ratio has a great effect on wind speed and CHTC inside the courtyard.

Parametric analysis of influence of courtyard microclimate on diminution of convective heat transfer through building's envelope

Abstract

The growing trend of using glass façade and the low thermal resistance of this material, has increased the importance of environmental loads on heat loss through the building's envelope. In this regards, creating microclimate spaces between buildings acts as a shelter against wind and sun, and thus convective and radiative heat transfer.

In this research, computational fluid dynamics microclimate software ENVI-met has been used to consider the relationship between optimum courtyard forms in decreasing the convective heat transfer coefficient (CHTC). A simple linear correlation was used to calculate the h_c ($\text{W m}^{-2} \text{K}^{-1}$) based on the wind speed (WS) near the façade within the courtyard.

The outcome of the research reveals that the microclimate of the courtyard, particularly for the strong ambient Winds (U_{10}), can diminish the CHTC in comparison with exposed surfaces. Moreover, among various design alternatives, the aspect ratio has a significant impact on WS and CHTC. It was observed that, for $U_{10} = 2.3$ (m s^{-1}), as aspect ratio (H/W) increases from 0.67 to 3.67, the average surface WS, up to the middle floor, on the windward and leeward façade inside the courtyard, located in Hanover, reduces by about 75%. This suggests that an appropriate selection of the courtyard geometry will help passively reduce heating load and let designers use less thickly insulated walls.

Keywords: Courtyard microclimate, Holistic microclimate simulation, Wind speed near the facade, Exterior convective heat transfer coefficient

Nomenclature			
α_s	Solar absorptance of the surface, dimensionless	Q_E	The turbulence induced by vegetation, ($m^2 s^{-2}$)
CFD	Computational fluid dynamics	Q_ϵ	The accelerated cascade of turbulence energy from large scales to smaller ones near plant foliage, ($m^2 s^{-2}$)
CHTC	Convective heat transfer coefficient, ($W m^{-2} K^{-1}$)	t	Time, s
$c_1; c_2 c_3$	Empiric constants, taken from (Launder & Spalding, 1974)	T_a	Air temperature, °C
D	Depth of the building, m	T_o	External air temperature, K
E	Local turbulent energy, ($m^2 s^{-2}$)	T_s	External surface temperatures, K
G	Total solar irradiance incident upon the surface, ($W m^{-2}$)	Th	The production and dissipation of turbulent energy caused by thermal stratification (buoyancy production), ($m^2 s^{-2}$)
g	Gravitational acceleration, ($m s^{-2}$)	U_{10}	Wind speed at 10m above the ground, ($m s^{-1}$)
H	Height of the courtyard, m	$u_i = \{u, v, w\}$	Wind velocity vectors, ($m s^{-1}$)
h_c	Convective heat transfer coefficient, ($W m^{-2} K^{-1}$)	v	Wind speed in front of the wall/roof element, ($m s^{-1}$)
$K_E, K\epsilon$	Turbulent and dissipation kinetic energy, ($m^2 s^{-2}$)	W	Width of the courtyard, m
L	Total long wave irradiance incident upon the surface, ($W m^{-2}$)	WS	Wind Speed, ($m s^{-1}$)
LE	The latent heat flux into the atmosphere due to the evaporation, L is the specific latent heat of evaporation, units ($J kg^{-1}$) and E is the evaporation rate, with units ($kg m^{-2} s^{-1}$)	WW	Windward
		$x_i = \{x, y, z\}$	Cartesian co-ordinates
LES	Large Eddy Simulation	y^+	Non-dimensional distance able to characterize the influences in the wall-adjacent cells
LW	Leeward	Z_0	Roughness length, m
Pr	Production and dissipation of turbulent energy caused by wind shearing, ($m^2 s^{-2}$)	<i>Greek letter</i>	
q	Net heat flow from or into the surface, $W m^{-2}$	ϵ	Turbulence dissipation ratio, ($m^2 s^{-3}$)

RH	Relative Humidity, %	σ	Stefan- Boltzmann constant = $5.6697 \times 10^{-8} (Wm^{-2}K^{-4})$
RANS	Reynolds-averaged Navier–Stokes	ε	Long-wave emittance of the surface (assumed equal to the long wave absorptance), dimensionless
Ri _b	Bulk Richardson Number, dimensionless	$\Delta\theta$	Temperature difference between wall and its surrounding, K
RMSE	Root mean square error	$\Delta\omega$	Distance between the surface and the first grid of air next to it, m

1. Introduction

The term ‘building envelope’ specifies the building components that surround the conditioned spaces, and thermal energy, depending on the inside-outside temperature difference, is transferred to or from the outdoor environment through it (Turner & Doty, 2013). Therefore, thermal control and understanding the mechanism of the heat transfer and the temperature distribution through building envelopes are important for assessing sustainable solutions for low energy consumption buildings (Straube, 2011).

The net sensible and latent energy balance at the external surface of the building can be expressed as:

$$q + \alpha_s G + \varepsilon L = \varepsilon \sigma T_s^4 + h_c (T_s - T_o) + LE \quad (1)$$

Accordingly, the heat transfer between the external surfaces of the building and its surroundings is a combination of conduction, convection, radiation and evaporation or condensation of water at the outside façade (DIN, 2003a; Turner & Doty, 2013). Therefore, increasing the mass and surface resistance of the system can reduce heat transfer through it. The first one can be improved by increasing the thermal properties of the exterior wall’s material (Long & Ye, 2016) and the second one requires sustainable designs with few exterior surfaces (Loukaidou, Michopoulos, & Zachariadis, 2017) and thermal bridge locations (Dumitrescu, Baran, & Pescaru, 2017), along with the use of climate control shields (Mauree, Coccolo, Kaempf, & Scartezzini, 2017). These obstacles restrict the solar radiation (MONTAVON, 2010) and wind (Azizi & Javanmardi, 2017), reduce the convective ($q_c = h_c (T_s - T_o)$) and irradiative ($q_{1-out} = \varepsilon \sigma T_s^4$) heat transfer (Erell et al., 2012). Therefore, the energy consumption of buildings does not depend only on the building’s material, and is very influenced by its geometry and surrounding microclimate (de la Flor & Domínguez, 2004; Grobman & Elimelech, 2016).

The convective heat losses are usually 2 – 7 times much larger than the radiative losses at low temperatures during the winter (Davies, 2004; Defraeye & Carmeliet, 2010; DIN, 2015; Loveday & Taki, 1998; Wen Yang, Zhu, & Liu, 2017). This parameter is more important, especially if the exterior surface is composed of materials with a relatively low thermal resistance (e.g. glass). Yang et al. (Wen Yang et al., 2017) found that when the h_c of the exterior surface increased from 10 to 50 ($\text{W m}^{-2} \text{K}^{-1}$), the heat transfer coefficient of the single glass wall increased by 61.5%, while this parameter is 8.2% for the heavy brick-concrete structure. Likewise, the consideration done by the Energy and Resources Institute et al. (Energy and Resources Institute, Institut Català d'Energia, & Asia Urbs Programme, 2004) indicates that the thermal transmittance of the single-glazed window increases by about 30% under severe exposure (open countryside) compared with sheltered conditions (urban location).

The heat loss through convective depends on two main factors, including the WS (Defraeye et al., 2011; Mirsadeghi, Cóstola, Blocken, & Hensen, 2013; Murakami, 1990; Yoshie et al., 2007) and the surface-to-air temperature differences (Mirsadeghi et al., 2013; Murakami, 1990; Yoshie et al., 2007). Since with free convection (by warming or cooling of the air) the h_c is in the range 3 to 10 ($\text{W m}^{-2} \text{K}^{-1}$) but with forced convection (by wind) this value is in the range 10 to 100 ($\text{W m}^{-2} \text{K}^{-1}$), it can be assumed that the external CHTC mostly depends on the WS distribution close to the walls (Bouyer, Inard, & Musy, 2011; Defraeye et al., 2011; Aya Hagishima, Tanimoto, & Narita, 2005; Y. Liu & Harris, 2007; Sharples, 1984; J. Xie, Cui, Liu, Wang, & Zhang, 2017; L. Zhang, Zhang, Zhao, & Chen, 2004). Therefore, improving the airflow and WS in urban microclimates can be instrumental for reducing the heat loss through envelopes.

A courtyard pattern is one of the traditional methods for optimization of the building form in relation to the external climate. The geometrical shape of the courtyard – which is isolated through the interior façade of buildings – generates a particular microclimate and a shield zone between the inside and the building outside, and provides an effective climate control system. Rodríguez- Algeciras (Rodríguez-Algeciras, Tablada, Chaos-Yeras, De la Paz, & Matzarakis, 2018) summarizes the results of previous studies on the effect of courtyard configuration on outdoor thermal conditions in various climates. Based on the findings, the courtyard's special form controls the insolation (among others (Al-Hafith et al., 2017; Berkovic et al., 2012; Ghaffarianhoseini, Berardi, & Ghaffarianhoseini, 2015; Muhaisen & Gadi, 2006; Rodríguez-Algeciras et al., 2018; Soflaei, Shokouhian, Abraveshdar, & Alipour, 2017; Mohammad Taleghani et al., 2014a)) and flow pattern (among others (Almhafdy et al., 2015; ALVAREZ et al., 1998; Hall et al., 1999; Micallef et al., 2016; Rojas et al., 2012; TABLADA et al., 2005)). This space has a great effect on reducing the WS and, consequently, CHTC throughout the envelopes through reducing the

building's edge, detachment or reattachment (Sharples, 1984) and the surface temperature difference with the surrounding air (Erell et al., 2012). Table 1 summarizes the average WS inside the semi-enclosed spaces, which has been measured in the past through various studies.

The measurements show that the WS inside the courtyard is 0.00 – 0.36 of the WS at 10m above ground (U_{10}). This ratio is affected by the configuration of the courtyard and design parameters, including: (1) aspect ratio (Micallef et al., 2016; TABLADA et al., 2005); (2) orientation relative to the ambient wind direction (P Moonen, Dorer, & Carmeliet, 2011); (3) step-up and step-down notch (Assimakopoulos, ApSimon, & Moussiopoulos, 2003; Chew, Nazarian, & Norford, 2017); (4) courtyard enclosure's depth (Hall et al., 1999); (5) surrounding building's roof shape (Badas, Ferrari, Garau, & Querzoli, 2017; Eliasson, Offerle, Grimmond, & Lindqvist, 2006; Louka, Belcher, & Harrison, 1998, 2000; Yassin, 2011); (6) courtyards' ground floor plan (Grobman & Elimelech, 2016); (7) the presence of openings in the walls (Hall et al., 1999) and (8) amount of surface exposed to solar radiation (Sini, Anquetin, & Mestayer, 1996; X. Xie, Huang, Wang, & Xie, 2005).

Despite the vast amount of studies conducted to consider the effect of courtyard configuration on flow pattern and WS, the impact of the courtyard space on reducing the WS near the façade and the CHTC had not been applied in heat load calculation and the most building energy simulation standards use the same value for h_c inside and outside the courtyard. Therefore, in this research, the parametric analysis is applied to determine the percentage diminution of surface CHTC inside the courtyard semi-closed spaces in comparison with the exposed area for various design alternatives.

In the light of above, this paper is structured in three main parts as follows. Section 2 provides and summarizes a detailed description about studied geometry and simulation procedures. The most important findings are then described in section 3. Section 4 summarizes the main outputs and describes effect of design scenarios on CHTC.

Table 1. Wind speed inside courtyard investigated through previous studies

Author	Location	Design Parameter	Courtyard Geometry	Surrounded building	Wind speed (m s ⁻¹)	Average wind speed inside the courtyard at 1 – 2m high (m s ⁻¹)	Investigation method
Comparative analysis							
Micalled et al. (Micallef et al., 2016)			(9 × 9 m) H/W= 1 H/W = 3 H/W= 5	Surrounded by same buildings repeated in periodic manner	U ₁₀ = 4	0.8 0.08 0.16	CFD – simulation with (ANSYS Fluent, k-ε model)
Tablada et al. (TABLADA et al., 2005)	Havana, Cuba	Aspect Ratio	10.6 length cavity W/H = 2 W/H = 1 W/H = 0.7 W/H = 0.5 W/H = 0.3	Such as underground building	U _{ref} = 8	V/ U _{ref} = -0.1 V/ U _{ref} = -0.1 V/ U _{ref} = -0.05 V/ U _{ref} = -0.02 V/ U _{ref} = -0.01	Wind Tunnel + 2D CFD Simulation
Hall et al. (Hall et al., 1999)	-		100 × 100 mm Range of heights from 10- 100 H/W = 5 – 1.5 H/W = 1 – 0.3 H/W = 0.2 – 0.1	The boundary layer was grown over an array of 10 mm square by 20 mm high roughness elements on a 50 mm spacing	U _{100mm} = 1.5	V/ U _{ref} = 0.00 V/ U _{ref} = -0.12 V/ U _{ref} = -0.01	Wind Tunnel

Table 1. Wind speed inside courtyard investigated through previous studies (continued)

Author	Location	Design Parameter	Courtyard Geometry	Surrounded building	Wind speed (m s ⁻¹)	Average wind speed inside the courtyard at 1 – 2m high (m s ⁻¹)	Investigation method
Alvarez et al. (ALVAREZ et al., 1998)	-		H/W = 0.1	Surrounded by same buildings	U _{ref} = 1	U/ U _{ref} = 0.00 – 0.2	Numerical simulation
			H/W = 0.3			U/ U _{ref} = -0.07 – 0.17	
			H/W = 0.5			U/ U _{ref} = -0.12 – 0.17	
			H/W = 1.0			U/ U _{ref} = -0.07 – 0.17	
			H/W = 1.5			U/ U _{ref} = -0.03 – 0.17	
			H/W = 5.0			U/ U _{ref} = -0.04 – 0.00	
Wong et al. (Wong N H, H, W, C, & W, 2000)	Singapore	Aspect Ratio	Square- shaped	Surrounded by same buildings and open at first floor	U _{ref} = 1 U _{ref} = 1.5 U _{ref} = 2 U _{ref} = 2.5	Minimum wind speed: 0.2	Wind tunnel
			1. Medium high-rise			Minimum wind speed: 0.05	
			2. Height rise				

Table 1. Wind speed inside courtyard investigated through previous studies (continued)

Author	Location	Design Parameter	Courtyard Geometry	Surrounded building	Wind speed (m s ⁻¹)	Average wind speed inside the courtyard at 1 – 2m high (m s ⁻¹)	Investigation method
Rafailidis (Rafailidis,1997)		Roof shape	W/H = 1 ----- W/H = 0.5	Surrounded by: 1. Flat roof 2. Slanted roof	U _{ref} = 5	1. U/ U _{ref} = 0.06 2. U/ U _{ref} = 0.08 ----- 1. U/ U _{ref} = 0.065 2. U/ U _{ref} = 0.1	Wind tunnel
Xie et al. (X. Xie et al., 2005)		Heated surface	Symmetrical street H/W = 1	1. Windward heated 2. Leeward heated 3. Floor heated 4. Non heated	U _{ref} = 2	Windward: 1. -0.35 – 0.1 2. -1 – -0.1 3. -1.1 – -0.1 4. -0.7 – -0.1 ----- Leeward: 1. -0.1 – 0.4 2. 0.1 – 1.0 3. 0.1 – 1.1 4. 0.1 – 0.6	CFD Simulation

Table 1. Wind speed inside courtyard investigated through previous studies (continued)

Author	Location	Design Parameter	Courtyard Geometry	Surrounded building	Wind speed (m s ⁻¹)	Average wind speed inside the courtyard at 1 – 2m high (m s ⁻¹)	Investigation method
Grobman and Elimelech (Grobman & Elimelech, 2016)		Geometry	Rectangle	One side open-cavity	Tangential velocities: 1. V _t = 1 2. V _t = 5 3. V _t = 10	1. 0.11 2. 0.4005 3. 1.98	CFD – simulation with (ANSYS Fluent, k-ε model)
			Triangle			1. 0.043 2. 0.258 3. 1.18	
			Circle			1. 0.377 2. 1.485 3. 2.83	
			Trapezoid			1. 0.086 2. 0.60 3. 0.57	
Single cases							
Ghaffarianhoseini et al. (Ghaffarianhoseini et al., 2015)	Kuala Lumpur, Hot-humid		Square- shaped courtyard (24 × 24 × 4m)	A single story building with the dimension of 60 × 60m (2.5 W)	U ₁₀ = 1.1	0.4	CFD Simulation, ENVI-met

Table 1. Wind speed inside courtyard investigated through previous studies (continued)

Author	Location	Design Parameter	Courtyard Geometry	Surrounded building	Wind speed (m s ⁻¹)	Average wind speed inside the courtyard at 1 – 2m high (m s ⁻¹)	Investigation method
Moonen et al. (P Moonen et al., 2011)	-		(16 × 8 × 16)m L/H = 1/2	Simulated inside large flat plate underground	U ₁₀ = 10	LES = 0.075 RANS = 0.05	CFD Simulation LES + RANS
Almhafdy et al. (Almhafdy et al., 2015)	Malaysia Hot – humid climate		U-shape courtyard (south side open)	Surrounded from north side with 5 floors, east side 4 floors and west side 3 floors.	-	0.3 – 2.7	Site-measurement 23th of October
Rajapaksha et al. (Rajapaksha, Nagai, & Okumiya, 2003)	Colombo, Sri Lanka Warm-Humid		Central rectangular courtyard (3.7 × 8.1 × 4.8)m The courtyard opened to the outdoor through two perpendicular axes passages	Surrounded single story building with pitched roof Building located on a large plat of land with tall trees	U ₁₀ = 1.5	0.08 – 0.1	Site-measurement 12 April- 3 May + CFD – simulation with (α- Flow, k-ε model)

Table 1. Wind speed inside courtyard investigated through previous studies (continued)

Author	Location	Design Parameter	Courtyard Geometry	Surrounded building	Wind speed (m s ⁻¹)	Average wind speed inside the courtyard at 1 – 2m high (m s ⁻¹)	Investigation method
Wang and Liu (F. Wang & Liu, 2002)	Jiang YaoZu, Mizhi	cold weather	(19.5 × 14.40 × 3 – 3.8)m	Surrounded by cave rooms	-	0.4 – 3.6	Site-measurement 15-18 th of January
Forouzandeh (Forouzandeh, 2018)	Hanover, Germany		(6 × 14 × 7 m)	Surrounded two story building with flat roof	U ₁₀ = 0.64 – 3.96	0 – 0.07	Site-measurement July – September January – February

2. Methodology

Comparative parametric simulations for analyzing the effect of different courtyard geometry on WS near the façade and h_c at different height levels have been carried out in this study through, several simulations on the same building while changing only a single design parameter. Considering the existing methods for CHTC measurements of exterior building surfaces – including full-scale experiments, wind-tunnel tests and computational fluid dynamics (CFD) (Defraeye et al., 2011) – the first method is only suitable for existing buildings and the second one is involved with limitations for complex building configurations and model designs. Therefore, for comparative analysis of the surface WS and CHTC for multiplex building forms, a CFD simulation method is more applicable than other techniques.

In recent years, many numerical simulations have been implemented to predict the CHTC at the external building's envelope through common turbulence models, including the Reynolds-averaged Navier–Stokes (RANS) (Defraeye, Blocken, & Carmeliet, 2010; Montazeri & Blocken, 2017) and Large Eddy Simulation (LES) (Hu, Cui, & Zhang, 2018; Jiying Liu, Heidarinejad, Gracik, & Srebric, 2015). Despite the high accuracy of LES methods, this method is more computationally expensive and thus less practical for large-scale environmental studies (Salim, Buccolieri, Chan, & Di Sabatino, 2011; Yoshie et al., 2007).

In addition, previous studies (Emmel, Abadie and Mendes, 2007; Blocken et al., 2009; Defraeye, Blocken and Carmeliet, 2011), mostly were inside generic urban areas under isothermal conditions (Toparlar et al., 2017) and diurnal temperature change on external surfaces due to solar radiation were not taken into account in calculations. Also the buoyancy effect, which is strong inside the courtyard with low wind speed and evidently affects the turbulence and CHTC (Allegrini, Dorer, Defraeye, & Carmeliet, 2012; Battista, 2017), was ignored in most of them.

The numerical value of the h_c is in a complicated way dependent on the temperature, the magnitude and direction of a possible air flow and the nature of the wall surface. In order to consider these parameters and overcome the previous studies shortcuts, in this study the h_c values are estimated by means of a validated three-dimensional microclimate ENVI-met model 4.0 (M. Bruse, 1999, 2004, 2016) inside real 3D urban areas located in Hanover, Germany. ENVI-met is one of the few microscale models that be capable to simulate parallel the various flow patterns inside the courtyard, including the heat transition around and between buildings envelope and vegetation, turbulence and thermal buoyancy.

Therefore, despite existing limitations for grid generation and wall function model (Blocken, Defraeye, Derome, & Carmeliet, 2009), the RANS simulation method used in ENVI-met is the preferred choice to consider daily buoyancy and radiation effects with reasonable simulation time.

Among the various available correlations for CHTC – Reported previously by Palyvos et al. (Palyvos, 2008) and Defraeye et al. (Defraeye et al., 2011) – ENVI-met uses the average wind speed near the façade (v) and calculates the h_c ($W m^{-2} K^{-1}$) according to universal standard DIN EN ISO 6946 (DIN, 2015) by the following equation:

$$h_c = 4 + 4v \quad (2)$$

This equation is accepted and applied, in most countries, to estimate CHTC in calculation of the buildings cooling load and according to the study has done by Colucci et al. (Colucci et al., 2017), it can predict the thermal energy demand of the building as accurate as other available equations.

2.1. Study site and Simulation days

Many previous studies have mainly investigated WS and CHTC, models with single building and did not consider the major urban parameters. However, generally known that wind speed over urban area is less than those open rural areas (Bornstein & Johnson, 1977) and it is more affected by area density, vegetation, building's construction and material. Therefore, in this research, in order to consider the reduction of CHTC inside urban areas, an existing building is selected as a base case. This building includes two regular courtyards and is located in the moderately vegetated urban texture in Hanover, Germany, which is associated with the Cfb category of Köppen's climate classification (Kottek et al., 2006).

The studied courtyard, as part of the Institute of Microbiology's building, is 6×14 m and completely enclosed by 7m tall buildings (on the windward side $(H/W) = 1.17$).

Regular geometric forms, the same facade materials, low urban density and displacement height and low distance from the meteorological station (≈ 80 m) make this case appropriate for parametric studies.

In order to determine the simulation time, the long simulation period is time-cost expensive and is inconceivable. Daily simulation is a good intermediate solution between decreasing time-costs and fitting with the impact of diurnal solar radiation changes.

Due to the high impact of convective heat loss at low temperatures, in this research, numerical simulations were conducted on 26 – 27 January 2017 with the typical atmospheric condition of winter weather in Hanover ($-3.6 \text{ }^\circ\text{C} < T_a < +5.6 \text{ }^\circ\text{C}$, $RH = 66.40\%$

(IMUK, 2016)). The simulations run for 48 h and since the numerical model requires an initialization time, in this case the results of first 24 h were ignored.

2.2. Characteristics of computational model and Studied cases

In order to consider the flow field in depending on wind intensity and thermal stratification, the turbulence closure scheme for 1D and 3D in ENVI-met is set as the “Prognostic 1.5 Order E-Epsilon Closure Model”. This allows the simulation of advection processes along with the incorporation of the influence of the horizontal non-homogeneity (M. Bruse, 1999, 2004, 2016), and is suitable for urban context (Institutes & Toudert, 2005). In the E- ϵ model, stand on the work of Mellor and Yamada (Mellor & Yamada, 1974), two further prognostic variables, including the local turbulence (E) and its dissipation rate (ϵ), are added to the model. Their distribution is given by the prognostic equation set:

$$\begin{aligned} \frac{\delta E}{\delta t} + u_i \frac{\delta E}{\delta x_i} &= K_E \left(\frac{\delta^2 E}{\delta x_i^2} \right) + Pr - Th + Q_E - \epsilon \\ \frac{\delta \epsilon}{\delta t} + u_i \frac{\delta \epsilon}{\delta x_i} &= K_\epsilon \left(\frac{\delta^2 \epsilon}{\delta x_i^2} \right) + c_1 \frac{\epsilon}{E} Pr - c_3 \frac{\epsilon}{E} Th - c_2 \frac{\epsilon^2}{E} + Q_\epsilon \end{aligned} \quad (3)$$

Where the term Pr denotes the production and dissipation of turbulent energy caused by wind shearing and Th considers thermal stratification (buoyancy production), one of common flows inside the courtyard (Rojas et al., 2012). In above equation, the turbulence production and dissipation at vegetation have been determined by Q_E and Q_ϵ (J Liu, Chen, Black, & Novak, 1996; Wilson, 1988).

On the other hand, due to low wind speed, natural convection inside the courtyard is important and has a great effect on the wind speed near the façade. Sini et al. (Sini et al., 1996), Nunez and Oke (Nunez & Oke, 1977), Cermak (Cermak, 1996) and, more recently, Xie et.al (X. Xie et al., 2005) found that in the symmetrical configuration of the canyon, solar heating has a great effect on the airflow pattern when the windward wall is heated.

The exchange coefficients between the ground or building surfaces and the air at the first grid point next to the surface are here decisive in the nature of free convection by the Bulk-Richardson number:

$$Ri_b = \frac{g \Delta\theta \cdot \Delta\omega}{\theta (\Delta u)^2} \quad (4)$$

In this research, twenty courtyard models, with various aspect ratios, orientations, depths of the enclosures and rise-to-run ratio of the pitched roofs were defined inside the three-dimensional computational domain for parametric Analysis (Fig. 1.). The area of courtyards is kept the constant, 6m wide and 14m length, as its surrounding's envelope change height.

The size of the three-dimensional computational domain is determined according to the guideline by Franke et al. (Franke, J., Hellsten, A., Schlünzen, H., Carissimo, 2007) and Tominaga et al. (Yoshihide Tominaga et al., 2008), where the lateral size of the domain is adjusted at least five times higher than the highest building and the height of the defined model is at least to ten times the height of the tallest structure. In the horizontal direction, a mesh of 81×81 grids was selected, with the resolution of 2m. 9 nesting grids were set for the area surrounding the main model for the reason of numerical stability. In the vertical direction, varying grid sizes with a 1 m base height were used ($y^+ \approx 200$, where a turbulent effect dominates). For having enough height for the model domain, telescoping grids were used for the space above 12m with a telescoping factor of 15%. Since the height of the computational domain has a significant influence on the airflow pattern in the courtyard (Forouzandeh, 2018) a large height ($\sim 276.64\text{m}$) with 39 grids is suggested here.

In the case of roof pitches, the model computational domain is shaped with $129 \times 129 \times 34 \text{ m}^3$ cells and 10 nesting grids. Due to ENVI-met limitations in the modeling pitched roofs, the slopes are resolved in fine steps and a small possible grid resolutions of 1, 1, 0.6 m are defined, in order to avoid the sharp edges. In this case, the models are rotated 12 (deg) out of grid north, which was considered by the adjustment of the wind direction.

The three-dimensional core model, includes a number of cells which represent different objects such as buildings, vegetation, soil or atmosphere. Accordingly, the radiation fluxes are calculated based on the cloud sky condition and modified for each cell inside the model by the shading from buildings and plants. Vegetation in ENVI-met is represented by clusters of cell having a leaf area density, and the effects of these cell clusters on the wind field and the radiation are considered (Simon, 2016).

The hourly meteorological data from the IMUK weather station is used to generate the forcing air temperature and relative humidity for the simulation and the variation of hourly global and diffuse radiation is set with cloud cover and solar adjust factor.

According to Figure 2, the 1D boundary model with its horizontally homogeneous vertical profiles ($z_0 = 0.1\text{m}$, correspond to the urban center with average surrounded building elevation of 8 m) is used to provide data on the borders of the 3D model. Inside the 3D model all the exterior walls and ground surface are specified as no-slip boundaries. The vertical motions, at the top boundary, are assumed to be zero (close boundary condition)

and due to the structure of the neighborhoods, which is similar to the studied case and based on the model validation results (Forouzandeh, 2018) the cyclic lateral boundary condition is set for turbulent inflow boundaries. In addition, to considering the stratification effect very small time step – steady state – is used for flow. Table 2 describes the fundamental input parameters into the ENVI-met model.

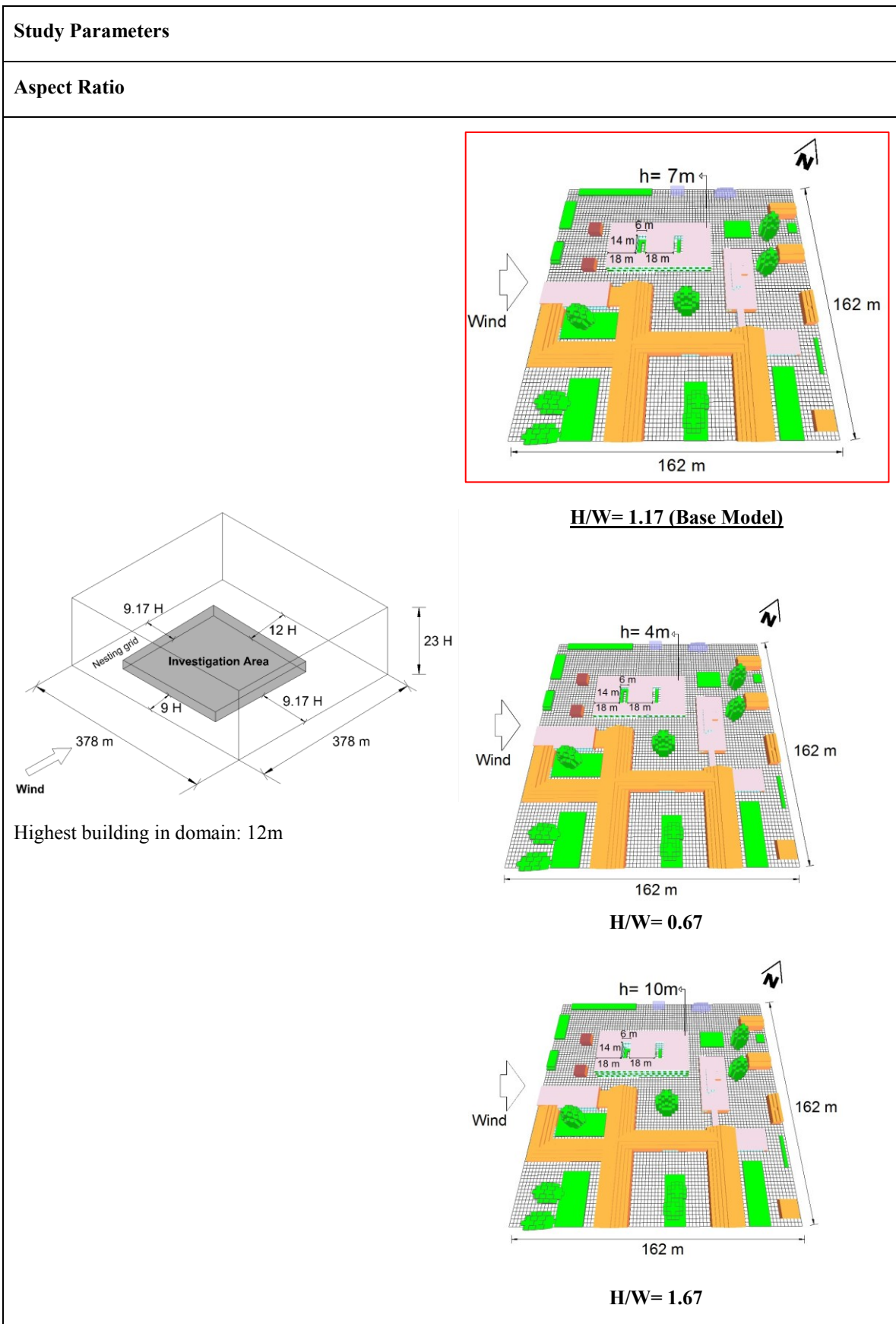


Fig. 1. Study cases

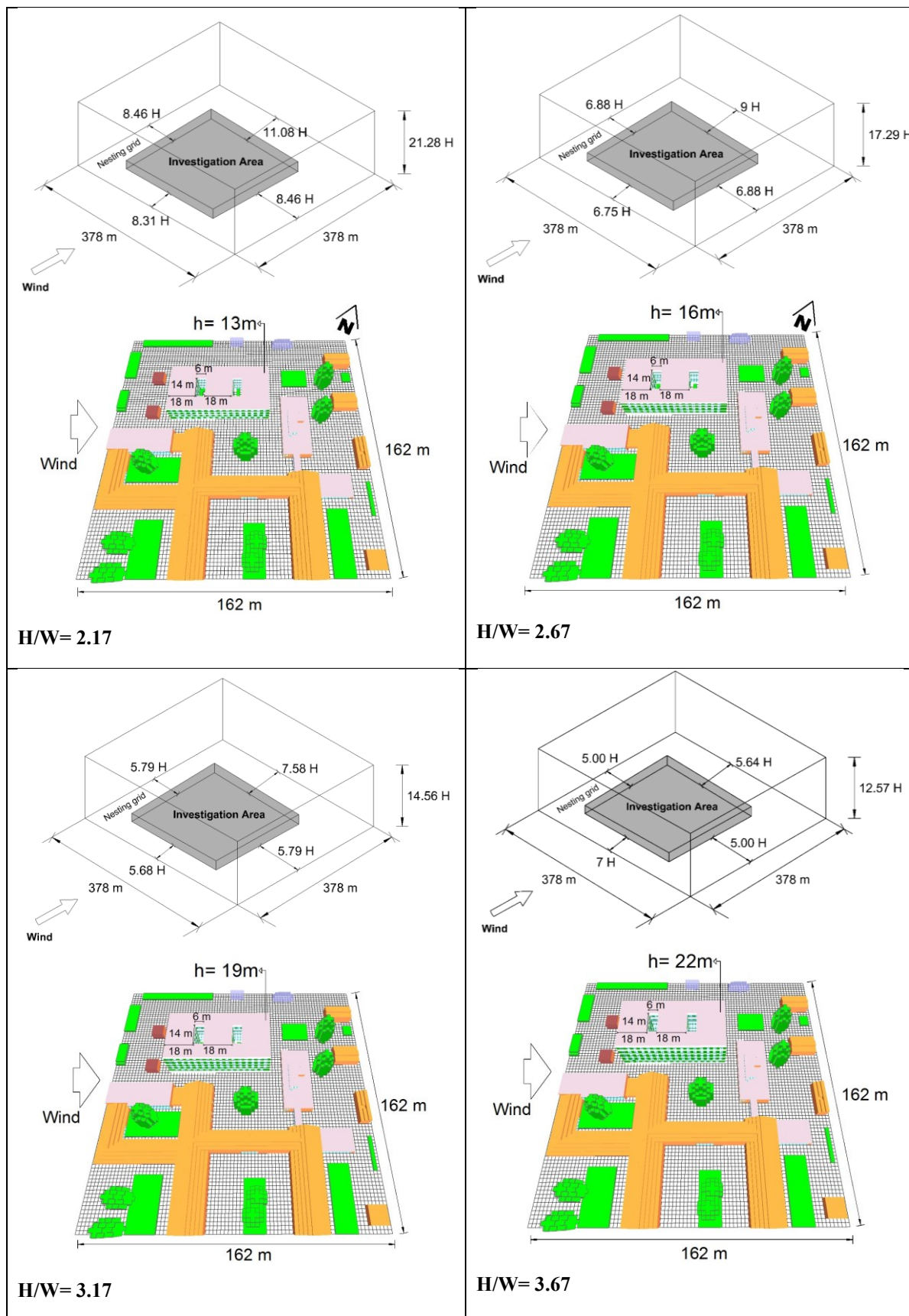


Fig. 1. Study cases (Continued)

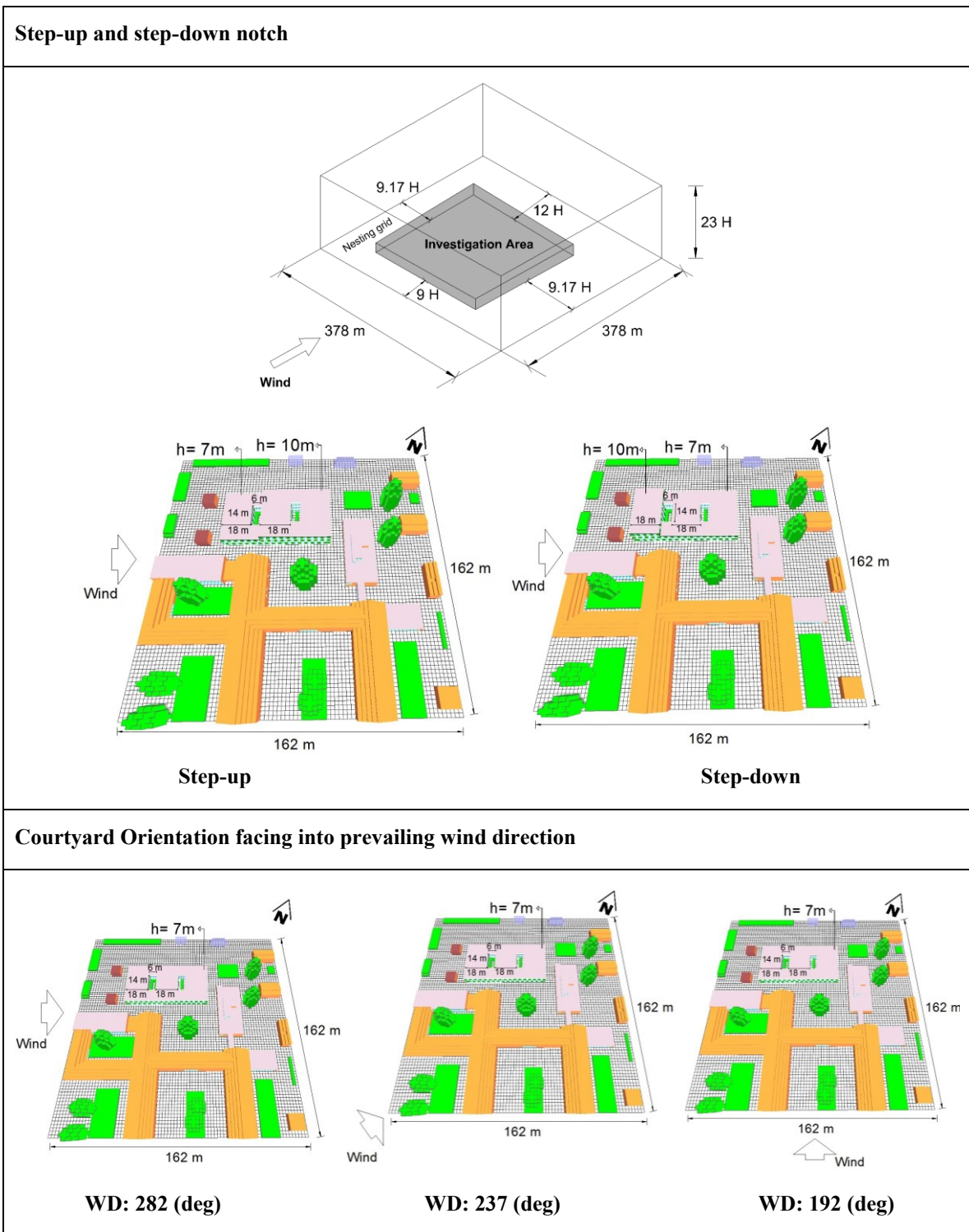


Fig. 1. Study cases (Continued)

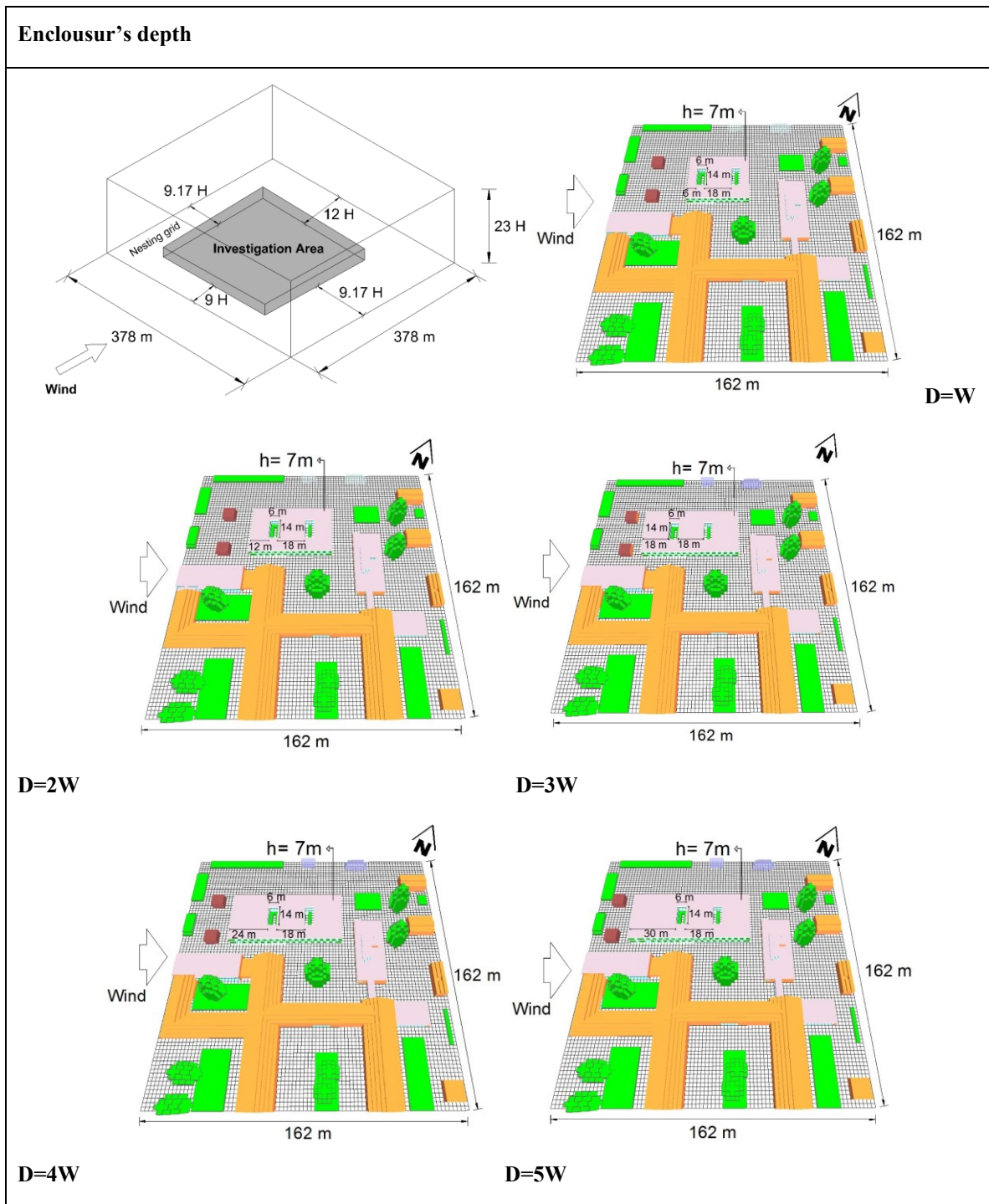


Fig. 1. Study cases (Continued)

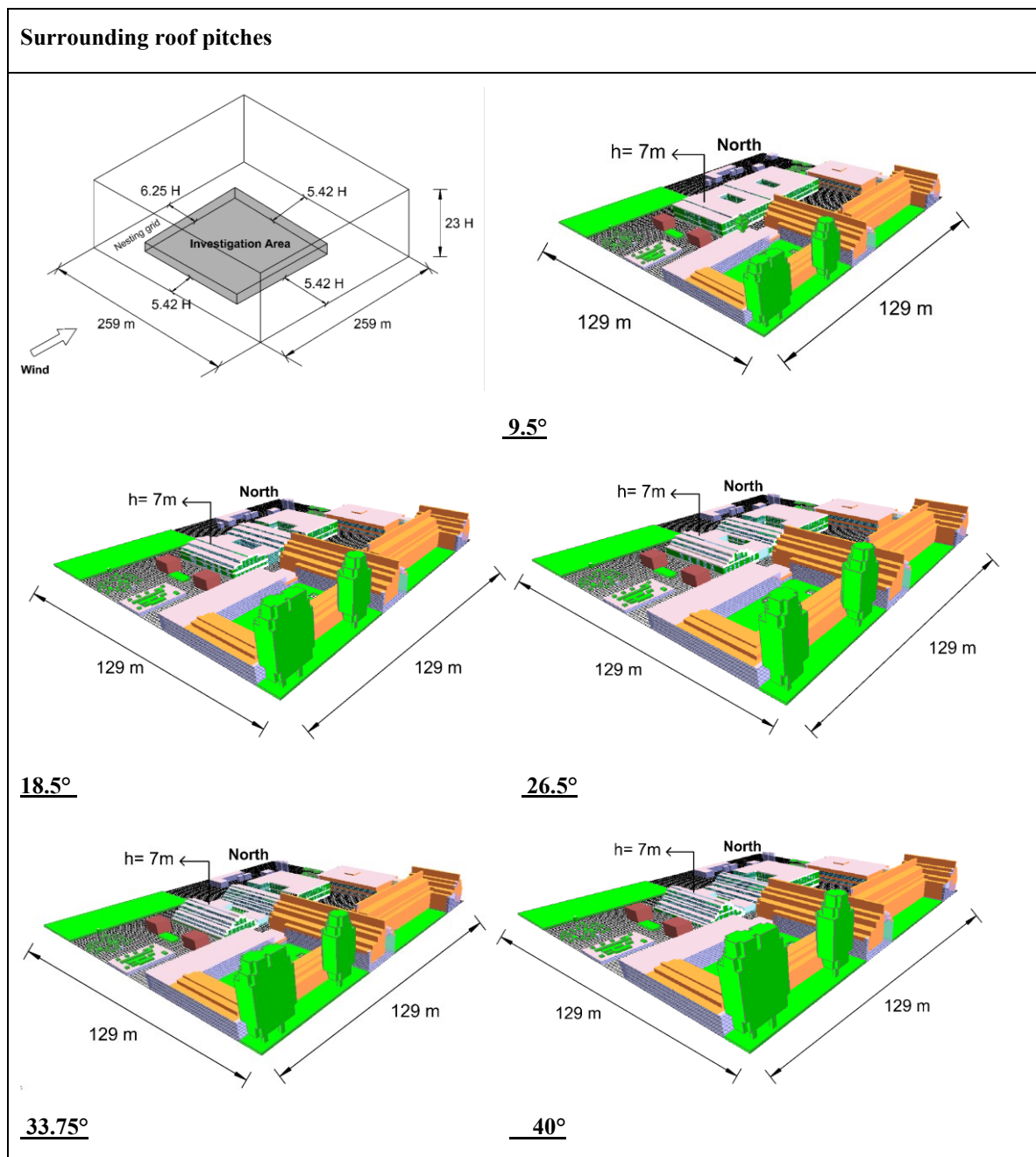


Fig. 1. Study cases (Continued)

ENVI-met uses the multiple-node model based on the works of Terjung and O'Rourke (Terjung & O'Rourke, 1980) to calculate the surface temperatures of walls and roofs. This model allows the construction of up to three layers with different thicknesses and materials. The outside surface temperature (node 1) is calculated by the facade's energy budget (Eq. (1)) equals zero, which considers the outside air temperature, the heat conduction coefficient of the wall, convection and the long-wave and short-wave radiation interchange along the outside wall surfaces. Subsequently, the temperatures of inner nodes are carried

out with the temperature of node n at time t and heat transfer coefficient of the layer along the distance of the nodes (Simon, 2016).

In all models, 70% of the courtyard is surrounded with the heat protection glass and the rest 30% with the Airtec ceramic glass façade. Figure 3 shows the heat balance on the construction of walls, surrounding the courtyard.

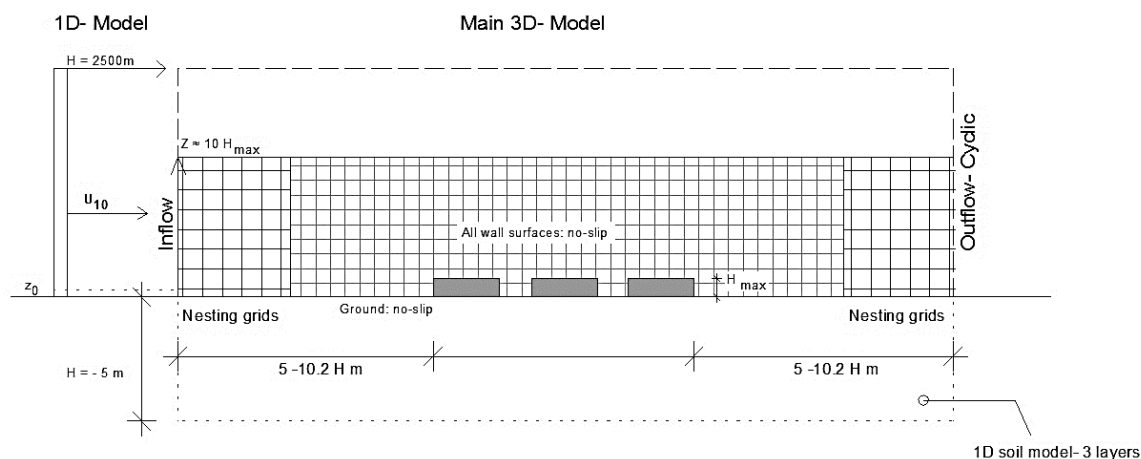


Fig. 2. A model description, computational domain in x-z plane including the boundaries

Table 2. Major input variables for ENVI-met simulation

Location	Hanover, Germany (Latitude: 52° 24' Longitude: 9° 44', elevation 57 m a.s.l)	
Simulation day	26 – 27 January 2017 (cold day)	
Simulation duration	48 h, from 3.00 am	
Meteorological inputs	Air temperature and relative humidity	Average Hourly data from Herrenhausen meteorological station (IMUK) (IMUK, 2016)
	Wind speed at 10m a.g.l	2.3 (m.s ⁻¹) (all phases) , 2.3, 3, 4, 6, 8, 10 (m s ⁻¹) (Section 3.6)
	Wind direction (12: N, 102: E, 192: S, 282: W)	282 (deg) (all cases, Wind flow orthogonal to the principle courtyard axis), 237 (deg)(intermediate directions), 192 (deg)(wind flow parallel to the principle courtyard axis) (Section 3.4)
	Solar radiation SW diffuse and Global	2/8 cloud cover , 0.7 solar adjustment factor
	Specific humidity in 2500m	1 (g kg ⁻¹)
	Roughness length at reference point	m
	Plants	3D tree
1D grass		Height 0.63/ Albedo 0.2/ LAD = 0.3
1D grass		Height 0.18/ Albedo 0.2/ LAD = 0.3
Building	Courtyard surrounded walls: Roof:	70%: one Layer Heat protected Glass; d = 3cm, $\lambda= 1$ (W m ⁻¹ K ⁻¹) 30%: 3 layers: including ceramic glass, air, brick wall; d = 50cm, U = 0.229 (W m ⁻² K ⁻¹) Concrete slab (hollow block) + insulation, d = 30cm, U = 0.22 (W m ⁻² K ⁻¹)
	Indoor Temperature (K)	293

Table 2. Major input variables for ENVI-met simulation (Continued)

Soil	Unsealed soil	Initial condition for soil (default)
	Concrete pavement Gray	Upper layer (0 – 20 cm): 273 K / 50%
	Loamy Soil	Middle Layer (20 – 50cm): 274 K / 60%
	Asphalt road	Deep Layer (50 – 200cm) : 276 K / 60%
	Plant processes	
Update Timing	Surface data	600 s
	Radiation/ Shadows	30 s
	Flow field	600 s
		0 s (Steady)

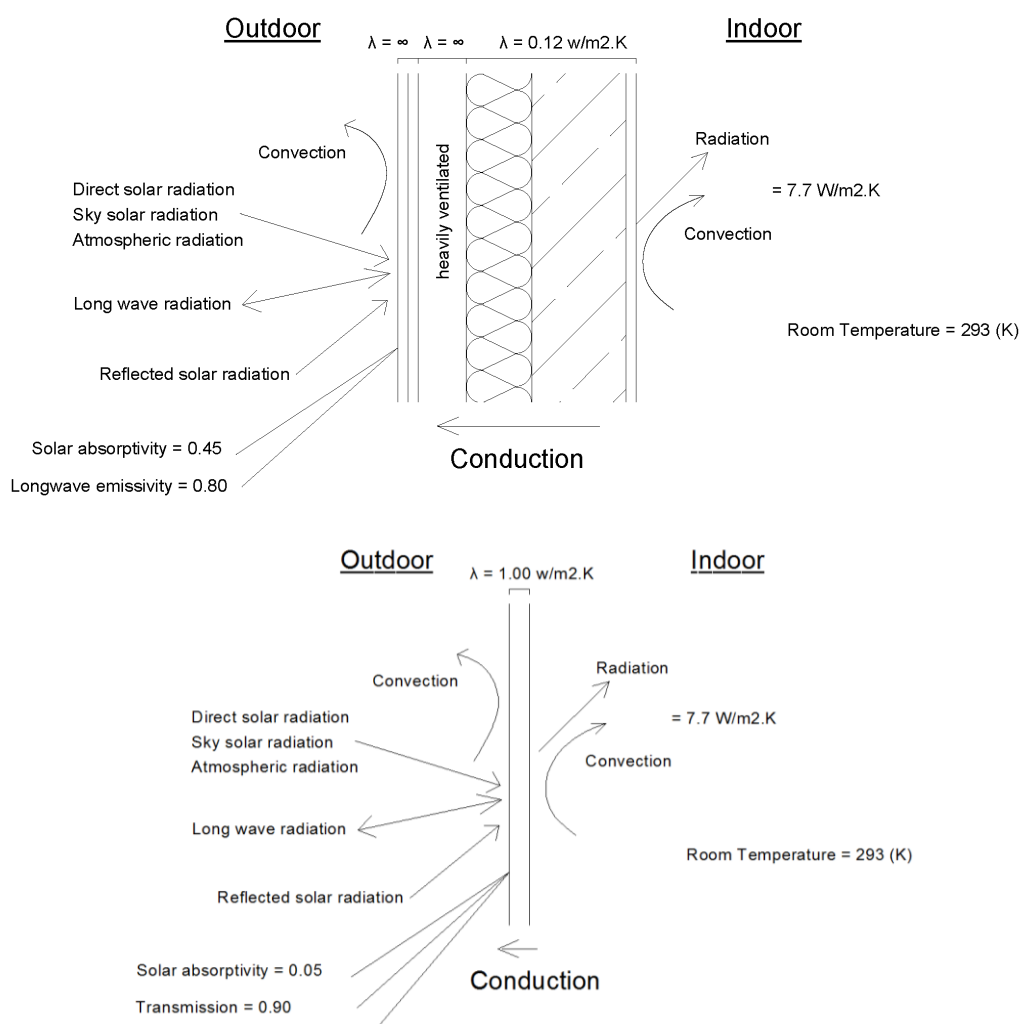


Fig. 3. Heat balances on outside and inside of the exterior walls, respectively on the Airtec glass façade and on the heat protection glass

2.3. Reliability of software

In this research a simple linear low correlation (Eq. (2)) is applied in order to consider CHTC at the outer built surfaces, which is based on WS near the faced. The accuracy of ENVI-met in predicting the WS has been evaluated previously. Srivanit et al. (Srivanit & Hokao, 2013) show that there is no significant difference between measured WS and ENVI-met predictions (≈ 0.05 (m s^{-1})) inside the urban environment. Krüger et al. (Krüger, Minella, & Rasia, 2011) indicate that when the initial WS is less than 2 m s^{-1} , the simulation values perfectly match the field measured values. However, ENVI-met tends to overestimate WS within the canyon for input wind speeds over 2 (m s^{-1}). Likewise, Huttner (Huttner, 2012) and the results of Ramses Project (De Ridder & Acero, J.; Lauwaet, D.; Lefebvre, W.; Maiheu, B.; Mendizabal, 2014) show that the root mean square error (RMSE) between the simulated values and the measured values is between 0.7 (m s^{-1}) and 0.2 (m s^{-1}).

Studies show that the veracity of this model depends on a set of boundary conditions and the optimal inflow wind boundary settings can strongly improve the accuracy of the numerical simulation. Therefore, the reliability of this model in real urban context and effect of various boundary conditions was validated and reported in an earlier publication (Forouzandeh, 2018). However, because of its importance for the present paper, a summary is provided below.

In order to verify the model, the output data for hourly WS at 1.5m above ground near the façade are compared with the data recorded using TESTO 480 data logger (resolution 0.01 (m s^{-1})). Figure 4 and 5 show the measurement points and results, respectively.

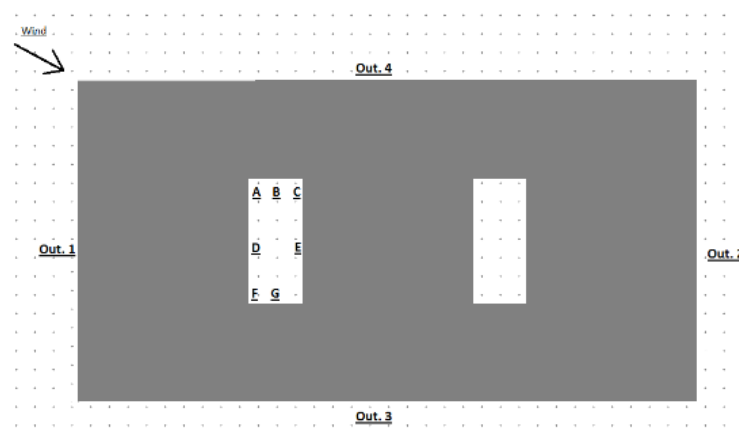


Fig. 4. Layout of the measured points

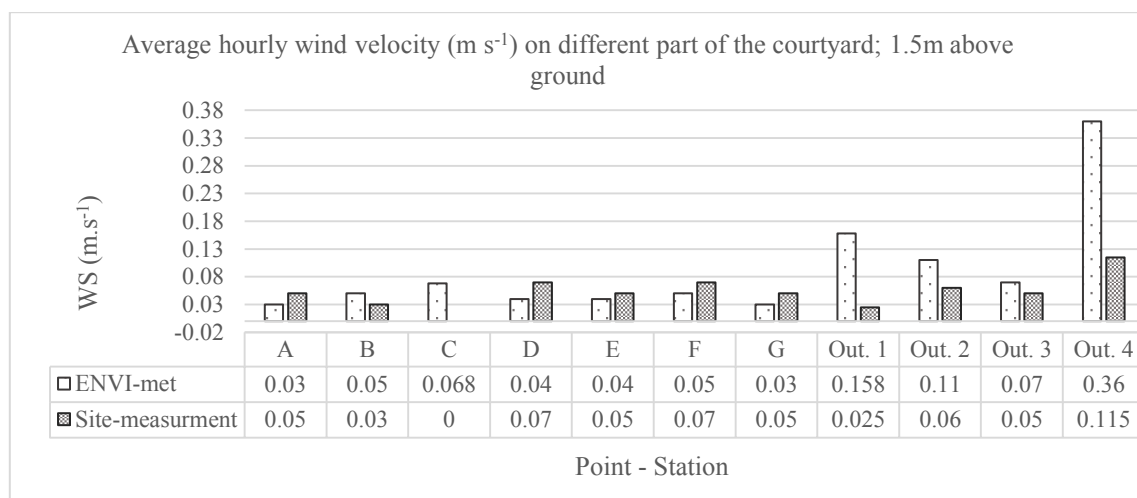


Fig. 5. Comparison of observed and modeled WS at 1.5m above ground, for measured points on 16-17 August, 2016

The results show that the predicted WS inside the courtyard, considerably, fits the observed values. However, for outside the courtyard, due to the limitations of the k - ϵ method (Huttner, 2012) – used for ENVI-met – the turbulent production in areas with a high acceleration or deceleration such as the flow around a building is slightly overestimated ($\approx 0.2 \text{ (m s}^{-1}\text{)}$).

3. Results and analysis

3.1. Flow Pattern inside the courtyards

The air flow pattern inside the courtyard spaces can vary depending on the configuration of the courtyard. Figure 6 discusses the flow pattern for all scenarios with the parameter changes.

As previously shown by Alvarez et al. (ALVAREZ et al., 1998), Rojas et al. (Rojas et al., 2012) and Micallef et al. (Micallef et al., 2016) comparing courtyards with aspect ratios that are less, equal and more than one concluded that for shallow courtyards there is no recirculation flow. Inside middle courtyards, $H/W = 1.17 - 1.67$, an isolated standing vortex is developed, while for more deep courtyards ($H/W > 2$) the stratification effects are strong and disturb the symmetrical lee vortex flow.

Similar to flow pattern inside a street canyon with step-up and down notches (Assimakopoulos et al., 2003; Chew et al., 2017; X. Xie et al., 2005), inside the courtyard when the upwind building wall is reduced in height the vortex is developed inside the

courtyard without the shear layer. However, when the downwind building is lower in height, the main vortex becomes weaker and the lee vortex shifted upward and may occur above the roof of the building. Furthermore, a weak secondary vortex is created in the lower part of the courtyard.

In the case of various thickness for the surrounding buildings, the results show estimate same flow pattern inside the courtyard.

According to the flow pattern, the shape of the roofs affects the depth and the strength of the shear layer at the roof level and therefore on the ventilation of the courtyard (Eliasson et al., 2006; Louka et al., 2000; Yassin, 2011). Louka et al. (Louka et al., 1998), Rafailidis (Rafailidis, 1997) and recently Badas et al. (Badas et al., 2017) found that pitched roofs create stronger turbulence intensities than flat roofs above the courtyard. This indicates that the pitched roofs increase the shear layer at roof level and induce more small turbulence than the flat roof inside the courtyard.

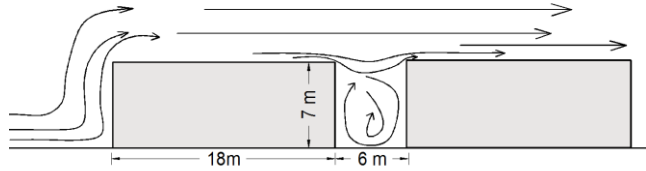
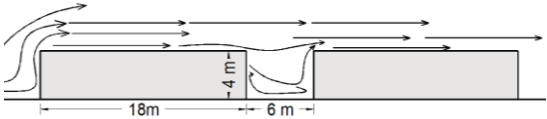
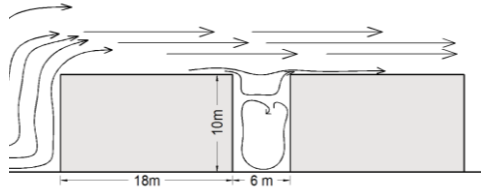
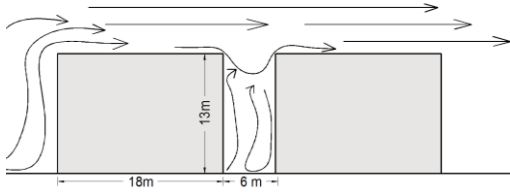
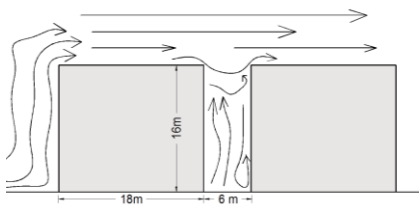
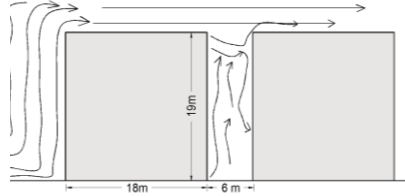
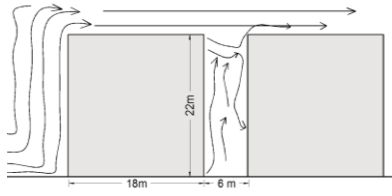
Aspect Ratio			
		<p>Base Model $H/W = 1.17$ $D = 3W$ $R.S. = 0.00^\circ$ <i>Skimming flow</i></p>	
	<p>$H/W = 0.67$ $D = 3W$ $R.S. = 0.00^\circ$ <i>Wake interference flow</i></p>		<p>$H/W = 1.67$ $D = 3W$ $R.S. = 0.00^\circ$ <i>Skimming flow</i></p>
	<p>$H/W = 2.17$ $D = 3W$ $R.S. = 0.00^\circ$ <i>Stratification flow</i></p>		<p>$H/W = 2.67$ $D = 3W$ $R.S. = 0.00^\circ$ <i>Stratification flow</i></p>
	<p>$H/W = 3.17$ $D = 3W$ $R.S. = 0.00^\circ$ <i>Stratification flow</i></p>		<p>$H/W = 3.67$ $D = 3W$ $R.S. = 0.00^\circ$ <i>Stratification flow</i></p>

Fig. 6. Sketches of flow pattern in courtyard of different cases. The sketches are not to scale and separate have been exaggerated

Step- up/ down			
	<p><i>Step-up</i> $D = 3W$ $R.S. = 0.00^\circ$ <i>Skimming flow</i></p>		<p><i>Step-down</i> $D = 3W$ $R.S. = 0.00^\circ$ <i>Skimming flow</i></p>
Courtyard enclosure's depth			
	<p>$H/W = 1.17$ $D = W$ $R.S. = 0.00^\circ$ <i>Skimming flow</i></p>		<p>$H/W = 1.17$ $D = 2W$ $R.S. = 0.00^\circ$ <i>Skimming flow</i></p>
	<p>$H/W = 1.17$ $D = 4W$ $R.S. = 0.00^\circ$ <i>Skimming flow</i></p>		<p>$H/W = 1.17$ $D = 5W$ $R.S. = 0.00^\circ$ <i>Skimming flow</i></p>

Fig. 6. Sketches of flow pattern in courtyard of different cases. The sketches are not to scale and separate have been exaggerated (Continued)

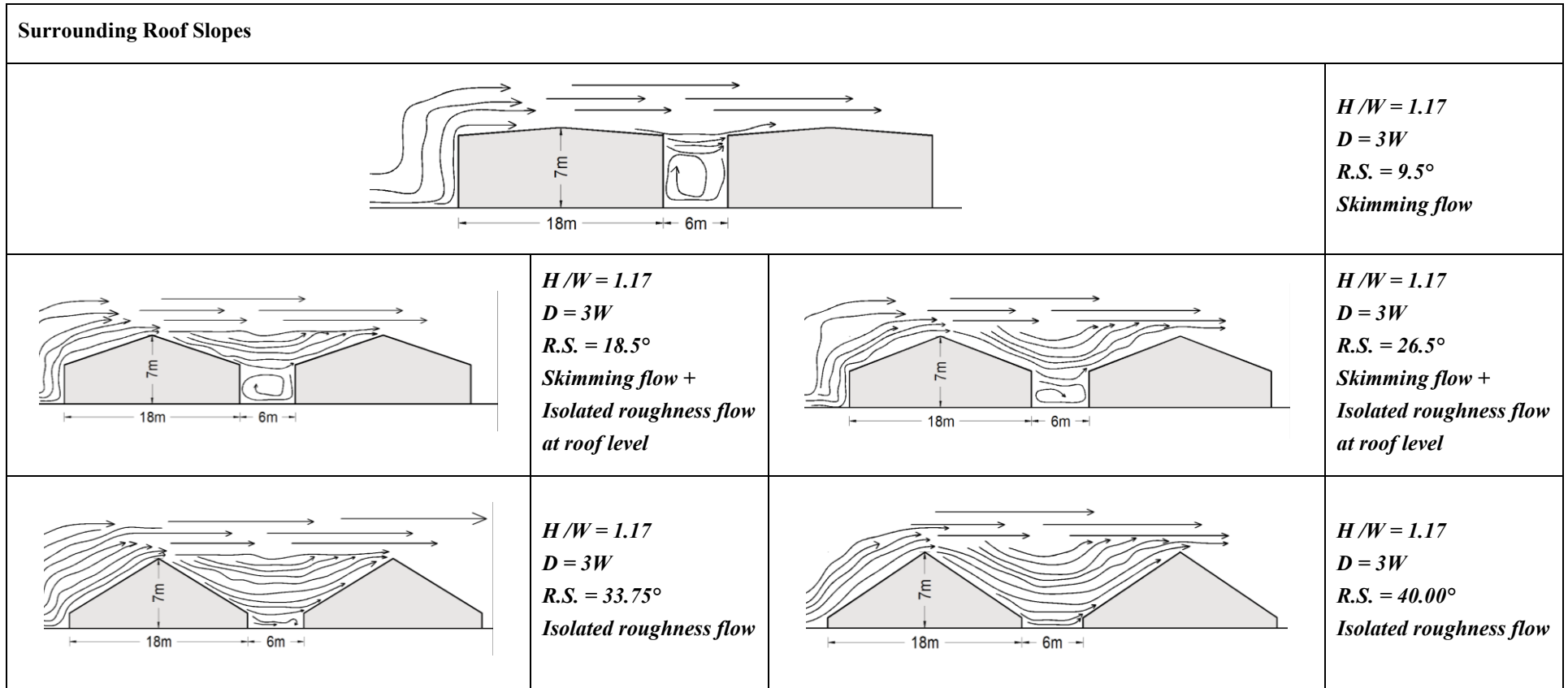


Fig. 6. Sketches of flow pattern in courtyard of different cases. The sketches are not to scale and separate have been exaggerated (Continued)

3.2. Diurnal variation of WS

To investigate the effect of courtyard on diurnal WS variation, WS with all three components of velocity was exported for eight points inside the courtyard at five different height levels (0.5m above the ground, 0.25H, 0.5 H, 0.75H and 1H) (Fig. 7.). Figure 8 and 9 show the diurnal WS on the windward and leeward façade inside the base model with $H/W = 1.17$.

The diurnal cycle of the near-surface WS is the function of geographic winds and thermal structure near the surface (He, Monahan, & McFarlane, 2013). In the present study, because the simulations have done during the winter with the cloudy condition, the surface temperature during the day slightly increase the WS and has no considerable effect on it.

According to the results, the WS vertical gradient is low at low levels of the courtyard, where the surface buoyancy is large and become larger with increasing the height from the bottom of the courtyard. At all height levels the maximum WS are recorded on the corners of the courtyard (at Point 4 and 5) at 12:00, which is considered in the next section as the maximum recorded velocities ($v_{max} (m s^{-1})$).

Finally, a comparison of the variation of the WS, between the windward (Point 5 – 8) and leeward (Point 1 – 4) sides of the building, does not show the considerable difference between both sides.

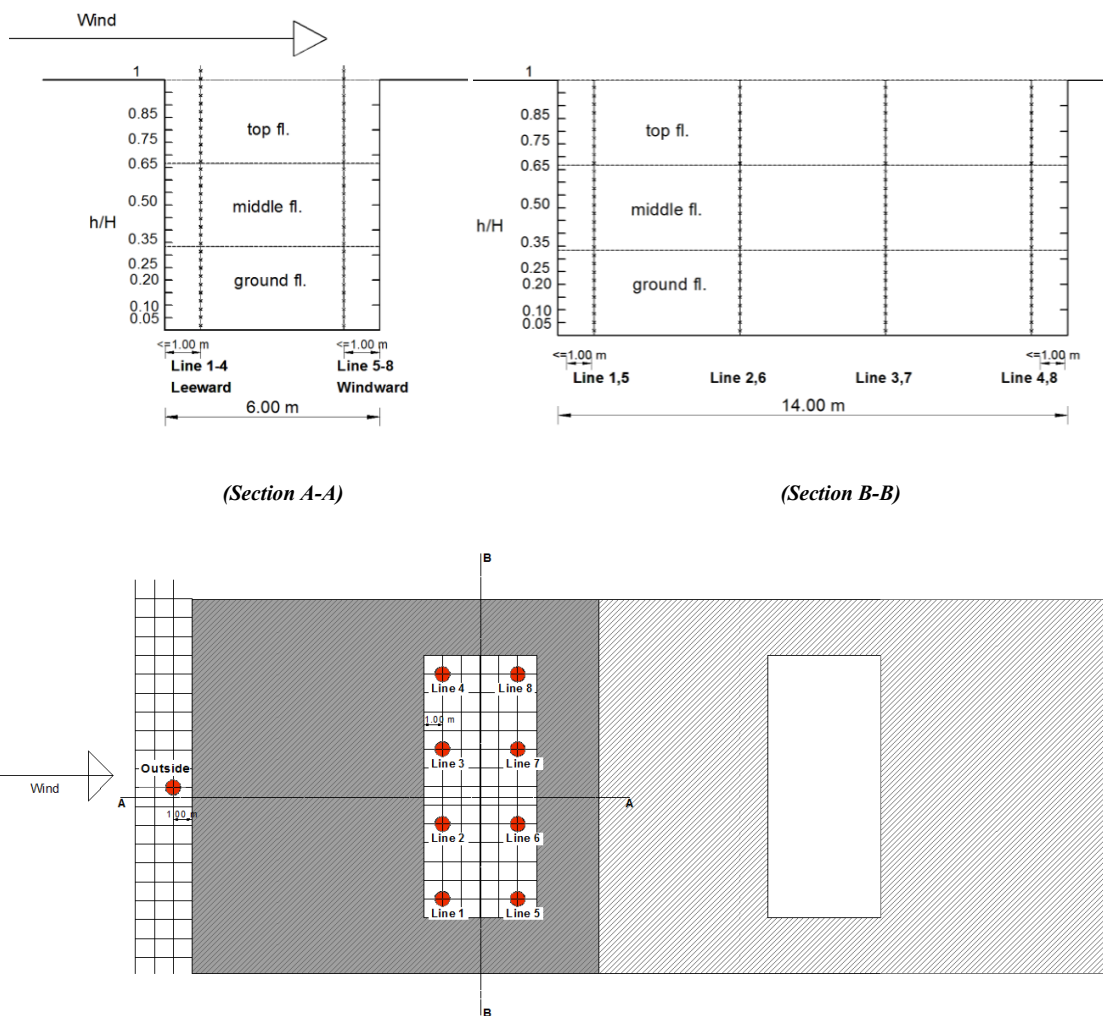


Fig. 7. Position of investigated planes relative to courtyard convention related to wind direction, respectively on side and top view

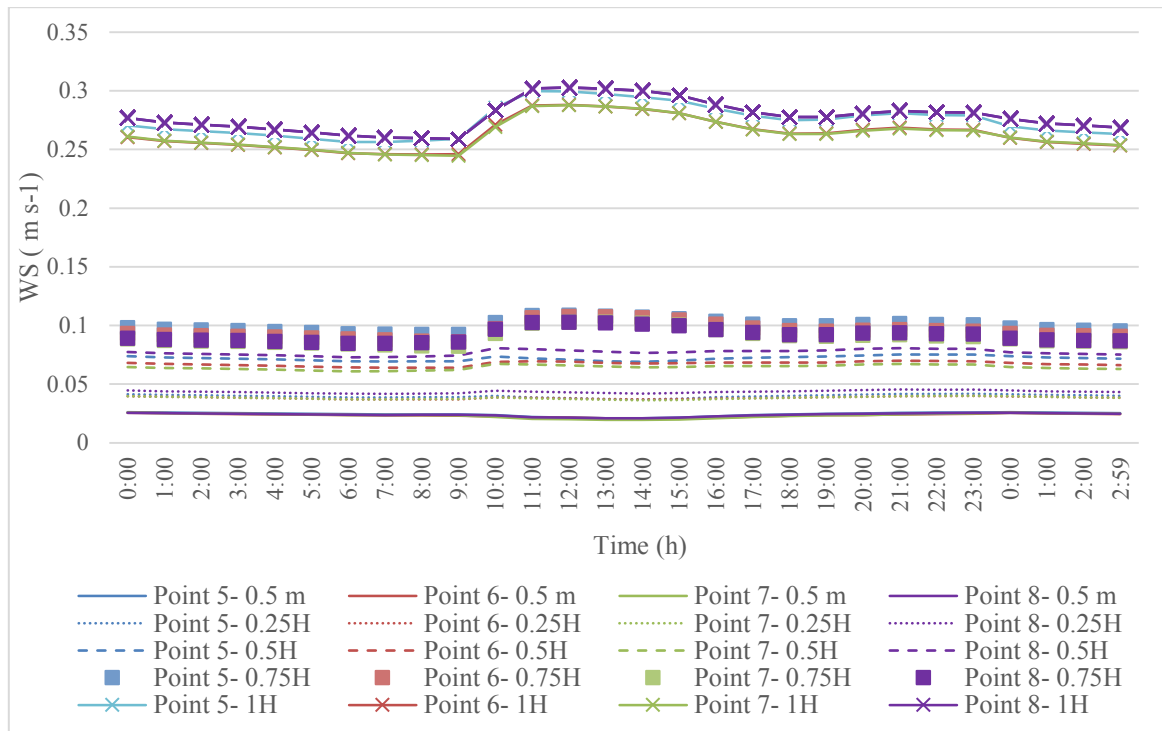


Fig. 8. Diurnal wind speed on courtyard windward surfaces based on mean hourly values for 27 January 2017

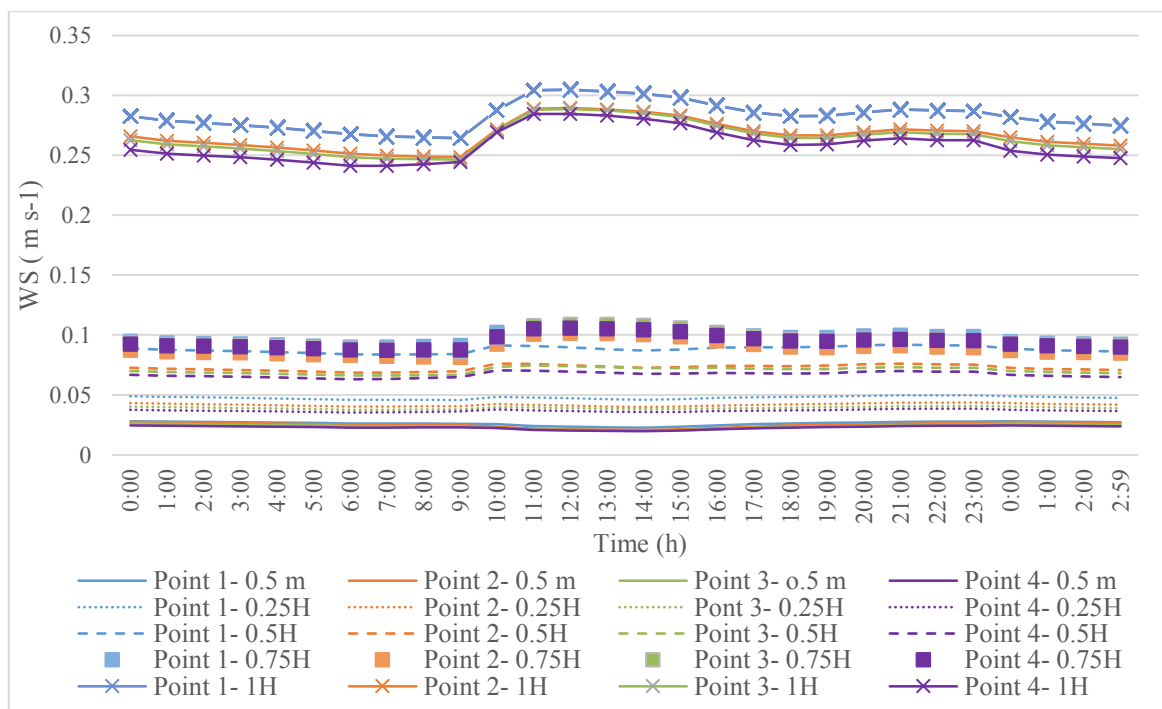


Fig. 9. Diurnal wind speed on courtyard Leeward surfaces based on mean hourly values for 27 January 2017

3.3. Effect of courtyard on WS and CHTC

This section discusses the effect of various parameters on CHTC difference between inside and outside the courtyard. In this way, the v_{max} ($m s^{-1}$) and $h_{c,max}$ ($W m^{-2} K^{-1}$) at all height levels inside the courtyard (Section 3.2, Fig. 7.) were compared with the v_{min} ($m s^{-1}$) and $h_{c,min}$ ($W m^{-2} K^{-1}$) near the windward outside wall, which is measured in the middle of the wall, apart from the de-reattachment effect. This method provides a more convenient comparison with outside WS and overcome the ENVI-met model shortcut, which overestimates the WS in front of exposed façade (Forouzandeh, 2018) and near the edges (BALDWIN & LOMAX, 1978; Kato, M., Launder, 1993).

3.3.1. Effect of courtyard aspect ratio (H/W)

In order to investigate changes in the aspect ratio of courtyards, seven different design scenarios with (H/W) of 0.67, 1.17, 1.67, 2.17, 2.67, 3.17 and 3.67 were defined. In all cases, the wind flow is assumed to be orthogonal to the principal courtyard, with a $U_{10} = 2.3$ ($m s^{-1}$).

The outcomes reveal that the height enclosures in the courtyard work as a wind shelter and decrease WS and as a result CHTC in front of the envelope walls. According to the Figure 10, the v_{max} ($m s^{-1}$) near the façade in all heights levels of the courtyard is considerably different than the minimum outside WS ($\sim 0.2 - 0.5$ ($m s^{-1}$)). Similarly, the CHTCs through the envelope façade inside the courtyard are 1 – 2 ($W m^{-2} K^{-1}$) less than the minimum CHTC throughout the outside façade.

Comparisons indicate that the aspect ratio exerts considerable influence on WS and CHTC inside the courtyard, based on whether the H/W is less than, equal to or more than one. In keeping with the Figure 10 and flow pattern inside the courtyard (Section 3.1), in the intermediate courtyards with $H/W = 1$ the WS up to middle level of the courtyard (0.65 H) is more than other cases. This happens due to a strong vortex and no stratification effect. With increasing the H/W, stratification becomes stronger and disturb the symmetrical lee vortex flow. Therefore, inside the deep courtyards ($H/W \geq 2.67$), the WS is almost zero throughout the courtyard at the ground level.

Based on the results, in the courtyard with the aspect ratio of 0.67, the velocity at 0 – 0.35H (courtyard height) differs by about 94% compared to the velocity at the top level of the courtyard (0.65 – 1H). This value is somewhat less ($\approx 90\%$) for the aspect ratio 1, due to full vortex, and increases slightly up to 99.5%, with increases in the enclosure heights.

Comparison between windward and leeward façade inside the courtyard (Figure 10, red and black lines) shows that the change trend of CHTCs, up to middle levels of the courtyard, was generally similar and total amount of CHTC is less than $4.5 \text{ (W m}^{-2} \text{ K}^{-1}\text{)}$ for all cases. However, at the top level of the courtyard, the WS and CHTC along the leeward wall is slightly more than the windward for all the experimental cases.

3.3.2. Effect of Step-up and step-down notch

In this section the effect of the step-up and step-down notches on WS and CHTC inside the courtyard was considered up to the roof of the shorter building.

The results confirm that the step-up/step-down design idea can limit the WS and CHTC inside the courtyard on both windward and leeward façades. According to Figure 11, the average WS up to the middle height of the courtyard is 45% lower for Step-up and 20% lower for step-down compared to WS across buildings of similar height. These configurations are more effective at top levels of the courtyard ($0.75 - 0.85H$) and can reduce the WS up to 70%.

In the case of step-down notches, the lee vortex shifts upward and occurs above at top level of the building; therefore, the WS and CHTC in this area ($0.65 - 0.75 H$), as shown in Fig 11, is slightly more in comparison with step-up, in which the vortex occurs at center and downside of the courtyard and has less interaction with the flow above the courtyard (Section 3.1).

Finally, considering the WS at outside the courtyard shows that this value decreases when step-down design idea is applied.

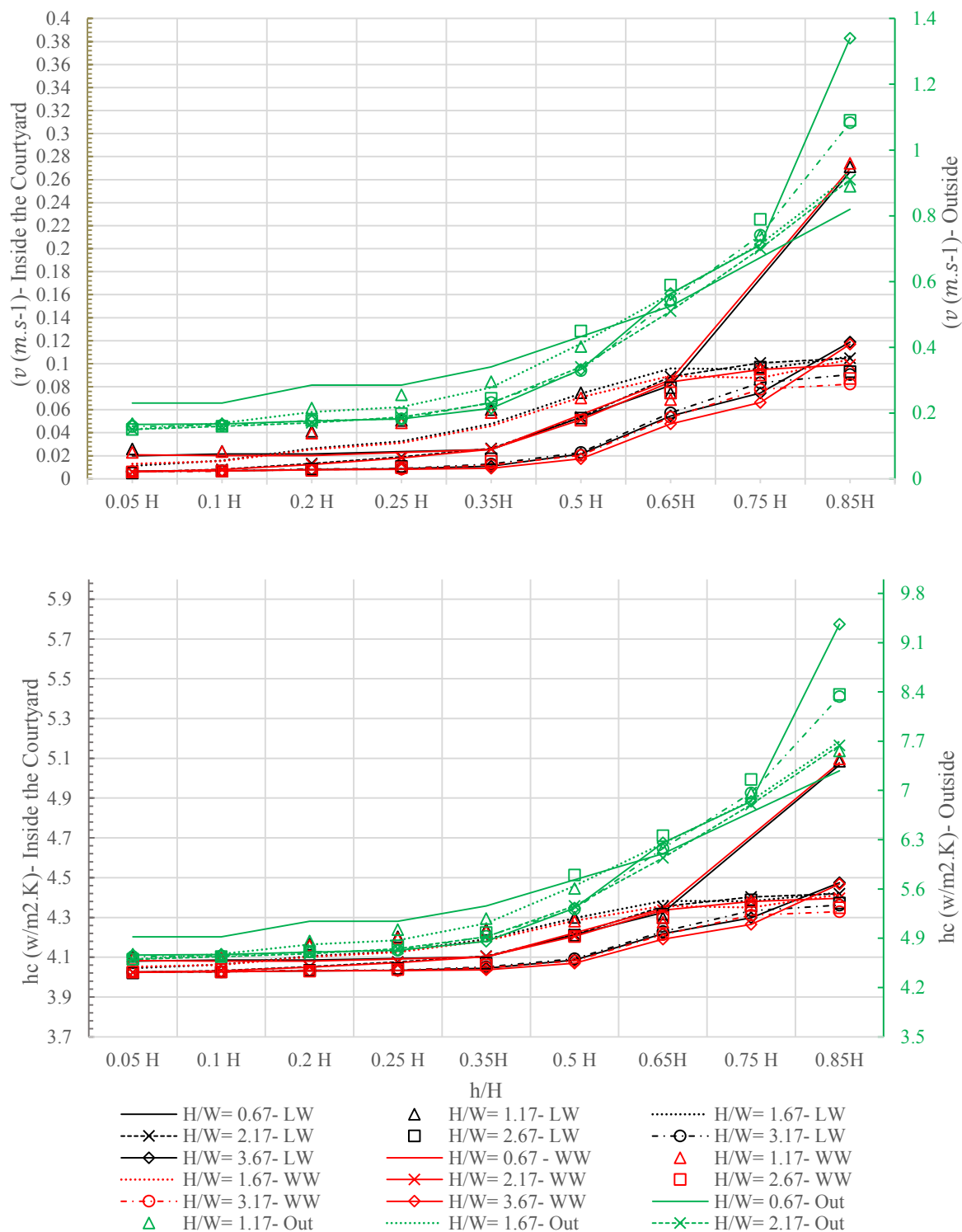


Figure 10. $v(m.s^{-1})$ and $h_c (W.m^{-2}.K^{-1}) = 4 + 4v(m.s^{-1})$ for the simulation period with various aspect ratios; Right y- axis: maximum on LW (Points 1-4) (black), WW (Points 5-8) (red); Left y-axis: minimum on outside in middle of WW wall (green)

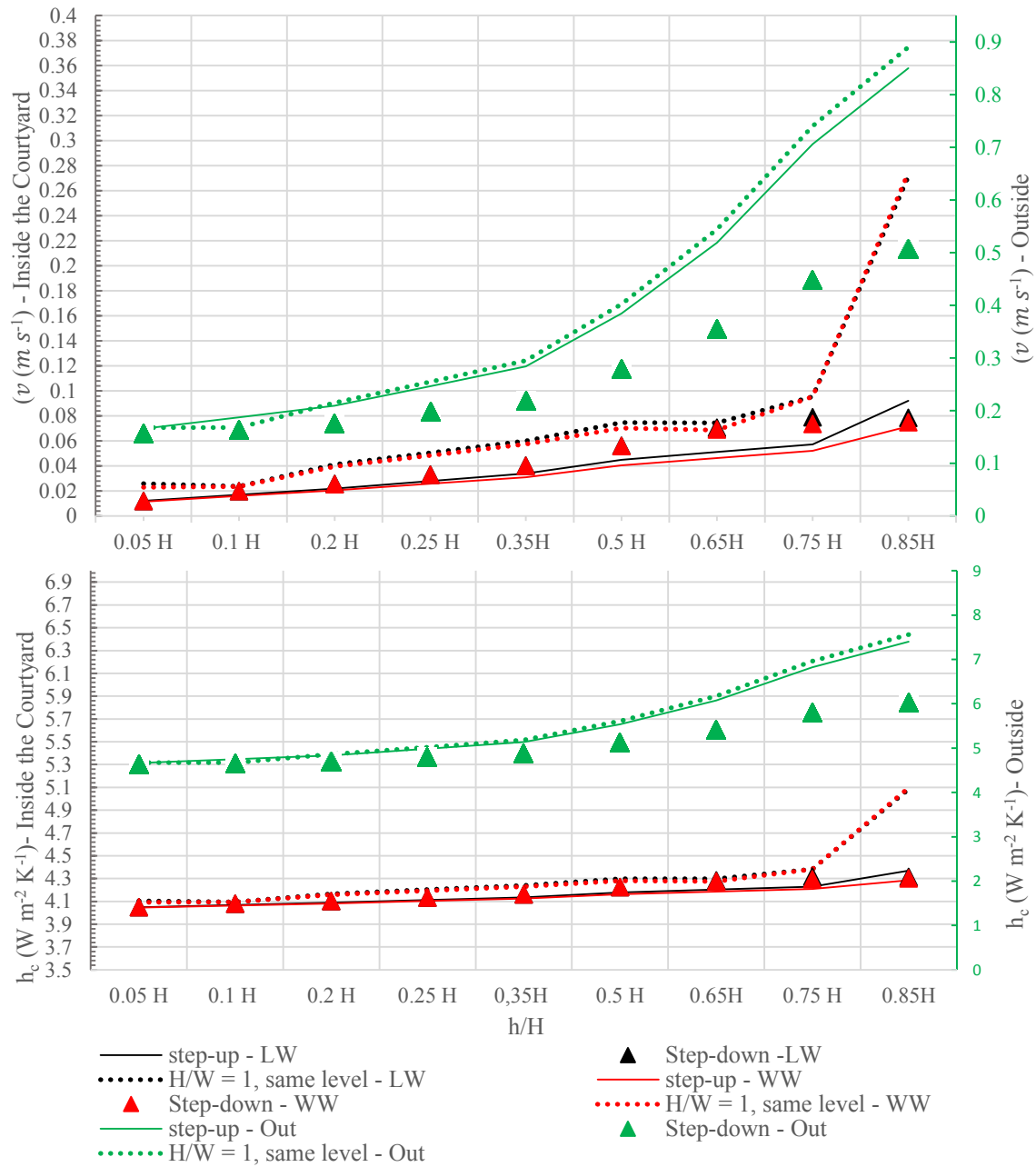


Fig. 11. v ($m s^{-1}$) and h_c ($W m^{-2} K^{-1}$) = $4 + 4v$ ($m s^{-1}$) for the simulation period with step-down /step-up; Right y- axis: maximum on LW (Points 1 – 4) (black), WW (Points 5 – 8) (red); Left y-axis: minimum on outside in middle of WW wall (green)

3.3.3. Effect of courtyard enclosure's depth

Analysis of flow fields shows that increasing the enclosure's thickness has two main effects: firstly it increases shear layer above the courtyard and reduces this space's ventilation (Hall et al., 1999) and secondly, as shown in Fig. 12., it enhances slightly the turbulence and the WS at the top level of the courtyard (0.75 – 0.85 H), Max 0.05 ($m s^{-1}$).

However, it does not have a great influence on the WS and CHTC, outside and at lower levels inside the semi-closed courtyard spaces.

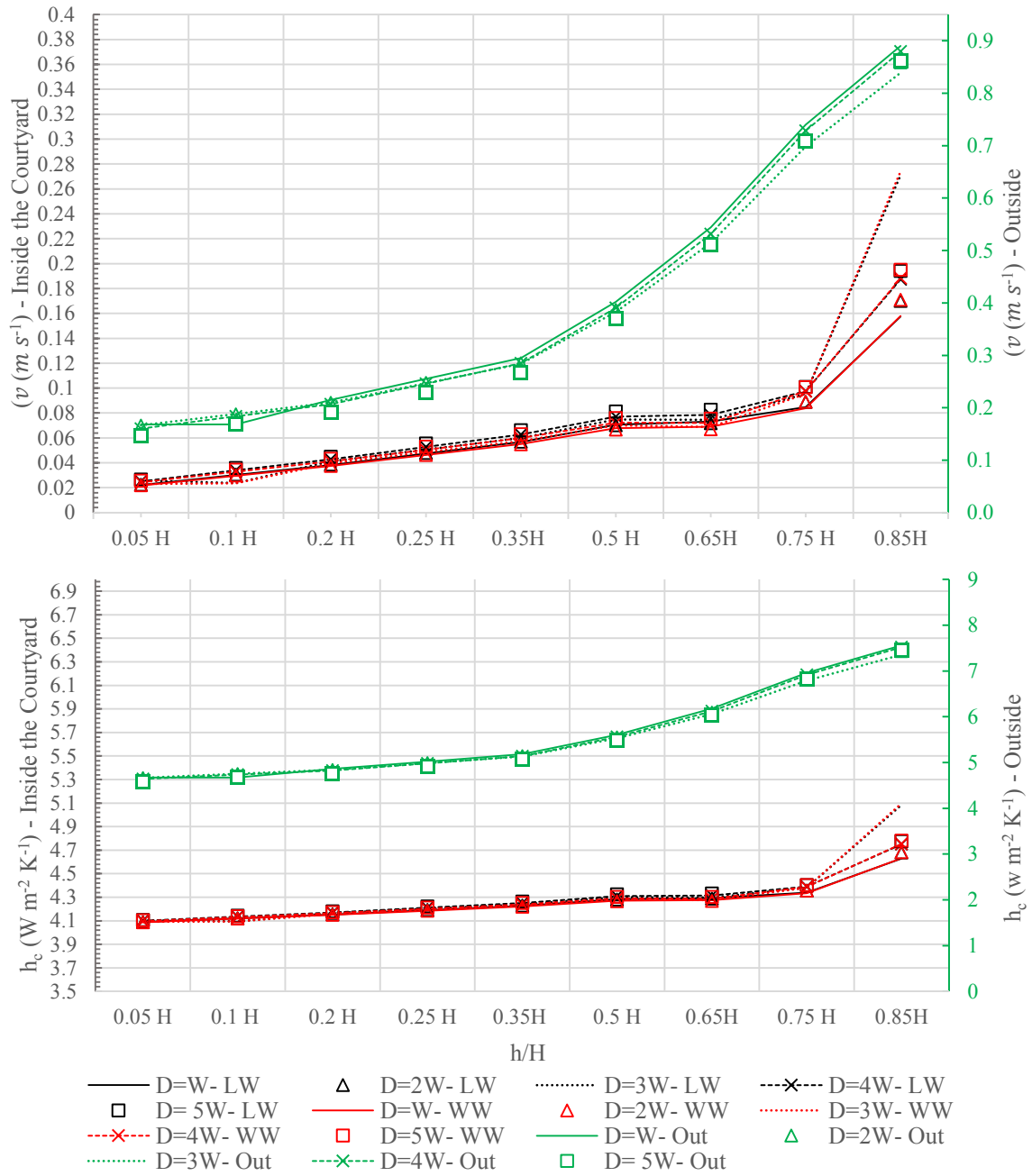


Fig. 12. v ($m s^{-1}$) and h_c ($W m^{-2} K^{-1}$) = $4 + 4v$ ($m s^{-1}$) for the simulation period with various depth-to-width ratios; Right y- axis: maximum on LW (Points 1 – 4) (black), WW (Points 5 – 8) (red); Left y-axis: minimum on outside in middle of WW wall (green)

3.3.4. Effect of courtyard orientation, facing into prevailing wind direction

Orientation plays an important role as it relates to the climate. In this part the simulation was repeated for the same geometrical model ($6 \times 14 \times 7 \text{ m}$) with various wind directions, including 282 (deg), when the wind flows orthogonal to the principle courtyard axis, 237 (deg), as intermediate directions and 192 (deg), when wind flows parallel to the principle courtyard axis.

Previously, Moonen et al. (P Moonen et al., 2011) and Sanyal et al. (Sanyal & Dalui, 2018) indicate that when the angle between the dominant wind direction and the main courtyard axis is about 15 – 30 (deg), the space exchange flux is maximal. In this research, the comparison of WS near the façade inside the courtyard (Fig. 13.) shows the same results. Based on the simulations, for 237 (deg) wind direction, the WS and therefore CHTC through the walls at the ground and top levels of the courtyard are greater than other cases. However, the wind velocity at the middle part of the courtyard is less affected by the courtyard orientation toward domain wind.

In the case of 192 (deg), the courtyard length-to-width relative to the ambient wind direction is increased and similar to shallow courtyard high WS and CHTC at low levels are recorded.

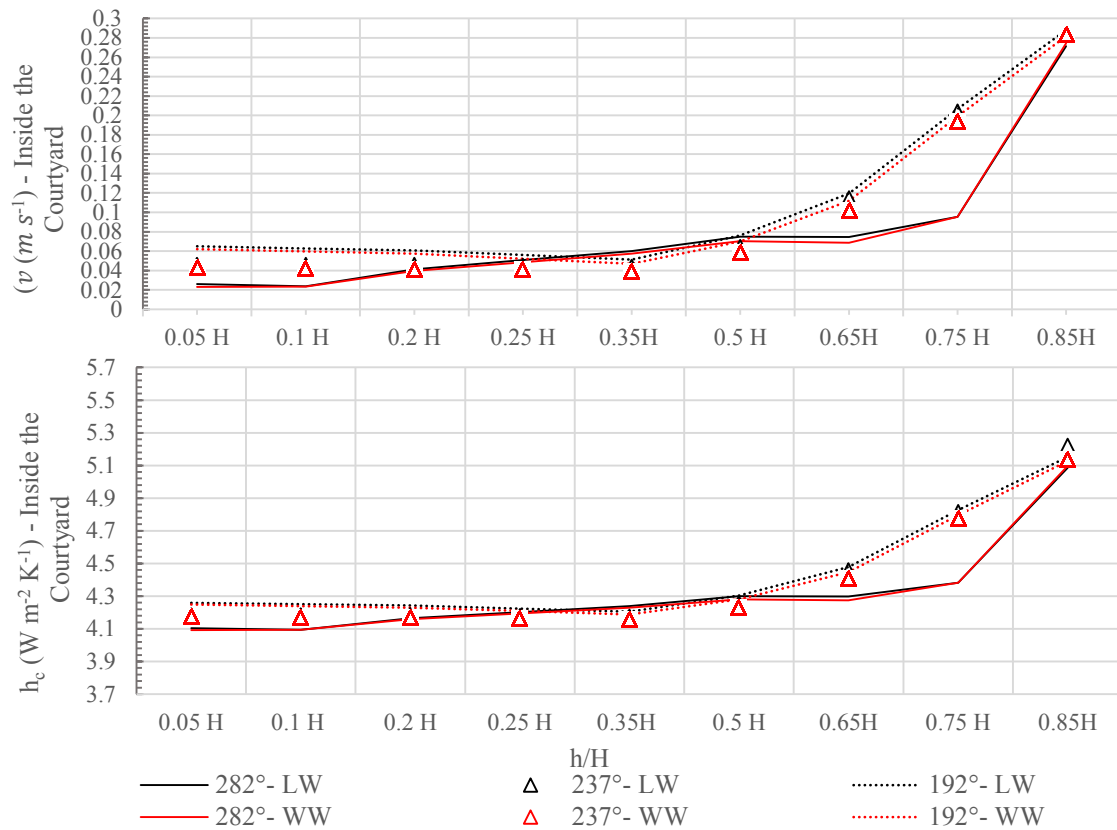


Fig. 13. v ($m s^{-1}$) and h_c ($W m^{-2} K^{-1}$) = $4 + 4v$ ($m s^{-1}$) for the simulation period with various dominant wind directions; maximum on LW (Points 1 – 4) (black), WW (Points 5 – 8) (red)

3.3.5. Effect of surrounding roof pitches

In this section the effect of various surrounding roof pitches (0 to 40 (deg)) on WS inside the courtyard are considered. The roofs are simulated with the same ridge height (7m) and the results are exported from the center of the first grid at the distance of 0.5m from the wall up to the eaves' height.

According to the WS results (Fig.14.) and flow pattern inside the courtyard (Section 3.1) the pitched roofs create stronger turbulence intensities than flat roofs above the courtyard, in the region between the eaves and the ridge height. Consequently, the vortex extends above the courtyard, and it was observed that the WSs in the front of the façade at ground and the middle part of the courtyard are about 50% lower than in the corresponding reference case. Therefore, higher pitch rise systematically leads to markedly lower CHTC throughout the envelope walls.

On the other hand, the WS variations outside the courtyard dos not show any specific relationship between WS and roof pitches (Fig. 14. – green lines).

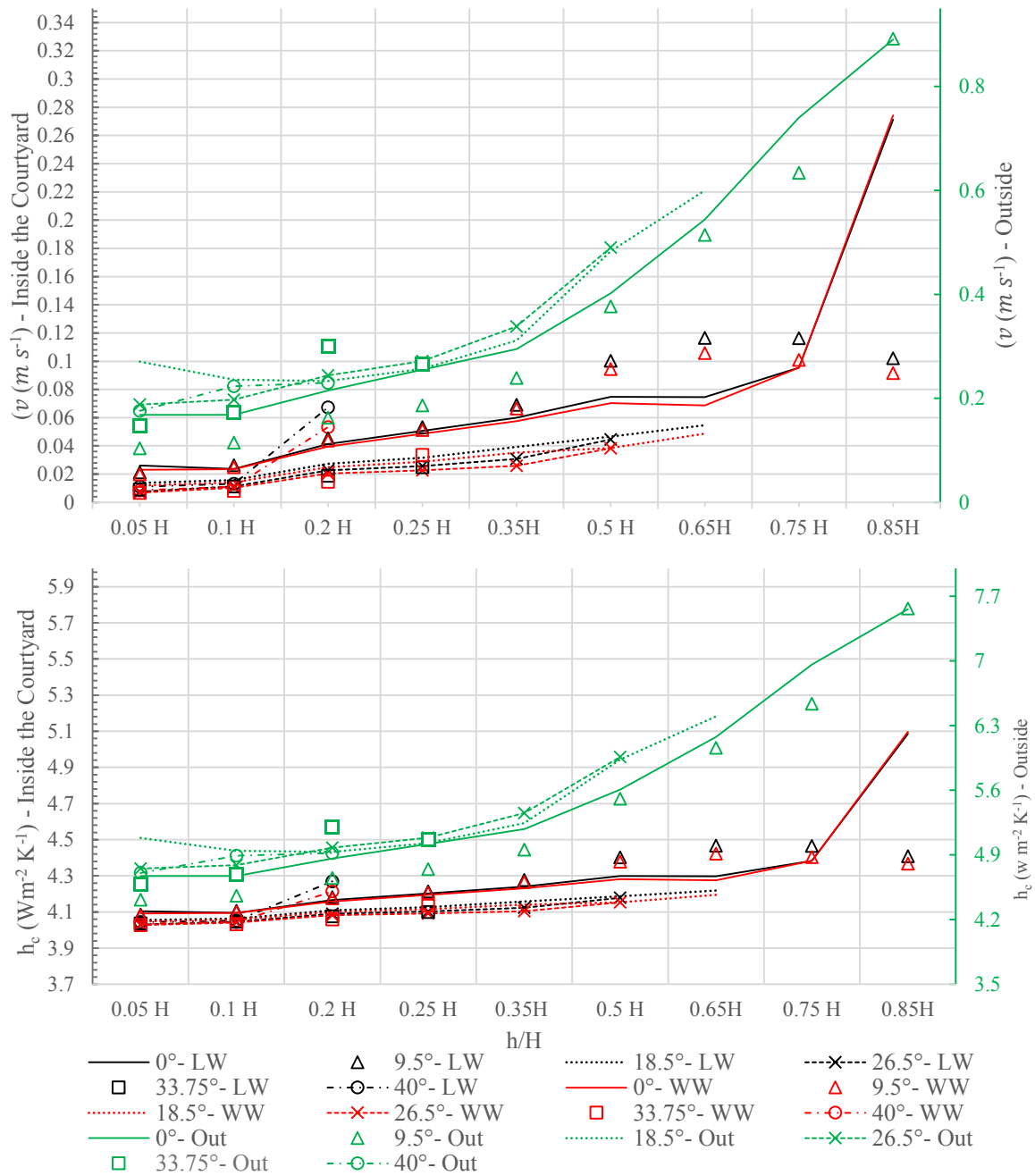


Fig. 14. v ($m s^{-1}$) and h_c ($W m^{-2} K^{-1}$) = $4 + 4v$ ($m s^{-1}$) for the simulation period with various roof slopes; Right y- axis: maximum on LW (Points 1 – 4) (black), WW (Points 5 – 8) (red); Left y-axis: minimum on outside in middle of WW wall (green)

3.3.6. Effect of ambient wind speed

In this step, the experimental models with $H/W = 1.17$ and 2.17 are selected and simulations, at different $U_{10} = 2.3, 3, 4, 6, 8$ and 10 ($m s^{-1}$), are performed to consider the effect of U_{10} on wind speed inside the courtyard.

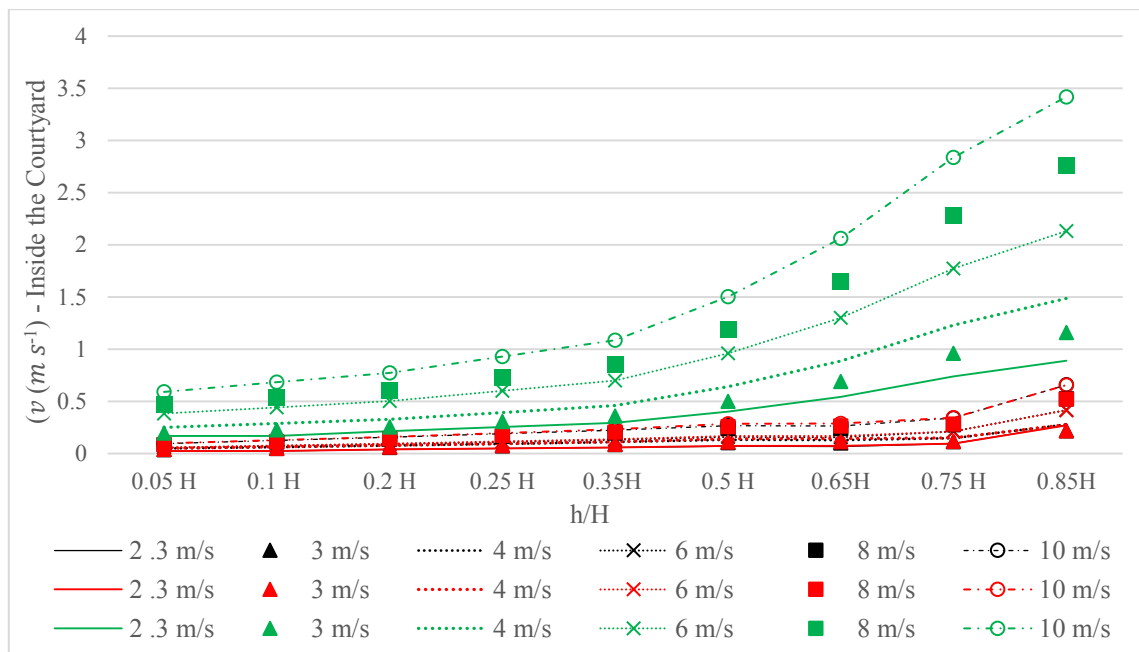


Fig. 15. v ($m s^{-1}$) for base model ($H/W = 1.17$) with various U_{10} , Right y- axis: LW (Points 1 – 4) (black), WW (Points 5 – 8) (red); Left y-axis: outside in middle of WW wall (green)

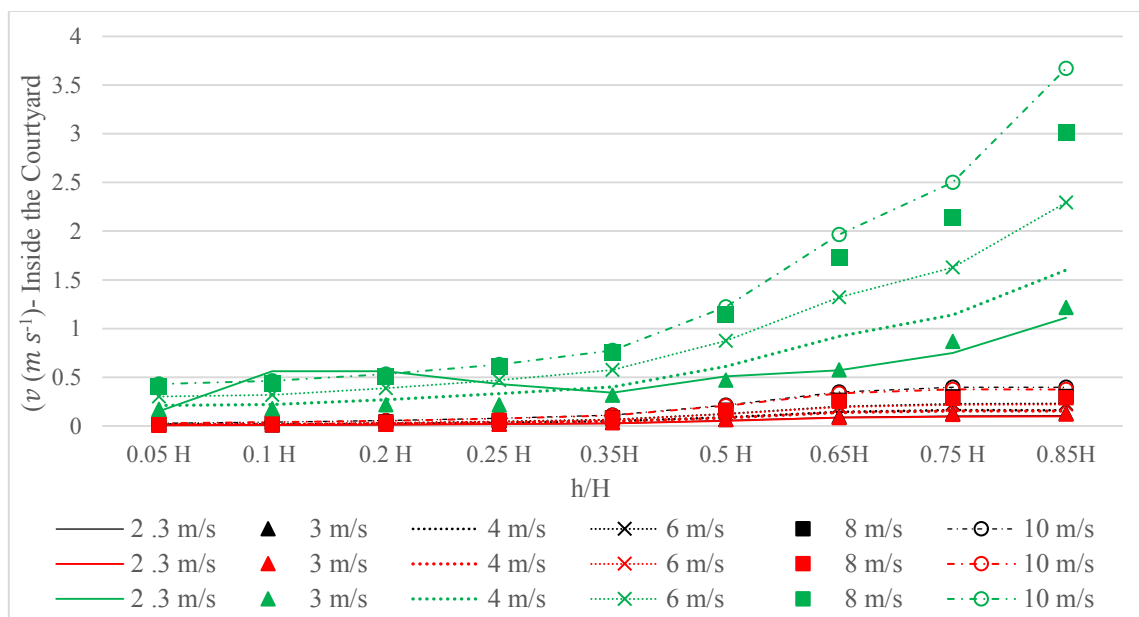


Fig. 16. v ($m s^{-1}$) for case study 4 ($H/W = 2.17$) with various U_{10} , Right y- axis: LW (Points 1 – 4) (black), WW (Points 5 – 8) (red); Left y-axis: outside in middle of WW wall (green)

According to Figure 15 and 16, an increase in the ambient WS has a negligible influence on the WS inside the courtyard. For both experimental cases ($H/W = 1.17$ and 2.17), the WS in front of the envelope façade inside the courtyard increases at the low and middle heights of the courtyard (up to $0.75H$) by about $0.00 - 0.03$ (m s^{-1}) and above $0.75H$ by about 0.2 (m s^{-1}), for each 1 (m s^{-1}) more U_{10} . However, this acceleration is more outside the courtyard and is ≈ 0.05 (m s^{-1}) up to $0.2H$, $0.1 - 0.2$ (m s^{-1}) up to $0.75H$ and reaches 0.7 (m s^{-1}) at the roof level of the building.

The results of this section indicate that the CHTC through the building's envelope inside the courtyard, in comparison with exposed surfaces, is less affected by the ambient WS.

4. Discussion

The percent difference between the maximum CHTC at the windward façade inside the courtyard and minimum CHTC on the middle of the outside windward wall for all experimental models are shown in Table 3 to compare the effectiveness of each scenario. The results of this part show the minimum effect of the courtyard on reducing CHTC and due to acceleration effect, the CHTC difference between the courtyard and the exterior edge of the building should be more (A Hagishima & Tanimoto, 2003).

This comparison highlights the potential of the courtyard to reduce wind loads on facade especially in the case with high ambient wind speeds. The findings also show that the difference between CHTC inside and outside the courtyard was continually increased with increasing the height of the surrounding buildings up to $H/W = 2.17$. However, the difference remains almost constant for deep cases. Meanwhile, it was found that step-up configuration more than other surrounding forms can reduce WS in front of the façade inside the courtyard.

Finally, according to the results, the ideal case with all the favorable parameters – including flat roof, step-up form and (H/W) up to shorter building = 3.67 – is defined.

The shape of the surrounding roofs and step-up form can change the vortex intensity and location and therefore WS near the envelopes in shallow and middle courtyards.

The flow inside the deep courtyards mostly depends on the stratification flow and not vortex. Therefore, step-up form and roof shape are not more effective here and the CHTC difference between inside and outside the courtyard is not changed considerably and is approximately equal to Case 7.

Table 3. Comparison between minimum CHTC on outside windward façade and maximum CHTC inside courtyard on windward façade for all experimental models


	Case study, Courtyard dimensions ($H \times W \times D$ m), dominant Wind direction , roof slope, D_{ww}, U_{10} ($m s^{-1}$)	CHTC_{min, outside facade} ($W m^{-2} K^{-1}$)	CHTC_{max, inside WW facade} ($W m^{-2} K^{-1}$)	Difference (%)
Case 1 ($4 \times 14 \times 6$), 270° , 0 (deg), 3W, $U_{10} = 2.3$ ($m s^{-1}$)	6.02	4.56	24.25%	
Case 2 ($7 \times 14 \times 6$), 270° , 0 (deg), 3W, $U_{10} = 2.3$ ($m s^{-1}$)	6.04	4.57	24.34%	
Case 3 ($10 \times 14 \times 6$), 270° , 0 (deg), 3W, $U_{10} = 2.3$ ($m s^{-1}$)	6.10	4.51	26.07%	
Case 4 ($13 \times 14 \times 6$), 270° , 0 (deg), 3W, $U_{10} = 2.3$ ($m s^{-1}$)	6.10	4.46	26.89%	
Case 5 ($16 \times 14 \times 6$), 270° , 0 (deg), 3W, $U_{10} = 2.3$ ($m s^{-1}$)	6.31	4.44	29.64%	
Case 6 ($19 \times 14 \times 6$), 270° , 0 (deg), 3W, $U_{10} = 2.3$ ($m s^{-1}$)	6.26	4.42	29.39%	
Case 7 ($22 \times 14 \times 6$), 270° , 0 (deg), 3W, $U_{10} = 2.3$ ($m s^{-1}$)	6.39	4.43	30.67%	
Case 9 ($7-10 \times 14 \times 6$) Step up, 270° , 0 (deg), 3W, $U_{10} = 2.3$ ($m s^{-1}$)	6.00	4.18	30.33%	
Case 10 ($10-7 \times 14 \times 6$) Step down, 270° , 0 (deg), 3W, $U_{10} = 2.3$ ($m s^{-1}$)	5.40	4.27	20.93%	
Case 11 ($7 \times 14 \times 6$), 270° , 0 (deg), W, $U_{10} = 2.3$ ($m s^{-1}$)	6.03	4.50	25.37%	
Case 12 ($7 \times 14 \times 6$), 270° , 0 (deg), 2W, $U_{10} = 2.3$ ($m s^{-1}$)	5.99	4.52	24.54%	

Table 3. Comparison between minimum CHTC on outside windward façade and maximum CHTC inside courtyard on windward façade for all experimental models (Continued)


	Case study, Courtyard dimensions ($H \times W \times D$ m), dominant Wind direction , roof slope, D_{ww}, U_{10} ($m\ s^{-1}$)	CHTC_{min, outside facade} ($W\ m^{-2}\ K^{-1}$)	CHTC_{max, inside WW facade} ($W\ m^{-2}\ K^{-1}$)	Difference (%)
Case 13 ($7 \times 14 \times 6$), 270° , 0 (deg), 4W, $U_{10} = 2.3$ ($m\ s^{-1}$)	6.00	4.56	24.00%	
Case 14 ($7 \times 14 \times 6$), 270° , 0 (deg), 5W, $U_{10} = 2.3$ ($m\ s^{-1}$)	5.94	4.83	18.69%	
Case 15 ($7 \times 14 \times 6$), 225° , 0 (deg), 3W, $U_{10} = 2.3$ ($m\ s^{-1}$)	-	4.62	-	
Case 16 ($7 \times 14 \times 6$), 192° , 0 (deg), 3W, $U_{10} = 2.3$ ($m\ s^{-1}$)	-	4.62	-	
Case 17 ($7 \times 14 \times 6$), 270° , 9.5 (deg), 3W, $U_{10} = 2.3$ ($m\ s^{-1}$) – Up to eaves height (6.90m)	5.96	4.38	26.51%	
Case 18 ($7 \times 14 \times 6$), 270° , 18.5 (deg), 3W, $U_{10} = 2.3$ ($m\ s^{-1}$) – Up to eaves height (4.50m)	5.43	4.14	23.76%	
Case 19 ($7 \times 14 \times 6$), 270° , 26.5 (deg), 3W, $U_{10} = 2.3$ ($m\ s^{-1}$) – Up to eaves height (3.90m)	5.23	4.11	21.41%	
Case 20 ($7 \times 14 \times 6$), 270° , 33.75 (deg), 3W, $U_{10} = 2.3$ ($m\ s^{-1}$) – Up to eaves height (1.50m)	4.88	4.03	17.42%	
Case 21 ($7 \times 14 \times 6$), 270° , 40 (deg), 3W, $U_{10} = 2.3$ ($m\ s^{-1}$) – Up to eaves height (0.90m)	4.88	4.13	15.37%	
Ideal case ($22 \times 14 \times 6$), 270° , 0 (deg), 3W, $U_{10} = 2.3$ ($m\ s^{-1}$), Step-up	6.00	4.17	30.50%	

Table 3. Comparison between minimum CHTC on outside windward façade and maximum CHTC inside courtyard on windward façade for all experimental models (Continued)



	Case study, Courtyard dimensions ($H \times W \times D$ m), dominant Wind direction , roof slope, D_{WW}, U_{10} ($m s^{-1}$)	CHTC_{min, outside facade} ($W m^{-2} K^{-1}$)	CHTC_{max, inside WW facade} ($W m^{-2} K^{-1}$)	Difference (%)
Effect of U_{10}				
Base model: ((7× 14 × 6), 270°, 0 (deg), 3W), $U_{10} = 2.3$ ($m s^{-1}$)	6.19	4.63	25.20%	
Base model: ((7× 14 × 6), 270°, 0 (deg), 3W), $U_{10} = 3$ ($m s^{-1}$)	6.60	4.73	28.33%	
Base model: ((7× 14 × 6), 270°, 0 (deg), 3W), $U_{10} = 4$ ($m s^{-1}$)	7.33	4.93	32.74%	
Base model: ((7× 14 × 6), 270°, 0 (deg), 3W), $U_{10} = 6$ ($m s^{-1}$)	8.88	5.29	40.43%	
Base model: ((7× 14 × 6), 270°, 0 (deg), 3W), $U_{10} = 8$ ($m s^{-1}$)	10.20	5.72	43.92%	
Base model: ((7× 14 × 6), 270°, 0 (deg), 3W), $U_{10} = 10$ ($m s^{-1}$)	11.74	6.08	48.21%	
Model 4 (H/W)=2.17: ((13× 14 × 6), 270°, 0 (deg), 3W), $U_{10} = 2.3$ ($m s^{-1}$)	6.10	4.53	26.89%	
Model 4 (H/W)=2.17: ((13× 14 × 6), 270°, 0 (deg), 3W), $U_{10} = 3$ ($m s^{-1}$)	6.60	4.59	30.45%	
Model 4 (H/W)=2.17: ((13× 14 × 6), 270°, 0 (deg), 3W), $U_{10} = 4$ ($m s^{-1}$)	7.47	4.78	36.01%	
Model 4 (H/W)=2.17: ((13× 14 × 6), 270°, 0 (deg), 3W), $U_{10} = 6$ ($m s^{-1}$)	8.98	5.11	43.10%	

Table 3. Comparison between minimum CHTC on outside windward façade and maximum CHTC inside courtyard on windward façade for all experimental models (Continued)

	Case study, Courtyard dimensions ($H \times W \times D$ m), dominant Wind direction , roof slope, D_{ww}, U_{10} ($m s^{-1}$)	CHTC_{min, outside facade} ($W m^{-2} K^{-1}$)	CHTC_{max, inside WW facade} ($W m^{-2} K^{-1}$)	Difference (%)
Model 4 ($H/W=2.17$): (($13 \times 14 \times 6$), 270° , 0 (deg), $3W$), $U_{10}= 8$ ($m s^{-1}$)	10.56	5.45	48.39%	
Model 4 ($H/W=2.17$): (($13 \times 14 \times 6$), 270° , 0 (deg), $3W$), $U_{10}= 10$ ($m s^{-1}$)	11.70	5.83	50.17%	

5. Conclusion

In recent years, as the use of glazing facades which have lower mass resistance increases, it becomes more necessary to improve climatic loads on exterior building envelopes. It was demonstrated that the microclimate of the courtyard creates a shield zone and improves surface resistance, which governs the convective and radiative heat exchange. In this study, the simple approach was used to investigate the effect of this space and various design alternatives on WS and CHTC using high-resolution 3D steady RANS simulations with ENVI-met.

The results agreed with the previous studies results (Table 1) and show that WS near the façade and therefore CHTC through the walls surrounding the courtyard, with various configurations, can be considered less than exposed surfaces in energy calculations. Moreover, a comparison of the CHTC inside the courtyard for various ambient WSs (3 – 10 (m s^{-1})) shows that the diminution rate is more for higher ambient velocities.

According to the results, the CHTC and WS in front of the façade inside the courtyard can also be affected by the design configurations. Various common strategies, including different proportions of height to width, step-up and step-down design concepts, the various thickness for surrounding buildings, three main different wind directions and various roof pitches, were considered in the five phases of this study. The findings show that among various design scenarios, the aspect ratio has a considerable effect on CHTC inside the courtyard and WS at low levels ($< 0.5H$) of the deep courtyards ($H/W > 2$) is near zero.

Finally, the results indicate that the developing microclimate spaces between buildings with reducing the CHTC through the building exterior surfaces can raise the thermal resistance without the need for expensive insulating materials and allows the designers to use large-scale glass facades.

In addition, it is important to do a heat load calculation with the decline in CHTC. However, it should be considered that the percentages calculated in this paper are only valid for comparison in this specific flow field. To obtain accurate correlations that can be applied in other cases, further investigations are needed.

References

- Al-Hafith, O., B K, S., Bradbury, S., & de Wilde, P. (2017). The Impact of Courtyard parameters on its shading level An experimental study in Baghdad, Iraq. *Energy Procedia*, 134, 99–109. <https://doi.org/https://doi.org/10.1016/j.egypro.2017.09.539>

- Allegrini, J., Dorer, V., Defraeye, T., & Carmeliet, J. (2012). An adaptive temperature wall function for mixed convective flows at exterior surfaces of buildings in street canyons. *Building and Environment*, *49*, 55–66. <https://doi.org/https://doi.org/10.1016/j.buildenv.2011.09.025>
- Almhafdy, A., Ibrahim, N., Ahmad, S. S., & Yahya, J. (2015). Thermal Performance Analysis of Courtyards in a Hot Humid Climate Using Computational Fluid Dynamics CFD Method. *Procedia - Social and Behavioral Sciences*, *170*, 474–483. <https://doi.org/http://dx.doi.org/10.1016/j.sbspro.2015.01.012>
- ALVAREZ, S., SANCHEZ, F., & MOLINA, J. L. (1998). Air flow pattern at courtyards. *Environmentally Freindly Cities*, 503–506. Retrieved from http://www.aivc.org/sites/default/files/airbase_11854.pdf
- Assimakopoulos, V. D., ApSimon, H. M., & Moussiopoulos, N. (2003). A numerical study of atmospheric pollutant dispersion in different two-dimensional street canyon configurations. *Atmospheric Environment*, *37*(29), 4037–4049. [https://doi.org/https://doi.org/10.1016/S1352-2310\(03\)00533-8](https://doi.org/https://doi.org/10.1016/S1352-2310(03)00533-8)
- Azizi, M. M., & Javanmardi, K. (2017). The Effects of Urban Block Forms on the Patterns of Wind and Natural Ventilation. *Procedia Engineering*, *180*, 541–549. <https://doi.org/https://doi.org/10.1016/j.proeng.2017.04.213>
- Badas, M. G., Ferrari, S., Garau, M., & Querzoli, G. (2017). On the effect of gable roof on natural ventilation in two-dimensional urban canyons. *Journal of Wind Engineering and Industrial Aerodynamics*, *162*, 24–34. <https://doi.org/https://doi.org/10.1016/j.jweia.2017.01.006>
- BALDWIN, B., & LOMAX, H. (1978). Thin-layer approximation and algebraic model for separated turbulentflows. In *16th Aerospace Sciences Meeting*. American Institute of Aeronautics and Astronautics. <https://doi.org/doi:10.2514/6.1978-257>
- Battista, G. (2017). Analysis of Convective Heat Transfer at Building Facades in Street Canyons. *Energy Procedia*, *113*, 166–173. <https://doi.org/https://doi.org/10.1016/j.egypro.2017.04.048>
- Berkovic, S., Yezioro, A., & Bitan, A. (2012). Study of thermal comfort in courtyards in a hot arid climate. *Solar Energy*, *86*(5), 1173–1186. <https://doi.org/10.1016/j.solener.2012.01.010>
- Blocken, B., Defraeye, T., Derome, D., & Carmeliet, J. (2009). High-resolution CFD simulations for forced convective heat transfer coefficients at the facade of a low-rise building. *Building and Environment*, *44*(12), 2396–2412. <https://doi.org/http://dx.doi.org/10.1016/j.buildenv.2009.04.004>
- Bornstein, R. D., & Johnson, D. S. (1977). Urban-rural wind velocity differences. *Atmospheric Environment (1967)*, *11*(7), 597–604. [https://doi.org/https://doi.org/10.1016/0004-6981\(77\)90112-3](https://doi.org/https://doi.org/10.1016/0004-6981(77)90112-3)
- Bouyer, J., Inard, C., & Musy, M. (2011). Microclimatic coupling as a solution to improve building energy simulation in an urban context. *Energy and Buildings*, *43*(7), 1549–1559. <https://doi.org/http://dx.doi.org/10.1016/j.enbuild.2011.02.010>

- Bruse, M. (1999). Die Auswirkungen kleinskaliger Umweltgestaltung auf das Mikroklima Michael Bruse aus Essen Bochum , 1999.
- Bruse, M. (2004). ENVI-met documentation.
- Bruse, M. (2016). ENVI_met. A holistic microclimate model. Retrieved September 1, 2016, from <http://www.model.envi-met.com/hg2e/doku.php?id=intro:modelconept>
- Cermak, J. E. (1996). Thermal effects on flow and dispersion over urban areas: Capabilities for prediction by physical modeling. *Atmospheric Environment*, 30(3), 393–401. [https://doi.org/http://dx.doi.org/10.1016/1352-2310\(95\)00142-5](https://doi.org/http://dx.doi.org/10.1016/1352-2310(95)00142-5)
- Chew, L. W., Nazarian, N., & Norford, L. (2017). Pedestrian-Level Urban Wind Flow Enhancement with Wind Catchers. *Atmosphere*, 8, 159. Retrieved from <http://www.mdpi.com/2073-4433/8/9/159>
- Colucci, C., Mauri, L., Grignaffini, S., Romagna, M., Cedola, L., & Kanna, R. (2017). Influence of the façades convective heat transfer coefficients on the thermal energy demand for an urban street canyon building. *Energy Procedia*, 126, 10–17. <https://doi.org/https://doi.org/10.1016/j.egypro.2017.08.047>
- Davies, M. G. (2004). *Building Heat Transfer*. Wiley. Retrieved from <https://books.google.de/books?id=mJXX3nRi3CYC>
- de la Flor, F. S., & Domínguez, S. A. (2004). Modelling microclimate in urban environments and assessing its influence on the performance of surrounding buildings. *Energy and Buildings*, 36(5), 403–413. <https://doi.org/https://doi.org/10.1016/j.enbuild.2004.01.050>
- De Ridder, K. ; A., & Acero, J. ; Lauwaet, D.; Lefebvre, W.; Maiheu, B.; Mendizabal, M. (2014). *WP 4 : Climate change scenarios for urban agglomerations D4 . 1 : Validation of agglomeration-scale climate projections*. RAMSES - Science for cities in transition.
- Defraeye, T., Blocken, B., & Carmeliet, J. (2010). CFD analysis of convective heat transfer at the surfaces of a cube immersed in a turbulent boundary layer. *International Journal of Heat and Mass Transfer*, 53(1), 297–308. <https://doi.org/https://doi.org/10.1016/j.ijheatmasstransfer.2009.09.029>
- Defraeye, T., Blocken, B., & Carmeliet, J. (2011). Convective heat transfer coefficients for exterior building surfaces: Existing correlations and CFD modelling. *Energy Conversion and Management*, 52(1), 512–522. <https://doi.org/http://doi.org/10.1016/j.enconman.2010.07.026>
- Defraeye, T., & Carmeliet, J. (2010). A methodology to assess the influence of local wind conditions and building orientation on the convective heat transfer at building surfaces. *Environmental Modelling & Software*, 25(12), 1813–1824. <https://doi.org/http://doi.org/10.1016/j.envsoft.2010.06.002>
- DIN. (2003). *DIN 4108-2*. Berlin: Deutsches Institut für Normung e. V.
- DIN. (2015). *DIN EN ISO 6946*. Berlin.

- Dumitrescu, L., Baran, I., & Pescaru, R. A. (2017). The Influence of Thermal Bridges in the Process of Buildings Thermal Rehabilitation. *Procedia Engineering*, *181*, 682–689. <https://doi.org/https://doi.org/10.1016/j.proeng.2017.02.450>
- Eliasson, I., Offerle, B., Grimmond, C. S. B., & Lindqvist, S. (2006). Wind fields and turbulence statistics in an urban street canyon. *Atmospheric Environment*, *40*(1), 1–16. <https://doi.org/http://dx.doi.org/10.1016/j.atmosenv.2005.03.031>
- Energy and Resources Institute, Institut Català d’Energia, & Asia Urbs Programme. (2004). *Sustainable Building - Design Manual: sustainable building design practices*. Energy and Resources Institute. Retrieved from <https://books.google.de/books?id=cihmupBhTWIC>
- Erell, E., Pearlmutter, D., & Williamson, T. (2012). *Urban Microclimate: Designing the Spaces Between Buildings*. Taylor & Francis. Retrieved from <https://books.google.de/books?id=LHwnWaYfPNkC>
- Forouzandeh, A. (2018). Numerical modeling validation for the microclimate thermal condition of semi-closed courtyard spaces between buildings. *Sustainable Cities and Society*, *36*(Supplement C), 327–345. <https://doi.org/https://doi.org/10.1016/j.scs.2017.07.025>
- Franke, J., Hellsten, A., Schlünzen, H., Carissimo, B. (2007). *Best Practice Guideline for the CFD Simulation of Flows in the Urban Environment*. Brussel, Belgium. <https://doi.org/ISBN:3-00-018312-4>
- Ghaffarianhoseini, A., Berardi, U., & Ghaffarianhoseini, A. (2015). Thermal performance characteristics of unshaded courtyards in hot and humid climates. *Building and Environment*, *87*, 154–168. <https://doi.org/http://dx.doi.org/10.1016/j.buildenv.2015.02.001>
- Grobman, Y. J., & Elimelech, Y. (2016). Microclimate on building envelopes: testing geometry manipulations as an approach for increasing building envelopes’ thermal performance. *Architectural Science Review*, *59*(4), 269–278. <https://doi.org/10.1080/00038628.2015.1025688>
- Hagishima, A., & Tanimoto, J. (2003). Field measurements for estimating the convective heat transfer coefficient at building surfaces. *Building and Environment*, *38*(7), 873–881. [https://doi.org/10.1016/S0360-1323\(03\)00033-7](https://doi.org/10.1016/S0360-1323(03)00033-7)
- Hagishima, A., Tanimoto, J., & Narita, K. (2005). Intercomparisons of Experimental Convective Heat Transfer Coefficients and Mass Transfer Coefficients of Urban Surfaces. *Boundary-Layer Meteorology*, *117*(3), 551–576. <https://doi.org/10.1007/s10546-005-2078-7>
- Hall, D. J., Walker, S., & Spanton, A. M. (1999). Dispersion from courtyards and other enclosed spaces. *Atmospheric Environment*, *33*(8), 1187–1203. [https://doi.org/10.1016/S1352-2310\(98\)00284-2](https://doi.org/10.1016/S1352-2310(98)00284-2)
- He, Y., Monahan, A. H., & McFarlane, N. A. (2013). Diurnal variations of land surface wind speed probability distributions under clear-sky and low-cloud conditions. *Geophysical Research Letters*, *40*(12), 3308–3314. <https://doi.org/10.1002/grl.50575>

- Hu, Z.-X., Cui, G.-X., & Zhang, Z.-S. (2018). Numerical study of mixed convective heat transfer coefficients for building cluster. *Journal of Wind Engineering and Industrial Aerodynamics*, 172, 170–180. <https://doi.org/https://doi.org/10.1016/j.jweia.2017.10.025>
- Huttner, S. (2012). Further development and application of the 3D microclimate simulation ENVI-met. *Mainz: Johannes Gutenberg-Universität in Mainz*, 147. Retrieved from <http://ubm.opus.hbz-nrw.de/volltexte/2012/3112/>
- IMUK. (2016). Weather & Climate > Measurement Data. Retrieved January 1, 2017, from <https://www.muk.uni-hannover.de/258.html?&L=1>
- Institutes, M., & Toudert, F. A. (2005). Berichte des Meteorologischen Institutes der Universität Freiburg Fazia Ali Toudert Dependence of Outdoor Thermal Comfort on Street Design in Hot and Dry Climate, (15).
- Kato, M., Launder, B. (1993). Three-dimensional modelling and heat-loss effects on turbulent flow in a nominally two-dimensional cavity. *Heat and Fluid Flow*, 16, 171–177.
- Kottke, M., Grieser, J., Beck, C., Rudolf, B., & Rubel, F. (2006). World map of the Köppen-Geiger climate classification updated. *Meteorologische Zeitschrift*, 15(3), 259–263. <https://doi.org/10.1127/0941-2948/2006/0130>
- Krüger, E. L., Minella, F. O., & Rasia, F. (2011). Impact of urban geometry on outdoor thermal comfort and air quality from field measurements in Curitiba, Brazil. *Building and Environment*, 46(3), 621–634. <https://doi.org/https://doi.org/10.1016/j.buildenv.2010.09.006>
- Launder, B. E., & Spalding, D. B. (1974). The numerical computation of turbulent flows. *Computer Methods in Applied Mechanics and Engineering*, 3(2), 269–289. [https://doi.org/https://doi.org/10.1016/0045-7825\(74\)90029-2](https://doi.org/https://doi.org/10.1016/0045-7825(74)90029-2)
- Liu, J., Chen, J. M., Black, T. A., & Novak, M. D. (1996). E- ϵ modelling of turbulent air flow downwind of a model forest edge. *Boundary-Layer Meteorology*, 77(1), 21–44. <https://doi.org/10.1007/BF00121857>
- Liu, J., Heidarinejad, M., Gracik, S., & Srebric, J. (2015). The impact of exterior surface convective heat transfer coefficients on the building energy consumption in urban neighborhoods with different plan area densities. *Energy and Buildings*, 86, 449–463. <https://doi.org/https://doi.org/10.1016/j.enbuild.2014.10.062>
- Liu, Y., & Harris, D. J. (2007). Full-scale measurements of convective coefficient on external surface of a low-rise building in sheltered conditions. *Building and Environment*, 42(7), 2718–2736. <https://doi.org/http://dx.doi.org/10.1016/j.buildenv.2006.07.013>
- Long, L., & Ye, H. (2016). The roles of thermal insulation and heat storage in the energy performance of the wall materials: a simulation study. *Scientific Reports*, 6, 24181. <https://doi.org/10.1038/srep24181>
- Louka, P., Belcher, S. E., & Harrison, R. G. (1998). Measurements of air flow in an urban environment. *Journal of Wind Engineering and Industrial Aerodynamics*, 74, 485–493.

- Louka, P., Belcher, S. E., & Harrison, R. G. (2000). Coupling between air flow in streets and the well-developed boundary layer aloft. *Atmospheric Environment*, *34*(16), 2613–2621. [https://doi.org/http://dx.doi.org/10.1016/S1352-2310\(99\)00477-X](https://doi.org/http://dx.doi.org/10.1016/S1352-2310(99)00477-X)
- Loukaidou, K., Michopoulos, A., & Zachariadis, T. (2017). Nearly-zero Energy Buildings: Cost-optimal Analysis of Building Envelope Characteristics. *Procedia Environmental Sciences*, *38*, 20–27. <https://doi.org/https://doi.org/10.1016/j.proenv.2017.03.069>
- Loveday, D. L., & Taki, A. H. (1998). Outside surface resistance: Proposed new value for building design. *Building Services Engineering Research and Technology*, *19*(1), 23–29. <https://doi.org/10.1177/014362449801900104>
- Mauree, D., Coccolo, S., Kaempf, J., & Scartezzini, J.-L. (2017). Multi-scale modelling to evaluate building energy consumption at the neighbourhood scale. *PLoS ONE*, *12*(9). Retrieved from <https://doi.org/10.1371/journal.pone.0183437>
- Mellor, G. L., & Yamada, T. (1974). A Hierarchy of Turbulence Closure Models for Planetary Boundary Layers. *Journal of the Atmospheric Sciences*, *31*(7), 1791–1806. [https://doi.org/10.1175/1520-0469\(1974\)031<1791:AHOTCM>2.0.CO;2](https://doi.org/10.1175/1520-0469(1974)031<1791:AHOTCM>2.0.CO;2)
- Micallef, D., Buhagiar, V., & Borg, S. P. (2016). Cross-ventilation of a room in a courtyard building. *Energy and Buildings*, *133*, 658–669. <https://doi.org/http://dx.doi.org/10.1016/j.enbuild.2016.09.053>
- Mirsadeghi, M., Cóstola, D., Blocken, B., & Hensen, J. L. M. (2013). Review of external convective heat transfer coefficient models in building energy simulation programs: Implementation and uncertainty. *Applied Thermal Engineering*, *56*(1), 134–151. <https://doi.org/http://dx.doi.org/10.1016/j.applthermaleng.2013.03.003>
- MONTAVON, M. (2010). *Optimisation of Urban Form by the Evaluation of the Solar Potentia*. EPFL.
- Montazeri, H., & Blocken, B. (2017). New generalized expressions for forced convective heat transfer coefficients at building facades and roofs. *Building and Environment*, *119*, 153–168. <https://doi.org/https://doi.org/10.1016/j.buildenv.2017.04.012>
- Moonen, P., Dorer, V., & Carmeliet, J. (2011). Evaluation of the ventilation potential of courtyards and urban street canyons using RANS and LES. *Journal of Wind Engineering and Industrial Aerodynamics*, *99*(4), 414–423. <https://doi.org/http://dx.doi.org/10.1016/j.jweia.2010.12.012>
- Muhaisen, A. S., & Gadi, M. B. (2006). Effect of courtyard proportions on solar heat gain and energy requirement in the temperate climate of Rome. *Building and Environment*, *41*(3), 245–253. <https://doi.org/http://dx.doi.org/10.1016/j.buildenv.2005.01.031>
- Murakami, S. (1990). Computational wind engineering. *Journal of Wind Engineering and Industrial Aerodynamics*, *36*, 517–538. [https://doi.org/http://dx.doi.org/10.1016/0167-6105\(90\)90335-A](https://doi.org/http://dx.doi.org/10.1016/0167-6105(90)90335-A)
- Nunez, M., & Oke, T. R. (1977). The Energy Balance of an Urban Canyon. *Journal of Applied*

- Meteorology*, 16(1), 11–19. [https://doi.org/10.1175/1520-0450\(1977\)016<0011:TEBOAU>2.0.CO;2](https://doi.org/10.1175/1520-0450(1977)016<0011:TEBOAU>2.0.CO;2)
- Palyvos, J. A. (2008). A survey of wind convection coefficient correlations for building envelope energy systems' modeling. *Applied Thermal Engineering*, 28(8–9), 801–808. <https://doi.org/10.1016/j.applthermaleng.2007.12.005>
- Rafailidis, S. (1997). Influence of Building Areal Density and Roof Shape on the Wind Characteristics Above a Town. *Boundary-Layer Meteorology*, 85(2), 255–271. <https://doi.org/10.1023/A:1000426316328>
- Rajapaksha, I., Nagai, H., & Okumiya, M. (2003). A ventilated courtyard as a passive cooling strategy in the warm humid tropics. *Renewable Energy*, 28(11), 1755–1778. [https://doi.org/http://dx.doi.org/10.1016/S0960-1481\(03\)00012-0](https://doi.org/http://dx.doi.org/10.1016/S0960-1481(03)00012-0)
- Rodríguez-Algeciras, J., Tablada, A., Chaos-Yeras, M., De la Paz, G., & Matzarakis, A. (2018). Influence of aspect ratio and orientation on large courtyard thermal conditions in the historical centre of Camagüey-Cuba. *Renewable Energy*, 125, 840–856. <https://doi.org/https://doi.org/10.1016/j.renene.2018.01.082>
- Rojas, J. M., Galán-Marín, C., & Fernández-Nieto, E. D. (2012). Parametric study of thermodynamics in the mediterranean courtyard as a tool for the design of eco-efficient buildings. *Energies*, 5(7), 2381–2403. <https://doi.org/10.3390/en5072381>
- Salim, S. M., Buccolieri, R., Chan, A., & Di Sabatino, S. (2011). Numerical simulation of atmospheric pollutant dispersion in an urban street canyon: Comparison between RANS and LES. *Journal of Wind Engineering and Industrial Aerodynamics*, 99(2), 103–113. <https://doi.org/http://dx.doi.org/10.1016/j.jweia.2010.12.002>
- Sanyal, P., & Dalui, S. K. (2018). Effects of courtyard and opening on a rectangular plan shaped tall building under wind load. *International Journal of Advanced Structural Engineering*, 10(2), 169–188. <https://doi.org/10.1007/s40091-018-0190-4>
- Sharples, S. (1984). Full-scale measurements of convective energy losses from exterior building surfaces. *Building and Environment*, 19(1), 31–39. [https://doi.org/http://dx.doi.org/10.1016/0360-1323\(84\)90011-8](https://doi.org/http://dx.doi.org/10.1016/0360-1323(84)90011-8)
- Simon, H. (2016). New and Improved Calculation Methods for the, (MICROSCALE MODELS), 233.
- Sini, J.-F., Anquetin, S., & Mestayer, P. G. (1996). Pollutant dispersion and thermal effects in urban street canyons. *Atmospheric Environment*, 30(15), 2659–2677. [https://doi.org/http://dx.doi.org/10.1016/1352-2310\(95\)00321-5](https://doi.org/http://dx.doi.org/10.1016/1352-2310(95)00321-5)
- Soflaei, F., Shokouhian, M., Abraveshdar, H., & Alipour, A. (2017). The impact of courtyard design variants on shading performance in hot- arid climates of Iran. *Energy and Buildings*, 143, 71–83. <https://doi.org/https://doi.org/10.1016/j.enbuild.2017.03.027>
- Srivanit, M., & Hokao, K. (2013). Evaluating the cooling effects of greening for improving the

- outdoor thermal environment at an institutional campus in the summer. *Building and Environment*, 66, 158–172. <https://doi.org/10.1016/j.buildenv.2013.04.012>
- Straube, J. (2011). BSD-011: Thermal Control in Buildings. *Building Science Corporation*. Retrieved from <https://buildingscience.com/documents/digests/bsd-011-thermal-control-in-buildings>
- Tablada, A., Blocken, B., Carmeliet, J., Troyer, F. DE, & Verschure, H. (2005). Geometry of building's courtyards to favour natural ventilation: Comparison between wind tunnel experiment and numerical simulation. In *World Sustainable Building Conference*. Tokyo. Retrieved from <http://www.irbnet.de/daten/iconda/CIB3858.pdf>
- Taleghani, M., Tenpierik, M., van den Dobbelsteen, A., & Sailor, D. J. (2014). Heat in courtyards: A validated and calibrated parametric study of heat mitigation strategies for urban courtyards in the Netherlands. *Solar Energy*, 103, 108–124. <https://doi.org/https://doi.org/10.1016/j.solener.2014.01.033>
- Terjung, W. H., & O'Rourke, P. A. (1980). Simulating the causal elements of urban heat islands. *Boundary-Layer Meteorology*, 19(1), 93–118. <https://doi.org/10.1007/BF00120313>
- Tominaga, Y., Mochida, A., Yoshie, R., Kataoka, H., Nozu, T., Yoshikawa, M., & Shirasawa, T. (2008). AIJ guidelines for practical applications of CFD to pedestrian wind environment around buildings. *Journal of Wind Engineering and Industrial Aerodynamics*, 96(10), 1749–1761. <https://doi.org/http://dx.doi.org/10.1016/j.jweia.2008.02.058>
- Toparlar, Y., Blocken, B., Maiheu, B., & van Heijst, G. J. F. (2017). A review on the CFD analysis of urban microclimate. *Renewable and Sustainable Energy Reviews*, 80, 1613–1640. <https://doi.org/https://doi.org/10.1016/j.rser.2017.05.248>
- Turner, W. C., & Doty, S. (2013). *Energy Management Handbook: 8th Edition*. Lulu.com. Retrieved from <https://books.google.de/books?id=T6lUCAAQBAJ>
- Wang, F., & Liu, Y. (2002). Thermal environment of the courtyard style cave dwelling in winter. *Energy and Buildings*, 34(10), 985–1001. [https://doi.org/10.1016/S0378-7788\(01\)00145-1](https://doi.org/10.1016/S0378-7788(01)00145-1)
- Wilson, J. D. (1988). A second-order closure model for flow through vegetation. *Boundary-Layer Meteorology*, 42(4), 371–392. <https://doi.org/10.1007/BF00121591>
- Wong, N H., Feriadi, H., Tham, K W., Sekhar, C., Cheong, K W. (2000). Natural ventilation characteristics of courtyard buildings in Singapore. *Air Distribution in Rooms: Ventilation for Health and Sustainable Environment*, 2, 1213–1218.
- Xie, J., Cui, Y., Liu, J., Wang, J., & Zhang, H. (2017). Study on Convective Heat Transfer Coefficient on Vertical External Surface of Island-reef Building Based on Naphthalene Sublimation Method. *Energy and Buildings*. <https://doi.org/https://doi.org/10.1016/j.enbuild.2017.09.092>
- Xie, X., Huang, Z., Wang, J., & Xie, Z. (2005). The impact of solar radiation and street layout on pollutant dispersion in street canyon. *Building and Environment*, 40(2), 201–212.

- <https://doi.org/http://dx.doi.org/10.1016/j.buildenv.2004.07.013>
- Yang, W., Zhu, X., & Liu, J. (2017). Annual experimental research on convective heat transfer coefficient of exterior surface of building external wall. *Energy and Buildings*. <https://doi.org/https://doi.org/10.1016/j.enbuild.2017.08.075>
- Yassin, M. F. (2011). Impact of height and shape of building roof on air quality in urban street canyons. *Atmospheric Environment*, 45(29), 5220–5229. <https://doi.org/http://dx.doi.org/10.1016/j.atmosenv.2011.05.060>
- Yoshie, R., Mochida, A., Tominaga, Y., Kataoka, H., Harimoto, K., Nozu, T., & Shirasawa, T. (2007). Cooperative project for CFD prediction of pedestrian wind environment in the Architectural Institute of Japan. *Journal of Wind Engineering and Industrial Aerodynamics*, 95(9), 1551–1578. <https://doi.org/http://dx.doi.org/10.1016/j.jweia.2007.02.023>
- Zhang, L., Zhang, N., Zhao, F., & Chen, Y. (2004). A genetic-algorithm-based experimental technique for determining heat transfer coefficient of exterior wall surface. *Applied Thermal Engineering*, 24(2), 339–349. <https://doi.org/http://dx.doi.org/10.1016/j.applthermaleng.2003.07.005>

Paper C

Note. Reprinted from “Accurate prediction of heating energy demand of courtyard’s surrounding envelopes using temperature correction factor” by A. Forouzandeh & T. Richter, 2019, Journal of Energy and Buildings, Volume 193, page 49-68. Copyright (2019) by Elsevier B.V. (Appendix 4)

Title	Accurate prediction of heating energy demand of courtyard’s surrounding envelopes using temperature correction factor
Author(s)	Aysan Forouzandeh, Torsten Richter
Publication outlet	Journal of Energy and Buildings
Publication type	Journal paper
Publication year	2019
Publication status	Published
Volume	193
Issue	-
Pages	49-68
DOI	https://doi.org/10.1016/j.enbuild.2019.03.030
Impact Factor	4.49
Highlights	<ul style="list-style-type: none"> • Air temperature inside courtyard semi-closed spaces, depending on its configuration can be more or less than ambient outside temperature and should be applied in calculation of the buildings energy consumption. • Thermal resistance of surrounding materials has a direct effect on the minimum temperature and $F_{x,Heat\ load}$, inside middle and narrow courtyards. • High reflective and absorptive glass facade can slightly mitigate courtyard cold island during sunny hours but have not a great effect on air temperature in early morning and therefore on $F_{x,Heat\ load}$.

Author contribution statements

Title: Accurate prediction of heating energy demand of courtyard's surrounding envelopes using temperature correction factor

DOI: <https://doi.org/10.1016/j.enbuild.2019.03.030>

Journal: Energy & Buildings

Corresponding and first author: Aysan Forouzandeh

Received at Editorial Office: 18 Sep 2018

Article accepted for publication: 18 Mar 2019

Authors: Aysan Forouzandeh, Torsten Richter

Department of Civil Engineering and Geodetic Science, Institute for building physics, Leibniz University, Hannover, Germany

1. Aysan Forouzandeh

- Conception or design of the work
- Conceived and planned the experiments and data collection (carried out the experiment measurement in Microbiological Institute of Leibniz University, VHV-Group office building)
- Performed the analytic calculations and performed the numerical simulations
- Data analysis and interpretation
- Drafting the article
- Critical revision of the article
- Final approval of the version to be published

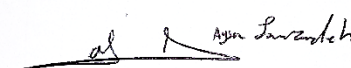
2. Torsten Richter

- Performed the site measurement in (VHV-Group office building)

All authors discussed the results and commented on the manuscript.

Author's signature:

Author 1: Aysan Forouzandeh



Author 2: Torsten Richter



Date: 21.03.2019

Accurate prediction of heating energy demand of courtyard's surrounding envelopes using temperature correction factor

Abstract

It is widely accepted that the climatic factors — including solar load, wind flow pattern and external air temperature — strongly affect building energy consumption. Meanwhile, the microclimate of semi-closed spaces between buildings has direct and indirect consequences on heat transfer through building envelopes.

This study demonstrates how courtyard configuration can modify the climate and external air temperature and how the microclimate condition can be considered for functionally accurate calculation of heat loss and thermal loads of buildings.

Based on the experimental and computational results, increasing the courtyard's depth by restricting the sky view factor (SVF) and the heat exchange with courtyard's outside at low levels, creates the individual microclimate. The thermal environment of this middle space is affected more than outside by surrounding rooms and the thermal properties of the building walls.

The findings, which are limited to experimental cases in the Hanover climate region, propose to consider the temperature of courtyard depending on its aspect ratio and glazing percentage with a temperature correction factor ($F_{x, \text{Heat load}}$) between 0.9 to 2.2.

Keywords: Courtyard microclimate, Heat transfer through building envelope, Temperature correction Factor, Aspect ratio (H/W)

Nomenclature			
A_i	Surface area of building element (i), m ²	R_{lw}	Long-wave radiation at the surface, (W m ⁻²)
A_{tl}	Heat transmitting surrounding area, m ²	RMSE	Root mean squared error, °C or K
α_s	Solar absorptance of the surface, dimensionless	SVF	Sky view factor, dimensionless
$c_1; c_2$ c_3	Empiric constants, taken from (Launder & Spalding, 1974)	t	Time, s
c_p	Specific heat capacity of the air with constant pressure, [1006 J kg ⁻¹ K ⁻¹ for 20 °C air temperature]	Th	The production and dissipation of turbulent energy caused by thermal stratification (buoyancy production), (m ² s ⁻²)
E	Local turbulent energy, (m ² s ⁻²)	To	External air temperature, K
$F_{x,i}$	Temperature correction factor for heat loss and heat load, dimensionless	T _s	External surface temperatures, K
G	Total solar irradiance incident upon the surface, (W m ⁻²)	U ₁₀	Wind speed at 10m above the ground, (ms ⁻¹)
g	Gravitational acceleration, (m s ⁻²)	$u_i = \{u,v,w\}$	Wind velocity vectors, (m s ⁻¹)
H	Height of the courtyard, m	W	Width of the courtyard, m
h_c	Convective heat transfer coefficient, (W m ⁻² K ⁻¹)	WW	Windward
K_E , $K\epsilon$	Turbulent and dissipation kinetic energy, (m ² s ⁻²)	$x_i = \{x,y,z\}$	Cartesian co-ordinates
K_θ	diffuse coefficient of heat, (m ² s ⁻¹)	Z ₀	Roughness length, m
L	Total (Incoming or outgoing) long-wave irradiance incident upon the surface, (Wm ⁻²)	<i>Greek letter</i>	
LAD	Leaf area density, (m ² m ⁻³)	ω	The maximum cutoff angle in special direction π
LE	The latent heat flux into the atmosphere due to the evaporation, L is the specific latent heat of evaporation, units (J kg ⁻¹) and E is the evaporation rate, with units (kg m ⁻² s ⁻¹)	σ	Stefan- Boltzmann constant = 5.6697×10^{-8} (W m ⁻² K ⁻⁴)
Pr	Production and dissipation of turbulent energy caused by wind shearing, (m ² s ⁻²)	ϵ	Long wave emittance of the surface (assumed equal to the long wave absorptance), dimensionless
q	Net heat flow from or into the surface, (W m ⁻²)	λ	Turbulence dissipation ratio, (m ² s ⁻³)
Q _c	Heat exchange between courtyard air and all the envelope surfaces through convection, (W m ⁻²)	θ_e	Thermal conductivity of material, (W m ⁻¹ K ⁻¹)
			Standard outside temperature, °C

Q_E	The turbulence induced by vegetation, ($m^2 s^{-2}$)	U_i	Mean thermal transmittance coefficient of building element, ($W m^{-2} K^{-1}$)
Q_G	Heat exchange between the courtyard air and the earth, ($W m^{-2}$)	ΔU_{TB}	Thermal bridge correction factor, generally $\Delta U_{TB} = 0.1 (W m^{-2} K^{-1})$
Q_V	Heat exchange by natural convection through the top of the courtyard, ($W m^{-2}$)	ρ	Density of air, ($Kg m^{-3}$)
Q_W	Conduction heat flux from or to the adjacent node inside the wall, ($W m^{-2}$)	θ_i	Standard inside temperature of the courtyard surrounding rooms (i), °C
Q_θ	Heat exchange between air and vegetation, ($W m^{-2}$)	θ_u	Temperature of the neighboring special room (x)(here courtyard), °C
R	Thermal resistance, ($m^2 K W^{-1}$)	θ	Potential air temperature, °C
RANS	Reynolds-averaged Navier–Stokes	ΔT	Temperature difference between building's inside and outside, K
RH	Relative Humidity, %	$\Delta \theta$	Temperature difference between wall and its surrounding, K
Ri_b	Bulk Richardson Number, dimensionless	$\Delta \omega$	Distance between the surface and the first grid of air next to it, m

1. Introduction

In recent years, more attention has been given to exploring the links between buildings and their surroundings. The results indicate that improving the exterior condition, by controlling the solar load, wind flow and external air temperature should have direct and indirect consequences on energy saving (de la Flor & Domínguez, 2004).

Considering the net energy balance at the external surface of the building:

$$q + \alpha_s G + \varepsilon L = \varepsilon \sigma T_s^4 + h_c (T_s - T_o) + LE$$

$$\begin{array}{ccc} \longleftarrow & \longleftrightarrow & \longrightarrow \\ \text{Heat Source} & & \text{Heat Sink} \end{array}$$

$$q = \frac{(\sum_{i=1}^n (F_{x,i} \cdot U_i \cdot A_i) + \Delta U_{TB} \cdot A_{tl}) \cdot (\Delta T)}{A_{tl}} \quad (1)$$

The thermal transmittance and thermal resistance of building enclosures are determined based on the thermal properties of materials, building shape and dimension of thermal bridges. Besides, it is commonly accepted that the energy consumption of buildings is strongly influenced by the thermal condition in front of it (Bouyer et al., 2011; Castaldo et al., 2018; Croome, 1981).

In this regard, applying innovative transitional spaces, such as courtyards, lets the building envelopes experience different climate condition (Allegrini, Kämpf, Dorer, & Carmeliet, 2013), which has an important impact on thermal condition and heating and cooling energy demand of surrounding buildings. Al-Hemiddi et al. (Al-Hemiddi & Megren Al-Saud, 2001), Aldwoud (Aldawoud, 2008), Taleghani et al. (Mohammad Taleghani, Kleerekoper, Tenpierik, & van den Dobbelsteen, 2015) and many other studies approved this response inside the courtyard space in different climate regions.

A courtyard is a very old form of human-made microclimate, traced back to 3000BC (Bednar, 1986) and was used by many urban civilizations with various climates (Pfeifer, Engelmann, & Brauneck, 2007). The microclimate of the courtyard reduces convective heat exchange and long-wave energy losses during the night and winter due to lower wind speeds and SVFs, respectively. This space can also modify the radiation balance due to its solar- shadowing effect (Allegrini et al., 2013).

The potential of the courtyard, in controlling wind and sun, affects the temperature difference between the interior and the exterior sides of the building envelope ($\theta_i - \theta_e$). As a result, the local air temperature inside the most of existing semi-closed courtyard spaces is warmer than an open space in winter and in the same way at nights, due to trapping the heat in the space. And in summer, since less solar radiation enters the space, it is cooler than outside (Sinou, 2007). Previous experiments (Table 1) show that inside the courtyard the average peak temperature drops and minimum temperature rises compare to ambient temperature. The difference varies between 276.15 – 280.15 K (3 - 7 °C), and can be considerably modified through courtyard's geometry (Rodríguez-Algeciras et al., 2018), vegetation (Charalampopoulos, Tsiros, Chronopoulou-Sereli, & Matzarakis, 2013) and physical properties of building material (Xinyan Yang, Li, & Yang, 2012).

Ignoring the difference between microclimate and outdoor air temperature on buildings energy consumption causes 30 – 60% overestimating the annual energy consumption of buildings (Brun, Spitz, Wurtz, & Mora, 2009; Erell & Williamson, 2006a; Liang, Huang, Jones, Wang, & Hang, 2018). In this regard, since the big part of the energy demand in Germany and most of European countries is related to heating (Mathiesen, 2017), DIN EN 12831-1 (DIN, 2017b) and DIN 4108-6 (DIN, 2003a) suggest a correction factor (F_x) for taking into account the effect of buffer spaces — such as sunspaces, attic, unheated basements — on the outside temperature:

$$F_{x, \text{Heat loss}} = (\theta_i - \theta_u) / (\theta_i - \theta_{e, \text{mean}}) \quad (2)$$

$$F_{x, \text{Heat load}} = (\theta_i - \theta_u) / (\theta_i - \theta_{e, \text{standard- outside temperature}}) \quad (3)$$

Where $F_{x, \text{Heat loss}}$ is related to the heat loss through envelopes and $F_{x, \text{Heat load}}$ applies in calculating the heating energy demand of the building. The former depends on the seasonal mean temperature and the latter relates to the lowest possible temperature in each climate zone.

Notwithstanding the fact that courtyard microclimate, mostly effects on the maximum and minimum outside temperature, in predicting building's energy consumption the temperature of the courtyard was theoretically defined equal to open spaces and the effect of interactions with the surroundings was ignored. Therefore, in this study, we focused especially on the effects of internal courtyards and their various configurations on the minimum air temperature in winter and $F_{x, \text{Heat load}}$ in the climatic condition of Hanover, Germany.

This correction factor is useful in the calculation phase of building's heating energy consumption and improves the accuracy of the predicted heat transfer loss for buildings with the courtyard in the climate area of Germany. The results can also be applied to the thermal design of a broad range of semi-enclosed configurations.

In this way, at the first step of the research four courtyards with different configurations in Hanover are selected and air temperature near the façade, away from direct solar radiation, is measured during the cold winter days. In the next step, since the extreme cold weather condition rarely happens, the minimum air temperature at different height levels of the courtyard is investigated under different aspect ratios, glazing percentage and glazing type, using the validated three-dimensional computational microclimate model ENVI-met. Finally, the appropriate values for temperature correction factors are suggested for different height levels of the studied cases.

Table 1. Air temperature inside the courtyard investigated through previous studies

Author	Climate	City	Courtyard description	Day	Outside temperature (°C)	Courtyard temperature
Kubota et al. (Kubota, Zakaria, Abe, & Toe, 2017)		Malaysia	Frontages 3.6 – 8.3m Depth vary from 2.1 – 84.5m Heights 2.6 – 8.9m	Sep. – Oct.	32 – 34 °C	In early morning not big difference, from 09:00 to 21:00, depends on courtyard depth, 2.5 – 5 °C less than outdoor
Almhafdy et al. (Almhafdy et al., 2015)	Af	Malaysia	u-shaped courtyard – 893 m ² – surrounded north side 5 floors, east side 4 floors and west side 3 floors	23 th Oct.		0.5 – 5 °C less than outdoor
Rajapaksha et al. (Rajapaksha et al., 2003)	Tropical climate	Colombia, Srilanka	Central rectangular courtyard The courtyard opened to the outdoor through two perpendicular axes passages, Surrounded single story building with pitched roof and tall trees	12 Apr. – 3 May	25.5 – 32.8 °C	2 °C less than ambient
Shanthi Pirya et al. (Shanthi Priya, Sundarraja, & Radhakrishnan, 2012)	Aw Tropical Savanna Climate	Nagapattinam, Cuddalore	H/W = 1 With wind catcher above	1. Nov. – Feb. 2. Mar. – Apr.	1.24 – 35 °C 2.24 – 40 °C	1. θ_{max} is 5 °C cooler than outside 2. θ_{max} is 7 °C cooler than outside Average 3 °C cooler than outside

Table 1. Air temperature inside the courtyard investigated through previous studies

Author	Climate	City	Courtyard description	Day	Outside temperature (°C)	Courtyard temperature
	BSk					
F. Wang et al. (F. Wang & Liu, 2002)	Tropical and Subtropical Steppe Climate	Loess Plateau of Northern China	(19.5 × 14.5 m), H = 3 – 3.8m	15 th – 18 th Jan.	-15 – +1 °C	-11 – +3 °C Courtyard 2 °C warmer than ambient
			Rectangular courtyard (6.80 × 23.40 × 7.25 m), H/W > 1	Jul. Feb.	39.9 – 43.4 °C 25.4 – 25.7 °C	39.6 – 41.5 °C 24.0 – 25.3 °C
			Square courtyard (14.16 × 14.16 × 14 m), H/W > 1	Jul. Feb.	39.6 – 40.8 °C 24.80 – 26.9 °C	33.6 – 39.4 °C 23.7 – 24.2 °C
	BWH					
Guedouh et al. (Guedouh & Zemmouri, 2017)	Hot desert climate	Biskra, Algeria	Square courtyard (11.50 × 11.50 × 7 m), H/W < 1	Jul. Feb.	37.8 – 38.8 °C 23.50 – 24.30 °C	37.5 – 37.9 °C 23.90 – 25.10 °C
			Rectangular courtyard (8.80 × 11.70 × 16.50 m), H/W > 1	Jul. Feb.	37.0 °C 17.6 °C	37.0 – 37.70 °C 16.90 – 17.20 °C
			Square courtyard (8.08 × 8.38 × 20 m), H/W > 1	Jul. Feb.	37.9 – 39.3 °C 19.2 – 19.8 °C	35.9 – 36 °C 20.10 – 20.70 °C

Table 1. Air temperature inside the courtyard investigated through previous studies (Continued)

Author	Climate	City	Courtyard description	Day	Outside temperature (°C)	Courtyard temperature
Berkovic et al. (Berkovic et al., 2012)		Negev area- hot-arid	(20 × 40 m), (40 × 20 m) and (28 × 28 m); H = 9 m	Jun.	26 – 30 °C	27 – 32 °C
A.Bagneid (AMR BAGNEID, 2006)	BWH	Cairo- Egypt	Square courtyard with H/W = 1	Dec. 29 th – Jan. 7 th		Maximum 10 F° warmer than outside all the day except from morning until noon
AL-Hemiddi et al. (Al-Hemiddi & Megren Al-Saud, 2001)	Hot desert climate	Riyadh, Saudi Arabia	Internal courtyard, surrounded single story building	19 th Aug. – 14 th Sep.	40 – 34 °C	1 – 4 °C less than outdoor
Meir et al. (Meir, Pearlmutter, & Etzion, 1995)		Negev Desert	(5.5 × 21 m) – Enclosed on three sides by 2.6 – 3.1 m buildings; H/W = 0.47 – 0.56	Aug. – Jul. Dec. – Jan.		7 °C higher than ambient 1.5 °C warmer than ambient
Ahmad et al. (AHMAD, KHETRISH, & Abughres, 1985)		Ghadames, Libya	Traditional courtyard house in indigenous urban cluster	Summer Winter	20 – 40 °C 4 – 23 °C	Constant at 28 °C 12 °C

Table 1. Air temperature inside the courtyard investigated through previous studies (Continued)

Author	Climate	City	Courtyard description	Day	Outside temperature (°C)	Courtyard temperature
Zhang et al. (Y. Zhang, Liu, & Mai, 2017)	Cfa Subtropical climate	Guangzhou, China	1. Square courtyard, surrounded by 24 m height walls (H/W = 1.15) 2. U-shape courtyard open to the west and surrounded by 20m height walls (H/W = 0.7)	Sunny days of summer May – Oct.		Daily mean air temperatures are lower by 1. 2.9 °C 2. 1.3 °C
Lopez- Cabeza et al. (López-Cabeza, Galán-Marín, Rivera-Gómez, & Roa-Fernández, 2018)		Seville, Spain	1. (7.4 × 3.1 × 12.6 m) 2. (7.0 × 11 × 8.9 m) 3. (7.5 × 13.2 × 10.7 m)	4 – 9 Jun.	17 – 40 °C	1. 22 – 33 °C 2. 18 – 33 °C 3. 18 – 36 °C
Rojas- Fernandez et al. (Rojas-Fernández, Galán-Marín, Roa-Fernández, & Rivera-Gómez, 2017)	Csa, Csb Mediterranean climate	South of Spain	1. (9.57 × 8.8 m), H/W=0.92 2. (28.5 × 27.5), H/W =3.66	Jun. – Oct.		Max average difference between roof and courtyards: 6.7 °C
Soltani et al. (Soltani & Sharifi, 2017)		Adelaide, Australian	Dense Street canyon	Winter- late afternoon midnight	2.7 °C 4.3 °C	3.9 °C 5.5 °C

Table 1. Air temperature inside the courtyard investigated through previous studies (Continued)

Author	Climate	City	Courtyard description	Day	Outside temperature (°C)	Courtyard temperature
Rojas et al. (Rojas et al., 2012)	Csa, Csb	Galicia, Spain Mediterranean	Deep central courtyard with H/W = 2.9	27 th Apr. – 5 th May	26.5 – 16 °C 31.23 – 20.13 °C	9 °C cooler than outside April: 18 – 23 °C May: 19 – 23 °C
Santamouris et al. (Santamouris, Papanikolaou, Koronakis, Livada, & Asimakopoulos, 1999)	Mediterranean climate	Athens, Greece	Deep Canyon H/W > 2	7 and 15 th Jul. Hot summer		At noon 1– 6°C and at night 1.5°C cooler than outside
Carrasco et al. (Carrasco & Reynolds, 1996)		Bornos, Spain	traditional courtyard house	Aug.	22 – 44 °C	26 – 29.5 °C

2. Methodology

In this study, the effect of the courtyard on minimum outside air temperature during the winter was investigated both numerically and experimentally (Fig. 1.). The method includes the following main steps:

- a) Selection of courtyards to consider the bottom winter air temperature
- b) Validation of the model for geometrical analysis
- c) Generation of various scenarios with different aspect ratio
- d) Critical assessment of possible temperature correction factor in terms of heat load calculation

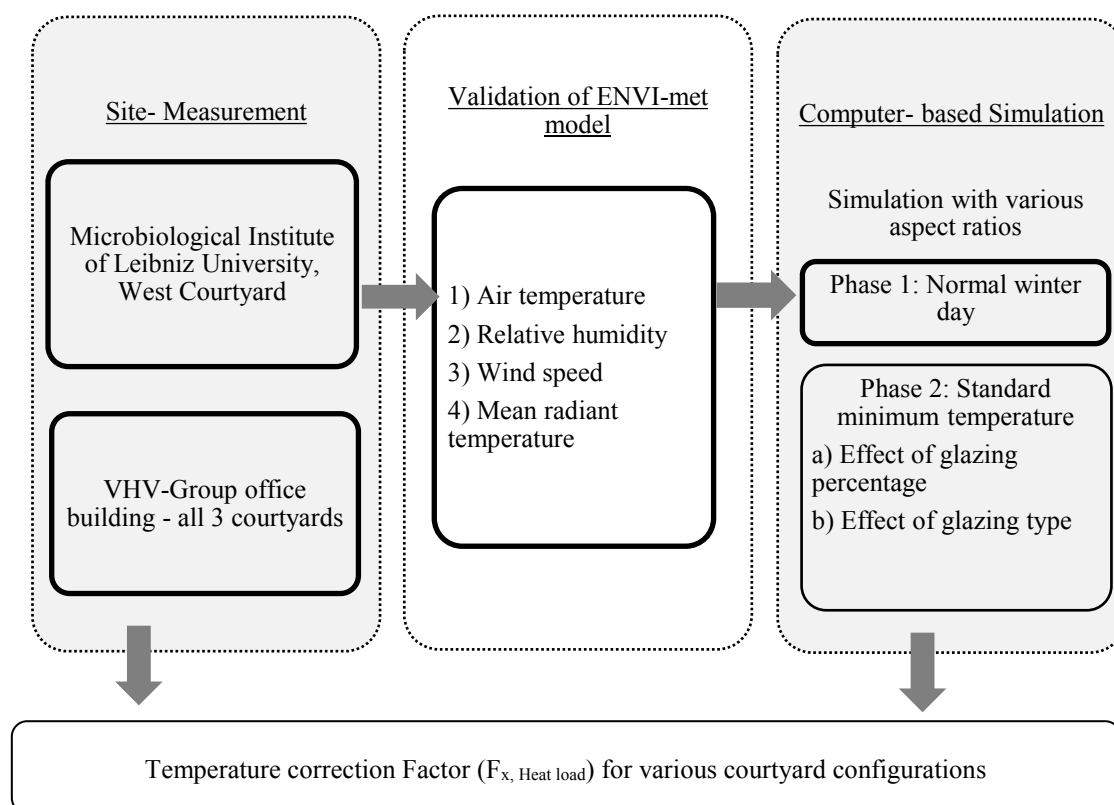


Fig. 1. An overview of methodology

2.1. Description of experimental studies

In order to consider the courtyards microclimate under real complex urban area, the study was started with field experiments. Neither wind tunnel measurements, nor computational simulation methods can fully reproduce this real complexity (Peter Moonen et al., 2012). The results, also used to validate the base computational model for the second part of the research.

2.1.1. Selected courtyards and field measurement

In the present study, an experimental model system was performed in the courtyard of the microbiological institute (IfMB) at Leibniz University and at the three courtyards of VHV-Group office building in the city of Hanover, Germany (52° 22' 13.87" N 9° 43' 59.59" E, elevation 57m a.s.l). The former is a central courtyard, which has a uniform form 6×17 m and is boarded by 7m height buildings, $H/W \approx 1$ (Fig. 2.). And the latter, including two rectangular courtyards (A; C) with aspect ratios $H/W = 0.78$ and $H/W = 2.04$ and one triangular shaped courtyard (B) with $H/W = 0.6$. The courtyard A and C are starting from the ground floor of the building and courtyard B starts from the second floor of the building (Fig. 3.). All courtyards are surrounded by the same glass facades with the same physical properties, which makes them ideal for comparison.

Table 2, describes the physical characteristics of experimental courtyards and measurement setups. The sensors used in observations are digital humidity and temperature sensors Testo 480 and Testo 177-H1 with an accuracy of ± 0.5 °C — over the range of -20 °C to + 70 °C — recording a data every 5 minutes during the January and February, with typical winter day conditions (-8 °C $< T_0 < 7.7$ °C). The production company (Testo) calibrated the sensors and the values recorded at same point are almost equal.

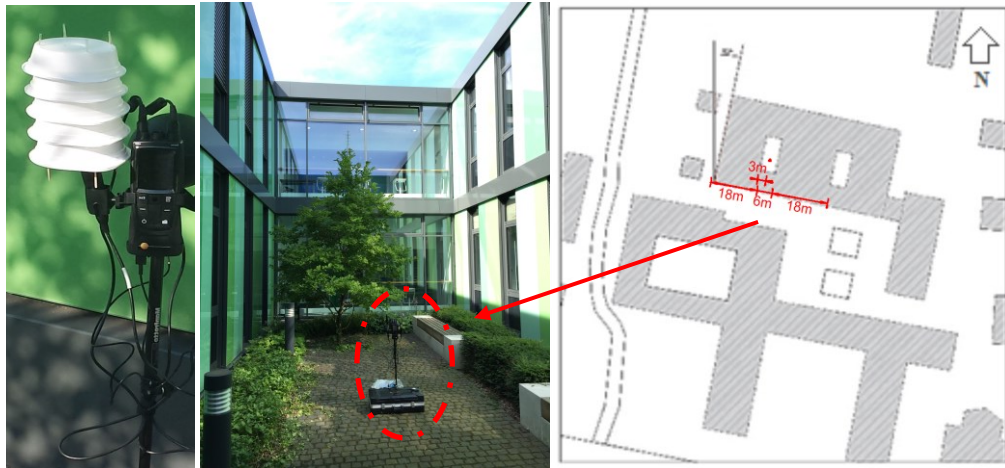


Fig. 2. Microbiological institute with the studied courtyard and measurement setup in courtyard

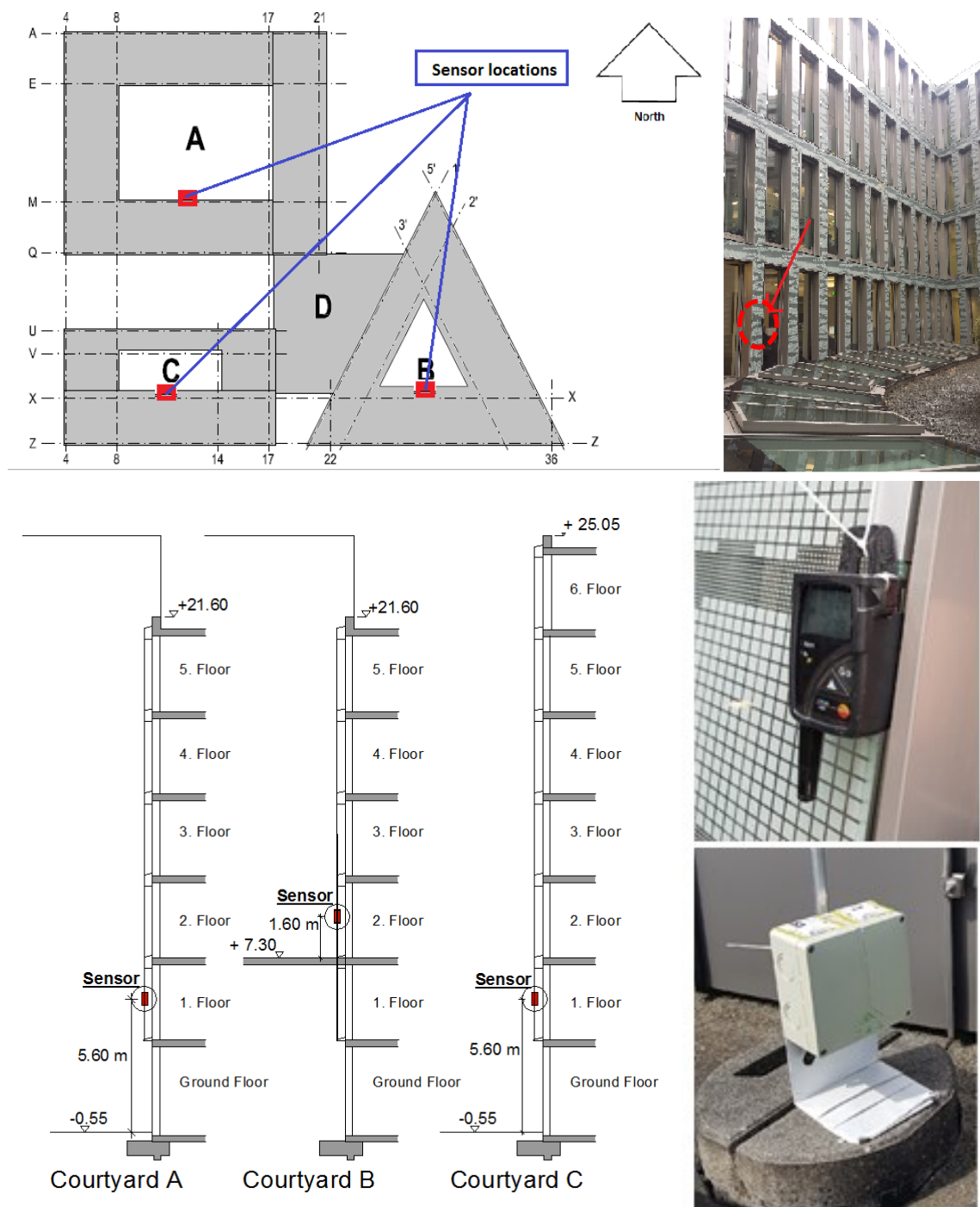


Fig. 3. VHV- Group office building with the studied courtyard spaces- Photo, plan and elevation drawing of measurement setup

The aim of the measurements was to compare the air temperature near the facade inside the courtyard with the corresponding outside temperature. In this way, inside the first case study (IfMB) the sensors were installed in shaded areas at 1.5m above the ground. The air temperatures for second three cases (VHV) were measured near the shading north-facing

walls inside the courtyard at 5.6 m above the ground for courtyard A and C and 1.6m above the ground for courtyard B (Fig. 3.). All sensors are installed on the glass cover of the strong ventilated double skin façade, which is less influenced by the inside thermal condition. In addition, the measurements have done on north façade and with considering the low heat absorption and thermal capacity of the glass, the effect of surface temperature on thermal balance can be ignored. The sensors are installed far away from the green area, since vegetation has a great effect on the air temperature (Mohammad Taleghani et al., 2014b).

Meanwhile, the outdoor temperature was registered through IMUK weather station, located 80 m away from the courtyard of IfMB. In case 2 (VHV), the weather stations are quite far away from the building and the recorded weather conditions differ from this urban context. Therefore, since it was approved that the roof temperature, recorded by the sensor, is very similar to the recorded temperature by the official weather stations (Rojas-Fernández et al., 2017), in this case, outdoor temperature was registered on the roof of the building C with a data logger. The sensor was shielded inside an opened white painted box to permit air circulation. In addition, due to the effect of building indoor temperature on the courtyard microclimate and $F_{x, \text{Heat load}}$, parallel with the measurement the temperature was recorded on the ground and first floor of the building.

Table 2. Geometrical dimensions of experimental courtyards and location of sensors

Courtyard	Plan form	dimensions						Plants/ Water bodies		Building's deep (m) (WW)	Glass façade (%)	Measuring date	Sensor	Sensor height (m)
		W (m)	D (m)	H (m)	H.diff (m)	Are. (m ²)	Vol. (m ³)	Green coverage (m ²)	Water bodies					
IfMB-Hanover	Rectangular	6	14	7	0	84	588	36	0	18	73	27.01.2017 02.02.2017	Testo 480	1.6
VHV-Group office building-Hanover	Rectangular (A)	28.35	36.95	22.15	3.45	1047.5	22349.4	~ 302.70	0	12.20	66			5.60
	Triangular (B)	21.05	21.05	14.30	3.45	247.71	3542.25	~ 62	0	10.70	62		Testo 177-H1	1.60
	Rectangular (C)	10.17	23.85	22.15	3.45	242.55	5372.50	~ 72.5	0	12.20 4.70	72.5	05. – 12.02.2018		5.60
	Inside temperature	-	-	-	-	-	-	-	-	-	-		Testo 480	Ground floor and first floor

2.1.2. Experimental results

In general, it was found that temperature gradients within the courtyard air were small and the courtyard spaces in winter were warmer than outside. However, the amount of θ_u diurnal variations are strongly depend on the configuration of the courtyard. While, for VHV office building, the ambient outdoor temperature has a deviation of 11.7 °C, from -7.80 °C to 3.90 °C, the air temperature in the courtyard A, B and C has a diurnal variation of 9.83°C (from -5.71 °C to 4.12 °C), 9.69 °C (from -5.37 °C to 4.33 °C) and 9.63 °C (from -4.69 °C to 4.93 °C), respectively. Similarly, inside the IfMB courtyard, the air fluctuation is 3 °C (from 4.70 °C to 7.70 °C), which is less than 4.7 °C (from 2.5 °C to 7.20 °C) for outside (Fig. 4 and 5).

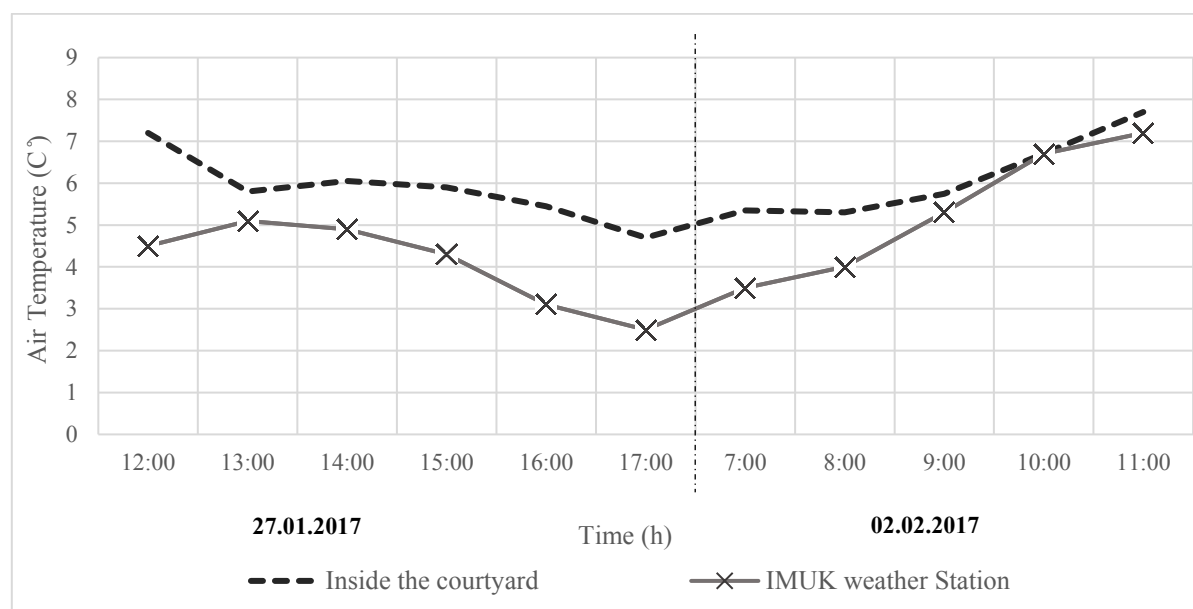


Fig. 4. Comparison of observed air temperature at 1.5m above ground inside IfMB-Hanover with measured average hourly air temperature at IMUK meteorological weather station

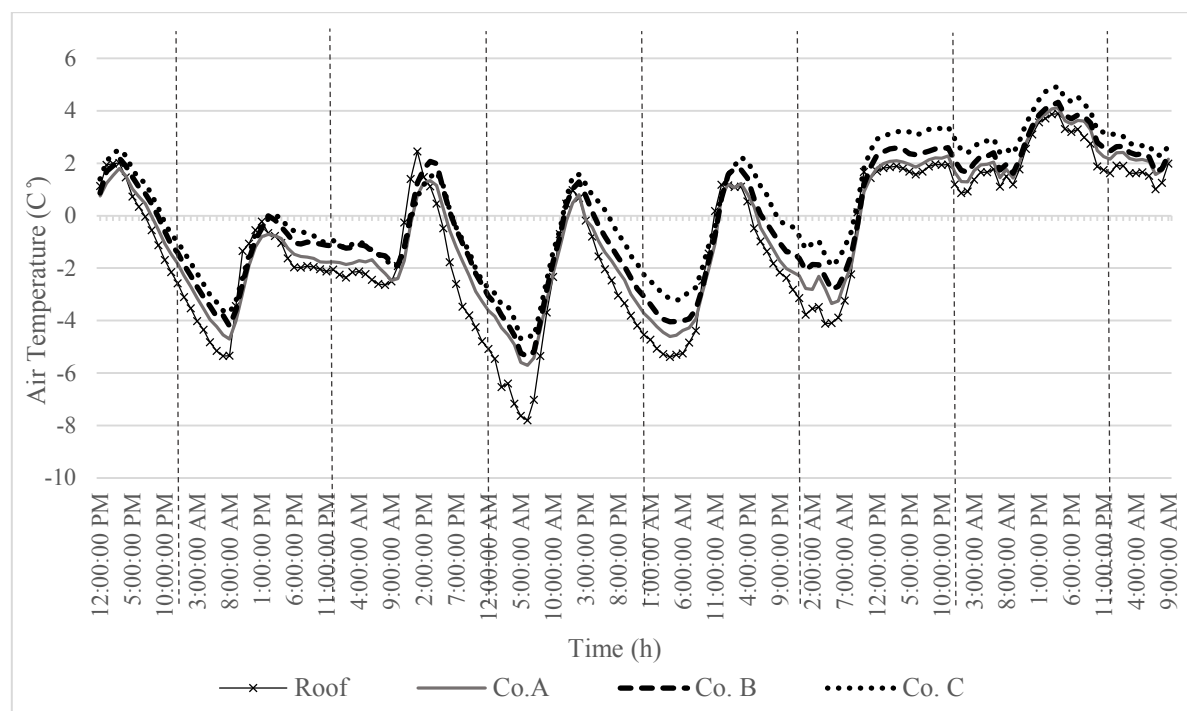


Fig. 5. Comparison of observed air temperature inside 3 courtyards of VHV with measured average hourly air temperature at roof level, 5–12 February

Analysis of the 24 hours measured air temperature inside the studied courtyards shows that, even though a higher building density decreases the solar gains inside the courtyard (Allegrini et al., 2013), this effect is less during the cloudy winter days with the low intensity of global radiation. And the courtyards studied here with reduction of the wind speed and keeping the heat, lead to a higher temperature than exposed areas during the winter.

According to the results, the air-tightness efficiency of the courtyard was good in the evening and reaches its maximum value around 06:00 in the early morning. The maximum average difference between the outside and the courtyard air temperature in the measured period was recorded during the night from 00:00 to 06:00, which due to courtyards small SVF lower energy losses into the sky (Yupeng Wang & Akbari, 2014). Also, the storage capacity of courtyard envelopes by releasing their heat during the night-time can lead to enhanced micro-scale heat island intensity inside the courtyard (F. Wang & Liu, 2002; Xinyan Yang et al., 2012). However, in the studied cases, due to a low thermal storage capacity of glass surrounding walls, this parameter is not more impressive.

The airtightness value for the courtyard decreased as the outside temperature increased. In this way, the air temperature difference between inside and outside (roof sensor) of the

considered courtyards was less during the day from 10:00 to 12:00, especially on sunny days.

As previously approved by Rojas et al. (Rojas-Fernández et al., 2017), the air temperature drop observed are more influenced by the severity of the climate. Considering the recorded temperatures, inside three courtyards located in VHV- Hanover (Fig. 5.), shows that most significant variation between outdoor and courtyard temperature, take places on coldest time of the measurement, 8th February at 6:00. In this way, the bottom temperature inside the courtyard C with $H/W = 2.04$ is $3.11\text{ }^{\circ}\text{C}$ more than outside the courtyard.

By reducing the aspect ratio, the difference between courtyard temperature and open area is reduced, where the bottom air temperature inside the courtyard A with $H/W = 0.76$ is $2.1\text{ }^{\circ}\text{C}$ more than outside.

The comparison of air temperature at 5.6m and 1.6m above ground inside the courtyards with the same aspect ratio (A and B) shows a difference between the various height levels inside the courtyard. Where θ_u at low levels, due to low wind speed and incoming heat from the ground, is more and reduces slightly with increasing the height.

Finally, $F_{x, \text{Heat load}}$ for experimental courtyards is calculated based on Eq. (3), by the recorded minimum temperature inside the courtyard and outside at roof levels or weather station, during the measurement period (Table 3). In this part, the $F_{x, \text{Heat load}}$ is exported at a fix average indoor temperature and the difference between air temperature at the ground floor ($21.82\text{ }^{\circ}\text{C}$) and upper floors ($22.69\text{ }^{\circ}\text{C}$) is ignored.

According to the results, the courtyards in all cases can create a local heat island, which its temperature can be considered in heat load calculations with the adjustment factor. In this research, we assume the air temperature inside the courtyard uniform and we suggest $F_{x, \text{Heat load}}$ for the measuring period. To calculate the exact values of the courtyard thermal function, longer observations in the different part of the courtyard space are necessary.

Table 3. Comparison between minimum air temperature inside experimental courtyards and outside in exposed area with suggested $F_{x, \text{Heat load}}$ in each case (Inside temperature: $22\text{ }^{\circ}\text{C}$)

Experimental courtyard	$T_{a.min}\text{ }(^{\circ}\text{C})$ inside courtyard	$T_{a.min}\text{ }(^{\circ}\text{C})$ Outside	$F_{x, \text{Heat load}}$
IfMB - Hanover	4.7	2.5	0.90
VHV - Hanover, Courtyard A	-5.71	-7.80	0.93
VHV - Hanover, Courtyard B	-5.37	-7.80	0.92
VHV - Hanover, Courtyard C	-4.58	-7.80	0.89

2.2. Computational studies: method and validation

In this section, the computer simulation method was selected, which offers a powerful method to test a wide range of configurations and extreme weather conditions.

Based on the experimental results and many other similar studies (Rodríguez-Algeciras et al., 2018; van Esch, Looman, & de Bruin-Hordijk, 2012; F. Wang & Liu, 2002; Y. Zhang et al., 2017) the thermal environment in courtyard microclimate greatly depends on the connection between the courtyard and its outside or the courtyard aspect ratio (H/W) than other parameters. Accordingly, in the following discussion, we focus our analysis on the minimum air temperature and its variation inside the courtyard with various aspect ratios.

The computational settings used in this section are treated based on the first case study IfMB. This building is an ideal case for various design scenarios. Since it is located in the low-density urban area and its regular geometry and same façade materials limit the influence of unpredictable environmental factors. In the following, the numerical method and computational settings are explained in detail.

2.2.1. Computational method and adjustments

The model for the mean air temperature inside the courtyard should be derived from a set of equations of heat balance between the courtyard, surrounding rooms, envelope surfaces and outside (Fig. 6.). In this way, the tools specifically dedicated to microclimate simulation in combination with the effects of building on its surrounding environment and conversely stay rare. Most of the models are often rough estimate the microclimate and the specific local urban elements and surface materials distribution are not realistic. To provide a more exact prediction of the microclimate thermal environment, appropriate tools are needed to assess the performance of the building's surfaces and indoor thermal condition, taking into account the 3D microclimate context. Among the numerical simulation tools, ENVI-met version 4 — which can simulate parallel the effect of various parameters in the microclimate simulation in combination with building physics — is selected in this project.

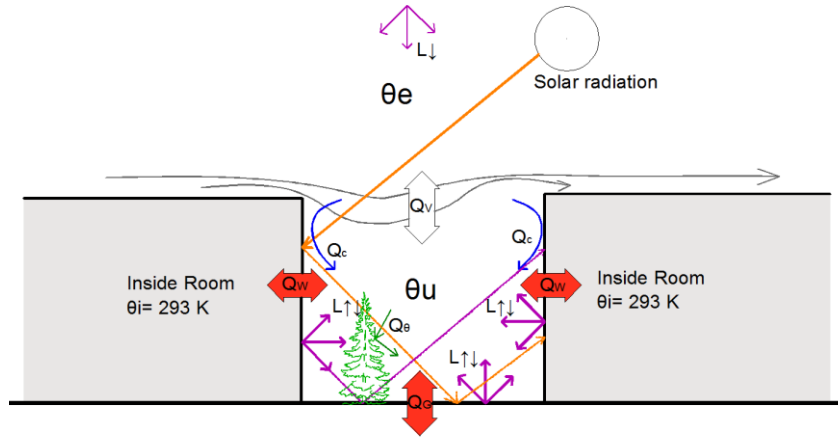


Fig. 6. Schematic diagram of heat exchange between courtyard and its surrounding

ENVI-met is based on the RANS method and is composed of four main systems: soil, vegetation, atmosphere and building. The physical model in this program identifies with a) mean air flow, b) temperature and humidity, c) turbulence and exchange processes, and d) radiative fluxes.

This comprehensive-holistic model provides the best choice for simulating, parallel with the wind flow, the thermal buoyancy and convection process, which are important inside the courtyard spaces (Maldonado & Yannas, 2014). In this way, atmospheric turbulence is set as the “Prognostic 1.5 Order E-Epsilon Closure Model”— stand on the work of Mellor and Yamada_(Mellor & Yamada, 1974) (Eq. (4)) — and the free convection exchange coefficients between the ground or building surfaces and the air at the first grid point next to the surface are calculated by the Bulk-Richardson number (Institutes & Toudert, 2005) (Eq. (5)):

$$\frac{\delta E}{\delta t} + u_i \frac{\delta E}{\delta x_i} = K_E \left(\frac{\delta^2 E}{\delta x_i^2} \right) + Pr - Th + Q_E - \epsilon$$

$$\frac{\delta \epsilon}{\delta t} + u_i \frac{\delta \epsilon}{\delta x_i} = K_\epsilon \left(\frac{\delta^2 \epsilon}{\delta x_i^2} \right) + c_1 \frac{\epsilon}{E} Pr - c_3 \frac{\epsilon}{E} Th - c_2 \frac{\epsilon^2}{E} + Q_\epsilon \quad (4)$$

$$Ri_b = \frac{g \Delta \theta \Delta \omega}{\theta (\Delta u)^2} \quad (5)$$

The Boussinesq-approximation (M. Bruse, 1999; Simon, 2016) is adopted for air density and the semi-empirical procedure by Taesler and Anderson (Taesler & Anderson, 1984) is used to calculate the atmospheric short-wave radiation fluxes.

Finally, the effect of heated building surfaces and vegetation from absorption of solar radiation (Allegrini et al., 2013), is considered in estimating the θ inside the courtyard by using the combined advection-diffusion equation as follows:

$$\frac{\partial \theta}{\partial t} + u_i \frac{\delta^2 \theta}{\delta x_i} = K_\theta \left(\frac{\delta^2 \theta}{\delta x_i^2} \right) + \frac{1}{c_p \rho} \frac{\delta R_{lw}}{\delta z} + Q_\theta \quad (6)$$

The simulations are done based on hourly weather data and to take into account the effect of buildings and vegetation on courtyards microclimate, three dimensional spatial forms of buildings, trees and other structures, and two-dimensional ground surfaces are simulated and divided into mesh grids, with a grid resolution of $2 \times 2 \times 1$ m (The grid resolution refinement has done in our previous work (Forouzandeh, 2018)).

In this research, eight different heights were defined for courtyard enclosures (Fig. 7.). The model area and the number of grids for each model are described in Table 4. In addition, to rise the numerical stability of the simulation with objects close to the border of the study area, 8-9 nesting grids are added on each side.

The size of the three-dimensional computational domain is determined according to the guideline by Franke et al. (Franke, J., Hellsten, A., Schlünzen, H., Carissimo, 2007) and Tominaga et al. (Yoshihide Tominaga et al., 2008). The lateral size of the domain is adjusted at least five times higher than the highest building and the height of the model is defined at least to ten times the height of the tallest structure (Fig. 8.). In the model, all solid surfaces, ground and buildings are simulated with a no-slip condition. Furthermore, the following properties were implemented:

1. Meteorological data: This part is divided into two phases, in order to consider air temperature near the courtyard envelopes during the winter, and while the heat load of the building and $F_{x, \text{heat load}}$ is calculated for extremely low temperature.

Phase 1: In this phase, the simulations are based on the weather data on the normal winter day, 27. January 2017 ($-3.6 \text{ }^\circ\text{C} < \text{Air Temperature} < +5.6 \text{ }^\circ\text{C}$, $51.60\% < \text{RH} < 83.40\%$). The initial hourly temperature is set to the whole vertical profile up to 2500m and the air humidity profile is calculated by means of specific humidity in $2500\text{m} = 1 \text{ (g kg}^{-1}\text{)}$ and the hourly RH at 2m. $U_{10} = 2.3 \text{ (m s}^{-1}\text{)}$ was set perpendicular to the building and is supposed to be constant during the simulation. In such a way, based on the input wind at 10m height and $z_0 = 0.1\text{m}$, the vertical wind flow profile

up to a height of 2500m, is calculated with the 1D model by applying a logarithmic law (Fig. 8.).

The solar radiation adjustment was based on the global radiation values measured at the IMUK weather station. In this way, a constant cloud cover value (2/8) was selected for the simulation period and to adjust the solar radiation, it was considered with factor 0.7. Since in Hanover during the winter the sky is overcast or mostly cloudy, approximately 70% of the time (“Weather Spark,” 2016), this assumption can be considered as typical Hanover average sky cover during the winter.

Phase 2: For calculating the $F_{x, \text{heat load}}$, the outside temperature at all hours of the day is set $-14\text{ }^{\circ}\text{C}$. This is in accordance with standard minimum external design temperature, in DIN EN 12831 Bbl.1 (DIN, 2017b), for building with the time constant less than 100 h located in Hanover. The U_{10} and RH are defined, based on the long-term average of the years 1950 – 2013 (Deutscher Wetterdienst, n.d.), equal to $3.8\text{ (m s}^{-1}\text{)}$ and 75%, respectively.

In this phase, the simulations are done without any cloud and the adjustment factor. Since clouds can moderate the winter night thermal condition by reducing net night sky radiation and increasing the counter radiation (Bainbridge & Haggard, 2011).

2. Building construction: The air temperature near the façade depends on the facing wall material and solar radiation oblique (Kakoniti, Georgiou, Marakkos, Kumar, & Neophytou, 2016). Therefore, in this study the thermos-physical data of construction materials such as emissivity, conductivity, and solar transmittance, absorption is assigned same for all scenarios. The whole volume of the buildings is assumed to be single rooms and the influence of the inner walls and roofs are not taken into consideration. The indoor air temperature is adjusted constant = 293 K and the energy exchange at the internal surfaces — including the radiative and convective exchange with indoor air — is considered to be constant at $7.7\text{ (W m}^{-2}\text{ K}^{-1}\text{)}$.

In the first phase, the existing real materials are defined for courtyards envelopes. 75% of the surrounding walls are simulated with 3cm thickness clear glass façade with a thermal conductivity coefficient equal to $1\text{ (W m}^{-1}\text{ K}^{-1}\text{)}$, and the three layers composed ceramic glass facade with 50 cm in thickness and thermal transmittance of $0.229\text{ (W m}^{-2}\text{ K}^{-1}\text{)}$ is defined for the rest of the envelope walls. A concrete slab with thickness 30cm and $U = 0.22\text{ (W m}^{-2}\text{ K}^{-1}\text{)}$ roofs the surrounding buildings.

In the second phase of the study, the effect of heat gain from envelopes and glazing type is considered by repeating the simulations for five different glazing percentage.

Furthermore, the effect of the physical properties of the glass façade is considered for three different glazing type (Fig. 9.), using the new IVS method, in which each urban element is considered using its actual state (sun reflection, thermal radiation) instead of averages fluxes (M. Bruse, 2017).

3. Soil and plant type: The prevalent soil for the study site is unsealed soil. In this way, the initial relative humidity is set to 50% for upper layer (0 – 20cm) and 60% for the middle (20 – 50cm) and lowest (> 50cm) layers. The initial temperature of the soil is adjusted to 0.1 °C, 1 °C and 2.5 °C for the upper, middle and lowest layer, respectively (Deutscher Wetterdienst, n.d.).

Since the type and arrangement of vegetation play an important role in microclimate condition (Guhathakurta & Gober, 2010; Mohammad Taleghani et al., 2015) and the accuracy of the ENVI-met model (Z. Liu, Zheng, & Zhao, 2018), inside the courtyard is simulated without any vegetation. And the 3D Crowns trees — which have the 5m width and 10m height with LAD = 2 (m² m⁻³) and albedo of 0.18 — are defined for green areas out of the courtyard within the computational domain.

4. Time steps: The main time step is set 600 s for radiation and plant processes and the surface data are updated every 30 s. In order to obtain the effect of stratification flow and show the thermal layers inside the courtyard, smaller time step $\Delta t = 0$ s is used for flow in the first phase of the simulation. However, since the results for air temperature with $\Delta t = 0$ s and 100 s are significantly similar (Forouzandeh, 2018), in order to save the computational time, the second phase was simulated with $\Delta t = 100$ s.

We ran ENVI-met for a 48 h period, starting at 03:00 on 26 Januarys. The first 24 h of the model run was discarded because the ENVI-met model requires spin-up time. The average hourly air temperature was exported at four different height levels (0.25 H, 0.5 H, 0.75 H and 1 H) for 6 points inside the courtyard and the coldest outside point in the 1m distance from the façade with the same material (Fig. 10.).

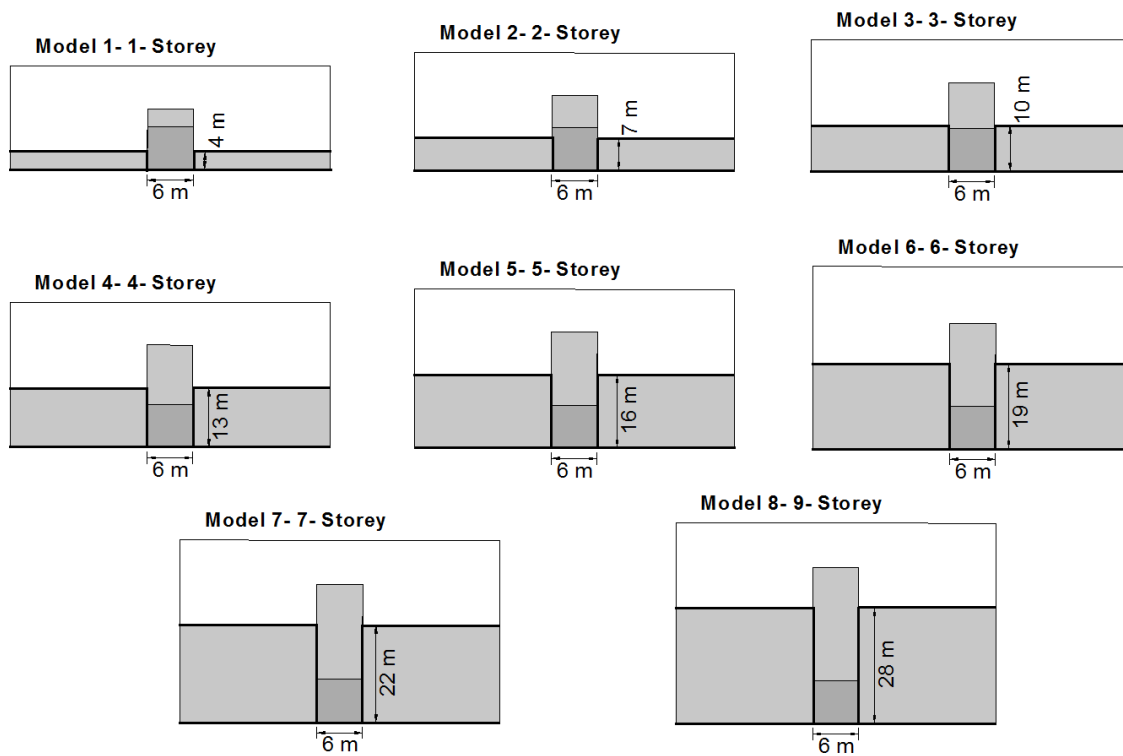
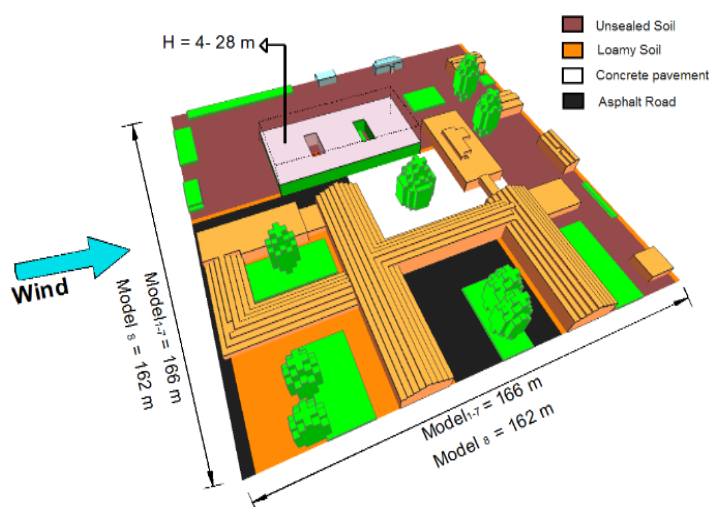
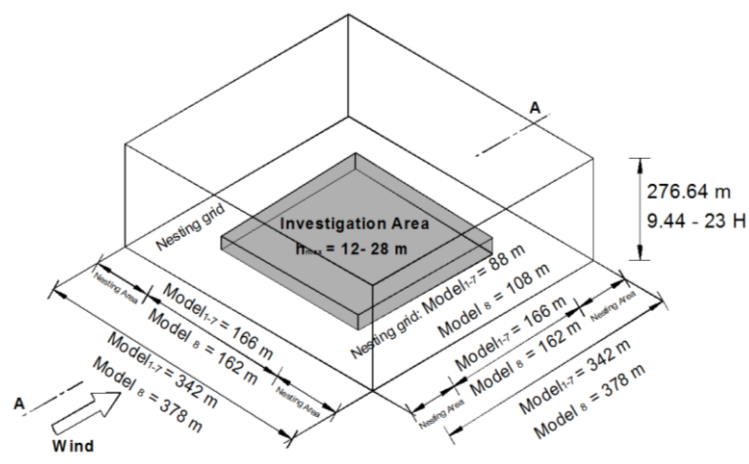


Fig. 7. Experimental models with different aspect ratios

Table 4. Overview of computational model

Model	Grids	Resolution	Core XY domain size (m)	Nesting grids	Extra space added by nesting area (m)	Height of 3D model top (m)	Highest building in domain (m)
Model 1 – 3	83 × 83 × 39	dx = 2 m, dy = 2m, dz = 1m	166 × 166	8	88	276.64	12
Model 4	83 × 83 × 39	dx = 2 m, dy = 2m, dz = 1m	166 × 166	8	88	276.64	13
Model 5	83 × 83 × 39	dx = 2 m, dy = 2m, dz = 1m	166 × 166	8	88	276.64	16
Model 6	83 × 83 × 39	dx = 2 m, dy = 2m, dz = 1m	166 × 166	8	88	276.64	19
Model 7	83 × 83 × 39	dx = 2 m, dy = 2m, dz = 1m	166 × 166	8	88	276.64	22
Model 8	81 × 81 × 39	dx = 2 m, dy = 2m, dz = 1m	162 × 162	9	108	276.64	28



1D- Model

Meteorological data

Main 3D- Model

Building - Vegetation

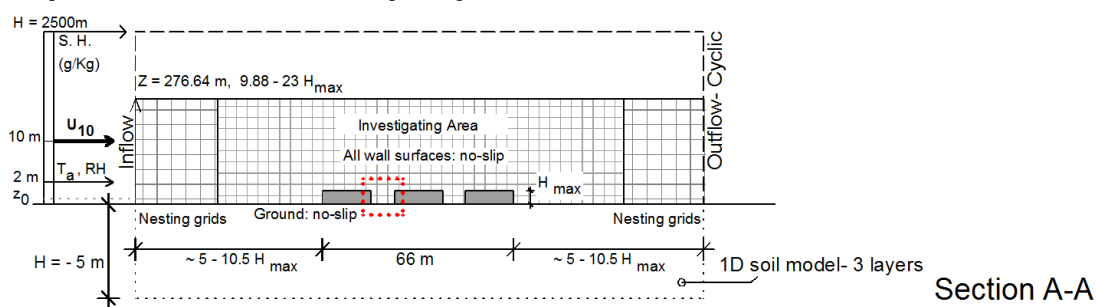


Fig. 8. Domain of computational model showing boundary conditions

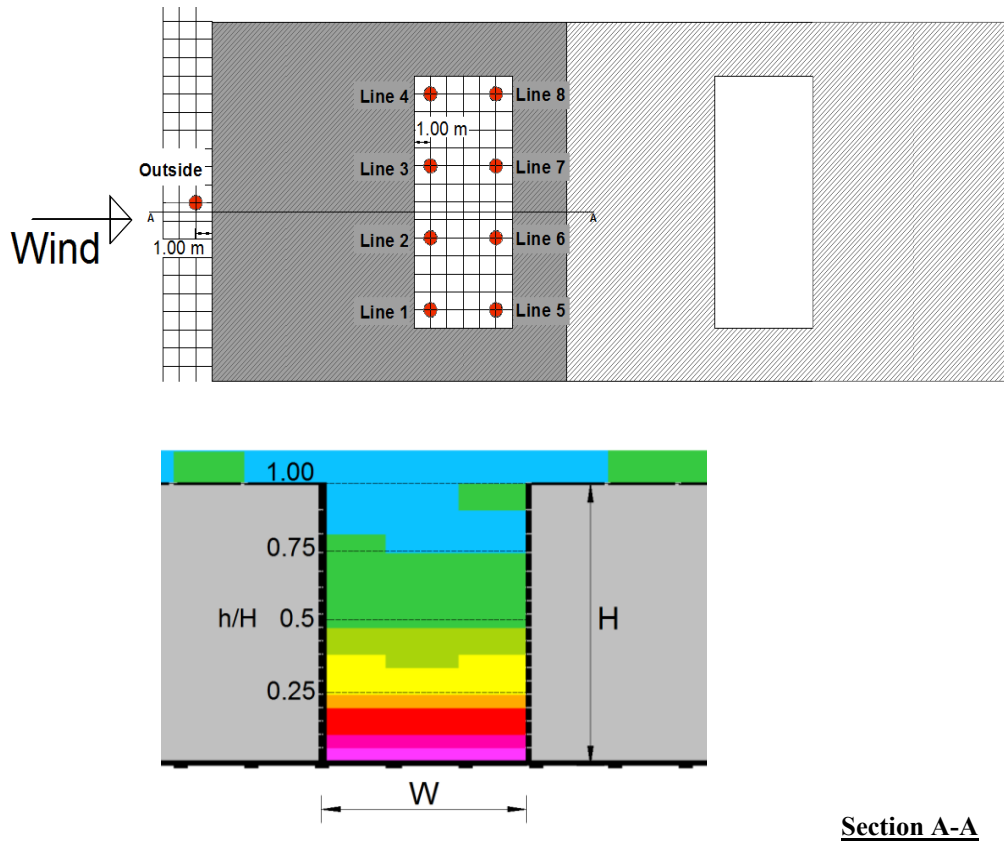


Fig. 10. Location and height levels of measurement points

2.2.2. Validation using experimental results

The accuracy of the ENVI-met in predicting the air temperature in various areas have been investigated more. Huttner (Huttner, 2012) compares the accuracy of the software between the open area and street canyon from 9:00 – 18:00 during the summer and found that with increasing the urban density the predicted air temperature is less than measured one (RMSE_{open area} = 0.86 °C and RMSE_{street canyon} = 1.70 °C). Similarly, López-Cabeza et al. (López-Cabeza et al., 2018) show RMSE for open areas varies between 0.73 – 0.82 °C while it is 1.52 – 3.35 °C inside semi-closed courtyard spaces and with decreasing the space size (deep courtyards) the error between monitoring and simulation results are increased. The reason can be attributed to ENVI-met shortcuts, which just the temperature of the inner nodes carried out in a transient state (Simon, 2016), and the outside surface temperature is calculated dynamically, without considering the amount of heat saved on the surfaces through the material's thermal capacity (Ali-Toudert & Mayer, 2006).

On the other hand, according to the Eq. (6), the term $\frac{1}{c_p \rho} \frac{\delta R_{lw}}{\delta z}$ describes the change in air temperature due to the divergence of the long-wave radiation inside the (thin) atmospheric layer (M. Bruse, 2004), which is a function of the vapor content and air temperature of the air layer concerned the surface temperature of the underlying soil and the temperature of

the upper atmosphere (M. Bruse, 2017). Therefore, the effect of horizontal long-wave fluxes between surfaces, which increase air temperature inside the semi-closed areas, has not taken into account.

On the other hand, the evaluation of IfMB base model (Table 5) — was reported on our previous work (Forouzandeh, 2018) — and similar studies by Jänicke et al. (Jänicke et al., 2015), Wu et al. (Wu, Kong, Wang, Sun, & Chen, 2016), Yafei Wang et al. (Yafei Wang, Bakker, de Groot, Wortche, & Leemans, 2015) and Gusson et al. (Gusson & Duarte, 2016) showed that during the night the mentioned errors becoming less effective, especially inside the semi-closed spaces, which are constructed from low thermal mass materials. In this way, ENVI-met slightly overestimates air temperature during the night, while it underestimates it during the day.

Table 5. RMSE of comparing air temperature for different spans of time during winter (27th January and 2th February) at IfMB (Forouzandeh, 2018)

Root mean squared error (RMSE)			
	7-11 CET	12-17 CET	Night
Inside the courtyard (Shaded area)*	1.08 °C Underestimate	2.28 °C Underestimate	0.35 °C Overestimate
Near the outside façade*	0.45 °C Underestimate		0.3 °C Overestimate

*Shaded area away from direct sunlight

Finally, since early morning is the coldest time of the day (Zielinski & Keim, 2005), in the next section, $F_{x, \text{Heat loss}}$ values are exported with calibrating the predicted θ_u for inside the courtyard with RMSE = 0.60 °C, 1.00 °C, 1.50 °C and 2.00 °C for $H/W < 1$, $1 < H/W < 2$, $2 < H/W < 4$ and $H/W > 4$, respectively. In this way, despite this value is initialized for 1.75m above the ground and not higher parts, for simplification we applied it for the whole height of the courtyard.

2.2.3. Results and discussions

2.2.3.1. Phase 1 : normal winter day

As previously proved by Kubota et al. (Kubota et al., 2017) and Micallef et al. (Micallef et al., 2016), it can be determined that the diurnal temperature variation in various height levels inside the internal courtyards strongly depends on radiation and the ventilation performance of the courtyard.

The modification of the long-wave and short-wave radiation fluxes, coming and leaving the courtyard, is modeled via an SVF, which ranges between 0 to 1. After calculating the SVF for 6 measurement points (Eq. (7)), the mean of the SVF value (Fig. 11.) was determined for each height level as expressed in Eq. (8):

$$SVF = \frac{1}{360} \sum_{\pi=0}^{360} \cos \omega(\pi) \quad (7)$$

$$SVF_a = \frac{\sum_{i=1}^6 SVF_i}{6} \quad (8)$$

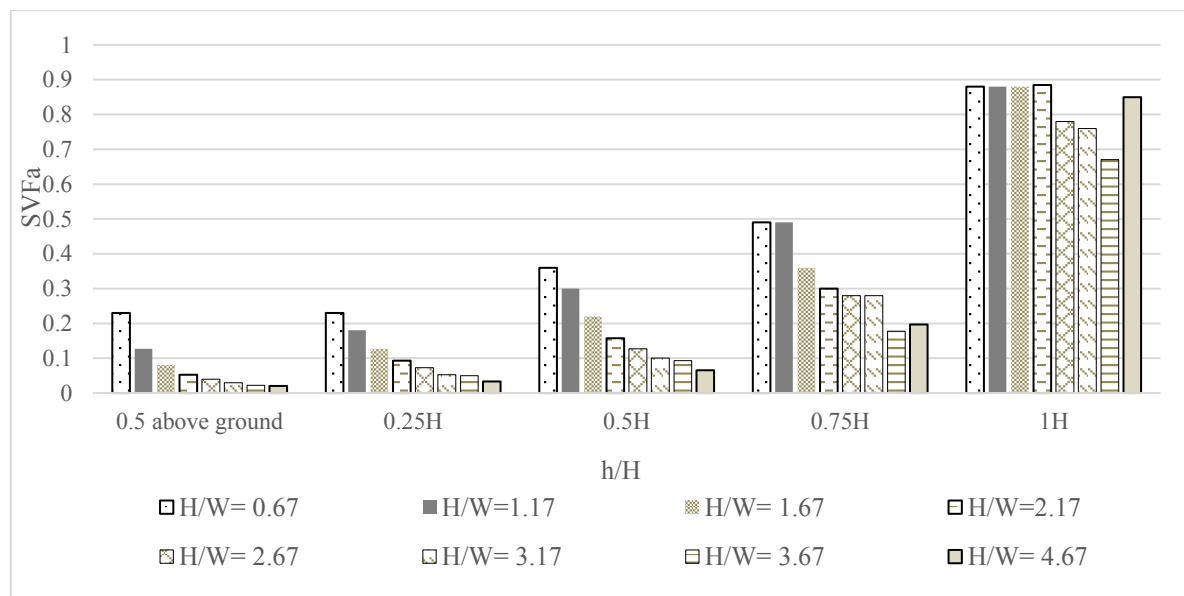


Fig. 11. Comparison of SVF at different height levels of the courtyard for each study case

An increase in the number of stories surrounding the courtyard leads to the reduction in the SVF (Fig. 11.). This reduces solar heat gain during the day (Chow & Roth, 2006; Erell & Williamson, 2006b) and during the night reduces the disposal of the long-wave radiation. In addition, increasing the aspect ratio isolates the whirlwind inside the courtyard and limits the air exchange through ventilation between the lower layers of the courtyard and its outside (P Moonen et al., 2011).

Based on the results (Fig. 12.), θ_u inside the courtyard at all height levels during winter typical day continuously reduces from 00:00 to 06:00 and reaches the bottom value at 06:00, irrespective of the aspect ratio. In this regard, increasing the height of the surrounding buildings, especially $H/W \geq 2.17$, results in a clear rise of θ_u , between 00:00 to 08:00.

On the contrary, deep courtyards limit the heat gain from solar radiation as well as heat loss by long-wave radiation and ventilation. Therefore, considering the air temperature at different height levels inside the courtyard, during the sunny hours, 10:00 to 16:00, does not show the great difference for different aspect ratio.

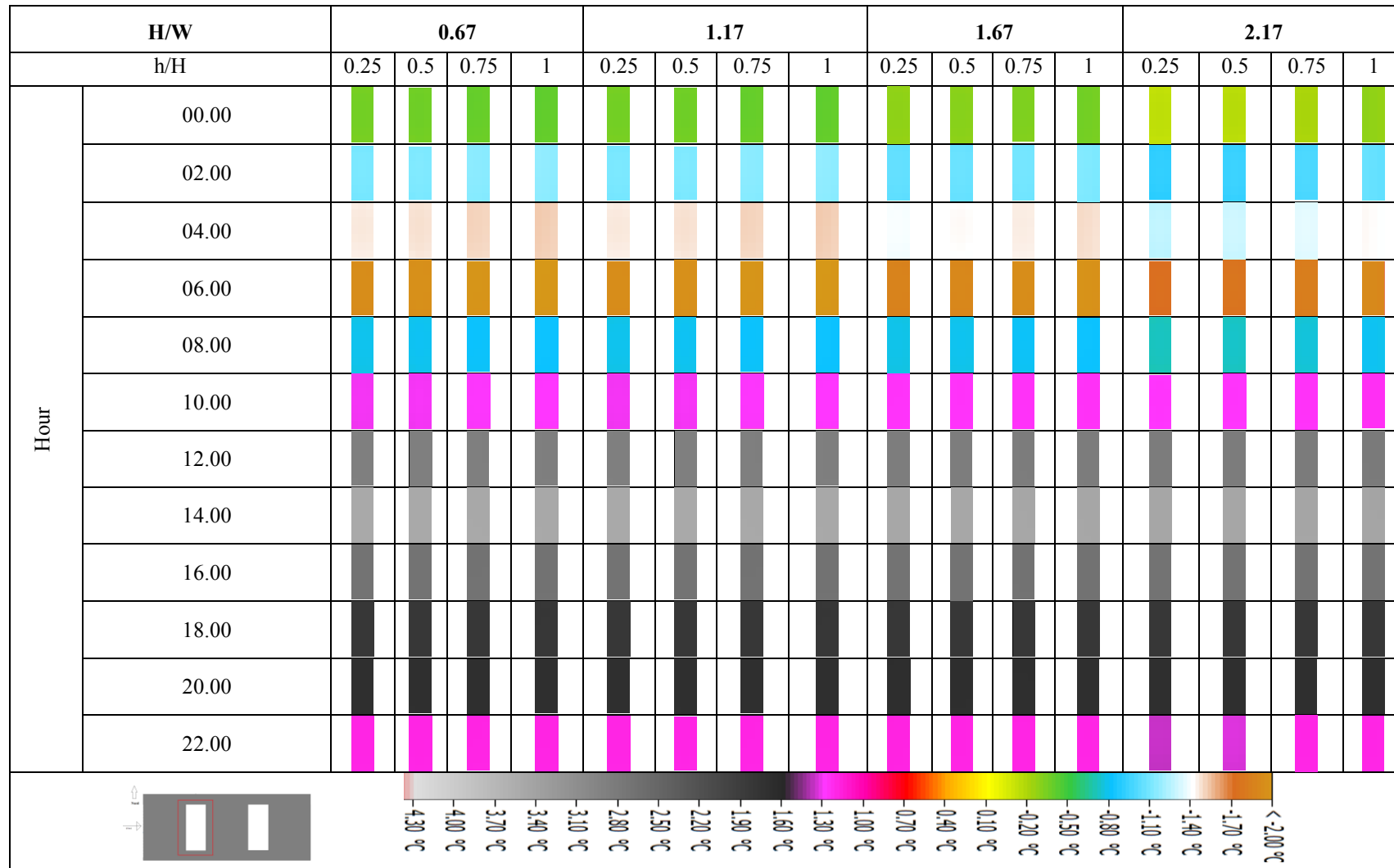


Fig. 12. Diurnal courses of θ_u °C for rectangular courtyards with different aspect ratios – (Typical winter day 27.01.2017)

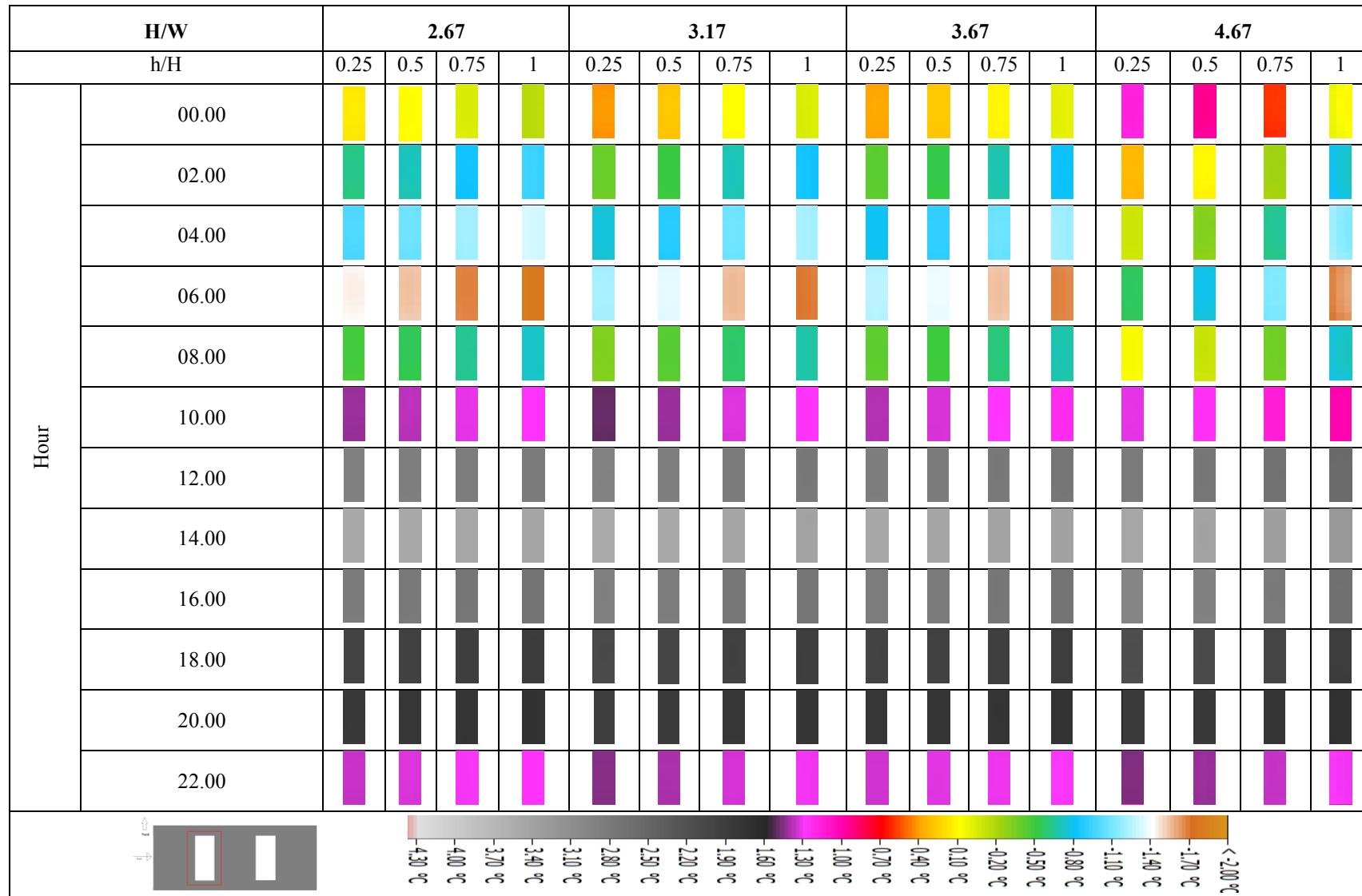


Fig. 12. Diurnal courses of θ_u °C for rectangular courtyards with different aspect ratios – (Typical winter day 27.01.2017) (Continued)

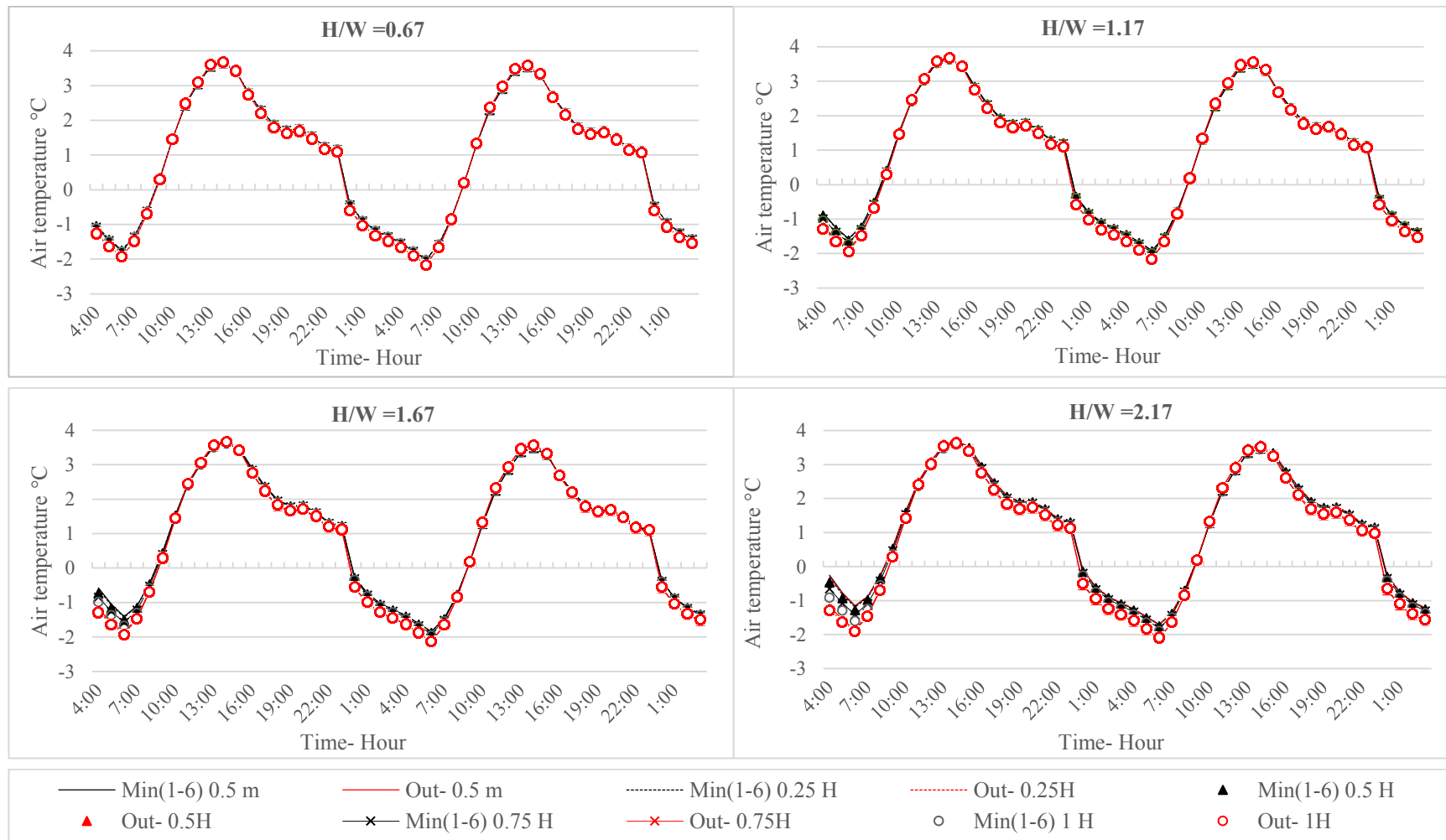


Fig. 13. Hourly distribution of temperature at different height levels of courtyard and it's outside for various aspect ratios on 27th January - (Min (1-6): the minimum recorded value inside the courtyard at point 1-6, Out: minimum recorded value near the outside facade)

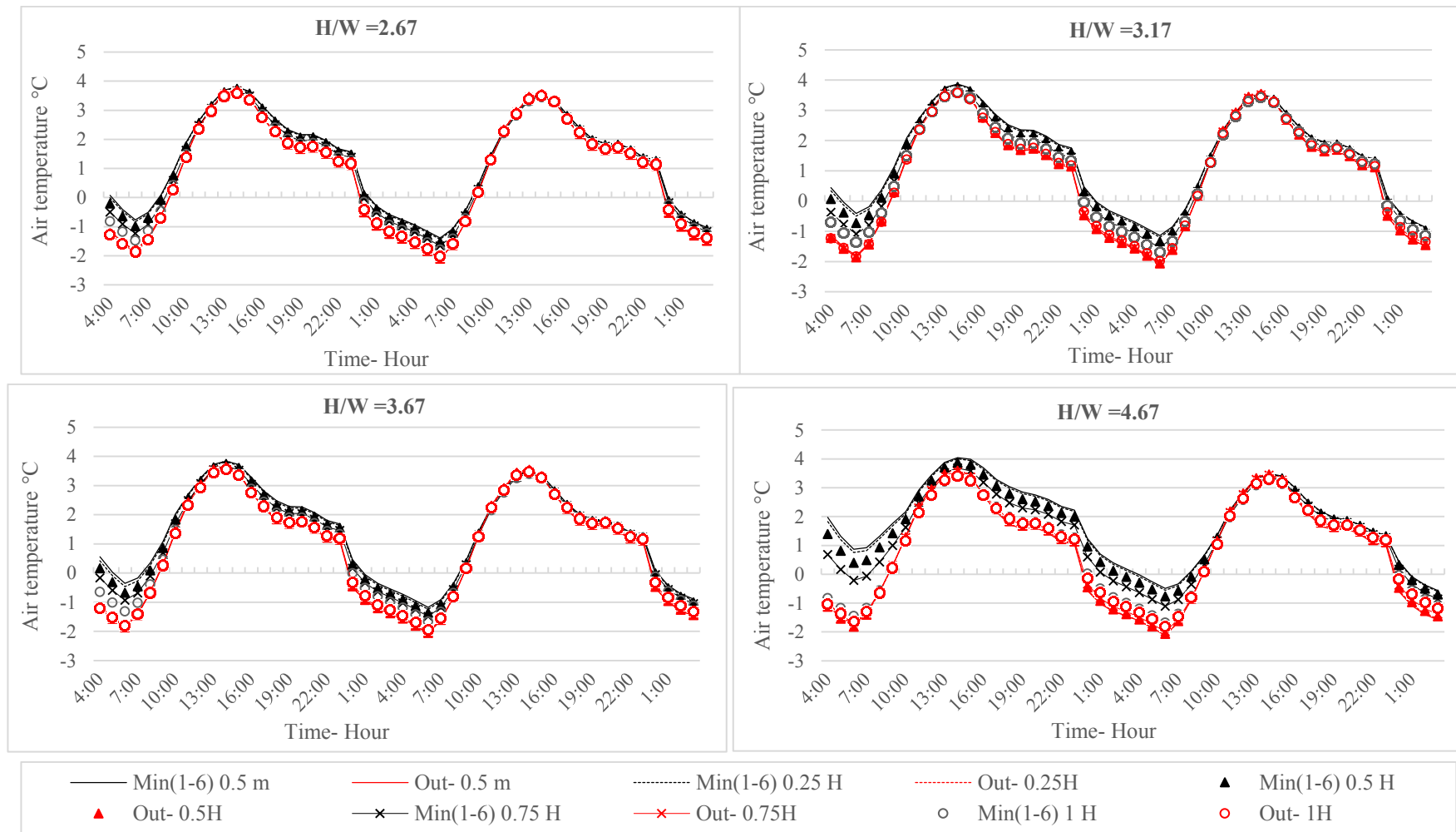


Fig. 13. Hourly distribution of temperature at different height levels of courtyard and it's outside for various aspect ratios on 27th January - (Min (1-6): the minimum recorded value inside the courtyard at point 1-6, Out: minimum recorded value near the outside facade) (Continued)

In addition, the level of bottom θ_u does not differ more at various height levels inside the courtyard with $H/W = 0.67 - 1.67$. However, increasing the aspect ratio, more than 2.17, resulting in different air temperature distribution patterns at different height levels of the space, particularly from 00:00 to 08:00.

Considering the 24 h daily minimum air temperature at different height levels inside the courtyard — 0.25 H, 0.5 H, 0.75 H and 1 H — and its difference with the same level minimum temperature in front of outside façade (Fig. 13) shows that, diurnal temperature variations are generally similar within all scenarios. Due to shading effects of the courtyard, the temperature difference between the outside and the courtyard at noon time is less (≈ 0.03 °C) for the courtyard with the $H/W = 0.67 - 4.67$. The micro-scale heat island phenomenon of highest courtyard begins to occur just after sunset. And it can be observed that very early in the day, 00:00 – 07:00, semi-enclosed space temperatures are much higher than outside.

The predicted temperature difference between the studied courtyards and their outside open area is varied from 0.15 °C to 1.56 °C, depending on the courtyard's aspect ratio. The midrise scenarios are warmer than in the corresponding low-rise scenarios and the bottom temperature is largest in the compact high-rise scenarios, which, at the same time are the coolest in mid-afternoon.

2.2.3.2. Phase 2: Standard- external temperature and $F_{x, \text{Heat load}}$

Courtyards limit heat discharge to the atmosphere and mostly connect with their surrounding rooms. Therefore, the thermal condition of courtyards' envelopes and transmission heat loss between the courtyards and their surroundings can also play a great role in their microclimate environment. In previous sections, the results are exported to courtyard spaces, of which large parts (> 60%) are surrounded with light glass materials. In this section, to further consider the effect of various design parameters, the bottom temperature and $F_{x, \text{Het load}}$ (Table 6) are calculated for various aspect ratios of the courtyard with different glazing percentage and glazing type.

Glass ratio:

The vertical temperature profile inside the courtyard showed a direct relation between the courtyard ventilation and its thermal condition. By increasing the depth of the courtyard, skimming flow replaced by the stratified flow (ALVAREZ et al., 1998), which limits the air exchange between the courtyard and its outside (Hall et al., 1999). Therefore, the thermal condition of the courtyards strongly associated with its surrounding envelopes. This relation is less for low depth ratio and increases with increasing the aspect ratio.

The results for θ_u inside the courtyards with various ratios of glass covering (Fig. 14.) show that increasing the glass façade, more than 75% of the courtyard, with low thermal resistance increases

access to indoor heat and therefore higher temperature inside the courtyard. In contrast, applying high insulated envelopes with limiting the connection between courtyard and building inside as the only heat source for deep levels results in very cold condition inside the courtyard, with $H/W > 1$, in comparison with open exposed areas. Accordingly, at the low part of the courtyard with aspect ratio 4.67, the air temperature can be much lower than outside ($\approx 40\text{ }^{\circ}\text{C}$) when $R > 1$. In opposite situation, when the whole of the courtyard is surrounded with low resistance glass façade, the courtyard can be up to $5\text{ }^{\circ}\text{C}$ warmer than outside. However, the first condition is rare, while, according to courtyard typology, we generally use the term of the courtyard for an area which is covered with glass to provide daylight and ventilation for indoor spaces (Edwards et al., 2006; Pfeifer et al., 2007).

Glass type:

In this section, the study aimed to investigate the effects of installing windows with heat reflection or absorption on thermal environments within the courtyard semi-closed space. The 8 experimental models are simulated with three different types of windows that are defined in the whole of the surface envelope of the courtyard: (1) heat protection clear glass, (2) heat protection reflected glass with 26% reflection, and (3) heat protection absorbing glass with 45% absorption. Hence, ENVI-met used for radiant analysis cannot evaluate the effects of a heat ray retro-reflective for surfaces in this case, each surface in the computational domain is assumed to be the perfect smooth surface which has a specular reflection downward inside the courtyard. Also, constant albedo values are applied during the simulation, spectral and angular independence.

Figure 15 illustrates the relationship between the type of the glass façade and the air temperature inside the courtyard at different height levels. As Yoshida et al. (Yoshida, Yumino, Uchida, & Mochida, 2016) and Sailor et al. (Sailor & Fan, 2002) show, higher solar reflectance can increase reflected solar radiation to near surfaces and trap solar radiation in semi-closed spaces. On the other hand, the use of highly-reflective facades inside the courtyard potentially reduces the air temperature on building surfaces (Akbari et al., 2016) and as a result of the convective heat transfer to the air and the emitted infrared radiation to surface in view (Fox, Osmond, & Peters, 2018).

The perceptible rise in air temperature inside the courtyard is caused by the increasing of the surface temperature and the difference between surface and ambient temperature through applying highly absorbing materials (Kandya & Mohan, 2018). This was also previously proved by Oke et al. (Oke, Johnson, Steyn, & Watson, 1991) for street canyons.

According to the results of this part for case 1 with $H/W < 1$, the air temperature inside the courtyard at all height levels is approximately the same for various glass type. By increasing the aspect ratio, the value of air temperature at noon can be up to $0.16\text{ }^{\circ}\text{C}$ and $0.25\text{ }^{\circ}\text{C}$ more for reflective and absorptive glass in comparison with clear glass. However, it was clarified that

increasing the surface reflectance, as previously approved by Yang et al. (Xinyan Yang et al., 2012), not greatly affect the minimum potential air temperature in the early hours of the day inside the courtyard and $F_{x, \text{Heat load}}$. Therefore, in the following, the $F_{x, \text{Heat load}}$ is predicted at each height level by comparing the minimum air temperature inside the courtyard with the same height level at the coldest point near the outside façade (Table 6) for various aspect ratios and glazing percentage.

The results show that the air temperature difference between shallow courtyards ($H/W < 1$) and the outside is negligible, when up to 75% of them are covered with glass facade. In this way, the predicted $F_{x, \text{Heat load}}$ for courtyard semi-closed spaces, which are completely enclosed with clear glass façade, is 0.9 for all aspect ratios. This factor is also applicable for deep courtyards ($H/W > 2$) with more than 75%, low isolate glass facade. However, the air temperature inside the middle and deep courtyards with $H/W > 1$, for which the thermal resistance of envelope walls is more than $1 \text{ (m}^2 \text{ K W}^{-1}\text{)}$, can be considerably less than its outside.

The findings of this part are in good agreement with experimental studies in section 2, regardless of the ENVI-met shortcut in considering the heat storage in building surface and horizontal long-wave radiation (Kubota, Toe, & Ossen, 2014). Furthermore, it is demonstrated that the semi-closed space of the courtyard can affect the outside air temperature, which should be considered in calculations of building's heat load.

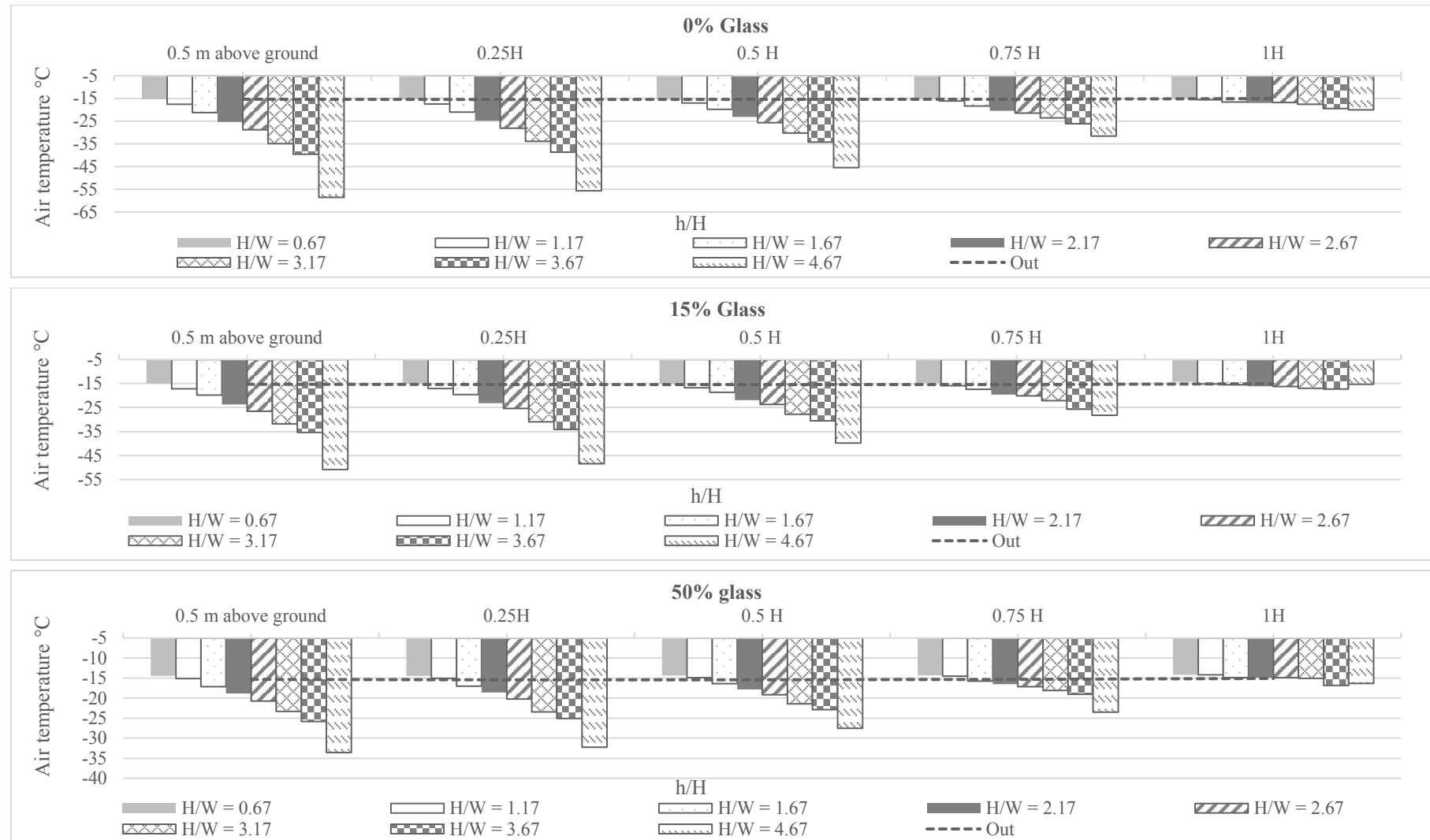


Fig. 14. Comparison of minimum air temperature at the different height of the courtyards with corresponding outside condition for various aspect ratio and glass cover percentage; The forced input air temperature is set -14 °C for all hours of the day.

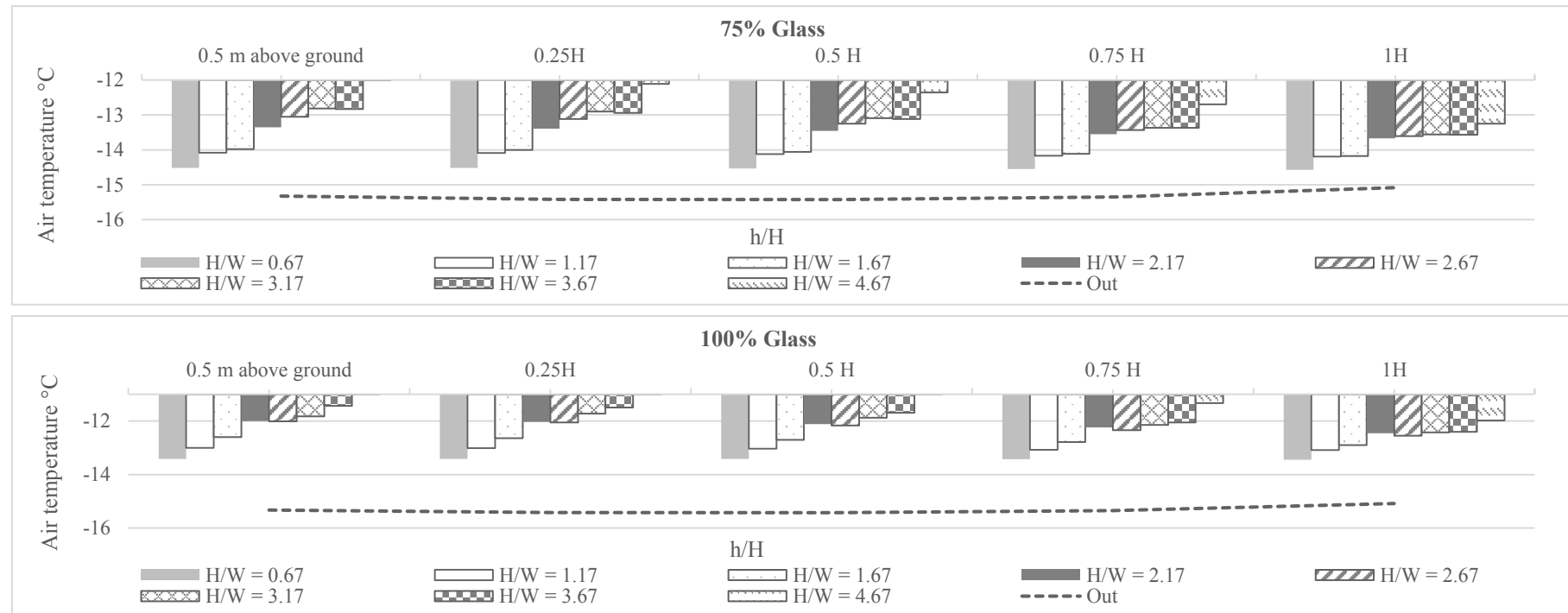


Fig.14. Comparison of minimum air temperature at the different height of the courtyards with corresponding outside condition for various aspect ratio and glass cover percentage; The forced input air temperature is set -14 °C for all hours of the day. (Continued)

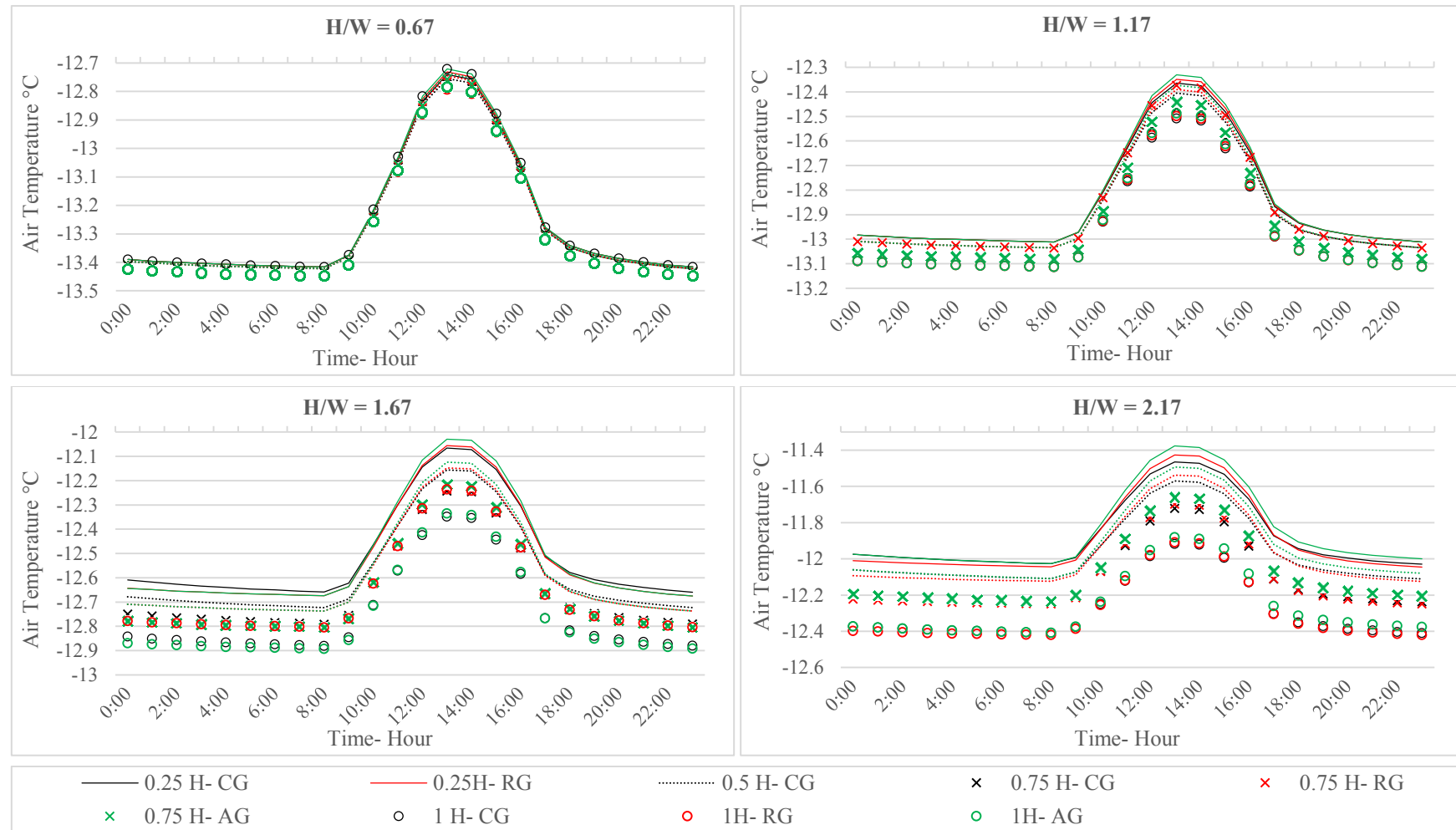


Fig. 15. The diurnal variation of temperature inside courtyard as affected by type of the surrounding glass façade, including clear glass (CG – black), reflecting glass (RG – red) and heat-absorbing glass (AG – green)

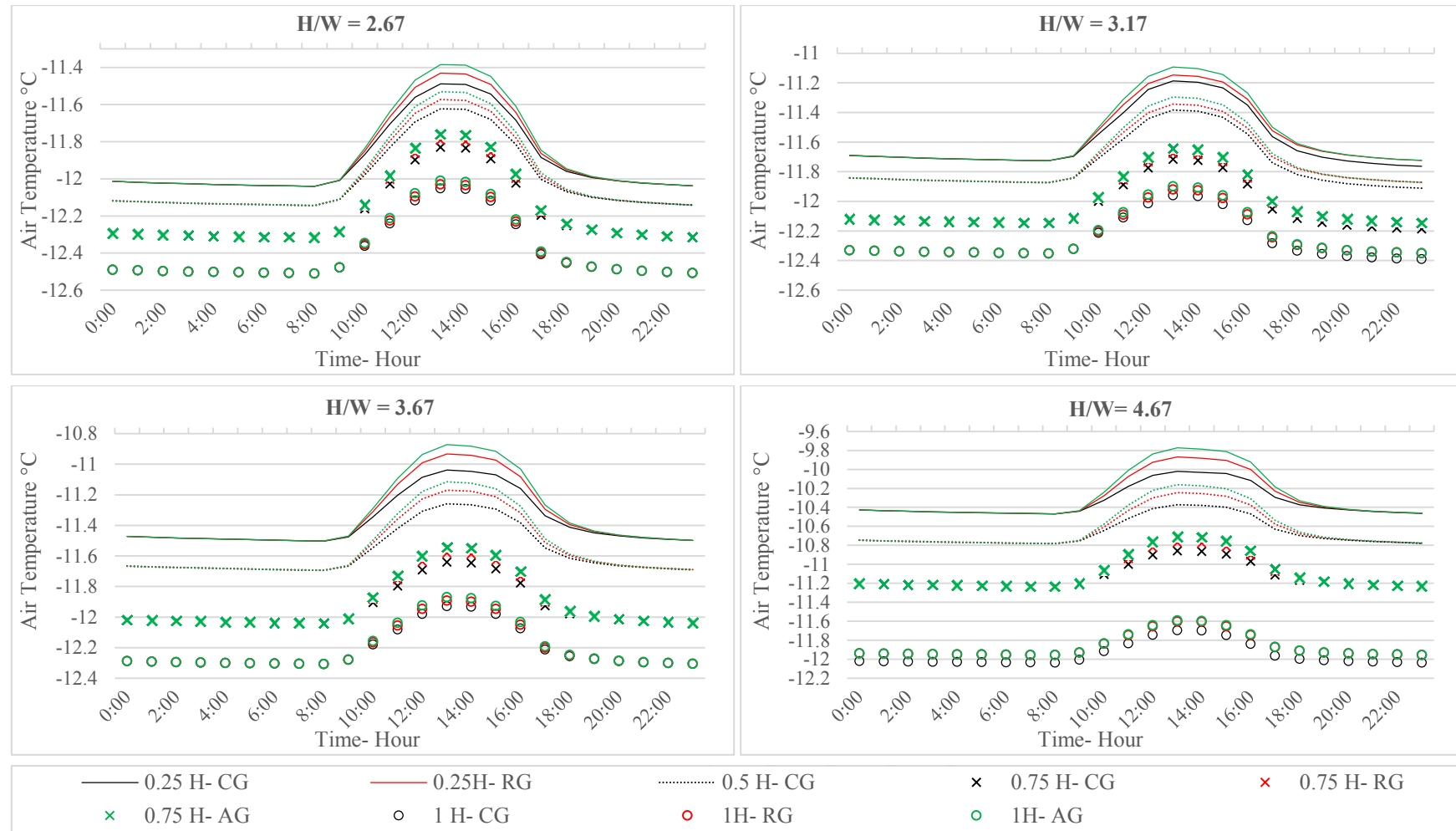


Fig. 15. The diurnal variation of temperature inside courtyard as affected by type of the surrounding glass façade, including clear glass (CG – black), reflecting glass (RG – red) and heat-absorbing glass (AG – green) (Continued)

Table. 6. Predicted $F_{x, \text{Heat load}}$ at different height levels inside the courtyards with various aspect ratios, simulation with minimum standard outside air temperature = $-14\text{ }^{\circ}\text{C}$ and Inside temperature = $20\text{ }^{\circ}\text{C}$

	H/W < 1					1 < H/W < 2					2 < H/W < 3									
% Glass	0%	15%	50%	75%	100%	0%	15%	50%	75%	100%	0%	15%	50%	75%	100%					
	R > 1 ($\text{m}^2 \text{K W}^{-1}$)					R < 1 ($\text{m}^2 \text{K W}^{-1}$)					R > 1 ($\text{m}^2 \text{K W}^{-1}$)					R < 1 ($\text{m}^2 \text{K W}^{-1}$)				
0.5m above ground	1.0	1.0	1.0	1.0	0.9	1.1	1.1	1.0	1.0	0.9	1.3	1.3	1.1	0.9	0.9					
0.25 h	1.0	1.0	1.0	1.0	0.9	1.1	1.1	1.0	1.0	0.9	1.3	1.2	1.1	0.9	0.9					
0.5 H	1.0	1.0	1.0	1.0	1.0	1.1	1.1	1.0	1.0	0.9	1.2	1.2	1.1	0.9	0.9					
0.75 h	1.0	1.0	1.0	1.0	1.0	1.1	1.0	1.0	1.0	0.9	1.2	1.1	1.0	0.9	0.9					
1 H	1.0	1.0	1.0	1.0	1.0	1.0	1.0	1.0	1.0	1.0	1.0	1.0	1.0	1.0	0.9					
	3 < H/W < 4					H/W > 4														
% Glass	0%	15%	50%	75%	100%	0%	15%	50%	75%	100%										
	R > 1 ($\text{m}^2 \text{K W}^{-1}$)					R < 1 ($\text{m}^2 \text{K W}^{-1}$)														
0.5m above ground	1.6	1.5	1.3	0.9	0.9	2.2	2.0	1.5	0.9	0.9										
0.25 h	1.6	1.5	1.2	0.9	0.9	2.1	1.9	1.5	0.9	0.9										
0.5 H	1.5	1.4	1.2	0.9	0.9	1.8	1.7	1.3	0.9	0.9										
0.75 h	1.3	1.2	1.1	0.9	0.9	1.4	1.4	1.2	0.9	0.9										
1 H	1.1	1.1	1.0	1.0	0.9	1.1	1.0	1.0	0.9	0.9										

3. Conclusions and future developments

The local microclimate near the façade strongly influences heat transfer through envelopes, due to conduction, convection and radiation. Meanwhile, the courtyard as one of the oldest urban microclimate, has different interactions with its outdoor environment, whose effect on energy demand of buildings is accepted through various studies. The main question in this research is how the temperature has been modified by using such a space and how this can be considered in the calculation of the building's energy consumption.

In this regard, at first step the temperature difference between the semi-closed courtyard and open area, outside the courtyard, is measured in four case studies located in Hanover, Germany and in the second step, the effect of the courtyard's aspect ratio and physical properties of surrounding envelopes were considered through multiple simulations, using ENVI-met. Based on the results, the temperature adjustment factors for various height levels inside the courtyards were calculated.

According to the results of the experimental measurements and the simulations, the heat accumulation in courtyard layers is affected by its geometry and properties of its surroundings. In so far the convection heat exchange between the courtyard and its outside and surface exposure to solar radiation during the day and clear sky during the night has a great effect on saving the heat inside the courtyard, the amount of the heat courtyard gains through its surrounding rooms can also change the thermal condition inside the courtyard during cold winter times. So the deep courtyards with more than 65% light envelope façade are warmer than open spaces while showing relatively lower temperatures with insulated envelopes. This indicates that the effect of heat savings through low ventilation can be mitigated by eliminating the courtyard's heat source, through its envelope as well as through the sunny sky during the day.

Even so, the high temperature inside the semi-closed spaces with glass surrounding façade does not necessarily mean that this idea reduces building energy consumption, but this temperature difference from outside can be considered with correction factor in the heat load calculations.

Finally, the findings of this research limit to experimental cases in a maritime temperate climate of Hanover. In order to reach general results and provide the appropriate adjustment factor, it was recommended to further research on the local heat island intensity of courtyard semi-closed space and its changes under the effect of various parameters including geometric, vegetation and the weather condition.

References

- AHMAD, I., KHETRISH, E., & Abughres, S. (1985). Thermal analysis of the architecture of old and new houses at Ghadames. *Building and Environment*, 20, 39–42.
- Akbari, H., Cartalis, C., Kolokotsa, D., Muscio, A., Pisello, A. L., Rossi, F., ... Zinzi, M. (2016). Local climate change and urban heat island mitigation techniques – the state of the art. *Journal of Civil Engineering and Management*, 22(1), 1–16. <https://doi.org/10.3846/13923730.2015.1111934>
- Al-Hemiddi, N. A., & Megren Al-Saud, K. A. (2001). The effect of a ventilated interior courtyard on the thermal performance of a house in a hot–arid region. *Renewable Energy*, 24(3), 581–595. [https://doi.org/http://dx.doi.org/10.1016/S0960-1481\(01\)00045-3](https://doi.org/http://dx.doi.org/10.1016/S0960-1481(01)00045-3)
- Aldawoud, A. (2008). Thermal performance of courtyard buildings. *Energy and Buildings*, 40(5), 906–910. <https://doi.org/http://dx.doi.org/10.1016/j.enbuild.2007.07.007>
- Ali-Toudert, F., & Mayer, H. (2006). Numerical study on the effects of aspect ratio and orientation of an urban street canyon on outdoor thermal comfort in hot and dry climate. *Building and Environment*, 41(2), 94–108. <https://doi.org/https://doi.org/10.1016/j.buildenv.2005.01.013>
- Allegrini, J., Kämpf, J. H., Dorer, V., & Carmeliet, J. (2013). Modelling the Urban Microclimate and its Influence on Building Energy Demands of an Urban Neighbourhood. *Proceedings of CISBAT 2013 Cleantech for Smart Cities and Buildings, II*, 631–1187. Retrieved from 10.5075/epfl-infoscience-190601
- Almhafdy, A., Ibrahim, N., Ahmad, S. S., & Yahya, J. (2015). Thermal Performance Analysis of Courtyards in a Hot Humid Climate Using Computational Fluid Dynamics CFD Method. *Procedia - Social and Behavioral Sciences*, 170, 474–483. <https://doi.org/http://dx.doi.org/10.1016/j.sbspro.2015.01.012>
- ALVAREZ, S., SANCHEZ, F., & MOLINA, J. L. (1998). Air flow pattern at courtyards. *Environmentally Freindly Cities*, 503–506. Retrieved from http://www.aivc.org/sites/default/files/airbase_11854.pdf
- AMR BAGNEID. (2006). The creation of a courtyard microclimate thermal model for the analysis of courtyard houses. Texas A&M University. Retrieved from <http://oaktrust.library.tamu.edu/bitstream/handle/1969.1/ETD-TAMU-1662/BAGNEID-DISSERTATION.pdf?sequence=1>
- Bainbridge, D., & Haggard, K. (2011). *Passive Solar Architecture: Heating, Cooling, Ventilation, Daylighting and More Using Natural Flows*. Chelsea Green Publishing. Retrieved from <https://books.google.de/books?id=gD687keMhLwC>
- Bednar, M. J. (1986). *The new atrium*. New York: McGraw-Hill.

- Berkovic, S., Yezioro, A., & Bitan, A. (2012). Study of thermal comfort in courtyards in a hot arid climate. *Solar Energy*, *86*(5), 1173–1186. <https://doi.org/10.1016/j.solener.2012.01.010>
- Bouyer, J., Inard, C., & Musy, M. (2011). Microclimatic coupling as a solution to improve building energy simulation in an urban context. *Energy and Buildings*, *43*(7), 1549–1559. <https://doi.org/http://dx.doi.org/10.1016/j.enbuild.2011.02.010>
- Brun, A., Spitz, C., Wurtz, E., & Mora, L. (2009). Behavioural comparison of some predictive tools used in a low-energy building. In *International IBPSA Conference*. Glasgow, Scotland.
- Bruse, M. (1999). Die Auswirkungen kleinskaliger Umweltgestaltung auf das Mikroklima Michael Bruse aus Essen Bochum , 1999.
- Bruse, M. (2004). ENVI-met documentation.
- Bruse, M. (2017). ENVI-met. A holistic microclimate model. Retrieved June 14, 2018, from [http://www.envi-met.info/doku.php?id=kb:lwflux&s\[\]=longwave](http://www.envi-met.info/doku.php?id=kb:lwflux&s[]=longwave)
- Carrasco, V., & Reynolds, J. S. (1996). Shade, Water and Mass: Passive cooling in Andalusia. In *21st Annual Passive Solar Conference*. Asheville: American Solar Energy Society.
- Castaldo, V. L., Pisello, A. L., Piselli, C., Fabiani, C., Cotana, F., & Santamouris, M. (2018). How outdoor microclimate mitigation affects building thermal-energy performance: A new design-stage method for energy saving in residential near-zero energy settlements in Italy. *Renewable Energy*, *127*, 920–935. <https://doi.org/https://doi.org/10.1016/j.renene.2018.04.090>
- Charalampopoulos, I., Tsiros, I., Chronopoulou-Sereli, A., & Matzarakis, A. (2013). Analysis of thermal bioclimate in various urban configurations in Athens, Greece. *Urban Ecosystems*, *16*(2), 217–233. <https://doi.org/10.1007/s11252-012-0252-5>
- Chow, W. T. L., & Roth, M. (2006). Temporal dynamics of the urban heat island of Singapore. *International Journal of Climatology*, *26*(15), 2243–2260. <https://doi.org/10.1002/joc.1364>
- Croome, D. J. (1981). Structures as climatic modifiers- the influence of vernacular architecture. *IABSE Reports of the Working Commissions*, *36*. <https://doi.org/http://doi.org/10.5169/seals-28272>
- de la Flor, F. S., & Domínguez, S. A. (2004). Modelling microclimate in urban environments and assessing its influence on the performance of surrounding buildings. *Energy and Buildings*, *36*(5), 403–413. <https://doi.org/https://doi.org/10.1016/j.enbuild.2004.01.050>
- Deutscher Wetterdienst. (n.d.). Langjährige Stationsmittelwerte für die Klimareferenzperiode 1981-2010, für aktuellen Standort und Bezugsstandort. Retrieved June 12, 2017, from <ftp://ftp-cdc.dwd.de/pub/CDC/>
- DIN. (2003). *DIN 4108-2*. Berlin: Deutsches Institut für Normung e. V.
- DIN. (2017). *DIN EN 12831-1*. Berlin: Deutsches Institute für Normung e.V.
- Edwards, B., Sibley, M., Land, P., & Hakmi, M. (2006). *Courtyard Housing: Past, Present and Future. Search*.

- Erell, E., & Williamson, T. (2006a). Comments on the correct specification of the analytical CTTC model for predicting the urban canopy layer temperature. *Energy and Buildings*, 38(8), 1015–1021. <https://doi.org/https://doi.org/10.1016/j.enbuild.2005.11.013>
- Erell, E., & Williamson, T. (2006b). Intra-urban differences in canopy layer air temperature at a mid-latitude city. *International Journal of Climatology*, 27(9), 1243–1255. <https://doi.org/10.1002/joc.1469>
- Forouzandeh, A. (2018). Numerical modeling validation for the microclimate thermal condition of semi-closed courtyard spaces between buildings. *Sustainable Cities and Society*, 36(Supplement C), 327–345. <https://doi.org/https://doi.org/10.1016/j.scs.2017.07.025>
- Fox, J., Osmond, P., & Peters, A. (2018). The Effect of Building Facades on Outdoor Microclimate—Reflectance Recovery from Terrestrial Multispectral Images Using a Robust Empirical Line Method. *Climate*, 6(3). <https://doi.org/https://doi.org/10.3390/cli6030056>
- Franke, J., Hellsten, A., Schlünzen, H., Carissimo, B. (2007). *Best Practice Guideline for the CFD Simulation of Flows in the Urban Environment*. Brussel, Belgium. <https://doi.org/ISBN:3-00-018312-4>
- Guedouh, M. S., & Zemmouri, N. (2017). Courtyard Building's Morphology Impact on Thermal and Luminous Environments in Hot and Arid Region. *Energy Procedia*, 119, 153–162. <https://doi.org/https://doi.org/10.1016/j.egypro.2017.07.063>
- Guhathakurta, S., & Gober, P. (2010). Residential Land Use, the Urban Heat Island, and Water Use in Phoenix: A Path Analysis. *Journal of Planning Education and Research*, 30(1), 40–51. <https://doi.org/10.1177/0739456X10374187>
- Gusson, C. S., & Duarte, D. H. S. (2016). Effects of Built Density and Urban Morphology on Urban Microclimate - Calibration of the Model ENVI-met V4 for the Subtropical Sao Paulo, Brazil. *Procedia Engineering*, 169, 2–10. <https://doi.org/http://dx.doi.org/10.1016/j.proeng.2016.10.001>
- Hall, D. J., Walker, S., & Spanton, A. M. (1999). Dispersion from courtyards and other enclosed spaces. *Atmospheric Environment*, 33(8), 1187–1203. [https://doi.org/10.1016/S1352-2310\(98\)00284-2](https://doi.org/10.1016/S1352-2310(98)00284-2)
- Huttner, S. (2012). Further development and application of the 3D microclimate simulation ENVI-met. *Mainz: Johannes Gutenberg-Universität in Mainz*, 147. Retrieved from <http://ubm.opus.hbz-nrw.de/volltexte/2012/3112/>
- Institutes, M., & Toudert, F. A. (2005). Berichte des Meteorologischen Institutes der Universität Freiburg Fazia Ali Toudert Dependence of Outdoor Thermal Comfort on Street Design in Hot and Dry Climate, (15).
- Jänicke, B., Meier, F., Hoelscher, M.-T., & Scherer, D. (2015). Evaluating the Effects of Façade Greening on Human Bioclimate in a Complex Urban Environment. *Advances in Meteorology*, 2015, 1–15. <https://doi.org/http://dx.doi.org/10.1155/2015/747259>

- Kakoniti, A., Georgiou, G., Marakkos, K., Kumar, P., & Neophytou, M. K.-A. (2016). The role of materials selection in the urban heat island effect in dry mid-latitude climates. *Environmental Fluid Mechanics*, *16*(2), 347–371. <https://doi.org/10.1007/s10652-015-9426-z>
- Kandya, A., & Mohan, M. (2018). Mitigating the Urban Heat Island effect through building envelope modifications. *Energy and Buildings*, *164*, 266–277. <https://doi.org/https://doi.org/10.1016/j.enbuild.2018.01.014>
- Kubota, T., Toe, D., & Ossen, D. (2014). Field Investigation of Indoor Thermal Environments in Traditional Chinese Shophouses with Courtyards in Malacca. *Journal of Asian Architecture and Building Engineering*, *13*, 247–254.
- Kubota, T., Zakaria, M. A., Abe, S., & Toe, D. H. C. (2017). Thermal functions of internal courtyards in traditional Chinese shophouses in the hot-humid climate of Malaysia. *Building and Environment*, *112*, 115–131. <https://doi.org/http://dx.doi.org/10.1016/j.buildenv.2016.11.005>
- Lauder, B. E., & Spalding, D. B. (1974). The numerical computation of turbulent flows. *Computer Methods in Applied Mechanics and Engineering*, *3*(2), 269–289. [https://doi.org/https://doi.org/10.1016/0045-7825\(74\)90029-2](https://doi.org/https://doi.org/10.1016/0045-7825(74)90029-2)
- Liang, W., Huang, J., Jones, P., Wang, Q., & Hang, J. (2018). A zonal model for assessing street canyon air temperature of high-density cities. *Building and Environment*, *132*, 160–169. <https://doi.org/https://doi.org/10.1016/j.buildenv.2018.01.035>
- Liu, Z., Zheng, S., & Zhao, L. (2018). Evaluation of the ENVI-Met Vegetation Model of Four Common Tree Species in a Subtropical Hot-Humid Area. *Atmosphere*, *9*(5).
- López-Cabeza, V. P., Galán-Marín, C., Rivera-Gómez, C., & Roa-Fernández, J. (2018). Courtyard microclimate ENVI-met outputs deviation from the experimental data. *Building and Environment*, *144*, 129–141. <https://doi.org/https://doi.org/10.1016/j.buildenv.2018.08.013>
- Maldonado, E., & Yannas, S. (2014). *Environmentally Friendly Cities: Proceedings of Plea 1998, Passive and Low Energy Architecture, 1998, Lisbon, Portugal, June 1998*. Taylor & Francis. Retrieved from <https://books.google.de/books?id=xaKWBQAAQBAJ>
- Mathiesen, B. V. (2017). *2015 Final Heating & Cooling Demand in Germany*. Retrieved from http://www.heatroadmap.eu/resources/HRE4-Country_presentation-Germany.pdf
- Meir, I. A., Pearlmutter, D., & Etzion, Y. (1995). On the microclimatic behavior of two semi-enclosed attached courtyards in a hot dry region. *Building and Environment*, *30*(4), 563–572. [https://doi.org/http://dx.doi.org/10.1016/0360-1323\(95\)00018-2](https://doi.org/http://dx.doi.org/10.1016/0360-1323(95)00018-2)
- Mellor, G. L., & Yamada, T. (1974). A Hierarchy of Turbulence Closure Models for Planetary Boundary Layers. *Journal of the Atmospheric Sciences*, *31*(7), 1791–1806. [https://doi.org/10.1175/1520-0469\(1974\)031<1791:AHOTCM>2.0.CO;2](https://doi.org/10.1175/1520-0469(1974)031<1791:AHOTCM>2.0.CO;2)
- Micallef, D., Buhagiar, V., & Borg, S. P. (2016). Cross-ventilation of a room in a courtyard building. *Energy and Buildings*, *133*, 658–669.

- <https://doi.org/http://dx.doi.org/10.1016/j.enbuild.2016.09.053>
- Moonen, P., Dorer, V., & Carmeliet, J. (2011). Evaluation of the ventilation potential of courtyards and urban street canyons using RANS and LES. *Journal of Wind Engineering and Industrial Aerodynamics*, 99(4), 414–423. <https://doi.org/http://dx.doi.org/10.1016/j.jweia.2010.12.012>
- Moonen, Peter, Defraeye, T., Dorer, V., Blocken, B., & Carmeliet, J. (2012). Urban Physics: Effect of the micro-climate on comfort, health and energy demand. *Frontiers of Architectural Research*, 1(3), 197–228. <https://doi.org/https://doi.org/10.1016/j.foar.2012.05.002>
- Oke, T. R., Johnson, G. T., Steyn, D. G., & Watson, I. D. (1991). Simulation of surface urban heat islands under ‘ideal’ conditions at night part 2: Diagnosis of causation. *Boundary-Layer Meteorology*, 56(4), 339–358. <https://doi.org/10.1007/BF00119211>
- Pfeifer, G., Engelmann, U., & Brauneck, P. (2007). *Courtyard Houses: A Housing Typology*. Birkhäuser Basel. Retrieved from <https://books.google.de/books?id=1mOGVfQf5FgC>
- Rajapaksha, I., Nagai, H., & Okumiya, M. (2003). A ventilated courtyard as a passive cooling strategy in the warm humid tropics. *Renewable Energy*, 28(11), 1755–1778. [https://doi.org/http://dx.doi.org/10.1016/S0960-1481\(03\)00012-0](https://doi.org/http://dx.doi.org/10.1016/S0960-1481(03)00012-0)
- Rodríguez-Algeciras, J., Tablada, A., Chaos-Yeras, M., De la Paz, G., & Matzarakis, A. (2018). Influence of aspect ratio and orientation on large courtyard thermal conditions in the historical centre of Camagüey-Cuba. *Renewable Energy*, 125, 840–856. <https://doi.org/https://doi.org/10.1016/j.renene.2018.01.082>
- Rojas-Fernández, J., Galán-Marín, C., Roa-Fernández, J., & Rivera-Gómez, C. (2017). Correlations between GIS-Based Urban Building Densification Analysis and Climate Guidelines for Mediterranean Courtyards. *Sustainability*, 9(12), 2255. <https://doi.org/10.3390/su9122255>
- Rojas, J. M., Galán-Marín, C., & Fernández-Nieto, E. D. (2012). Parametric study of thermodynamics in the mediterranean courtyard as a tool for the design of eco-efficient buildings. *Energies*, 5(7), 2381–2403. <https://doi.org/10.3390/en5072381>
- Sailor, D. J., & Fan, H. (2002). Modeling the diurnal variability of effective albedo for cities. *Atmospheric Environment*, 36(4), 713–725. [https://doi.org/https://doi.org/10.1016/S1352-2310\(01\)00452-6](https://doi.org/https://doi.org/10.1016/S1352-2310(01)00452-6)
- Santamouris, M., Papanikolaou, N., Koronakis, I., Livada, I., & Asimakopoulos, D. (1999). Thermal and air flow characteristics in a deep pedestrian canyon under hot weather conditions. *Atmospheric Environment*, 33(27), 4503–4521. [https://doi.org/https://doi.org/10.1016/S1352-2310\(99\)00187-9](https://doi.org/https://doi.org/10.1016/S1352-2310(99)00187-9)
- Shanthi Priya, R., Sundarraja, M. C., & Radhakrishnan, S. (2012). Experimental study on the thermal performance of a traditional house with one-sided wind catcher during summer and winter. *Energy Efficiency*, 5(4), 483–496. <https://doi.org/10.1007/s12053-012-9155-9>
- Simon, H. (2016). *Modeling urban microclimate - Development, implementation and evaluation of new and improved calculation methods for the urban microclimate model ENVI-met*. Mainz :

Univ.

- Sinou, M. (2007). *Design and Thermal Diversity of Semi-enclosed Spaces*. Melrose Books. Retrieved from <https://books.google.de/books?id=etUVAQAIAAJ>
- Soltani, A., & Sharifi, E. (2017). Daily variation of urban heat island effect and its correlations to urban greenery: A case study of Adelaide. *Frontiers of Architectural Research*, 6(4), 529–538. <https://doi.org/https://doi.org/10.1016/j.foar.2017.08.001>
- Taesler, R., & Anderson, C. (1984). A method for solar radiation computations using routine meteorological observations. *Energy and Buildings*, 7, 341–352.
- Taleghani, M., Kleerekoper, L., Tenpierik, M., & van den Dobbelsteen, A. (2015). Outdoor thermal comfort within five different urban forms in the Netherlands. *Building and Environment*, 83, 65–78. <https://doi.org/https://doi.org/10.1016/j.buildenv.2014.03.014>
- Taleghani, M., Tenpierik, M., van den Dobbelsteen, A., & Sailor, D. J. (2014). Heat mitigation strategies in winter and summer: Field measurements in temperate climates. *Building and Environment*, 81, 309–319. <https://doi.org/https://doi.org/10.1016/j.buildenv.2014.07.010>
- Tominaga, Y., Mochida, A., Yoshie, R., Kataoka, H., Nozu, T., Yoshikawa, M., & Shirasawa, T. (2008). AIJ guidelines for practical applications of CFD to pedestrian wind environment around buildings. *Journal of Wind Engineering and Industrial Aerodynamics*, 96(10), 1749–1761. <https://doi.org/http://dx.doi.org/10.1016/j.jweia.2008.02.058>
- van Esch, M. M. E., Looman, R. H. J., & de Bruin-Hordijk, G. J. (2012). The effects of urban and building design parameters on solar access to the urban canyon and the potential for direct passive solar heating strategies. *Energy and Buildings*, 47, 189–200. <https://doi.org/http://dx.doi.org/10.1016/j.enbuild.2011.11.042>
- Wang, F., & Liu, Y. (2002). Thermal environment of the courtyard style cave dwelling in winter. *Energy and Buildings*, 34(10), 985–1001. [https://doi.org/10.1016/S0378-7788\(01\)00145-1](https://doi.org/10.1016/S0378-7788(01)00145-1)
- Wang, Yafei, Bakker, F., de Groot, R., Wortche, H., & Leemans, R. (2015). Effects of urban trees on local outdoor microclimate: synthesizing field measurements by numerical modelling. *Urban Ecosystems*, 18(4), 1305–1331. <https://doi.org/10.1007/s11252-015-0447-7>
- Wang, Yupeng, & Akbari, H. (2014). Effect of Sky View Factor on Outdoor Temperature and Comfort in Montreal. *Environmental Engineering Science*, 31, 272–287. Retrieved from 10.1089/ees.2013.0430
- Weather Spark. (2016). Retrieved August 1, 2016, from <https://weatherspark.com/averages/28636/Hanover-Niedersachsen-Germany>
- Wu, Z., Kong, F., Wang, Y., Sun, R., & Chen, L. (2016). The Impact of Greenspace on Thermal Comfort in a Residential Quarter of Beijing, China. *International Journal of Environmental Research and Public Health*, 13(12), 1217. <https://doi.org/10.3390/ijerph13121217>
- Yang, X., Li, Y., & Yang, L. (2012). Predicting and understanding temporal 3D exterior surface temperature distribution in an ideal courtyard. *Building and Environment*, 57, 38–48.

<https://doi.org/https://doi.org/10.1016/j.buildenv.2012.03.022>

Yoshida, S., Yumino, S., Uchida, T., & Mochida, A. (2016). Numerical Analysis of the Effects of Windows with Heat Ray Retro-reflective Film on the Outdoor Thermal Environment within a Two-dimensional Square Cavity-type Street Canyon. *Procedia Engineering*, *169*, 384–391. <https://doi.org/https://doi.org/10.1016/j.proeng.2016.10.047>

Zhang, Y., Liu, D., & Mai, J. (2017). The CTTC model for predicting courtyard air temperature in South China. *Building Simulation*, *10*(5), 663–676. <https://doi.org/10.1007/s12273-017-0364-1>

Zielinski, G. A., & Keim, B. D. (2005). *New England Weather, New England Climate*. University Press of New England. Retrieved from <https://books.google.de/books?id=k-ASosvSGW8C>

Appendix 1

Existing correlations for convective heat transfer coefficient at exterior building surface

Knowledge on the convective heat transfer at exterior building surface is of interest for several building and urban engineering purposes (Defraeye & Carmeliet, 2010; Aya Hagishima et al., 2005). These studies determined the CHTCs for buildings with three main techniques:

1. Flat plate

Estimations of CHTCs ($\text{W m}^{-2} \text{K}^{-1}$) for exterior building surfaces have often been based on CHTC - U_∞ correlations for flat plates, where U_∞ is the free-stream air speed (m s^{-1}). Some of these flat-plate correlations were based on the heat and momentum transfer analogy, using only empirical information of the flow field, and they can be represented by Eq. (1) for forced convection (Cebeci & Bradshaw, 1988; Lienhard, 2013):

$$Nu_x = aRe_x^b Pr^c \quad (1)$$

Where a , b and c are empirical parameters, Nu_x is the Nusselt number, based on the distance along the plate ($x - \text{m}$), Pr is the Prandtl number of air and Re_x is the Reynolds number, based on x and U_∞ . Where the exponent b is about 0.8 for turbulent flow and 0.5 for laminar flow (Sharples, 1984).

$$\text{Laminar flow} \quad Nu_x = 0.644Re_x^{0.5} Pr^{c0.33} \quad (2)$$

$$\text{Turbulent flow} \quad Nu_x = 0.036Re_x^{0.8} Pr^{c0.33} \quad (3)$$

Other flat –plate correlations were based on convective heat transfer experiments on flat plates such as McAdams model (Mac Adams, 1954). The expression by MacAdams

considers rough and smooth surfaces on the building's roof and applies air velocity outside the atmospheric boundary layer.

McAdams model (Mac Adams, 1954) was grounded on the experiments by Jürges (Jürges, 1924), which have been used extensively for building applications:

$$h_{c,e} = 4.0U_{\infty} + 5.6 \quad U_{\infty} < 5 \text{ (m s}^{-1}\text{)} \quad (4)$$

$$h_{c,e} = 7.1U_{\infty}^{0.78} \quad U_{\infty} > 5 \text{ (m s}^{-1}\text{)} \quad (5)$$

The influence of Jürges's work has persisted for nearly 60 years. His results still form the basis for the design values of h given in the CIBS guide. These values are calculated from the CIBS's expression (Chartered Institution of Building services (CIBS), 1982):

$$h_{c,e} = 4.1V_{loc} + 5.8 \quad (6)$$

Where V_{loc} is the local wind speed at a building surface.

The limitations of this method are include (Sharples, 1984):

- Real building do not provide an exact physical equivalence with Jürges experimental conditions.
- Some details are fail such as the influence of building shape, façade location and wind direction on convective losses.
- The free of Reynold number effects on the dependence of convective heat transfer on the size and temperature of the heated surface.

All these empirical correlations somehow lack physical similarity regarding the flow pattern, as flow along a building surface and its turbulence content can be considerably different from that along a flat plate. Thereby it is also difficult to obtain a reliable estimate of U_{∞} , being "some" undefined wind speed near the building surface, and usually the exact location where U_{∞} is evaluated, is chosen in a rather arbitrary way (Defraeye et al., 2011). Furthermore, many of these correlations incorporate dimensionless numbers such as the Nusselt number¹ and Sherwood number, which are in turn functions of the Prandtl number and Reynold number. Setting a value of these numbers requires an appropriate

¹ $Nu = \frac{h_c L}{\lambda_{fl}}$, with λ_{fl} thermal conductivity of the fluid. Multiplying the left and right term in equation with the characteristic length. A large Nu means high fluid velocities.

representative length- which is difficult to define in complex and variable urban environments (Erell et al., 2012).

2. Full- scale experiments

There have been also several attempts to express h_c as a function of air speed near outdoor surfaces, including typically flat roofs and vertical building surfaces (i.e. walls). Table 1 summarizes the obtained correlations, for building facades, and the experimental conditions. These correlations are shaped based on the wind speed at height of 10m above ground (U_{10}), wind speed at some distance above the roof (U_R); and the wind speed near the building surface (U_S).

Significant differences are found between different empirical correlations which are to some extent related to the limitations of the experiments. This limitations are:

- a) The CHTC was only measured at one or a limited number of locations on building surface.
- b) The CHTC at a certain location on the surface, are in reality related to the specific flow field near the building surface, which is influenced by the specific building geometry, building surroundings and location of measurement.
- c) In most cases, the influence of turbulent fluctuations on the CHTC has not been taken into account in the correlations.
- d) Mostly smooth surfaces were considered.
- e) The effect of different flow pattern during the daytime and nighttime are not considered and the values are obtained depending on the measuring period.

Therefore, the correlation are case-specific and are not always applicable for other types of buildings and other boundary conditions (Defraeye et al., 2011).

3. Wind-tunnel experiments

A significant amount of research has been performed by wind- tunnel experiments, which in contrast to full-scale experiments, include detailed information about flow field and flow direction. But because most of these experiments were not performed in the context of building engineering, they were usually carried out for rather thin turbulent boundary layers, with respect to the body height, and at relatively low Reynold numbers compared to those typically encountered for buildings (Defraeye et al., 2011).

4. Computational fluid dynamics experiments

Recently, computational fluid dynamics (CFD) was used to predict convective heat transfer at exterior building surfaces. The main advantages of this attitude are:

- Specific and complex building form can be analyzed
- Very high resolution data are obtained
- High Reynolds number flows for atmospheric condition can be considered
- Detailed information on the flow field as well as thermal field is available

Table 1. CHTC correlations derived from full-scale measurements on building surface

Author	Wind speed			Surface	CHTC equation	Comments
	Value	Location	Range (m s ⁻¹)			
(Gerhart, 1967)	U _R	6m above roof	-	roof	No consistent correlation	Building, 30m height
(Sturrock, 1971)	U _R	-	-	WW ² Normal surface	6.1 U _R + 11.4 6.0 U _R + 5.7	Tower, 26m high
(ASHRAE. ASHRAE Task Group., 1975)	U _S	0.3m from facade	-	WW + LW	18.6 U _S ^{0.605}	6 floors building U _S = 0.5 (m s ⁻¹) if U ₁₀ < 2 (m s ⁻¹) U _S = 0.25 (m s ⁻¹) if U ₁₀ ≥ 2 (m s ⁻¹)
(Nicol, 1977)	U _R	-	0 – 5	WW + LW	4.35 U _R + 7.55	Rectangular building
(Clark & Berdahl, 1980)	U _S		< 0.076		0.8	Wind speed low and surface is colder than ambient air, free convection, i.e. the flow is laminar
	U _S		< 0.45		3.5	Surface is warmer than ambient air and there is free convection
	U _S		3.35 < U _S < 4.5		1.8 U _S + 3.8	
(Givoni, 1982)					1 + 6 U _S ^{0.75}	
(Sharples, 1984)	U _S	1m from facade	0.5 – 20	WW + LW	1.7 U _S + 5.1	18 story tower (20 × 36 × 78m)

² WW: Windward

LW: Leeward

Table 1. CHTC correlations derived from full-scale measurements on building surface (Continued)

Author	Wind speed			Surface	CHTC equation	Comments
	Value	Location	Range (m s ⁻¹)			
(Yazdanian & Klems, 1994)	U ₁₀	-	0 – 12	WW	$\sqrt{(0.84 \Delta T^{1/3})^2 + (2.38 U_{10}^{0.89})^2}$	Small, single story, rectangular building
				LW	$\sqrt{(0.84 \Delta T^{1/3})^2 + (2.86 U_{10}^{0.617})^2}$	
(Jayamaha, Wijesundera, & Chou, 1996)	U _R	Above vertical wall	0 – 4	WW + LW	1.444 U _R + 4.955	Vertical wall (1.2m × 1.8m)
(Loveday & Taki, 1996)	U _S	1m from facade	0.5 – 9	WW	16.15 U _S ^{0.397}	Rectangular building with L-shaped ground floor (21 × 9 × 28m)
				LW	16.15 U _S ^{0.503}	
(A Hagishima & Tanimoto, 2003)	U _S	0.13m from facade	0.5 – 3	Roof	3.96√ $\bar{u}^2 + \bar{v}^2 + \bar{w}^2 + 2K$ + 6.42	Two adjacent rectangular buildings (2 floors building shielded by a 4 story building)
				Wall	10.21 U _S +4.47	
(L. Zhang et al., 2004)	U _S	0.2m from facade	1 – 7	WW + LW	-0.0203 U _S ² + 1.766 U _S + 12.263	Small building (3 × 3 × 3m)
(Y. Liu & Harris, 2007)	U _S	0.5m from facade	0-3.5	WW	6.31 U _S + 3.32	Rectangular building
				LW	5.03 U _S + 3.19	
(Y. Liu & Harris, 2007)	U _R	1m above roof	0-9	WW	2.08 U _R + 2.97	Rectangular building
				LW	1.57 U _R + 2.66	
(Y. Liu & Harris, 2007)	U ₁₀		0-16	WW	1.53 U ₁₀ + 1.43	Rectangular building
				LW	0.90 U ₁₀ + 3.28	

Table 2. CHTC correlations derived from CFD simulations

Author	Wind speed		Range (m s ⁻¹)	Surface	CHTC equation	Comments
	Value	Location				
(Emmel, Abadie, & Mendes, 2007)	U ₁₀	-	1 – 15	WW	5.15 U ₁₀ ^{0.81} (short wall) 4.84 U ₁₀ ^{0.82} (long wall)	Rectangular Building (6 × 8 × 2.7m)
(Blocken et al., 2009)	U ₁₀		1 – 4	WW	4.60 U ₁₀ ^{0.89}	Cubic building, 10m high
(Defraeye et al., 2011)	U ₁₀		0.005 – 7.5	WW LW	5.01 U ₁₀ ^{0.85} 2.27 U ₁₀ ^{0.83}	Cubic building, 10m high

References

- ASHRAE. ASHRAE Task Group. (1975). *Procedure for determining heating and cooling loads for computerising energy calculations, Algorithms for building heat transfer subroutines*. New York.
- Blocken, B., Defraeye, T., Derome, D., & Carmeliet, J. (2009). High-resolution CFD simulations for forced convective heat transfer coefficients at the facade of a low-rise building. *Building and Environment*, 44(12), 2396–2412. <https://doi.org/http://dx.doi.org/10.1016/j.buildenv.2009.04.004>
- Cebeci, T., & Bradshaw, P. (1988). *Physical and Computational Aspects of Convective Heat Transfer*. New York: Springer. Retrieved from <https://link.springer.com/book/10.1007%2F978-1-4612-3918-5>
- Chartered Institution of Building services (CIBS). (1982). *CIBS Guide Book A, Section A3*. London: Chartered Institute of Building Services.
- Clark, E., & Berdahl, P. (1980). Radiative cooling: Resource and Applications. In H. Miller (Ed.), *Proceedings of the Passive Cooling Workshop* (pp. 177–212). Amherst: Center for Energy Efficient Design, Berkeley.
- Defraeye, T., Blocken, B., & Carmeliet, J. (2011). Convective heat transfer coefficients for exterior building surfaces: Existing correlations and CFD modelling. *Energy Conversion and Management*, 52(1), 512–522. <https://doi.org/http://doi.org/10.1016/j.enconman.2010.07.026>
- Defraeye, T., & Carmeliet, J. (2010). A methodology to assess the influence of local wind conditions and building orientation on the convective heat transfer at building surfaces. *Environmental Modelling & Software*, 25(12), 1813–1824.

- <https://doi.org/http://doi.org/10.1016/j.envsoft.2010.06.002>
- Emmel, M. G., Abadie, M. O., & Mendes, N. (2007). New external convective heat transfer coefficient correlations for isolated low-rise buildings. *Energy and Buildings*, 39(3), 335–342. <https://doi.org/10.1016/j.enbuild.2006.08.001>
- Erell, E., Pearlmutter, D., & Williamson, T. (2012). *Urban Microclimate: Designing the Spaces Between Buildings*. Taylor & Francis. Retrieved from <https://books.google.de/books?id=LHwnWaYfPNkC>
- Gerhart, K. (1967). Model experiments on the distribution of convective heat transfer at building facades (Modellversuche über die verteilung des konvektiven wärmeüberganges an gebäudefassaden). *Kältetechn-Klimatisier*, 5, 122–128.
- Givoni, B. (1982). Cooling by longwave radiation. *Passive Sol. J.(United States)*, 1:3, 131–150.
- Hagishima, A., & Tanimoto, J. (2003). Field measurements for estimating the convective heat transfer coefficient at building surfaces. *Building and Environment*, 38(7), 873–881. [https://doi.org/10.1016/S0360-1323\(03\)00033-7](https://doi.org/10.1016/S0360-1323(03)00033-7)
- Hagishima, Aya, Tanimoto, J., & Narita, K. (2005). Intercomparisons of Experimental Convective Heat Transfer Coefficients and Mass Transfer Coefficients of Urban Surfaces. *Boundary-Layer Meteorology*, 117(3), 551–576. <https://doi.org/10.1007/s10546-005-2078-7>
- Jayamaha, S. E. G., Wijesundera, N. E., & Chou, S. K. (1996). Measurement of the heat transfer coefficient for walls. *Building and Environment*, 31(5), 399–407. [https://doi.org/http://dx.doi.org/10.1016/0360-1323\(96\)00014-5](https://doi.org/http://dx.doi.org/10.1016/0360-1323(96)00014-5)
- Jürges, W. (1924). *Der Wärmeübergang an einer ebenen Wand*. R. Oldenbourg. Retrieved from <https://books.google.de/books?id=2uGfGwAACAAJ>
- Lienhard, J. H. (2013). *A Heat Transfer Textbook: Fourth Edition*. Dover Publications. Retrieved from <https://books.google.de/books?id=HM7DAgAAQBAJ>
- Liu, Y., & Harris, D. J. (2007). Full-scale measurements of convective coefficient on external surface of a low-rise building in sheltered conditions. *Building and Environment*, 42(7), 2718–2736. <https://doi.org/http://dx.doi.org/10.1016/j.buildenv.2006.07.013>
- Loveday, D. L., & Taki, A. H. (1996). Convective heat transfer coefficients at a plane surface on a full-scale building facade. *International Journal of Heat and Mass Transfer*, 39(8), 1729–1742. [https://doi.org/10.1016/0017-9310\(95\)00268-5](https://doi.org/10.1016/0017-9310(95)00268-5)
- Mac Adams, W. H. (1954). *Heat Transmission*. McGraw-Hill. New York.
- Nicol, K. (1977). The energy balance of an exterior window surface, Inuvik, N.W.T., Canada. *Building and Environment*, 12(4), 215–219. [https://doi.org/http://dx.doi.org/10.1016/0360-1323\(77\)90022-1](https://doi.org/http://dx.doi.org/10.1016/0360-1323(77)90022-1)
- Sharples, S. (1984). Full-scale measurements of convective energy losses from exterior building surfaces. *Building and Environment*, 19(1), 31–39.

[https://doi.org/http://dx.doi.org/10.1016/0360-1323\(84\)90011-8](https://doi.org/http://dx.doi.org/10.1016/0360-1323(84)90011-8)

Sturrock, N. (1971). *Localised boundary layer heat transfer from external building surfaces*.

Yazdanian, M., & Klems, J. H. (1994). Measurement of the exterior convective film coefficient for windows in low-rise buildings. *ASHRAE Transactions*, 1087–1096.

Zhang, L., Zhang, N., Zhao, F., & Chen, Y. (2004). A genetic-algorithm-based experimental technique for determining heat transfer coefficient of exterior wall surface. *Applied Thermal Engineering*, 24(2), 339–349.
<https://doi.org/http://dx.doi.org/10.1016/j.applthermaleng.2003.07.005>

Appendix 2

Effect of courtyard on surface temperature of surrounding envelopes and accuracy of ENVI-met in predicting building surface temperature

This study conducted field measurements both during the day and the night in June and September 2017 in order to investigate changes in the building surface temperatures across time.

The external surface temperature measurements were made by using DK311 TempLog with input for external temperature sensors. The temperature sensors installed with same color tape on façade. The external measurements were taken every 1 minute, sequentially at inside and outside the courtyard (Fig. 1.). Field measurement data were collected in 3 days for both summer and winter (Fig. 2. and 3.).

Analyzing climate data collected from a representative sample of the hottest time of a summer day—3 – 5 June 2017, at noon — the surface temperatures observed inside and outside the courtyard varied up to 20 °C.

During the winter — 22 – 24th December 2017 — there is not big difference (Max 2 °C) between the building surface temperature inside the courtyards and the outside facades, and recorded values are about same.

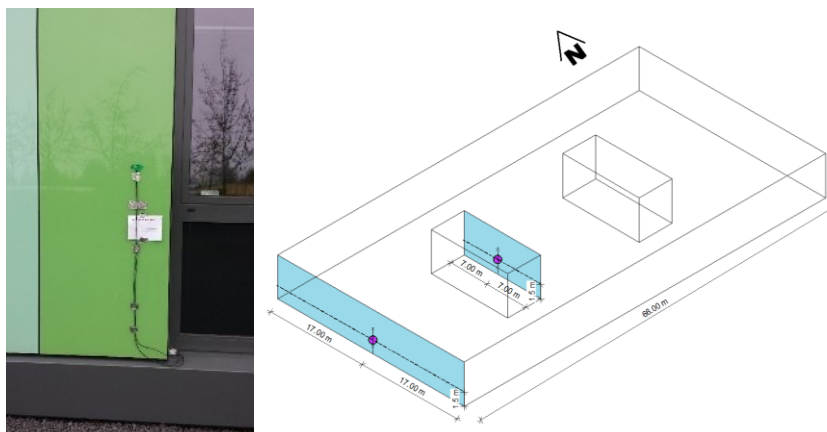


Fig. 1. Views of the instruments and sensors position inside and outside of courtyard

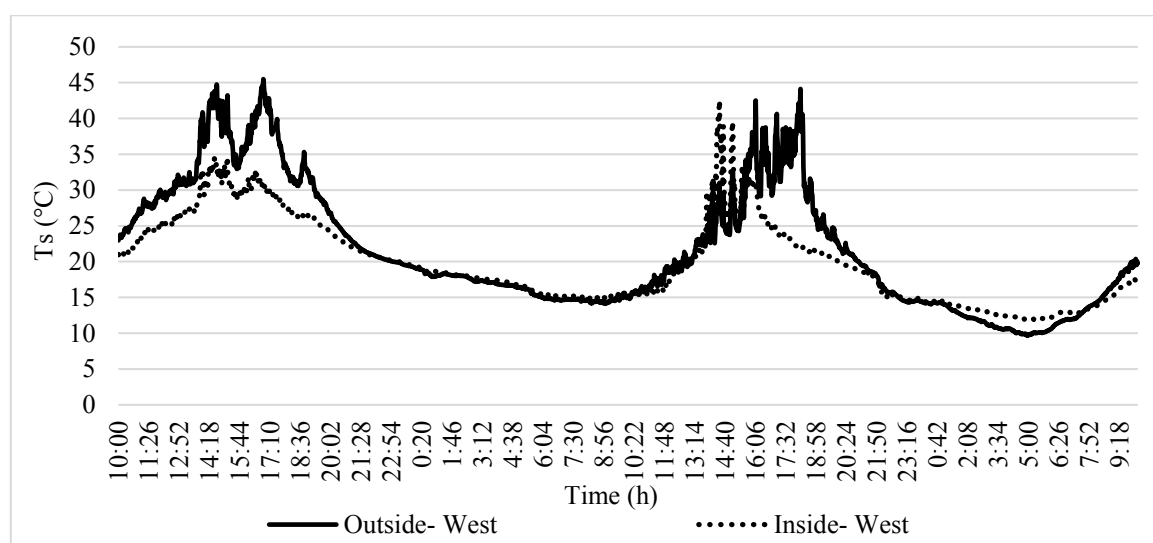


Fig. 2. Comparison of building surface temperature inside and outside of courtyard on west façade of IfMB, Hanover (3 – 5th June 2017)

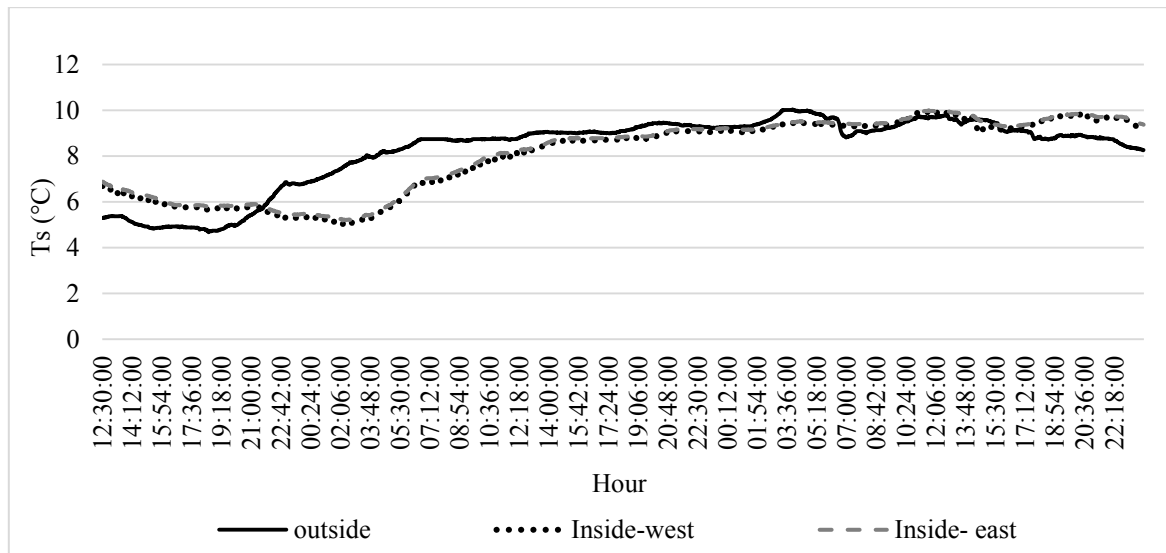


Fig. 3. Comparison of building surface temperature inside and outside of courtyard on west façade of IfMB, Hanover (22 – 24th December 2017)

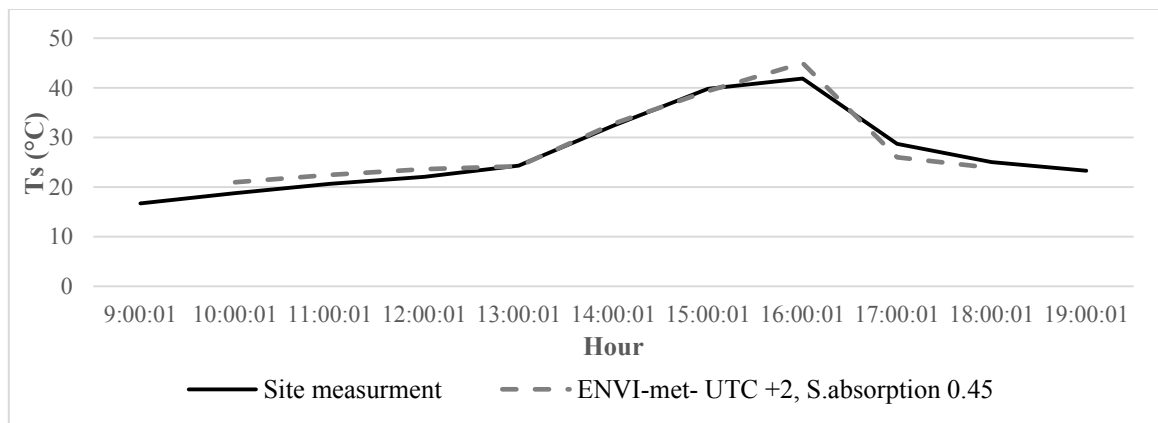


Fig. 4. Comparison of difference between calculated and site measurement surface temperature inside IfMB courtyard (west façade), 5 – 6th June 2017

Additionally, meteorological data were measured on the testing site and provided by the IMUK, air temperature and humidity, wind speed, wind direction, shortwave radiation (direct and diffuse) and long wave radiation – were used as boundary conditions for ENVI-met model validation.

Overall, the results (Fig. 4.) demonstrate that, with the advancements of the multiple-node model and absorption factor of 0.45, ENVI-met is capable of simulating building physics process in complex environments.

Appendix 3

Software: Microclimate model ENVI-met, features and codes

This research investigated a three-dimensional microclimate model ENVI-met ([M Bruse, 2016](#)), which was designed to simulate the microclimate thermal condition with a typical spatial resolution of a few meters and a time step between 1 and 5 s. Development of the model was started in 1995 by Michael Bruse at the Ruhr-University of Bochum. ENVI-met runs in contrast to many other climate simulation – on a standard x86 personal computer with a Microsoft Windows operating system.

ENVI-met is a prognostic model based on the fundamental laws of fluid dynamics and thermodynamics, including simulation of several phenomena (Fig. 1. – left). The main numerical calculation equations and presumptions are include ([M. Bruse, 1999](#); [Szucs, 2013](#)):

- 1.The atmospheric model (maximal height of the model is 2500m), which calculates the air movement, three-dimensional turbulence, temperature, relative humidity and takes into account obstacles such as buildings and vegetation.
- 2.The surface model, which calculates the emitted long wave, and the reflected short wave radiation from the different surfaces, taking into account the incident long-wave and short-wave radiation.
- 3.The vegetation model, which calculates the foliage temperature and the energy balance of the leaves taking into account the physiological and meteorological parameters.
- 4.The soil model, which calculates the thermo and hydrodynamic processes that take place in the soil. This model takes into account the combination of the natural and artificial surfaces of the urban quarter.
- 5.The biometeorological model, which is able to calculate the PMV index from the meteorological data.

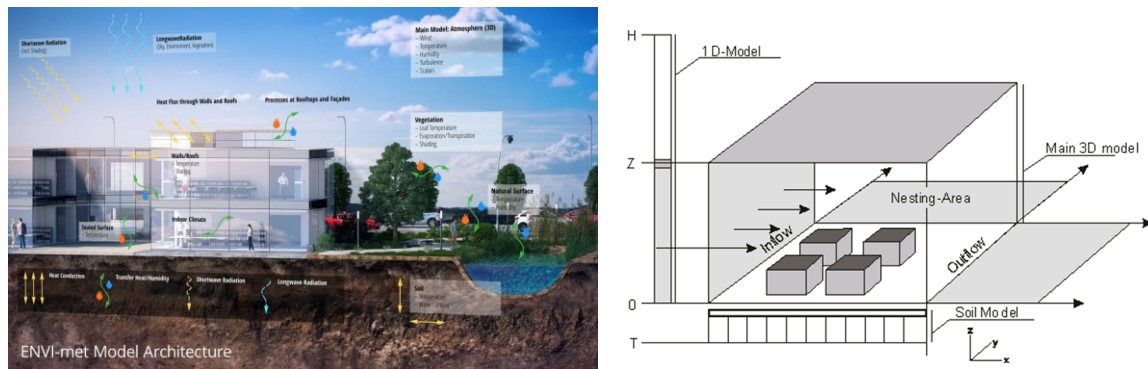


Fig. 1. Schematic of sub models of ENVI-met (left) and basic model layout (right)(image after (M. Bruse, 2016))

1. General model properties

The ENVI-met model basically consists of a one-dimensional boundary model that includes vertical profiles of different meteorological parameters up until a height of 2500 meters (approx. the height of the planetary boundary layer) and a three dimensional core model that includes all atmosphere, soil, building and vegetation processes. A so called ‘nesting’ area surrounds the core model is used to create stable lateral boundary conditions for the core model (Fig. 1. – right) (M. Bruse, 1999).

1.1. 1D boundary model

Due to the fact that ENVI-met only simulates part of the atmosphere, boundary conditions are required for the lateral and vertical borders of the 3D model. To provide these boundary conditions, the 1D boundary model generates one-dimensional profiles for meteorological parameters such as air temperature, specific humidity, wind vectors (horizontal), kinetic energy and turbulent exchange. To ensure stable laminar conditions the boundary model extends to an altitude of 2500m (average height of the planetary boundary layer). The top of the 1D model (H) at 2500m above ground, is determined via an iteration that splits the remaining height $H - Z$ into 15 cells with a telescoping grid. The one-dimensional boundary model with its horizontally homogeneous vertical profiles is then used to provide data on the borders of the 3D model (M. Bruse, 1999).

1.2. The 3D core model

The three-dimensional core model consists of three orthogonal orientated axes, which generate a three-dimensional cube, the model area. The model area consists of a number of cells which represent different objects such as buildings, vegetation or atmosphere. The

number of cells is dependent on the model area dimensions and its spatial resolution. Each cell is defined by its physical properties. For example, a building cell is defined by its material types, and the material type is defined by the specific heat capacity and other parameters. In combination with databases of all the different objects, this structure allows a detailed reconstruction of an urban environment. In the default settings the lowest atmospheric grid cell is vertically split into 5 smaller cells to better replicate the dynamic processes at the boundary layer close to the ground surface (M. Bruse, 1999).

At the bottom side, this three-dimensional atmosphere model is linked to a three dimensional soil model which reaches down to a depth of five meters (Simon, 2016).

1.2.1. The atmosphere model

In the atmosphere model the main processes on the urban climate are simulated: wind field, air temperature and humidity distribution, turbulence, gas and particle dispersion, radiation, exchange processes on ground and building surfaces.

1.2.1.1. Wind flow

The spatial and temporal evolution of the wind field is calculated using the non-hydrostatic three-dimensional Navier-Stokes equation. For further simplification the Boussinesq-approximation is used to eliminate the density ρ from the Navier-Stokes equations which can then - using the Einstein summation – be written as (M. Bruse, 1999; Michael Bruse & Fleer, 1998c; Huttner, 2012; Simon, 2016):

$$\frac{\delta u}{\delta t} + u_i \frac{\delta u}{\delta x_i} = - \frac{\delta p'}{\delta x} + K_m \left(\frac{\delta^2 u}{\delta x_i^2} \right) + f(v - v_g) - S_u$$

$$\frac{\delta v}{\delta t} + u_i \frac{\delta v}{\delta x_i} = - \frac{\delta p'}{\delta y} + K_m \left(\frac{\delta^2 v}{\delta x_i^2} \right) + f(u - u_g) - S_v$$

$$\frac{\delta \omega}{\delta t} + u_i \frac{\delta \omega}{\delta x_i} = - \frac{\delta p'}{\delta z} + K_m \left(\frac{\delta^2 \omega}{\delta x_i^2} \right) + g \frac{\theta(z)}{\theta_{ref}(z)} - S_\omega \quad (1)$$

With p' as the local pressure perturbation, K_m as the local exchange coefficient, $\theta(z)$ as the potential temperature at height level z , f as the Coriolis parameter³, describes the rotation of the wind near ground compared to the geostrophic wind components u_g and v_g (currently switched off). S_u , S_v and S_ω as local source / sink terms accounting for wind speed reduction due to vegetation and u_i , x_i as the three-dimensional advection and diffusion terms written in Einstein summation ($u_i = u$; v ; ω ; $x_i = x$; y ; z).

Due to the air now being treated as an incompressible fluid an additional continuity equation has to be satisfied (M. Bruse, 1999; Huttner, 2012):

$$\frac{\delta u}{\delta x} + \frac{\delta v}{\delta y} + \frac{\delta \omega}{\delta z} = 0 \quad (2)$$

1.2.1.2. Temperature and humidity

The potential temperature θ can be calculated by using the combined advection-diffusion equation:

$$\frac{\partial \theta}{\partial t} + u_i \frac{\delta^2 \theta}{\delta x_i} = K_h \left(\frac{\delta^2 \theta}{\delta x_i^2} \right) + \frac{1}{c_p \rho} \frac{\delta R_{lw}}{\delta z} + Q_\theta \quad (3)$$

Q_θ , is a term that defines the heat exchange between air and vegetation and K_h is the turbulent exchange coefficient for heat. The term $\frac{1}{c_p \rho} \frac{\delta R_{lw}}{\delta z}$ describes the change in air temperature due to divergence of the long wave radiation. For the humidity the advection-diffusion equation can be written as:

$$\frac{\partial q}{\partial t} + u_i \frac{\delta^2 q}{\delta x_i} = K_q \left(\frac{\delta^2 q}{\delta x_i^2} \right) + Q_q \quad (4)$$

Q_q defines the exchange of humidity between air and vegetation and K_q is the turbulent exchange coefficient for humidity.

The internal sources and sinks of the equations present linkages to the vegetation model - quantifying the effects of the exchange processes of vegetation and atmosphere on the

³ The Coriolis parameter can be calculated as $f = 2\Omega \sin \varphi$, where $\Omega = 7.10^{-5} \text{ s}^{-1}$ is the pulsance of the earth's rotation and φ is the latitude of the models location. The Coriolis parameter is implemented in ENVI-met but is switched off by default (M. Bruse, 1999; Huttner, 2012).

distribution of the air temperature and humidity in the atmosphere⁴ (M. Bruse, 1999; Huttner, 2012).

1.2.1.3. Atmospheric Turbulence

To simulate turbulences in a coarser resolution and in less computation time, turbulences in ENVI-met are parameterized using a E- ϵ 1.5 order closure model (M. Bruse, 1999; Institutes & Toudert, 2005). The E- ϵ model basically consists of two prognostic equations, one describing the production for turbulent energy and the other its dissipation (Mellor & Yamada, 1974, 1982):

$$\frac{\partial E}{\partial t} + u_i \frac{\partial E}{\partial x_i} = K_E \left(\frac{\partial^2 E}{\partial x_i^2} \right) + Pr - Th + Q_E - \epsilon$$

$$\frac{\partial \epsilon}{\partial t} + u_i \frac{\partial \epsilon}{\partial x_i} = K_\epsilon \left(\frac{\partial^2 \epsilon}{\partial x_i^2} \right) + c_1 \frac{\epsilon}{E} Pr - c_3 \frac{\epsilon}{E} Th - c_2 \frac{\epsilon^2}{E} + Q_\epsilon \quad (5)$$

With c_1 ; c_2 and c_3 as empiric constants (The default values used in ENVI-met are taken from Launder and Spalding (Launder & Spalding, 1974)), Q_E as the turbulence induced by vegetation and Q_ϵ as the accelerated cascade of turbulence energy from large scales to smaller ones near plant foliage (J Liu et al., 1996; Wilson, 1988).

In above formula the terms Pr and Th denote the production and dissipation of turbulent energy caused by wind shearing (Pr) and thermal stratification (buoyancy production) (Th) (Under stable conditions Th can be neglected).

1.2.1.4. Gas and particle dispersion model

The gas and particle dispersion model allows the simulation of emission and dispersion of various gases and particles in the model area. Apart from the dispersion and emission, ENVI-met also simulates the deposition as well as chemical reactions of gases NO, NO₂ and O₃. The dispersion of gases and particulate matter in the atmosphere is calculated using the advection- diffusion equation with local concentration of the gas/particle (unit: mg per kg (Air)). The sources in ENVI-met can have a diurnal variation. The database features 24 entries, each corresponding to an emission rate for each of the 24 hours of the day. The emission rates for points in time in between are linearly interpolated (Simon, 2016).

⁴ ENVI-met does not model the phase transformation between water and water vapour and vice versa. This means that the relative humidity is always below 100%.

1.2.1.5. Radiation

The calculation of the incoming short-wave and long-wave fluxes is based on a two-stream approximation in combination with some empiric formula (Gross, 2012; Taesler & Anderson, 1984).

The atmospheric radiation budget is defined by the absorption and emission coefficients of the different atmospheric layers. These coefficients depend on the optical thickness of the atmosphere, i.e. the number of aerosols and the amount of water vapor, carbon dioxide, ozone, and other greenhouse gases within the layer of atmosphere. For an accurate calculation of the radiative fluxes it would therefore be necessary to know the exact distribution of aerosols and greenhouse gases within the atmosphere and to account for their partly overlapping emission and absorption spectra. Since this information is usually not available, ENVI-met uses a much simpler approximation that only takes the water vapor into account. In a model with N layers the incoming long wave radiation at a height z can be calculated as (Paltridge & Platt, 1976):

$$Q_{lw}^{\downarrow}(z) = \sum_{n=1}^N \sigma T^4(n) [\epsilon_n(m + \Delta m) - \epsilon_n(m)] \quad (6)$$

Here m is the amount of water vapor between height z and the lower boundary of layer n , $(m + \Delta m)$ the amount of water vapour between height z and the upper boundary of layer n . ϵ_n is the emissivity (calculated based on an empiric formula (Kuhn, 1963; Pielke, 2002)), T the absolute temperature of layer n .

The incoming shortwave radiation at the upper boundary of the model area is calculated by integrating the radiation intensity of the sun I_0 from the wavelength $\lambda = 0.29\mu\text{m}$ to $\lambda = 4.0\mu\text{m}$:

$$Q_{sw}^* = \int_{0.29}^{4.0} I_0(\lambda) \exp\{-\alpha_R(\lambda)m + \alpha_M(\lambda)m\} d\lambda \quad (7)$$

The optical air mass m depends on the sun height h^5 , $\alpha_R(\lambda) = 0.00816 \cdot \lambda^{-4}$ and $\alpha_M(\lambda) = \lambda^{-1.3} \beta_{tr}$ are the coefficients for Rayleigh and Mie scattering, with $0.004 \leq \beta_{tr} \leq 1$ as the opacity coefficient.

The direct shortwave radiation on the upper boundary of the model $Q_{sw,dir}^0$ results from the difference of the incoming shortwave radiation Q_{sw}^* and the absorption of the shortwave radiation by water vapor $Q_{sw,abs}$.

$$Q_{sw,dir}^0 = Q_{sw}^* - Q_{sw,abs} \quad (8)$$

The diffuse shortwave radiation for a cloudless sky depends on the incoming direct shortwave radiation and the sun height (h) (Brown & Isfält, 1974):

$$Q_{sw,dif}^0 = R_{sw,dir}^0 \sin h \left(\frac{\gamma(h)}{1 - \gamma(h)} \right) \quad (9)$$

With:

$$\gamma(h) = \frac{1}{1 + 8(\sin h)^{0.7}} \quad (10)$$

If clouds are present the terms for the direct and diffuse radiation have to be adapted (Taesler & Anderson, 1984):

$$Q_{sw,dir}^0(\text{clouds}) = Q_{sw,dir}^0 \left(1 - \frac{N}{8} \right)$$

$$Q_{sw,dif}^0(\text{clouds}) = \left(\frac{Q_{sw,dir}^0 \sin h}{1 - \gamma(h)} \right) \left(\frac{\alpha_s - 1}{a_s a_c - 1} \right) - Q_{sw,dir}^0(\text{clouds}) \sin h \quad (11)$$

With N as the cloud cover in eighths, a_c as the mean albedo of the clouds depending on their height level and α_s as the mean albedo of the soil.

$$m = \begin{cases} \frac{1}{\sin h} & \text{if } h > 10 \\ 1.22 \left(\frac{1.0144}{\sin(h+1.44)} - 0.49 \right) & \text{if } h \leq 10. \end{cases}$$

Within the model area the radiation fluxes are strongly modified by (partial) shading from buildings and vegetation. This modification of the long wave and shortwave radiation fluxes is modeled via a number of coefficients σ that range between 0 (i.e. the radiation flux is completely blocked) to 1 (i.e. the radiation flux is not disturbed (M. Bruse, 1999; Michael Bruse & Fler, 1998c; Institutes & Toudert, 2005; Simon, 2016)). The five reduction coefficients are:

- Sky View Factor (SVF) σ_{svf}
- Effects of vegetation on the direct shortwave radiation $\sigma_{sw,dir}$
- Effects of vegetation on the diffuse shortwave radiation $\sigma_{sw,dif}$
- Effects of vegetation on the incoming long-wave radiation σ_{lw}^{\downarrow}
- Effects of vegetation on the outgoing long-wave radiation σ_{lw}^{\uparrow}

The SVF (σ_{svf}) is a measure for the amount of sky seen from the center of a grid cell:

$$\sigma_{svf} = \frac{1}{360} \sum_{\pi=0}^{360} \cos \omega(\pi) \quad (12)$$

Where w denotes the maximum cutoff angle in spatial direction π .

Other coefficients describe the influence of vegetation on direct $\sigma_{sw,dir}$ and diffuse $\sigma_{sw,dif}$ shortwave radiation and on upward σ_{lw}^{\uparrow} and downward σ_{lw}^{\downarrow} long wave radiation:

$$\sigma_{sw,dir} = \exp(F \cdot LAI^*(z)) \quad (13)$$

$$\sigma_{sw,dif} = \exp(F \cdot LAI(z, z_p)) \quad (14)$$

$$\sigma_{lw}^{\uparrow} = \exp(F \cdot LAI(0, z)) \quad (15)$$

$$\sigma_{lw}^{\downarrow} = \exp(F \cdot LAI(z, z_p)) \quad (16)$$

Where LAI is the vertical leaf area index of the plant from level z up to the top of the plant z_p or down to the ground $z = 0$. For shortwave solar radiation LAI^* replaces LAI . For the calculation of LAI^* the angle of incidence of the incoming sun rays is taken into account. The shortwave radiation budget can be summed up as:

$$Q_{sw}(z) = \sigma_{sw,dir}(z)Q_{sw,dir}^0 + \sigma_{sw,dif}(z)\sigma_{svf}(z)Q_{sw,dif}^0 + \left(1 - \sigma_{svf}(z)\right)Q_{sw,dir}^0 \bar{a} \quad (17)$$

With $Q_{sw,dir}^0$ as the direct and $Q_{sw,dif}^0$ as the diffuse shortwave radiation at the top of the model area. The term \bar{a} denotes the average albedo of all walls within the model area.

The long wave radiation fluxes can be written as:

$$Q_{lw}^{\downarrow}(z) = \sigma_{lw}^{\downarrow}(z, z_p)Q_{lw}^{\downarrow,0} + \left(1 - \sigma_{lw}^{\downarrow}(0, z)\right)\epsilon_f \sigma_B \bar{T}_{f+}^4 + (1 - \sigma_{svf}(z))Q_{lw}^{\leftrightarrow} \quad (18)$$

$$Q_{lw}^{\uparrow}(z) = \sigma_{lw}^{\uparrow}(0, z)\epsilon_s \sigma_B T_0^4 + (1 - \sigma_{lw}^{\uparrow}(0, z))\epsilon_f \sigma_f \bar{T}_{f-}^4 \quad (19)$$

\bar{T}_{f-}^4 and \bar{T}_{f+}^4 are the average foliage temperature of the underlying, respectively overlying vegetation. ϵ_s and ϵ_f denote the emissivity of the surface and foliage. T_0 is the surface temperature and $R \leftrightarrow lw$ is the horizontal long wave radiation flux from surrounding walls. σ_B is the Stefan-Boltzmann constant: $\sigma_B = 5.67 \cdot 10^{-8}$ (W m⁻² K⁻⁴) (Huttner, 2012; Simon, 2016).

1.2.2. Surface model: Ground and building surfaces

In contrast to the upper and lateral boundaries of the 3D model, ground and building surfaces represent actual physical boundaries (M. Bruse, 1999).

1.2.2.1. Ground surfaces

For the calculation of the temperature T_0 at the ground surface the energy balance at ground level has to be solved (M. Bruse, 1999; Huttner, 2012; Simon, 2016):

$$0 = Q_{sw;net} + Q_{lw;net} - G_0 - H_0 - LE_0 \quad (20)$$

$Q_{sw;net}$ is the net shortwave radiation at the surface, $Q_{lw;net}$ the net long-wave radiation at the surface, G_0 is the soil heat flux, H_0 the sensible and LE_0 the latent turbulent heat flux.

$$Q_{sw;net} = (\cos \beta \times Q_{sw;dir(z=0)} + Q_{sw;dif(z=0)}) - (1 - \alpha_s) \quad (21)$$

The net shortwave radiation of the ground surface ($z = 0$) is calculated taking into account the direct shortwave radiation $Q_{sw;dir}$, the diffuse shortwave radiation $Q_{sw;dif}$ and the albedo of the surface α_s . For the incoming direct radiation ($Q_{sw;dir}$) Lambert's cosine law is used to estimate the actual radiation on the surface with β as the angle between sun height and the normal of the surface. Since the diffuse radiation is assumed isotropic, the angle of the diffuse radiation ($Q_{sw;dif}$) does not need to be taken into account. For artificial surfaces the albedo (α_s) is taken directly from the database entry and used as a constant, while the albedo for natural surfaces is calculated dynamically taking into account the sun's height angle, the soil moisture of the topmost layer and the water content at saturation after Idso et al. (Idso, Jackson, Reginato, Kimball, & Nakayama, 1975).

The calculation of the net long-wave radiation is taking into account the unobstructed net long-wave radiation ($Q_{lw;net}^{unobs}$) from the sky and the net long-wave radiation emitted by objects like buildings or vegetation ($Q_{lw;net}^{obs}$) (M. Bruse, 1999):

$$Q_{lw,net} = \sigma_{svf} Q_{lw,net}^{unobs} + (1 - \sigma_{svf}) Q_{lw,net}^{obs} \quad (22)$$

The soil heat flux G_0 is calculated by:

$$G_0 = \lambda_s(k = -1) \frac{T_0 - T_{k=-1}}{0.5\Delta z_{k=-1}} \quad (23)$$

with $k = -1$ as the topmost height level of the soil model, λ_s as the heat transfer coefficient of the soil layer, T_0 as the surface temperature, $T_{k=-1}$ as the temperature of the soil layer in the depth $k = -1$ and $\Delta z_k = -1$ as the thickness of the topmost grid cell of the soil model.

The turbulent sensible and latent heat fluxes H_0 and LE_0 are implemented as functions of the turbulent exchange coefficients between the ground surface and the lowest grid cell of the atmosphere (Huttner, 2012; Institutes & Toudert, 2005; Simon, 2016).

1.2.2.2. Building surfaces

In versions prior to ENVI-met 4.0 the calculation of the outside wall/roof surface temperature was based on a simple steady-state energy balance. This approach has several shortcomings:

1. Parameters taken into account were the general thermal properties of the facade element (albedo, emissivity and U-value) in addition to the sensible heat transfer between the atmosphere and the facade and the heat conduction through the wall material, are identical for all wall and roof elements within the model domain. This

means that there was no possibility to assign individual values to a single wall or roof element.

2. The heat exchange between the outer and the inner side of the wall was driven by the heat transfer coefficient was not exactly equal to the U-value of the wall which can often be found in literature.
3. In earlier version the indoor temperature was set to a constant value and the inner wall is assumed to have the same temperature as the indoor air. Consequently, the heat exchange depends only on the temperature gradient between the outer and the inner surface of the wall or roof element.
4. In order to get more realistic temperatures of the facade, the heat storage within the wall was completely neglected, and the absorbed incoming short-wave radiation $Q_{sw;net}^{abs}$ for walls was set to half of its actual value. For roofs, which are assumed to be much thinner and to therefore have a much lower heat storage capacity than walls, $Q_{sw;net}^{abs}$ was left untouched. This lack of heat storage has two consequences:
5. When the wall/roof element is exposed to the sun (i.e. direct short wave radiation) the increase in wall/roof temperature is strongly overestimated
6. Once the wall/roof element is no longer in the sun the temperature of the façade immediately steeply declines. The release of energy from the facade element to the atmosphere during the night - one of the characteristics of the urban heat island - can therefore not be simulated.

The first consequence is not solved but at least mitigated by using only 50% of the incoming shortwave solar radiation $Q_{sw;net}^{abs}$ within the calculation.

Since Version 4.0 the calculation of the surface temperature of buildings is carried out using a three-node model which is based on the works of Terjung and O'Rourke (1980) (Terjung & O'Rourke, 1980). Terjung and O'Rourke's multiple-node transient state model allows the calculation of facade temperatures for an infinite amount of nodes in a wall. For the first implementation of the method in ENVI-met (Huttner, 2012), three nodes were applied to a wall, allowing the calculation of the temperature on the outside, the inside and the center of the wall (Fig. 2.).

The physical properties of the wall/roof included in the calculation of the proposed transient state model are: reflectivity, absorption, transmission, emissivity, heat transfer coefficient, specific heat capacity and the thickness of the wall (Huttner, 2012; Simon, 2016; Terjung & O'Rourke, 1980). For non-greened facades, the humidity at building facades is set to the humidity of the adjacent atmosphere cell (Simon, 2016).

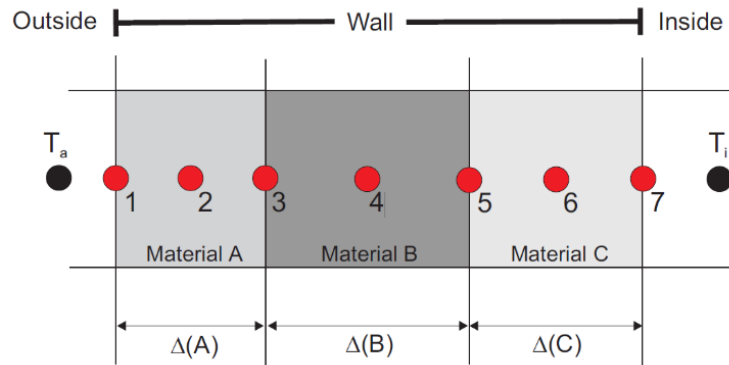


Fig. 2. Schematic of the new 3-node model (Simon, 2016)

The outside surface temperature (node 1) is calculated by the façade's energy budget. It is adjusted until the balance of the energy budget equals zero.

$$EB = Q_{sw,net}^{abs} + \epsilon \cdot (Q_{lw} - \sigma T_1^4) - H_w - LE_w - G_w \cong 0 \quad (24)$$

With $Q_{sw,net}^{abs}$ as the net short-wave radiation absorbed by the façade surface, σ = Stefan – Boltzmann, $\epsilon \cdot (Q_{lw} - \sigma T_1^4)$ as the longwave radiation balance depending on the surface temperature of the outside node T_1 and the incoming long-wave radiation Q_{lw} , H_w as the sensible heat flux into the atmosphere, LE_w as the latent heat flux into the atmosphere due to evaporation or condensation of water at the outside face surface and G_w as the conduction heat flux from or to adjacent node inside the wall - roof (Simon, 2016).

Radiative Fluxes

The incoming shortwave radiation $Q_{sw,net}^{abs}$ is provided as a boundary condition from the main model. The net short-wave radiation absorbed by the façade surface calculates through following equations for opaque and transparent surfaces:

$$Q_{sw,net}^{abs} = (Q + q)(1 - a_{c1}), \text{ for solid surface like concrete}$$

$$Q_{sw,net}^{abs} = (Q + q)(1 - a_{c1} - t_G), \text{ for glass surface} \quad (25)$$

Q: direct solar radiation (W m^{-2}), q: diffuse solar radiation, a_{c1} = albedo, $(1 - a_{c1})$: absorptivity, t_G transmissivity of glass (Terjung & O'Rourke, 1980).

Estimate of absorbed long wave radiation: For the calculation of the absorbed long wave radiation $Q_{lw,net}^{abs}$ separate view factors for each wall/roof element are used in the new approach. These view factors contain detailed information about the fraction of ground, sky, buildings and vegetation within the field of view of the facade. Using these new view factors, the long wave radiation absorbed by a wall/roof element can be written as:

$$Q_{lw,net}^{abs} = \epsilon_f (fvf_{ground} Q_{lw,ground} + fvf_{buildings} Q_{lw,buildings} + fvf_{sky} Q_{lw,sky} + fvf_{veg} Q_{lw,veg}) \quad (26)$$

The wall/roof view factors for soil (fvf_{ground}), buildings ($fvf_{buildings}$), sky (fvf_{sky}) and vegetation (fvf_{veg}) are calculated at the beginning of the simulation by the use of a ray tracing algorithm. This algorithm checks for every grid cell which elements can be seen from the center of the grid cell. The step width of the angles at which the tracing rays are emitted from the facade is 10° in the horizontal as well as the vertical direction. All in all 36×18 rays are emitted and traced from each grid cell. E.g. the fvf_{ground} can be calculated as:

$$fvf_{ground} = \sum_{i=-9}^8 \sum_{j=0}^{35} \frac{1}{36} (\sin(10 + i \times 10) - \sin(i \times 10)) I_{ground} \quad (27)$$

With I_{ground} , equal to 1 if ground is first obstacle in path of traced ray and 0 otherwise. The factor $(\sin(10 + i \times 10) - \sin(i \times 10))$ (takes the geometrics of the hemisphere into account, i.e. the fact that the percentage of the field of view attributed to one ray depends upon the angle at which the ray is emitted. The view factors have to sum up as:

$$fvf_{ground} + fvf_{buildings} + fvf_{sky} + fvf_{vegetation} = 1 \quad (28)$$

For an accurate calculation of the incoming long wave radiation at the surface of the wall/roof element this ray tracing procedure would have to be repeated at every time step the facade temperature is calculated. Due to computational limits this is not implemented. Instead a mean temperature value of all surfaces / buildings / vegetation within the model area is used for the calculation of $Q_{lw,ground}$, $Q_{lw,building}$ and $Q_{lw,veg}$.

Turbulent Fluxes

The turbulent flux of sensible heat H_w is given by (Bruse, 2018):

$$H_w = h_{c,w} (T_1 - T_a) \quad (29)$$

The convection coefficient at the wall surface $h_{c,w}$ in ($\text{W m}^{-2} \text{K}^{-1}$) is calculated according to DIN EN ISO 6946 (DIN, 2015):

$$h_{c,w} = 4 + 4v \quad (30)$$

Where v is the tangential wind velocity above the wall surface of interest.

Conductive Fluxes

The heat conduction G_w between the next inner node T_2 can be easily calculated using the material properties of material A and the temperature of the next inner node T_2 . G_w is then given by (Bruse, 2018):

$$G_w = \frac{\lambda(A)}{0.5 \Delta(A)} (T_1 - T_2) \quad (31)$$

Inner wall surface temperature

As the model does not include detailed information on indoor surfaces such as the floor, inner walls or furniture, we assume that all other surfaces seen by node 7 have more or less the same temperature. In addition, the reflection of shortwave radiation inside the building is not taken into account. With this assumptions, the energy budget equation for node T_7 as (Bruse, 2018):

$$EB = G_w - H_w \cong 0 \quad (32)$$

Where G_w is the conduction heat flux and calculated with:

$$G_w = \frac{\lambda(C)}{0.5 \Delta C} (T_6 - T_7) \quad (33)$$

H_w is the sensible heat transfer between the inner wall surface and the indoor air with :

$$H_w = h_w (T_7 - T_i) \quad (34)$$

With the heat transfer coefficient $h_{c,w}$ taken constant for the inner wall with $7.7 \text{ (W m}^{-2} \text{ K}^{-1}\text{)}$ according to DIN 6946.

Solving the Fourier- Equations for the inner nodes

The Fourier-Equation linked equations defining the temperature dynamics at the inner wall nodes T_2 to T_6 . In general, this system can be solved in either an explicit or an implicit way. While the explicit solution is easy to calculate, it tends to be numerically unstable and requires small time steps, especially if the material is thin and the heat conduction is fast. The implicit solution of the equation system is numerically more expensive, but allows larger time step and has only little tendency to generate unstable solutions. As most of the prognostic equations in ENVI-met are solved implicitly, an implicit solution of the wall temperature system was chosen (Bruse, 2018). Setting up the equations for the implicit solution process starts with the finite difference discretization of the Fourier Equation.

The calculation of the temperatures of inner nodes are carried out by using the one dimensional Fourier Equation:

$$\frac{\partial T_i}{\partial t} = k_i \frac{\partial^2 T}{\partial \Delta^2} \quad (35)$$

$$\frac{T_i^* - T_i}{\Delta t} = \frac{1}{\Delta_{ic}} \left[k_{i-} \left(\frac{T_{i-1}^* - T_i^*}{\Delta_{i-}} \right) - k_{i+} \left(\frac{T_i^* - T_{i+1}^*}{\Delta_{i+}} \right) \right] \quad (36)$$

With T_i^* as the temperature of the node i in the future time-step $t^* = t + \Delta t$, T_i as the temperature of the node i for the current time t , k_i as the thermal diffusivity ($\text{m}^2 \text{ s}^{-1}$) at node i and Δ_{ic} , Δ_{i-} , Δ_{i+} as the center, left and right differences between the nodes (Simon, 2016).

For example, T_2^* and T_3^* can then directly be calculated via following equations (Simon, 2016):

$$T_2^* = (PT_2 + T_1^* + \frac{P}{2}T_3R + \frac{h_{c,i}\Delta x}{\lambda} T_iR) \frac{1}{P+2-R} \quad (37)$$

$$T_3^* = \left(T_2^* + \frac{P}{2} T_3 + \frac{h_{c,i} \Delta x}{\lambda} T_i \right) R \quad (38)$$

$$\text{with } R = \left(\frac{P}{2} + \frac{h_c \Delta x}{\lambda} + 1 \right)^{-1} \quad (39)$$

$$\text{with } P = \frac{\Delta x^2 c_{wall} \rho_\omega}{\lambda \Delta t} \quad (40)$$

In which λ is the heat conductivity ($\text{W m}^{-1} \text{K}^{-1}$) of wall material and $c_{wall} \rho_\omega$ is the volumetric heat capacity ($\text{J m}^{-3} \text{K}^{-1}$) calculated as the product of specific heat c_{wall} ($\text{J Kg}^{-1} \text{K}^{-1}$) and density ρ_ω (Kg m^{-3}) of the material.

Indoor temperature:

The calculation of the building indoor temperature is not only a required helper variable, but an important parameter to analyze and control a buildings thermal performance. There are two different ways the indoor temperature can be handled in ENVI-met:

- (a) as a prognostic variable progressing with respect to the calculated energy fluxes at the building envelope (non-climate controlled building) and,
- (b) as a constant value defined by the user.

For the calculation of the indoor air temperature, the indoor air volume must be known. Therefore, the model will automatically divide buildings into separate air volumes. Alternatively, the user can manually define horizontally and vertically separated building zones within a building that represent confined spaces inside the building. The model then uses the respective inside air volumes in these zones to calculate the indoor air temperatures. The energy fluxes into the zones are sensible heat transfer from the indoor wall and the transmission of direct radiation through transparent wall elements such as windows.

The incoming and outgoing fluxes are balanced according to the indoor air volume enclosed in the building zones. The lack or gain of energy through the walls or roofs results in a change of the indoor temperature. Since, heat transfer between adjacent building zones and heat storage of indoor walls are neglected as of yet the calculation of the indoor temperature must still be regarded as only a rough estimation (Simon, 2016).

1.2.3. Soil model

The soil model is connected to the underside of the atmosphere model. Within the soil model hydrological and thermodynamically processes up to a depth of $z = -5\text{m}$ are calculated. The vertical extent of 5 meters guarantees constant conditions regarding the temperature and water content of the soils within the typical simulation periods of 24 hours to 5 days as well as providing enough space for roots of large plants. Since soils have a great impact on the microclimate and are typically vertically inhomogeneous ENVI-met soil are organized in layers of different soil types which each have different adjustable hydrological and thermo-dynamical parameters.

As the dynamics of the hydrological and thermo-dynamical processes decrease with increasing depth, ENVI-met's soil profiles are horizontally divided into 20 non-equidistant layers where the upper layers show finer vertical resolutions (five topmost layer thickness $\Delta z = 0.01\text{m}$) than deeper layers (bottom layer thickness $\Delta z = 0.5\text{m}$).

Within natural soils heat and water exchange is simulated whereas in impermeable surfaces only heat fluxes are calculated.

$$\frac{\partial T_s}{\partial t} = k_s \frac{\partial^2 T_s}{\partial z^2} \quad (41)$$

$$\frac{\partial \eta}{\partial t} = D_\eta \frac{\partial^2 \eta}{\partial z^2} + \frac{\partial K_\eta}{\partial z} - S_\eta(z) \quad (42)$$

With T_s as the soil temperature, t as the time, η as the volumetric water content, D_η as the hydraulic diffusivity of the soil, K_η as the hydraulic conductivity of the soil and S_η as the water extraction from the soil by plants. For natural soils the thermal diffusivity k_s is a function of the soil moisture η , for impermeable soils k_s is a user defined, constant parameter (M. Bruse, 1999; Michael Bruse & Fleer, 1998b; Huttner, 2012; Simon, 2016).

1.2.4. Vegetation model

Vegetation in ENVI-met is represented by clusters of cells having a leaf area density in the atmosphere model and root area density in the soil model, allowing the remodeling of the distribution and shape of roots and crowns of plants. Apart from the effects of these cell clusters on the wind field and the radiation, the modeled plants use biological control mechanisms that regulate the exchange of CO₂ and water vapor with the atmosphere.

Based on the calculation of the stomatal conductance using Jacobs' A - g_s model (Jacobs, 1994; Simon, 2016).

The vegetation in ENVI-met interacts with the atmospheric model as well as with soil model and the radiation model. The exchange of heat and moisture on the leaf surfaces are implemented as sources and sinks in the calculation of air temperature and humidity with z as the height, Q_θ as the potential temperature and Q_q as the specific humidity.

$$Q_\theta(z) = LAD(z)J_{f,h} \quad (43)$$

$$Q_q(z) = LAD(z)(J_{f,evapo} + J_{f,trans}) \quad (44)$$

The direct heat flux $J_{f,h}$, the evaporation flux $J_{f,evap}$ and the transpiration flux $J_{f,trans}$ that define the interactions between vegetation and atmosphere can be written as (Michael Bruse & Fleer, 1998c):

$$J_{f,h} = 1.1 r_a^{-1} (T_f - T_a) \quad (45)$$

$$J_{f,evap} = r_a^{-1} \Delta q \delta_c f_w + r_a^{-1} (1 - \delta_c) \Delta q \quad (46)$$

$$J_{f,trans} = \delta_c (r_a + r_s)^{-1} (1 - f_w) \Delta q \quad (47)$$

With T_a as the air temperature, T_f as the leaf temperature, Δq as the humidity gradient between leaf and atmosphere, r_s as the stomatal resistance, r_a as the aerodynamic resistance of the leaf, f_w as the ratio of moistened leaf area and δ_c as a factor being 1 if transpiration or evaporation can occur ($\Delta q \geq 0$) and being 0 if only condensation can occur (Simon, 2016).

To simulate the complex behavior of living organisms that react and interact with the microclimatic environment, the vegetation model includes a stomata model calculating the stomatal conductance based on the works of Jacobs' empirical A - g_s model (Jacobs, 1994). The main hypothesis of the A - g_s model is that the goal of plants is to operate the stomatal conductance in a way that while the water loss of the plant is minimized, the CO₂ assimilation and thus the carbon gain is maximized (DAMOUR, SIMONNEAU, COCHARD, & URBAN, 2010; Jacobs, 1994; Simon, 2016).

The basic relation of the model can be summed up as:

$$g_s = 1.6 \frac{A_n}{c_s - c_i} \quad (48)$$

With C_s and C_i as the CO₂ concentrations at the surface and inside the leaf. The factor 1.6 accounts for the different diffusivities of CO₂ and H₂O (Jacobs, 1994).

1.2.5. Biometeorological model

ENVI-met includes a simple biometeorological model to predict the thermal comfort inside the model area. At the moment ENVI-met supports the calculation of PMV⁶ (predicted mean vote) (Fanger, 1970) and the more modern “physiologically equivalent temperature” (PET) (Höppe, 1999).

The calculation of all of these biometeorological indices does not require any feedback from ENVI-met but just the output results for air temperature, wind speed, air humidity and radiant temperature.

1.2.5.1. Calculation of the mean radiant temperature in ENVI-met

ENVI-met calculates the mean radiant temperature T_{mrt} for a cylindrical shaped body:

$$T_{mrt} = \left(\frac{1}{\sigma} \left(Q_{lw,in} + \frac{\alpha k}{\epsilon} \times (Q_{sw-diff,in} + Q_{sw-dir,in}) \right) \right)^{0.25} \quad (49)$$

Where the emission coefficient of the human body (ϵ) is set to 0.97 and αk as the absorption coefficient of the human body for short wave radiation is set to 0.7. σ is the Stefan-Boltzmann constant.

The incoming long wave radiation $Q_{lw,in}$ is assumed to come to 50% from the sky, buildings and vegetation and to 50% from the ground surface.

⁶ PMV predicts the mean judgment of a large group of people on the ASHRAE thermal sensation scale, which runs from -4 (very cold) to +4 (hot) (Höppe, 1999)

$$Q_{lw,in} = 0.5 \times \left(vf_{veg} \overline{\epsilon_{veg}} \sigma \overline{T_{veg}}^4 + vf_{bldg} \overline{\epsilon_{bldg}} \sigma \overline{T_{bldg}}^4 + vf_{sky} Q_{lw,sky} + vf_{bldg} (1 - \overline{\sigma_{bldg}}) Q_{lw,sky} \right) + 0.5 \times (\sigma \epsilon_{ground} T_{ground}^4) \quad (50)$$

The view factors vf give the percentage of vegetation/ buildings/ sky that can be seen from the specific grid point. The physical correct approach would be to calculate the long wave radiation fluxes based on the emissivity and temperature of the elements within view. This would however require considerable amounts of CPU time and RAM.

Therefore the average emissivity $\bar{\epsilon}$ and temperature \bar{T} of all plants/ building surfaces within the model area are used instead. The incoming long wave radiation from the sky $Q_{lw,sky}$ is calculated based on the air temperature, air humidity and some empirical parameters (Oke, 1987). For long wave radiation coming from the ground only the emissivity and surface temperature of the grid corresponding grid cell are taken into account.

The diffuse incoming short wave radiation $Q_{sw-dir,in}$ is calculated accordingly (Huttner, 2012):

$$Q_{sw-dir,in} = 0.5 \times (vf_{bldg} \overline{rf_{bldg}} Q_{sw-dir,sky} + vf_{sky} Q_{sw-diff,sky}) + 0.5 \times (rf_{ground} Q_{sw,ground}) \quad (51)$$

With rf as the reflectivity and $Q_{sw,ground}$ as the overall shortwave radiation at the ground surface of the corresponding grid cell.

The incoming direct short wave radiation $Q_{sw-dir,in}$ is calculated as the direct short wave radiation within the grid cell multi-plicate with a projection factor pf :

$Q_{sw-dir,in} = pf \times Q_{sw-dir}$. This projection factor depends on the azimuth angle of the sun Φ (Huttner, 2012):

$$pf = 0.42 \times \cos \Phi + 0.043 \times \sin \Phi \quad (52)$$

2. Numerical solution techniques in ENVI-met

The differential equations are solved by using the finite difference method and are solved forward in time:

$$\frac{\partial \phi}{\partial t} \rightarrow \frac{\phi^{n+1} - \phi^n}{\Delta t} \quad (53)$$

with Δt as the time step, i.e. the interval at which the equations are solved and ϕ^n the (known) variable at the previous time step and ϕ^{n+1} the (searched for) variable at the next time step.

For the solution of the combined advection-diffusion equations the so called Alternating Direction Implicit (ADI) method is used.

In order to get a numerically stable calculation of the turbulence and its dissipation the size of the time step between calculations has to be chosen carefully. The maximum allowed time step depends on the velocity of the wind (u ; v ; w) and the size of the grid cells (Δx ; Δy ; Δz) and can be calculated as:

$$\Delta t_{max} = \frac{0.8}{|u/\Delta x|_{max} + |v/\Delta y|_{max} + |\omega/\Delta z|_{max}} \quad (54)$$

Experience has shown that this criterion is not sufficient in some conditions, it allows time steps that are too large and lead to numerical instability. Therefore an arbitrary maximum value is defined: $\Delta t = 0.3$ s (Huttner, 2012).

3. Shortcoming of ENVI-met

ENVI-met is continually being updated and new features are introduced regularly. However ENVI-met is far from being a perfect simulation of reality and has some (major) limitations. The following list gives a short overview on the most prominent shortcomings of ENVI-met:

1. The standard E- ϵ closure used by ENVI-met is known to have a tendency to overestimate the turbulent intensity. This behavior can often be found in simulations with ENVI-met. Other methods for the closure of the turbulent kinetic energy like Direct Numerical Simulation (DNS) or Large Eddy Simulation would require a complete reprogramming of ENVI-met and are therefore not applicable to ENVI-met in the foreseeable future.
2. ENVI-met is able to simulate the effects of plants onto the microclimate quite accurately but is not capable of assessing the effects of microclimate onto plants

since plants are represented by loose clusters of grid cells rather than a uniform object organism (Simon, 2016).

3. The attenuation of the diffuse radiation by vegetation is not yet taken into account.
4. while the chemistry model is able to simulate the formation of tropospheric ozone by photolyzation of nitrogen dioxide and its destruction by reacting with nitrogen monoxide, the release of isoprene and its additional contribution to the formation of tropospheric ozone is disregarded as of yet (Simon, 2016).
5. Overestimation of short-wave downward radiation in ENVI-met (Huttner, 2012).
6. The scattering of the upward and downward diffuse radiation is considered to be isotropic (Huttner, 2012).

Despite the limitations, through various researches the strong correlation found between the measured values and test run results, indicates that the ENVI-met model is a reliable tool for studying the microclimate condition in the space between buildings.

4. Example data for ENVI-met model (.SIM files)

Paper B

```

%---- ENVI-met V4 main configuration file -----
%---- generated with ProjectWizard -----
Fileversion                =4.0
JobID                      =Simulation
% Main data .....
Name for Simulation (Text):      =.....
Area Input File to be used      =.....INX
Filebase name for Output (Text): =.....
Output Directory:              =C:\ENVImet projects\Paper 2- .....
Start Simulation at Day (DD.MM.YYYY):    =26.01.2017
Start Simulation at Time (HH:MM:SS):     =03:00:00
Total Simulation Time in Hours:         =48
Wind Speed in 10 m ab. Ground [m/s]     =2.3
Wind Direction (0:N..90:E..180:S..270:W..) =282
Roughness Length z0 at Reference Point [m] =0.1
Initial Temperature Atmosphere [K]      =273.950
Specific Humidity in 2500 m [g Water/kg air] =1
Relative Humidity in 2m [%]             =56.17
% End main data .....
[OUTPUTTIMING]_____
Output interval main files (min)        =60.00
Output interval text output files (min)  =30.00
Include Nesting Grids in Output (0:n,1:y) =1

```

[SOLARADJUST] _____

Factor of shortwave adjustment (0.5 to 1.5) =0.70

[CLOUDS] _____

Fraction of LOW clouds (x/8) =0.00

Fraction of MIDDLE clouds (x/8) =2.00

Fraction of HIGH clouds (x/8) =0.00

[TIMING] _____

Update Surface Data each ? sec =30.00

Update Wind field each ? sec =0.00

Update Radiation and Shadows each ? sec =600.00

Update Plant Data each ? sec =600.00

[SOILDATA] _____

Initial Temperature Upper Layer (0-20 cm) [K]=273.25

Initial Temperature Middle Layer (20-50 cm) [K]=274.15

Initial Temperature Deep Layer (below 50 cm)[K]=275.65

Relative Humidity Upper Layer (0-20 cm) =50.00

Relative Humidity Middle Layer (20-50 cm) =60.00

Relative Humidity Deep Layer (below 50 cm) =60.00

[SIMPLEFORCE] _____

Hour 00h [Temp, rH] = 271.15, 83.40

Hour 01h [Temp, rH] = 270.95, 83.10

Hour 02h [Temp, rH] = 270.65, 83.20

Hour 03h [Temp, rH] = 270.55, 81.70

Hour 04h [Temp, rH] = 270.35, 80.70

Hour 05h [Temp, rH] = 270.05, 81.10

Hour 06h [Temp, rH] = 269.75, 81.60

Hour 07h [Temp, rH] = 270.85, 75.50

Hour 08h [Temp, rH] = 272.25, 68.40

Hour 09h [Temp, rH] = 273.85, 63.20

Hour 10h [Temp, rH] = 275.65, 57.70

Hour 11h [Temp, rH] = 277.15, 54.00

Hour 12h [Temp, rH] = 277.65, 53.00

Hour 13h [Temp, rH] = 278.25, 51.60

Hour 14h [Temp, rH] = 278.05, 53.00

Hour 15h [Temp, rH] = 277.45, 56.00

Hour 16h [Temp, rH] = 276.25, 60.60

Hour 17h [Temp, rH] = 275.65, 62.80

Hour 18h [Temp, rH] = 275.05, 65.60

Hour 19h [Temp, rH] = 274.95, 64.70

Hour 20h [Temp, rH] = 275.15, 62.20

Hour 21h [Temp, rH] = 274.75, 64.30

Hour 22h [Temp, rH] = 274.25, 65.60

Hour 23h [Temp, rH] = 274.25, 64.40

[LBC-TYPES] _____

LBC for T and q (1:open, 2:forced, 3:cyclic) =2

LBC for TKE (1:open, 2:forced, 3:cyclic) =3

[PARALLEL_CPU] _____

CPU usage settings =ALL

relax =0.7

Paper C- Phase 2

```

%---- ENVI-met V4 main configuration file -----
%---- generated with ProjectWizard -----
Fileversion                =4.3
JobID                      =Simulation
% Main data .....
Name for Simulation (Text):    =....
Area Input File to be used    =....INX
Filebase name for Output (Text): =....
Output Directory:            =C:\ENVI-met projects\....
Start Simulation at Day (DD.MM.YYYY):    =26.01.2017
Start Simulation at Time (HH:MM:SS):    =03:00:00
Total Simulation Time in Hours:        =48
Wind Speed in 10 m ab. Ground [m/s]    =3.8
Wind Direction (0:N..90:E..180:S..270:W..) =282
Roughness Length z0 at Reference Point [m] =0.1
Initial Temperature Atmosphere [K]     =259.150
Specific Humidity in 2500 m [g Water/kg air] =1
Relative Humidity in 2m [%]            =75%
% End main data .....
[OUTPUTTIMING]_____
Output interval main files (min)        =60.00
Output interval text output files (min)  =30.00
Include Nesting Grids in Output (0:n,1:y) =1
[TIMING]_____
Update Surface Data each ? sec          =30.00
Update Wind field each ? sec            =100.00
Update Radiation and Shadows each ? sec  =600.00

```

Update Plant Data each ? sec =600.00

[SOILDATA] _____

Initial Temperature Upper Layer (0-20 cm) [K]=273.25

Initial Temperature Middle Layer (20-50 cm) [K]=274.15

Initial Temperature Deep Layer (below 50 cm)[K]=275.65

Relative Humidity Upper Layer (0-20 cm) =50.00

Relative Humidity Middle Layer (20-50 cm) =60.00

Relative Humidity Deep Layer (below 50 cm) =60.00

[SIMPLEFORCE] _____

Hour 00h [Temp, rH] = 259.15, 75.00

Hour 01h [Temp, rH] = 259.15, 75.00

Hour 02h [Temp, rH] = 259.15, 75.00

Hour 03h [Temp, rH] = 259.15, 75.00

Hour 04h [Temp, rH] = 259.15, 75.00

Hour 05h [Temp, rH] = 259.15, 75.00

Hour 06h [Temp, rH] = 259.15, 75.00

Hour 07h [Temp, rH] = 259.15, 75.00

Hour 08h [Temp, rH] = 259.15, 75.00

Hour 09h [Temp, rH] = 259.15, 75.00

Hour 10h [Temp, rH] = 259.15, 75.00

Hour 11h [Temp, rH] = 259.15, 75.00

Hour 12h [Temp, rH] = 259.15, 75.00

Hour 13h [Temp, rH] = 259.15, 75.00

Hour 14h [Temp, rH] = 259.15, 75.00

Hour 15h [Temp, rH] = 259.15, 75.00

Hour 16h [Temp, rH] = 259.15, 75.00

Hour 17h [Temp, rH] = 259.15, 75.00

Hour 18h [Temp, rH] = 259.15, 75.00

Hour 19h [Temp, rH] = 259.15, 75.00

Hour 20h [Temp, rH] = 259.15, 75.00

Hour 21h [Temp, rH] = 259.15, 75.00

Hour 22h [Temp, rH] = 259.15, 75.00

Hour 23h [Temp, rH] = 259.15, 75.00

[LBC-TYPES] _____

LBC for T and q (1:open, 2:forced, 3:cyclic) =2

LBC for TKE (1:open, 2:forced, 3:cyclic) =3

relax =0.7

[PARALLEL_CPU] _____

CPU usage settings =ALL

[IVSRADIATION] _____

Use IVS radiation transfer scheme (0:n,1:y) = 1

[NEWBUILDING] _____

Initial Indoor temp [K] =293.00

Keep Indoor temp (0:no, 1:yes) =1

[SORMODE] _____

SOR solver (0: classic, 1:parallel) =0

References

- Brown, G., & Isfält, E. (1974). *Solinstrålning och solavskärmning: Solar irradiation and sun shading devices*. Stockholm: Statens inst. för byggnadsforskning.
- Bruse, M. (1999). Die Auswirkungen kleinskaliger Umweltgestaltung auf das Mikroklima Michael Bruse aus Essen Bochum , 1999.
- Bruse, M. (2016a). ENVI_met. A holistic microclimate model. Retrieved September 1, 2016, from <http://www.model.envi-met.com/hg2e/doku.php?id=intro:modelconept>
- Bruse, M. (2016b). ENVI-met 4.0, (Science). ESSEN.
- Bruse, Michael, & Flerer, H. (1998a). Simulating surface–plant–air interactions inside urban environments with a three dimensional numerical model. *Environmental Modelling & Software*, 13(3), 373–384. [https://doi.org/https://doi.org/10.1016/S1364-8152\(98\)00042-5](https://doi.org/https://doi.org/10.1016/S1364-8152(98)00042-5)
- Bruse, Michael, & Flerer, H. (1998b). With a Three Dimensional Numerical Model. *Environmental Modelling & Software*, 13(3–4), 373–384.
- Bruse, M., Simon, H., Kropp, T., Sohni, F., (2018). Development and implementation of a high-resolution dynamical wall and roof model for ENVI-met, (Not Published).
- DAMOUR, G., SIMONNEAU, T., COCHARD, H., & URBAN, L. (2010). An overview of models of stomatal conductance at the leaf level. *Plant, Cell & Environment*, 33(9), 1419–1438. <https://doi.org/10.1111/j.1365-3040.2010.02181.x>
- DIN. (2015). *DIN EN ISO 6946*. Berlin.
- Fanger, P. O. (1970). *Thermal comfort: Analysis and applications in environmental engineering*. Danish Technical Press. Retrieved from <https://books.google.de/books?id=S0FSAAAAMAAJ>
- Gross, G. (2012). *Numerical Simulation of Canopy Flows*. Springer Berlin Heidelberg. Retrieved from <https://books.google.de/books?id=sNm9BwAAQBAJ>
- Höppe, P. (1999). The physiological equivalent temperature -- a universal index for the biometeorological assessment of the thermal environment. *International Journal of Biometeorology*, 43(2), 71–75. <https://doi.org/10.1007/s004840050118>
- Huttner, S. (2012). Further development and application of the 3D microclimate simulation ENVI-met. *Mainz: Johannes Gutenberg-Universität in Mainz*, 147. Retrieved from <http://ubm.opus.hbz-nrw.de/volltexte/2012/3112/>
- Idso, S. B., Jackson, R. D., Reginato, R. J., Kimball, B. A., & Nakayama, F. S. (1975). The Dependence of Bare Soil Albedo on Soil Water Content. *Journal of Applied Meteorology*, 14(1), 109–113. [https://doi.org/10.1175/1520-0450\(1975\)014<0109:TDOBSA>2.0.CO;2](https://doi.org/10.1175/1520-0450(1975)014<0109:TDOBSA>2.0.CO;2)

- Institutes, M., & Toudert, F. A. (2005). Berichte des Meteorologischen Institutes der Universität Freiburg Fazia Ali Toudert Dependence of Outdoor Thermal Comfort on Street Design in Hot and Dry Climate, (15).
- Jacobs, C. M. J. (1994). *Direct impact of atmospheric CO2 enrichment on regional transpiration*. Wageningen University.
- Kuhn, P. M. (1963). Radiometersonde Observations of Infrared Flux Emissivity of Water Vapor. *Journal of Applied Meteorology*, 2(3), 368–378. [https://doi.org/10.1175/1520-0450\(1963\)002<0368:ROOIFE>2.0.CO;2](https://doi.org/10.1175/1520-0450(1963)002<0368:ROOIFE>2.0.CO;2)
- Lauder, B. E., & Spalding, D. B. (1974). The numerical computation of turbulent flows. *Computer Methods in Applied Mechanics and Engineering*, 3(2), 269–289. [https://doi.org/https://doi.org/10.1016/0045-7825\(74\)90029-2](https://doi.org/https://doi.org/10.1016/0045-7825(74)90029-2)
- Liu, J., Chen, J. M., Black, T. A., & Novak, M. D. (1996). E-\$\$\$ modelling of turbulent air flow downwind of a model forest edge. *Boundary-Layer Meteorology*, 77(1), 21–44. <https://doi.org/10.1007/BF00121857>
- Mellor, G. L., & Yamada, T. (1974). A Hierarchy of Turbulence Closure Models for Planetary Boundary Layers. *Journal of the Atmospheric Sciences*, 31(7), 1791–1806. [https://doi.org/10.1175/1520-0469\(1974\)031<1791:AHOTCM>2.0.CO;2](https://doi.org/10.1175/1520-0469(1974)031<1791:AHOTCM>2.0.CO;2)
- Mellor, G. L., & Yamada, T. (1982). Development of a turbulence closure model for geophysical fluid problems. *Reviews of Geophysics*, 20(4), 851–875. <https://doi.org/10.1029/RG020i004p00851>
- Oke, T. R. (1987). *Boundary Layer Climates*. Routledge. Retrieved from https://books.google.de/books?id=K_2dW7crfVIC
- Paltridge, G. W., & Platt, C. M. R. (1976). *Radiative processes in meteorology and climatology*. Elsevier. Retrieved from <https://books.google.de/books?id=m-HVoAEACAAJ>
- Pielke, R. A. (2002). *Mesoscale Meteorological Modeling*. Academic Press. Retrieved from <https://books.google.de/books?id=hyUEI7NK7bUC>
- Simon, H. (2016). *Modeling urban microclimate - Development, implementation and evaluation of new and improved calculation methods for the urban microclimate model ENVI-met*. Mainz : Univ.
- Szucs, Á. (2013). Wind comfort in a public urban space-Case study within Dublin Docklands. *Frontiers of Architectural Research*, 2(1), 50–66. <https://doi.org/10.1016/j.foar.2012.12.002>
- Taesler, R., & Anderson, C. (1984). A method for solar radiation computings using routine meteorological observations,. *Energy and Buildings*, 7, 341–352.
- Terjung, W. H., & O'Rourke, P. A. (1980). Simulating the causal elements of urban heat islands. *Boundary-Layer Meteorology*, 19(1), 93–118. <https://doi.org/10.1007/BF00120313>

Wilson, J. D. (1988). A second-order closure model for flow through vegetation. *Boundary-Layer Meteorology*, 42(4), 371–392. <https://doi.org/10.1007/BF00121591>

Appendix 4- Original published Papers

1. Paper A

DOI: <https://doi.org/10.1016/j.scs.2017.07.025>



Numerical modeling validation for the microclimate thermal condition of semi-closed courtyard spaces between buildings



Aysan Forouzandeh*

Department of Civil Engineering and Geodetic Science, Institute for Building Physics, Leibniz University, Hannover, Germany

ARTICLE INFO

Keywords:
Courtyard microclimate variables
ENVI-met model
Field experiment
Model evaluation

ABSTRACT

In this study, the microclimate model ENVI-met version 4 was evaluated with field data inside courtyard spaces. The measurements were planned in different climate conditions in summer and winter at different points inside the courtyard located in Hannover, Germany. Climate variables—including air temperature (T_a), relative humidity (RH), wind speed (WS) and mean radiant temperature (T_{mrt})—were investigated. The comparison between observation and prediction was performed while considering the accuracy of the model with the different domain and cell sizes, the different lateral boundary conditions for turbulence (LBC for TKE) and the time step size for flow. Consequently, the $2 \times 2 \times 1 \text{ m}^3$ cell-sized model with cyclic LBC for TKE and $t_{flow} = 0 \text{ s}$ lead to quicker simulation and reliable results.

This study provides further confidence that the ENVI-met model is capable of predicting the microclimate variables inside medium-narrow courtyards with an acceptable accuracy. The root mean square error (RMSE) value at the center of the shaded courtyard was calculated as approximately $0.73 \text{ }^\circ\text{C}$ for T_a , 3.34% for RH, 0.01 m/s for WS and $8.44 \text{ }^\circ\text{C}$ for T_{mrt} . However, due to the model resolution, inaccuracies in the values are displayed for T_{mrt} in the sun-exposed areas.

1. Introduction

The courtyard as a private and isolated space through which all living rooms are grouped around, offered an endemic sense of well-being, permitting residents to live either indoors or outdoors in natural surroundings more protected from the external climatic agents such as sun, wind and strong temperature fluctuations (among others (Berkovic, Yeziro, & Bitan, 2012; Edwards, Sibley, Land, & Hakmi, 2006; Polyzoides, Sherwood, & Tice, 1992; Randhawa, 1999; Rojas, Galán-Marín, & Fernández-Nieto, 2012)). This space with special microclimate conditions can also reduce heat loss or gain through building envelopes, consequently reducing the heating and cooling energy demand of buildings.

The courtyard microclimate thermal condition can be significantly influenced by the geometry and orientation of buildings (among others (Edwards et al., 2006; Fabbri, Di Nunzio, Gaspari, Antonini, & Boeri, 2017; Hall, Walker, & Spanton, 1999; Martinelli & Matzarakis, 2017; Muhaisen, 2006; Muhaisen & B Gadi, 2006; Rojas et al., 2012; Yaşa & Ok, 2014)) and other elements (e.g. vegetation) (Berkovic et al., 2012; Taleghani, Tenpierik, van den Dobbelen, & Sailor, 2014b), the materials used in construction (Nazarian & Kleissl, 2015; Wang & Liu, 2002) and land use characteristics (Collier, 2006). Therefore, the best

approach to assess the impact of geometrical parameters on courtyard microclimate and building envelope heat loss is to simulate the project with the help of microclimate modeling software that meets the following requirements (Huttner, 2012; Noro & Lazzarin, 2015):

- The model should have an adequate grid size – i.e. $\leq 10 \text{ m}$ –, according to building resolution
- The model has to implement the energy balance of surfaces of all types
- The model has to simulate the physical and physiological properties of plants
- The model should calculate the atmospheric processes, prognostic and transient

Accordingly, in this project, as a first step the appropriate modeling software should be selected based on the required accuracy and project resources.

Common turbulence models can be classified based on computational expense into two main approaches, The Reynolds-averaged Navier–Stokes (RANS) and Large Eddy Simulation (LES). Despite the increasing popularity of LES methods over the past three years, this method has the drawback that most LES microscale models only focus

* Correspondence to: Appelstraße 9A, 30167 Hannover, Germany.
E-mail address: forouzandeh@ifbp.uni-hannover.de.

2. Paper B

DOI: <https://doi.org/10.1007/s12273-019-0528-2>

BUILD SIMUL
<https://doi.org/10.1007/s12273-019-0528-2>

Parametric analysis of influence of courtyard microclimate on diminution of convective heat transfer through building's envelope

Aysan Forouzandeh (✉)

Department of Civil Engineering and Geodetic Science, Institute for Building Physics, Leibniz University, Hannover, Germany

Abstract

The growing trend of using glass facade and the low thermal resistance of this material, has increased the importance of environmental loads on heat loss through the building's envelope. In this regards, creating microclimate spaces between buildings acts as a shelter against wind and sun, and thus convective and radiative heat transfer. In this research, computational fluid dynamics microclimate software ENVI-met has been used to consider the relationship between optimum courtyard forms in decreasing the convective heat transfer coefficient (CHTC). A simple linear correlation was used to calculate the h_c ($\text{W}\cdot\text{m}^{-2}\cdot\text{K}^{-1}$) based on the wind speed (WS) near the facade within the courtyard. The outcome of the research reveals that the microclimate of the courtyard, particularly for the strong ambient winds (U_{10}), can diminish the CHTC in comparison with exposed surfaces. Moreover, among various design alternatives, the aspect ratio has a significant impact on WS and CHTC. It was observed that, for $U_{10} = 2.3$ ($\text{m}\cdot\text{s}^{-1}$), as aspect ratio (H/W) increases from 0.67 to 3.67, the average surface WS, up to the middle floor, on the windward and leeward facade inside the courtyard, located in Hanover, reduces by about 75%. This suggests that an appropriate selection of the courtyard geometry will help passively reduce cooling load and let designers use less thickly insulated walls.

Keywords

courtyard microclimate, holistic microclimate simulation, wind speed near the facade, exterior convective heat transfer coefficient

Article History

Received: 12 November 2018
 Revised: 1 February 2019
 Accepted: 13 February 2019

© Tsinghua University Press and Springer-Verlag GmbH Germany, part of Springer Nature 2019

1 Introduction

The term 'building envelope' specifies the building components that surround the conditioned spaces, and thermal energy, depending on the inside-outside temperature difference, is transferred to or from the outdoor environment through it (Doty and Turner 2013). Therefore, thermal control and understanding the mechanism of the heat transfer and the temperature distribution through building envelopes are important for assessing sustainable solutions for low energy consumption buildings (Straube 2011).

The energy balance at the external surface of the building can be expressed as:

$$q + \alpha_s G + \varepsilon L = \varepsilon \sigma T_s^4 + h_c (T_s - T_o) + LE \quad (1)$$

Accordingly, the heat transfer between the external surfaces of the building and its surroundings is a combination of conduction, convection, radiation and evaporation or condensation of water at the outside facade (DIN 2003;

Doty and Turner 2013). Therefore, increasing the mass and surface resistance of the system can reduce heat transfer through it. The first one can be improved by increasing the thermal properties of the exterior wall's material (Long and Ye 2016) and the second one requires sustainable designs with few exterior surfaces (Loukaidou et al. 2017) and thermal bridge locations (Dumitrescu et al. 2017), along with the use of climate control shields (Mauree et al. 2017). These obstacles restrict the solar radiation (Montavon 2010) and wind (Azizi and Javanmardi 2017), reduce the convective ($q_c = h_c (T_s - T_o)$) and irradiative ($q_{1-out} = \varepsilon \sigma T_s^4$) heat transfer (Erell et al. 2012). Therefore, the energy consumption of buildings does not depend only on the building's material, and is very influenced by its geometry and surrounding microclimate (de la Flor and Dominguez 2004; Grobman and Elimelech 2016).

The convective heat losses are usually 2–7 times much larger than the radiative losses at low temperatures during the winter (Davies 2004; Defraeye and Carmeliet 2010;

3. Paper C

DOI: <https://doi.org/10.1016/j.enbuild.2019.03.030>

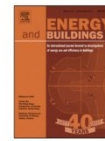
Energy & Buildings 193 (2019) 49–68



Contents lists available at ScienceDirect

Energy & Buildings

journal homepage: www.elsevier.com/locate/enbuild



Accurate prediction of heating energy demand of courtyard's surrounding envelopes using temperature correction factor

Aysan Forouzandeh*, Torsten Richter

Department of Civil Engineering and Geodetic Science, Institute for Building Physics, Leibniz University, Appelstraße 9A, Hanover 30167, Germany



ARTICLE INFO

Article history:

Received 18 September 2018

Revised 13 March 2019

Accepted 18 March 2019

Available online 20 March 2019

Keywords:

Courtyard microclimate
Heat transfer through building envelope
Temperature correction Factor
Aspect ratio (H/W)

ABSTRACT

It is widely accepted that the climatic factors—including solar load, wind flow pattern and external air temperature—strongly affect building energy consumption. Meanwhile, the microclimate of semi-closed spaces between buildings has direct and indirect consequences on heat transfer through building envelopes.

This study demonstrates how courtyard configuration can modify the climate and external air temperature and how the microclimate condition can be considered for functionally accurate calculation of heat loss and thermal loads of buildings.

Based on the experimental and computational results, increasing the courtyard's depth by restricting the sky view factor (SVF) and the heat exchange with courtyard's outside at low levels, creates the individual microclimate. The thermal environment of this middle space is affected more than outside by surrounding rooms and the thermal properties of the building walls.

The findings, which are limited to experimental cases in the Hanover climate region, propose to consider the temperature of courtyard depending on its aspect ratio and glazing percentage with a temperature correction factor ($F_{x, \text{Heat load}}$) between 0.9 to 2.2.

© 2019 Elsevier B.V. All rights reserved.

1. Introduction

In recent years, more attention has been given to exploring the links between buildings and their surroundings. The results indicate that improving the exterior condition, by controlling the solar load, wind flow and external air temperature should have direct and indirect consequences on energy saving [2].

Considering the net energy balance at the external surface of the building:

$$q + \alpha_s G + \alpha_L L = \varepsilon \sigma T_s^4 + h_c (T_s - T_0) + LE$$

$$q = \frac{\left(\sum_{i=1}^n (F_{x,i} U_i A_i) + \Delta U_{TB} \cdot A_{tl} \right) \cdot (\Delta T)}{A_{tl}} \quad (1)$$

The thermal transmittance and thermal resistance of building enclosures are determined based on the thermal properties of materials, building shape and dimension of thermal bridges. Besides, it is commonly accepted that the energy consumption of buildings is strongly influenced by the thermal condition in front of it [3–5].

In this regard, applying innovative transitional spaces, such as courtyards, lets the building envelopes experience different climate condition [6], which has an important impact on thermal condition and heating and cooling energy demand of surrounding buildings. Al-Hemiddi and Megren Al-Saud [7], Aldwoud [8], Taleghani et al. [9] and many other studies approved this response inside the courtyard space in different climate regions.

A courtyard is a very old form of human-made microclimate, traced back to 3000 BC [10] and was used by many urban civilizations with various climates [11]. The microclimate of the courtyard reduces convective heat exchange and long-wave energy losses during the night and winter due to lower wind speeds and SVFs, respectively. This space can also modify the radiation balance due to its solar-shadowing effect [6].

The potential of the courtyard, in controlling wind and sun, affects the temperature difference between the interior and the exterior sides of the building envelope ($\theta_i - \theta_e$). As a result, the local air temperature inside the most of existing semi-closed courtyard spaces is warmer than an open space in winter and in the same way at nights, due to trapping the heat in the space. And in summer, since less solar radiation enters the space, it is cooler than outside [12]. Previous experiments (Table 1) show that inside the courtyard the average peak temperature drops and minimum temperature rises compare to ambient temperature. The difference

* Corresponding author.

E-mail address: forouzandeh@fbp.uni-hannover.de (A. Forouzandeh).

CURRICULUM VITAE

Aysan Forouzandeh (M. Sc.)

Personal Data

Date of Birth 29.07.1985
Place of Birth Tabriz (Iran)
Nationality Iranian
Contact Address Appelstrasse 9A, 30167 Hanover.
Institute for Building Physic, Room: 326 (3408)
Phone +49 511 762 3718
E-mail forouzandeh@ifbp.uni-hannover.de



EDUCATION

04/2013– Present PHD, Institute for Building Physics
Leibniz University Hanover, Germany
Thesis: Effect of courtyard microclimate on heat loss through
building's envelope and heating energy demand
Supervisor: Prof. Dr.-Ing. Nabil A. Fouad

2008 – 2010 Master of Science (M. Sc.), Architectural Engineering
Tabriz Art University, Iran
Thesis: Designing research center for building's modern technology
by applying transformable skins
Supervisor: Dr. Maziar Asefi.
GPA: 19.13/20

2004 – 2008 Bachelor of Science (B. Sc.), Architectural Engineering
Tabriz Art University, Iran
Thesis: Designing research Centre for renewable energies with
Sustainable design Methods
Supervisor: Dr. A. Ghafarri.
GPA: 18.87/20

AWARDS

2010 Graduated as best student of the year
(„Architecture Engineering M. Sc.“, Tabriz Art University Iran)

2008 Graduated as best student of the year
(„Architecture Engineering B. Sc.“, Tabriz Art University Iran)

ACADEMIC RELATED ACTIVITIES

02/2015– Present Research and Teaching Assistant, Institute for Building Physics,
Department of Civil Engineering and Geodetic Science, Leibniz
University, Hanover, Germany

2014-2015 Student Assistant, Institute for Building Physics, Department of Civil
Engineering and Geodetic Science, Leibniz University, Hanover,
Germany

2010-2012 Research and Teaching Assistant, Department of Civil Engineering and
Geodetic Science, Tabriz University, Tabriz, Iran

2009-2010 Research and Teaching Assistant, Department of Architecture, Tabriz Art
University, Tabriz, Iran

2009 Member of the Research Team in the Project: “Seismic rehabilitation of
the buildings of Tabriz Art University”

2008-2009 Student Assistant, Department of Architecture, Tabriz Art University,
Tabriz, Iran

NON-ACADEMIC WORK EXPERIENCE

- 04/2018– Present Technical Draftsman for fire Protection Plans, 3B Bauconsult GmbH
§ Co.KG, Hanover, Germany
- 2015 – 2018 Architect, ALMA Bauprojekte, Hanover, Germany
- 2014 Practical Training, ALMA Bauprojekte, Hanover, Germany
- 2006- 2011 Member of Design-Teams, Abadkaran Building Firm, Tabriz, Iran
- 2009.2010 Member of Design-Teams in the Project: Tabriz’s miniature park,
Nemodar Design- Company, Tabriz, Iran

PUBLICATIONS AND MANUSCRIPTS

- Apr. 2019 Forouzandeh, Aysan (2019): Parametric analysis of influence of
courtyard microclimate on diminution of convective heat transfer
through building’s envelope (2019). *Building Simulation* 04/2019;
DOI:10.1007/s12273-019-0528-2
- Mar. 2019 Forouzandeh, Aysan, Richter, T. (2019): Accurate prediction of heating
energy demand of courtyard's surrounding envelopes using temperature
correction factor. *Energy and Buildings* 03/2019; 193.
DOI:10.1016/j.enbuild.2019.03.030
- Jan. 2018 Forouzandeh, Aysan (2018): Numerical modeling validation for the
microclimate thermal condition of semi-closed courtyard spaces
between buildings. *Sustainable Cities and Society* 01/2018;
36(Supplement C):327-345.
DOI:10.1016/j.scs.2017.07.025

- Sep.2014 Forouzandeh, Aysan. Malekshahi, Shahin (2014): The Evaluation of Structural Strengthening of Historic Building on the Basis of Architectural and Restoration Consideration". Journal of Civil Engineering and Architecture Research .Vol. 1, No. 3, Sept.2014.
- Jun.2011 Asefi, Maziar and Forouzandeh, Aysan. (2011): Nature and Kinetic Architecture: The Development of a New Type of Transformable Structure for Temporary Applications". Journal of Civil Engineering and Architecture, ISSN 1934-7359, USA. pp. 513-526.
- 2010 Nogrekar.A & Hamzenejad. M & Forouzandeh.A.(2010): Eternity secret of architectural works (In two artistic isms ,modernism and post modernism). Bagh-I-NAzar.12. The quartered scientific journal. Iran, (In Persian).
- 2010 Bagheri .Mohammad & Forouzandeh.Aysan : Customers' preferences in design of shopping centers' (A Case Study in Tabriz, Iran)
(Not Published).
- 2010 Forouzandeh. Aysan, Kafashian.Z & Pirbabaei.M.: Evaluation of the Rehabilitation Method of Shahid Beheshti Square
(In Persian)(Not Published)

CONFERENCE PRESENTATION AND PARTICIPATION

- Jun.2012 Forouzandeh,Aysan (2012): Technology transfer from nature in to kinetic adaptive structures". 6th International Conference on Relating Design in Nature with Sciences and Engineering. Spain (Abstract)
- Nov.2010 Asefi, M. & Forouzandeh, A. (2010): Nature and Kinetic Architecture: The Development of a New Type of Transformable Structure for Temporary Applications, IASS2010, Shanghai, China
- Jun.2010 Forouzandeh, A & Asefi.M. (2010): Nature and kinetic architecture. Design and Nature 2010. 28 – 30 June 2010. Pisa, Italy. (Abstract)
- Oct.2009 Forouzandeh, A. (2009): The ways of using sun energy in the buildings. The 4th International Renewable and Clean Energy Conference. Yerevan. Armenia. October 5 – 7, 2009 (Poster presentation)

- May.2008 Interior Design Conference , Tabriz, Iran
- 2007 International Conference on Structures and architecture, Tehran University, Teheran

TEACHING. LECTURE NOTES

- Oct.2015 Fouad, N. Richter, T., Forouzandeh, A. (2015): CAD für Bauingenieure- Grundlagen zur Erstellung von Bauzeichnungen, Electronic format. Leibniz University of Hanover

PROFESSIONAL MEMBERSHIP

- 2010– Present East-Azerbaijan Fellowship for Architects and Civil Engineers

WORKSHOPS

- Feb.2007 Solar responsive Design, Professor Norbert from Auburn University, Faculty for Architecture, Tabriz Islamic Art University, Iran

SKILLS

Languages

Language	Level
Persian	Mother Tongue
Azerbaijani	Mother Tongue
English	IELS 7.0, TOEFL IBP 80 (Fluent)
German	B2 (Upper Intermediate)
Turkish	Elementary

Computers

Software	Level
Microsoft office-Tools (word, PowerPoint, Excel, ...)	Advanced
AutoCAD	Advanced
3Ds Max	Advanced
IBP18599	Advanced
Flixo (Das Wärmebrücken Analyse)	Advanced
Photoshop	Upper- Intermediate
SketchUp	Advanced
Trnsys	Upper- Intermediate
Ecotect + Winair	Advanced
Allplan	Advanced
ENVI-met	Advanced
